Contents of issue 1 vol. XLV

Polish Academy of Sciences

Institute of Fundamental Technological Research

Archives of Mechanics

Archiwum Mechaniki Stosowanej

volume 45 issue 1

Polish Scientific Publishers PWN

Warszawa 1993

ARCHIVES OF MECHANICS IS DEVOTED TO Theory of elasticity and plasticity • Theory of nonclassical continua •Physics of continuous media • Mechanics of discrete media • Nonlinear mechanics • Rheology • Fluid gas-mechanics • Rarefied gases • Thermodynamics

Printed in Poland, Editorial Office: Świętokrzyska 21,
00-049 Warszawa (Poland)

Arkuszy wydawniczych 13,5. Arkuszy drukarskich 10,25
Papier offset. kl. III 70 g. B1. Oddano do składania w kwietniu 1993 r.
Druk ukończono w sierpniu 1993 r.
Skład i łamanie *ArtGraph*
Druk i oprawa „Graphield"

Arch. Mech., 45, 1, pp. 3–38, Warszawa 1993

On deformation-induced plastic anisotropy of sheet metals(*)

W. SZCZEPIŃSKI (WARSZAWA)

PROBLEMS CONNECTED with the theoretical description of plastic flow of polycrystalline sheet metals are discussed and commented. Sheet metals display distinct anisotropic properties in the plastic range of deformation. It is observed that these properties may be different depending on the plastic deformation histories in the course of the manufacturing process. Much attention has been devoted to the experimental tests of plastic anisotropy of sheet metals and to the comparison of test results with various theoretical descriptions.

1. Introduction

POLYCRYSTALLINE SHEET metals display anisotropic plastic properties caused by complex deformation processes, like multistage rolling and stretching connected with heat treatment of the material during the manufacturing process. An important factor, difficult to be included into the theoretical description, is the non-homogeneity of anisotropy through the thickness of the sheet. This effect is usually averaged in theoretical analyses.

Depending on the history of deformations during the manufacturing process, the plastic anisotropy of sheet metals may be of different form. In sheet metals it is usually the orthotropy: two axes of orthotropy lie in sheet's plane, and the third axis is directed normally to this plane.

As a very important case of orthotropy, the so-called normal anisotropy, when the sheet is isotropic in its plane, while its plastic properties in the direction normal to the sheet's surface are different, should be mentioned. A more general case of anisotropy one can observe when the sheet under loadings acting in its plane displays quasi-orthotropic plastic properties, while the direction normal to sheet's surface does not constitute the orthotropy axis. Such a behaviour will be referred to in this paper as the quasi-orthotropy. Sheet metals may also display the so-called generalized Bauschinger effect.

The proper definition of the type of anisotropy of a sheet metal in question is especially important, when it is used as the material for manufacturing products with the use of various drawing techniques, since the anisotropy plays an important role in overall deformability of sheet metals. These problems are, for example, discussed in the book by MARCINIAK [1]. The practical significance of the anisotropy of sheet metals stimulated the development of various experimental techniques allowing to measure anisotropy parameters. The complexity of the phenomena connected with the plastic flow of anisotropic materials makes useful its theoretical description because, first of all, such a theory allows us to rationalize any experimental program and the proper interpretation of the obtained results.

(*) The Editorial Committtee is extremely sorry to inform the Readers that the papers by W. Szczepiński "*On deformation-induced plastic anisotropy of sheet metals*" which appeared in the former issue of "Archives of Mechanics" contained numerous printer's errors making it difficult to follow the text: some illustrations were misplaced by the Printing House. In this situation it has been decided that the paper should be printed again in the present issue of our journal. We would like to apologize to the Author and to the Readers for all the inconveniences following from that fact.

In the present paper a certain attempt has been made to discuss more deeply the mechanics of plastic flow of sheet metals with the analysis of various experimental methods concerning such a flow. The possible practical applicability of the less studied variants of the theory for interpretation of experimental results has been also analysed.

2. Fundamentals of the classical mechanics of plastic flow of anisotropic bodies

The theory of plastic flow of anisotropic bodies originated in 1928 when the classical paper by MISES [2] appeared. It has been written in connection with plastic deformations of single crystals. In the following papers of other authors the concept proposed by Mises was used for theoretical description of plastic behaviour of polycrystalline metals with deformation-induced anisotropy.

MISES in his work [2] proposed the following general yield function for crystals:

$$\begin{aligned}(2.1)\quad \psi = {} & h_{11}\sigma_x^2 + h_{22}\sigma_y^2 + h_{33}\sigma_y^2 + h_{44}\tau_{xy}^2 + h_{55}\tau_{yz}^2 + h_{66}\tau_{zx}^2 + 2h_{12}\sigma_x\sigma_y \\ & + 2h_{13}\sigma_x\sigma_z + 2h_{14}\sigma_x\tau_{xy} + 2h_{15}\sigma_x\tau_{yz} + 2h_{16}\sigma_x\tau_{zx} + 2h_{23}\sigma_y\sigma_z + 2h_{24}\sigma_y\tau_{xy} \\ & + 2h_{25}\sigma_y\tau_{yz} + 2h_{26}\sigma_y\tau_{zx} + 2h_{34}\sigma_z\tau_{xy} + 2h_{35}\sigma_z\tau_{yz} + 2h_{36}\sigma_z\tau_{zx} \\ & + 2h_{45}\tau_{xy}\tau_{yz} + 2h_{46}\tau_{xy}\tau_{zx} + 2h_{56}\tau_{yz}\tau_{zx}\,.\end{aligned}$$

It was assumed here that the yield function is quadratic with respect to stress components $\sigma_x, \sigma_y, \ldots, \tau_{zx}$. It contains 21 various coefficients (moduli) $h_{ij}(i, j = 1, 2, \ldots, 6)$ of anisotropy. Function (2.1) remains unchanged when the signs of all stress components are changed. Thus, when using it, we cannot take into account the Bauschinger effect. Since in the yield function (2.1) there are terms containing products of normal and shear stresses, it is necessary to establish a rule concerning the sign of the latter in the assumed Cartesian coordinate system x, y, z.

Yield condition for anisotropic bodies corresponding to yield function (2.1) can be written as

$$(2.2)\qquad H_{ijkl}\sigma_{ij}\sigma_{kl} = \text{const.}$$

For metals the hydrostatic component p of the stress tensor has no influence on the plastic yielding. Thus, for obtaining the same form of the yield condition after introducing new stresses $\sigma_x - p$, $\sigma_y - p$, $\sigma_z - p$ instead of original stresses $\sigma_x, \sigma_y, \sigma_z$, it is necessary to reduce the number of anisotropy coefficients to 15. The yield condition takes then the form

$$\begin{aligned}(2.3)\quad f(\sigma_{ij}) = {} & k_{12}(\sigma_x - \sigma_y)^2 + k_{23}(\sigma_y - \sigma_z)^2 + k_{31}(\sigma_z - \sigma_x)^2 + 2\tau_{xy}[k_{16}(\sigma_z - \sigma_x) \\ & + k_{26}(\sigma_z - \sigma_y)] + 2\tau_{yz}[k_{24}(\sigma_x - \sigma_y) + k_{34}(\sigma_x - \sigma_z)] + 2\tau_{zx}[k_{35}(\sigma_y - \sigma_z) \\ & + k_{15}(\sigma_y - \sigma_x)] - 2k_{45}\tau_{yz}\tau_{zx} - 2k_{56}\tau_{zx}\tau_{xy} - 2k_{64}\tau_{xy}\tau_{yz} \\ & + k_{44}\tau_{yz}^2 + k_{55}\tau_{zx}^2 + k_{66}\tau_{xy}^2 - 1 = 0\,.\end{aligned}$$

OLSZAK and URBANOWSKI [3, 4, 5] have generalized this yield condition for simultaneously anisotropic and non-homogeneous bodies. In such a case all coefficients k_{ij} in Eq. (2.3) are known functions of the coordinates. The form of the yield condition remains the same as above.

Function (2.3) may be treated as the so-called plastic potential. Plastic strain rates are then connected with the stress components by the flow law

$$(2.4)\qquad \dot{\varepsilon}_{ij} = \lambda\frac{\partial f}{\partial \sigma_{ij}}\,,$$

where λ is a proportionality factor. Relations (2.4) are referred to as the associated flow law.

Physical interpretation of anisotropy coefficients k_{ij} in Eq. (2.3) may be found by considering various uniaxial stress states, each with one non-vanishing stress component only. By considering uniaxial tension (compression) we arrive at the relations (cf. [3])

$$
\begin{aligned}
k_{12} &= \frac{1}{2}\left(\frac{1}{Y_x^2} + \frac{1}{Y_y^2} - \frac{1}{Y_z^2}\right), \\
k_{23} &= \frac{1}{2}\left(-\frac{1}{Y_x^2} + \frac{1}{Y_y^2} + \frac{1}{Y_z^2}\right), \\
k_{31} &= \frac{1}{2}\left(\frac{1}{Y_x^2} - \frac{1}{Y_y^2} + \frac{1}{Y_z^2}\right),
\end{aligned} \tag{2.5}
$$

where Y_x, Y_y, Y_z stand for the yield loci of the material under uniaxial tension in directions x, y, z, respectively. Exact realization of such tests is rather difficult for materials with the general type of anisotropy, since application of the standard testing techniques produces distortion of the tensioned specimens, which assume the form of the letter S. This problem has been analysed for example by Boehler et al. [6]. To minimize the arising curvature of the test piece they have designed special grips with knife-edged joints.

Even more difficult is realization of shear tests which are necessary, if yield loci in shear Q_{xy}, Q_{yz}, Q_{zx} are to be directly measured. These yield loci are related to the respective anisotropy coefficients by the formulae

$$
k_{44} = \frac{1}{Q_{yz}^2}, \qquad k_{55} = \frac{1}{Q_{zx}^2}, \qquad k_{66} = \frac{1}{Q_{xy}^2}. \tag{2.6}
$$

The anisotropy coefficients are often measured indirectly, especially for sheet metals, by making use of the anisotropy of plastic strain increments that are connected with the yield condition (2.3) by the associated flow law (2.4). We obtain from that flow law the expressions for strain increments

$$
\begin{aligned}
d\varepsilon_x &= 2d\lambda[k_{12}(\sigma_x - \sigma_y) - k_{31}(\sigma_z - \sigma_x) - k_{16}\tau_{xy} + (k_{24} + k_{34})\tau_{yz} - k_{15}\tau_{zx}], \\
d\varepsilon_y &= 2d\lambda[-k_{12}(\sigma_x - \sigma_y) + k_{23}(\sigma_y - \sigma_z) - k_{26}\tau_{xy} - k_{24}\tau_{yz} + (k_{35} + k_{15})\tau_{zx}], \\
d\varepsilon_z &= 2d\lambda[-k_{23}(\sigma_y - \sigma_z) + k_{31}(\sigma_z - \sigma_x) + (k_{16} + k_{26})\tau_{xy} - k_{34}\tau_{yz} - k_{35}\tau_{zx}].
\end{aligned} \tag{2.7}
$$

The corresponding expressions for shear strain increments are not given here, since they are difficult to be measured in the laboratory tests and therefore such expressions are not used in practice.

When using relations (2.7) for indirect measuring anisotropy coefficients we should be aware that often the values of these coefficients measured indirectly differ remarkably from those measured directly. Respective examples will be discussed later on. Nevertheless, it should be emphasized that in some cases indirect measuring methods based on relations (2.7) are the only methods possible for practical realization.

3. Fundamentals of the classical mechanics of plastic flow of orthotropic bodies

Orthotropy is an important particular case of general anisotropy. At each point of the body three orthogonal planes of symmetry of plastic properties can be distinguished. Intersections of these planes are called the axes of orthotropy. Directions of orthotropy

axes may vary from point to point. Let us now discuss various types of orthotropy that are of practical significance.

3.1. Basic relations of plastic orthotropy

In the case of orthotropy the general yield condition (2.3) reduces to the form containing six plastic moduli only. Assuming that the axes of orthotropy coincide with the axes x, y, z of the Cartesian coordinate system we can write (cf. [3])

$$k_{12}(\sigma_x - \sigma_y)^2 + k_{23}(\sigma_y - \sigma_z)^2 + k_{31}(\sigma_z - \sigma_x)^2 + k_{44}\tau_{yz}^2 + k_{55}\tau_{zx}^2 + k_{66}\tau_{xy}^2 = 1 . \tag{3.1}$$

In HILL'S book [7] this yield condition is written in the equivalent form

$$F(\sigma_y - \sigma_z)^2 + G(\sigma_z - \sigma_x)^2 + H(\sigma_x - \sigma_y)^2 + 2L\tau_{yz}^2 + 2M\tau_{zx}^2 + 2N\tau_{xy}^2 = 1 . \tag{3.1a}$$

If directions of the principal stresses σ_1, σ_2, σ_3 coincide with the directions of orthotropy axes, condition (3.1) takes the form

$$k_{12}(\sigma_1 - \sigma_2)^2 + k_{23}(\sigma_2 - \sigma_3)^2 + k_{31}(\sigma_3 - \sigma_1)^2 = 1 . \tag{3.2}$$

By substituting relations (2.5) we obtain the equivalent form of yield condition (3.2)

$$\left(\frac{1}{Y_x^2} + \frac{1}{Y_y^2} - \frac{1}{Y_z^2}\right)(\sigma_1 - \sigma_2)^2 + \left(-\frac{1}{Y_x^2} + \frac{1}{Y_y^2} + \frac{1}{Y_z^2}\right)(\sigma_2 - \sigma_3)^2 + \left(\frac{1}{Y_x^2} - \frac{1}{Y_y^2} + \frac{1}{Y_z^2}\right)(\sigma_3 - \sigma_1)^2 = 2 . \tag{3.3}$$

Here the orthotropy coefficients have been replaced by the yield loci in orthotropy directions.

Note that for orthotropic bodies, the measurements of yield loci under simple tension or compression in orthotropy direction can be performed with the use of standard experimental methods, because the test pieces cut out from the material in these directions will not suffer any distortion.

Yield condition (3.3) may be represented in the space of principal stresses σ_1, σ_2, σ_3 as an infinitely long cylinder with elliptical cross-section and the axis making the same angle with all three axes of principal stresses. In Fig. 1 two projections of that cylinder are presented. Cross-section of the cylinder by an octahedral plane

$$\sigma_1 + \sigma_2 + \sigma_3 = 3\sigma^0$$

is also shown in the figure. In the lower part a triangular portion of the octahedral plane with this elliptical cross-section is presented. Dimensions and orientation of the ellipse depend on the yield loci in the directions of the orthotropy axes

$$Y_1 \equiv Y_x, \quad Y_2 \equiv Y_y, \quad Y_3 \equiv Y_z .$$

We shall find the equation of the ellipse on the octahedral plane with the axes σ_1^0, σ_2^0, σ_3^0 on that plane being projections of the original axes σ_1, σ_2, σ_3, respectively. Geometrical relations for the tetrahedron shown in Fig. 1 are used to find positions of points representing the respective yield loci on the axes σ_1^0, σ_2^0, σ_3^0 (Fig. 2)

$$Y_1^0 = Y_1\sqrt{\frac{2}{3}}, \quad Y_2^0 = Y_2\sqrt{\frac{2}{3}}, \quad Y_3^0 = Y_3\sqrt{\frac{2}{3}} .$$

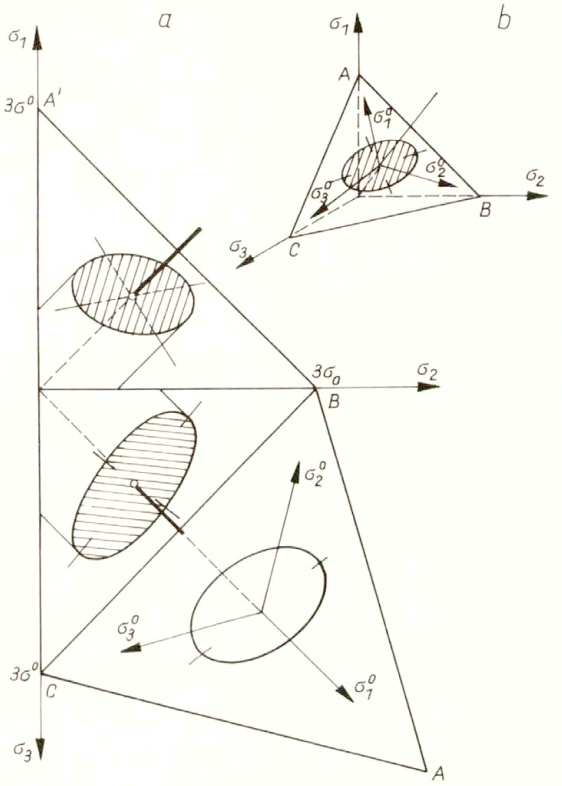

FIG. 1.

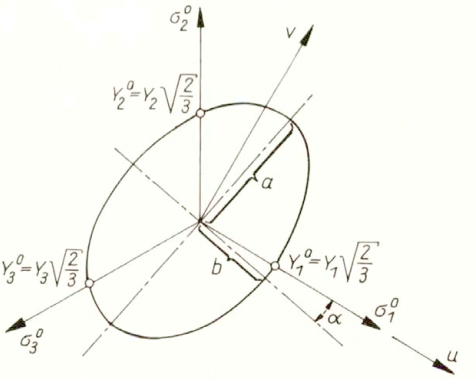

FIG. 2.

The ellipse with the centre at the origin of coordinates and passing through these three points has the equation

$$\frac{3}{2Y_1^2}u^2 + \sqrt{3}\left(\frac{1}{Y_2^2} - \frac{1}{Y_2^2}\right)uv + \left(\frac{1}{Y_2^2} + \frac{1}{Y_3^2} - \frac{1}{2Y_1^2}\right)v^2 = 1 \tag{3.4}$$

in the auxiliary coordinate system u, v (Fig. 2).

Note that the yield surface presented in Fig. 1 does not determine uniquely the yield condition of an orthotropic body. It is valid for arbitrary values of anisotropy coefficients k_{44}, k_{55}, k_{66} appearing in the generally written yield condition (3.1). Thus it corresponds only to particular stress states, when directions of principal stresses coincide with those of orthotropy.

Now we shall consider a certain particular case of orthotropy, that can occur in commercial metals, especially in sheet metals.

3.2. Transversal isotropy

Transversal isotropy is a particular case of orthotropy, when all directions perpendicular to one of orthotropy axes, say z-axis, are equivalent. Such a type of orthotropy characterises certain sedimentary soils and rocks, like e.g. diatomite (cf. [8, 9, 10]). However, for such materials the yield conditions discussed here do not apply, since plastic yielding of them depends on the first stress invariant, which is neglected in these conditions.

Transversal isotropy is often observed in sheet metals. Thus its practical significance is obvious. Yield condition for transversally isotropic materials results from Eq. (3.1), if the following relations and new notations (cf. [4])

$$k_{23} = k_{31} = k_1, \qquad k_{44} = k_{55} = k_2, \qquad k_{66} = 2(k_1 + 2k_{12})$$

are introduced. Then the yield condition for transversally isotropic materials takes the form

$$(3.5) \quad k_1[(\sigma_y - \sigma_z)^2 + (\sigma_z - \sigma_x)^2] + k_{12}(\sigma_x - \sigma_y)^2 + k_2(\tau_{zy}^2 + \tau_{zx}^2) + 2(k_1 + 2k_{12})\tau_{xy}^2 = 1 .$$

Since now we have $Y_x = Y_y = Y_0$, from Eqs. (2.5) result the expressions for the anisotropy coefficients

$$k_1 = \frac{1}{2Y_z^2}, \qquad k_{12} = \frac{1}{Y_0^2} - \frac{1}{2Y_z^2} .$$

Now the yield condition (3.5) may be written in equivalent form

$$(3.5') \quad \frac{1}{2Y_z^2}[(\sigma_y - \sigma_z)^2 + (\sigma_z - \sigma_x)^2] + \left(\frac{1}{Y_0^2} - \frac{1}{2Y_z^2}\right)(\sigma_x - \sigma_y)^2 + k_2(\tau_{yz}^2 + \tau_{zx}^2) + \left(\frac{4}{Y_0^2} - \frac{1}{Y_z^2}\right)\tau_{xy}^2 = 1 .$$

Let us assume such a stress state when the direction of the principal stress σ_3 coincides with the orthotropy axis which has been chosen as the z-axis. The remaining two principal stresses can be oriented arbitrarily in the plane of transversal isotropy. For such stress states the yield condition (3.5′) can be written in the form

$$(3.6) \quad \frac{1}{2Y_z^2}[(\sigma_2 - \sigma_3)^2 + (\sigma_3 - \sigma_1)^2] + \left(\frac{1}{Y_0^2} - \frac{1}{2Y_z^2}\right)(\sigma_1 - \sigma_2)^2 = 1 .$$

Yield condition (3.6) may be represented in the space of principal stresses by a certain cylinder with elliptical cross-section, in the similar manner as for the case of general orthotropy. Its elliptical cross-section is determined on the octahedral plane by the equation

$$(3.7) \quad \frac{3}{2Y_0^2}u^2 + \sqrt{3}\left(\frac{1}{Y_z^2} - \frac{1}{Y_0^2}\right)uv + \left(\frac{1}{2Y_0^2} + \frac{1}{Y_z^2}\right)v^2 = 1 .$$

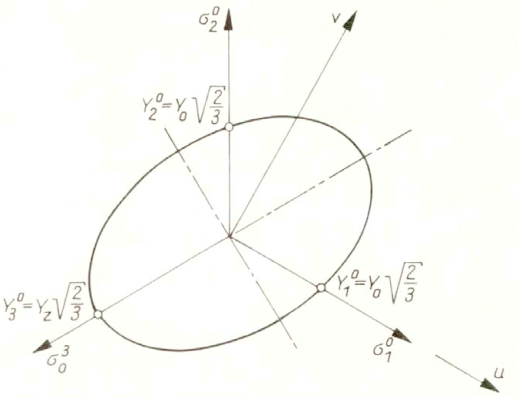

FIG. 3.

One of the principal axes of the ellipse coincides with the σ_3^0-axis on that plane (Fig. 3).

A certain peculiar type of transversal isotropy occurs when yield loci are identical for all three directions, that is when

$$Y_x = Y_y = Y_z = Y_0 . \tag{3.8}$$

In such a case yield condition (3.5′) reduces to the form

$$(\sigma_x - \sigma_y)^2 + (\sigma_y - \sigma_z)^2 + (\sigma_z - \sigma_x)^2 + 6\tau_{xy}^2 + 2k_2 Y_0^2(\tau_{yz}^2 + \tau_{zx}^2) = 2Y_0^2 . \tag{3.9}$$

For particular stress states, when the direction of the principal stress σ_3 coincides with the orthotropy direction z, yield condition (3.9) reduces to the form

$$(\sigma_1 - \sigma_2)^2 + (\sigma_2 - \sigma_3)^2 + (\sigma_3 - \sigma_1)^2 = 2Y_0^2 . \tag{3.10}$$

This form of the yield condition of the material with a special type of orthotropy is identical with that of the Huber–Mises yield condition for isotropic materials. The cross-section of the cylinder in the space of principal stresses is circular. However, there is now a distinct difference with respect to isotropic materials, since yield condition (3.10) and the respective cylindrical yield surface in the space of principal stresses correspond to particular stress states only, when principal stress σ_3 is directed along the axis z of orthotropy. For other stress states yield condition (3.10) is not valid.

3.3. Cubic orthotropy

Cubic orthotropy (cf. [4] is still another particular type of orthotropy characterized by identical values of yield stress under uniaxial tension (compression) in the directions of orthotropy — cf. Eq. (3.8). However, now all three orthotropy axes are fixed, while in the previous case the problem of transversal isotropy was dealt with. Let us assume that the axes x, y, z of the coordinate system coincide with the axes of orthotropy.

In the yield condition

$$(\sigma_x - \sigma_y)^2 + (\sigma_y - \sigma_z)^2 + (\sigma_z - \sigma_x)^2 + 2k_2 Y_0^2(\tau_{xy}^2 + \tau_{yz}^2 + \tau_{zx}^2) = 2Y_0^2 \tag{3.11}$$

we have two material constants Y_0 and k_2.

When principal stresses are directed along the respective orthotropy axes, this yield condition reduces to the form Eq. (3.10), which is represented by the cylinder with circular cross-section in the space of principal stresses. Thus the Huber–Mises cylinder

may correspond to various yield conditions including that for isotropic materials and those for materials with various particular cases of orthotropy.

4. Yield conditions for anisotropic bodies displaying Bauschinger effect

In sheet metals and in metal rods, a generalized form of the Bauschinger effect can be observed caused by plastic deformations induced during the manufacturing process. Generally speaking, this effect manifests itself as a difference between the absolute values of yield points of the material loaded by stress states of opposite signs. Bauschinger published his results in 1879 [11]. Interesting information concerning the history of investigations concerning this effect may be found in Bell's book [12]. Starting from the early fifties, scores of papers have appeared, in which a more generally understood Bauschinger effect induced in metals by previous plastic deformation was investigated. We shall mention only few earlier works, [13] to [17]. A comprehensive review of such papers was published by IKEGAMI [18, 19].

Interpretation of experimental results presented in the mentioned papers requires certain explanations if they are to be considered in terms of the theory of plastic anisotropy of commercial metals. Such metals underwent, during the manufacturing process, complex and usually not clearly known plastic deformations. In the experimental works referred to, the deformation history was strictly prescribed and registered. Thus it was possible to analyse the results of tests in terms of various strain-hardening hypothesis. Various definitions of yield point were assumed. In numerous papers the yield point was identified with the proportionality limit.

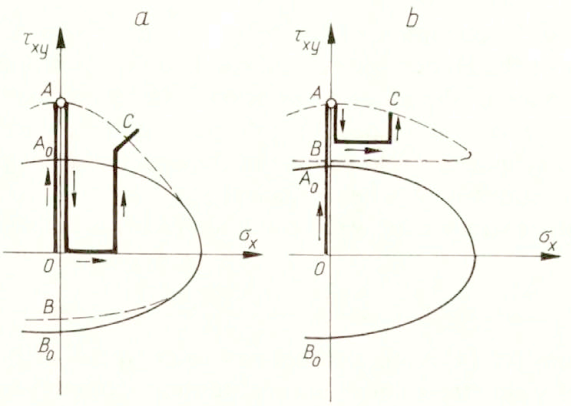

FIG. 4.

Two methods of performing experiments concerning the effect of plastic deformation on the yield condition may be distinguished. The scheme of the first of them is presented in Fig. 4a — which corresponds to the experimental procedure used in [13]. Thin-walled tubular specimens were twisted beyond the initial yield locus. Then, after total unloading, they were subsequently loaded by various combinations of axial force and twisting moment. One of such subsequent loading paths is shown in the figure. During each subsequent loading a point C corresponding to the new conventional yield limit was

found. The experimentally determined new yield surface of prestressed material, shown in the figure by the dashed line, differs remarkably from the initial yield surface shown by the continuous line. The new yield surface may be treated as that of the material with deformation-induced anisotropy.

Such a statement cannot be formulated if the new yield surface is determined according to the other experimental procedure presented schematically in Fig. 4b. It corresponds to the procedure being used e.g. in [15]. It was used also in numerous investigations of other authors. As in the first method, thin-walled tubular specimens were prestressed by twisting up to the point A, beyond the initial yield point A_0. Then they were only partly unloaded to a certain value of the twisting moment and subsequently reloaded along various loading paths — cf. Fig. 4b. In such a manner consecutive points C corresponding to the new conventional yield surface have been experimentally determined. If the predeformation is sufficiently large, the origin of the reference system lies outside the new yield surface identified with the surface of the proportionality limit.

In both papers [13] and [15] subsequent loading was interrupted when the first nonlinear deformations appeared. Thus the information on the plastic behaviour of prestressed material was limited. More information may be found in the works of other authors. Interesting results were obtained by DEAK [20], who measured (with great accuracy) the deformations in twisted thin-walled tubes during loading, and also during unloading. It was found that, even after a comparatively small plastic deformations, the unloading diagrams are curvilinear almost from the beginning of the unloading process. It means that the position of point B in Fig. 4b depends on the accuracy of strain measurements.

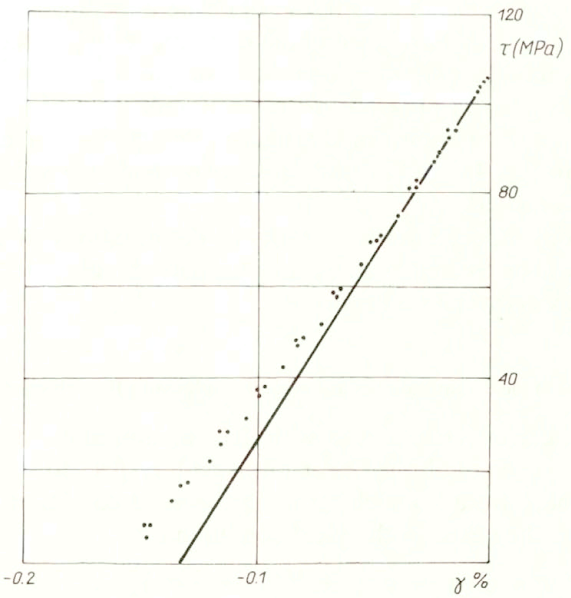

FIG. 5.

One of the unloading diagrams obtained in [20] for a tubular steel specimen prestressed by twisting until 3.6 percent of the permanent deformation is shown in Fig. 5. The diagram is curvilinear almost from the beginning. Thus, assuming the point at which the first

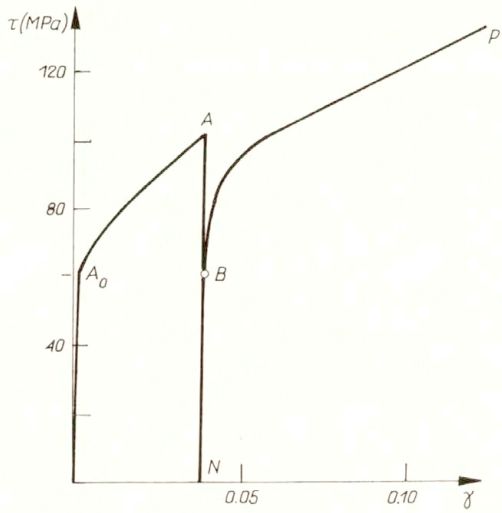

FIG. 6.

symptoms of nonlinearity of the unloading diagram are observed as the yield point, one obtains a subsequent yield surface such as that shown in Fig. 4b.

If experimental results are to be used for the description of the deformation-induced anisotropy, then the subsequent yield locus should rather be identified with the stresses at which plastic yielding during subsequent loading begins from the stress-free state. The diagram (Fig. 6) for a steel tube twisted in opposite directions, taken from [20], demonstrates how points A and B have been obtained in the testing procedure shown in Fig. 4a. The specimen was initially twisted in one direction (sector $A_0 - A$) and then, after total unloading, it was twisted in opposite direction (sector $N - B - P$) — absolute values of stresses and strains are shown in the figure. Points A_0, A and B correspond to the respective points in Fig. 4a. In [13] the subsequent loading was interrupted immediately after point B was reached.

Plastic anisotropy induced in the material by deformations connected with the manufacturing process will be treated as an existing property of the material, without connecting it with the previous deformation history.

4.1. On a general form of yield condition for anisotropic bodies with Bauschinger effect

If the Bauschinger effect in metals with deformation-induced anisotropy is to be accounted for in the yield condition, linear terms with respect to stress components should be introduced. There were no such terms in the yield conditions discussed in previous Sections. However, they exist in the yield condition

$$(4.1)\quad F(\sigma_y - \sigma_z)^2 + G(\sigma_z - \sigma_x)^2 + H(\sigma_x - -\sigma_y)^2 + 2L\tau_{yz}^2 + 2M\tau_{zx}^2 + 2N\tau_{xy}^2 - C\sigma_x - D\sigma_y - E\sigma_z = 1$$

proposed by OTA *et al.* [21] — cf. also [22, 23].

Constants C, D, E must satisfy the equality

$$C + D + E = 0,$$

if the plastic yielding is to be independent of the hydrostatic component of the stress tensor.

We shall analyse a more general form of the yield condition for materials displaying the Bauschinger effect. By analogy to Eq. (2.3), we shall write

$$
\begin{aligned}
(4.2)\quad f(\sigma_{ij}) = {} & k_{12}(\sigma_x - \sigma_y)^2 + k_{23}(\sigma_y - \sigma_z)^2 + k_{31}(\sigma_z - \sigma_x)^2 \\
& + 2\tau_{xy}[k_{16}(\sigma_z - \sigma_x) + k_{26}(\sigma_z - \sigma_y)] + 2\tau_{yz}[k_{24}(\sigma_x - \sigma_y) + k_{34}(\sigma_x - \sigma_z)] \\
& + 2\tau_{zx}[k_{35}(\sigma_y - \sigma_z) + k_{15}(\sigma_y - \sigma_x)] \\
& - 2k_{45}\tau_{yz}\tau_{zx} - 2k_{56}\tau_{zx}\tau_{xy} - 2k_{64}\tau_{xy}\tau_{yz} + k_{44}\tau_{yz}^2 + k_{55}\tau_{zx}^2 + k_{66}\tau_{xy}^2 \\
& - b_{12}(\sigma_x - \sigma_y) - b_{23}(\sigma_y - \sigma_z) - b_{31}(\sigma_z - \sigma_x) + b_{44}\tau_{yz} + b_{55}\tau_{zx} + b_{66}\tau_{xy} = 1 .
\end{aligned}
$$

Physical interpretation of some of the anisotropy coefficients k_{ij} and b_{ij} may be determined by analysing uniaxial stress states, each with only one non-vanishing stress component. By considering uniaxial tension (compression) we obtain the relations (cf. [22])

$$
\begin{aligned}
k_{12} &= \frac{1}{2}\left(\frac{1}{Y_x Z_x} + \frac{1}{Y_y Z_y} - \frac{1}{Y_z Z_z}\right), \\
(4.3)\qquad k_{23} &= \frac{1}{2}\left(-\frac{1}{Y_x Z_x} + \frac{1}{Y_y Z_y} + \frac{1}{Y_z Z_z}\right), \\
k_{31} &= \frac{1}{2}\left(\frac{1}{Y_x Z_x} - \frac{1}{Y_y Z_y} + \frac{1}{Y_z Z_z}\right),
\end{aligned}
$$

where Y_x, Y_y, Y_z stand for the yield limits of the material uniaxially tensioned in the directions x, y, z, respectively, and Z_y, Z_y, Z_z are the yield limits under uniaxial compressive loading.

Considering uniaxial tensile (compressive) loadings, we obtain also the following relations:

$$
\begin{aligned}
b_{31} - b_{12} &= \frac{1}{Y_x} - \frac{1}{Z_x}, \\
(4.4)\qquad b_{12} - b_{23} &= \frac{1}{Y_y} - \frac{1}{Z_y}, \\
b_{23} - b_{31} &= \frac{1}{Y_z} - \frac{1}{Z_z},
\end{aligned}
$$

for the moduli b_{12}, b_{23}, b_{31}. This system of equations has no unique solution since its characteristic determinant is equal to zero. By assuming that one of the moduli, say b_{31}, is equal to zero we obtain

$$
(4.5)\qquad b_{31} = 0, \quad b_{12} = -\frac{1}{Y_x} + \frac{1}{Z_x}, \quad b_{13} = \frac{1}{Y_z} - \frac{1}{Z_z}.
$$

Another variants are

$$
(4.5')\qquad b_{12} = 0, \quad b_{23} = -\frac{1}{Y_y} + \frac{1}{Z_y}, \quad b_{31} = \frac{1}{Y_x} - \frac{1}{Z_x},
$$

or

$$(4.5'') \qquad b_{23} = 0, \quad b_{12} = \frac{1}{Y_y} - \frac{1}{Z_y}, \quad b_{31} = -\frac{1}{Y_z} + \frac{1}{Z_z}.$$

From Eqs. (4.4) the relation follows

$$(4.6) \qquad \frac{1}{Y_x} + \frac{1}{Y_y} + \frac{1}{Y_z} = \frac{1}{Z_x} + \frac{1}{Z_y} + \frac{1}{Z_z}.$$

Let R_{xy} be the yield limit under simple shearing by the shear stress τ_{xy} acting in positive direction, and let S_{xy} be the yield limit under shear stress τ_{xy} acting in negative direction. Similarly R_{yz}, S_{yz} and R_{zx}, S_{zx} stand for the respective yield limits under loading by shear stresses τ_{yz} and τ_{zx}, respectively. Then the anisotropy coefficients k_{44}, k_{55}, k_{66} and b_{44}, b_{55}, b_{66} can be related to these yield limits

$$(4.7) \qquad \begin{aligned} k_{44} &= \frac{1}{R_{yz}S_{yz}}, \quad b_{44} = \frac{1}{R_{yz}} - \frac{1}{S_{yz}}, \\ k_{55} &= \frac{1}{R_{zx}S_{zx}}, \quad b_{55} = \frac{1}{R_{zx}} - \frac{1}{S_{zx}}, \\ k_{66} &= \frac{1}{R_{xy}S_{xy}}, \quad b_{66} = \frac{1}{R_{xy}} - \frac{1}{S_{xy}}. \end{aligned}$$

4.2. Associated plastic strain increments

The anisotropy of plastic strain increments may be used, as it was mentioned above, for undirect measuring of the values of the anisotropy coefficients appearing in yield conditions. For materials with Bauschinger effect the expressions for plastic strain increments associated with yield condition (4.2) are — cf. expressions (2.7) — as follows:

$$(4.8) \qquad \begin{aligned} d\varepsilon_x &= d\lambda\{2[k_{12}(\sigma_x - \sigma_y) - k_{31}(\sigma_z - \sigma_x) - k_{16}\tau_{xy} \\ &\qquad + (k_{24} + k_{34})\tau_{yx} - k_{15}\tau_{zx}] - b_{12} + b_{31}\}, \\ d\varepsilon_y &= d\lambda\{2[-k_{12}(\sigma_x - \sigma_y) + k_{23}(\sigma_y - \sigma_z) - k_{26}\tau_{xy} \\ &\qquad - k_{24}\tau_{yz} + (k_{35} + k_{15})\tau_{zx}] + b_{12} - b_{23}\}, \\ d\varepsilon_z &= d\lambda\{2[-k_{23}(\sigma_y - \sigma_z) + k_{31}(\sigma_z - \sigma_x) \\ &\qquad + (k_{16} + k_{26})\tau_{xy} - k_{34}\tau_{yz} - k_{35}\tau_{zx}] + b_{23} - b_{31}\}. \end{aligned}$$

These expressions will be used in the analysis of stress states in sheet metals.

4.3. Particular cases of anisotropic yield conditions for materials displaying Bauschinger effect

The following particular form of the yield condition (4.2)

$$(4.9) \qquad \begin{aligned} &k_{12}(\sigma_x - \sigma_y)^2 + k_{23}(\sigma_y - \sigma_z)^2 + k_{31}(\sigma_z - \sigma_x)^2 + k_{44}\tau_{yz}^2 + k_{55}\tau_{zx}^2 + k_{66}\tau_{xy}^2 \\ &\qquad - b_{12}(\sigma_x - \sigma_y) - b_{23}(\sigma_y - \sigma_z) - b_{31}(\sigma_z - \sigma_x) \\ &\qquad + b_{44}\tau_{yz} + b_{55}\tau_{zx} + b_{66}\tau_{xy} = 1 \end{aligned}$$

is of practical significance. By substituting Eqs. (4.3), (4.5) and (4.7) we can obtain a more convenient, equivalent form of this condition which, for the sake of brevity, is not given here. Another equivalent forms may be obtained if relations (4.5′) or (4.5″) are used.

If directions of principal stresses σ_1, σ_2, σ_3 coincide with the axes of the reference system x, y, z, yield condition (4.9) can be written as

$$(4.10)\quad k_{12}(\sigma_1-\sigma_2)^2+k_{23}(\sigma_2-\sigma_3)^2+k_{31}(\sigma_3-\sigma_1)^2 - b_{12}(\sigma_1-\sigma_2)-b_{23}(\sigma_2-\sigma_3)-b_{31}(\sigma_3-\sigma_1)=1,$$

or in the equivalent form

$$(4.10')\quad \left(\frac{1}{Y_xZ_x}+\frac{1}{Y_yZ_y}-\frac{1}{Y_zZ_z}\right)(\sigma_1-\sigma_2)^2 + \left(-\frac{1}{Y_xZ_x}+\frac{1}{Y_yZ_y}+\frac{1}{Y_zZ_z}\right)(\sigma_2-\sigma_3)^2 + \left(\frac{1}{Y_xZ_x}-\frac{1}{Y_yZ_y}+\frac{1}{Y_zZ_z}\right)(\sigma_3-\sigma_1)^2 - 2\left(\frac{1}{Y_x}-\frac{1}{Z_x}\right)(\sigma_1-\sigma_2)-2\left(\frac{1}{Y_z}-\frac{1}{Z_z}\right)(\sigma_2-\sigma_3)=2.$$

This yield condition may be represented in the space of principal stresses as an infinitely long cylinder with elliptical cross-section. The axis of the cylinder is inclined at the same angle to each of the axes of principal stresses. However, now it does not pass through the origin of the reference system.

In the particular case when

$$(4.11)\quad \frac{1}{Y_xZ_x}=\frac{1}{Y_yZ_y}=\frac{1}{Y_zZ_z},$$

yield condition (4.10′) takes the following form:

$$(4.12)\quad (\sigma_1-\sigma_2)^2+(\sigma_2-\sigma_3)^2+(\sigma_3-\sigma_1)^2 - 2Y_xZ_x\left[\left(\frac{1}{Y_x}-\frac{1}{Z_x}\right)(\sigma_1-\sigma_2)+\left(\frac{1}{Y_z}-\frac{1}{Z_z}\right)(\sigma_2-\sigma_3)\right]=2Y_xZ_x.$$

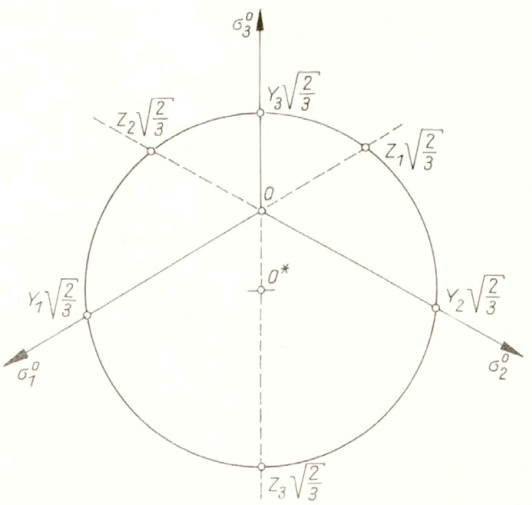

FIG. 7.

This particular form of the yield condition is represented in the space of principal stresses by the cylinder with circular cross-section. Such a cross-section is shown on the octahedral plane in Fig. 7.

4.4. Comparison of theoretical yield conditions with experimental data

Numerous experimental data show that plastic anisotropy induced in metals by previous complex plastic deformations is very complicated. Thus it is difficult to expect that it can be described by an universal theory. All the forms of yield conditions discussed above are based on certain simplifications and, therefore, they should be treated as approximate conditions only. Let us use the following examples to illustrate how far this approximation can be from the actual plastic properties of metals which underwent previous plastic deformation.

Let us analyse the experimental yield surface of prestressed material shown in Fig. 4a by dashed line. It has been determined in [13] by a simultaneous twisting and tension of thin-walled tubular specimen. The stress state reduces to two stress components σ_x and τ_{xy} if the x-axis is directed along the generatrix on tube's surface and the y-axis has circumferential direction.

For such a particular loading mode, the yield condition (4.9) reduces to the form

$$\frac{1}{Y_x^2}\sigma_x^2 + \frac{1}{R_{xy}S_{xy}}\tau_{xy}^2 + \left(\frac{1}{R_{xy}} - \frac{1}{S_{xy}}\right)\tau_{xy} = 1\,, \tag{4.13}$$

if the assumption that $Y_x = Z_x$, corresponding to the conditions of this experimental test, is introduced.

The experimental values Y_x, R_{xy}, S_{xy} can be estimated from the experimental curve as shown in Fig. 8. Thus the ellipse (4.13) is uniquely determined. A remarkable difference between this theoretical ellipse and the experimental curve is clearly seen. Similar differences can be observed when other experimental results concerning the effect of plastic deformation on the yield condition are compared with various anisotropic theoretical yield conditions.

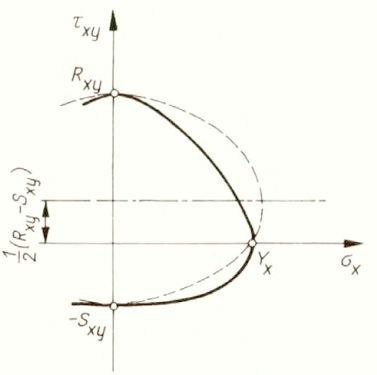

FIG. 8.

In numerous experimental investigations of the effect of plastic deformation on the yield condition, the yield limit is identified with the stresses at which the first deviation

from the proportionality between strains and stresses appears. Such an experimental procedure has been used in the mentioned paper [13] from which the experimental curve shown in Fig. 8 was taken. Another experimental procedure in which several conventional yield surfaces have been determined was used by JAGN and SHISHMARIEV [14] and by SZCZEPIŃSKI [16]. Usually such conventional yield loci are determined as the stress levels at which permanent deformations are reaching a certain prescribed conventional small magnitude. The shape and dimensions of a conventional yield surface strongly depend on that prescribed magnitude.

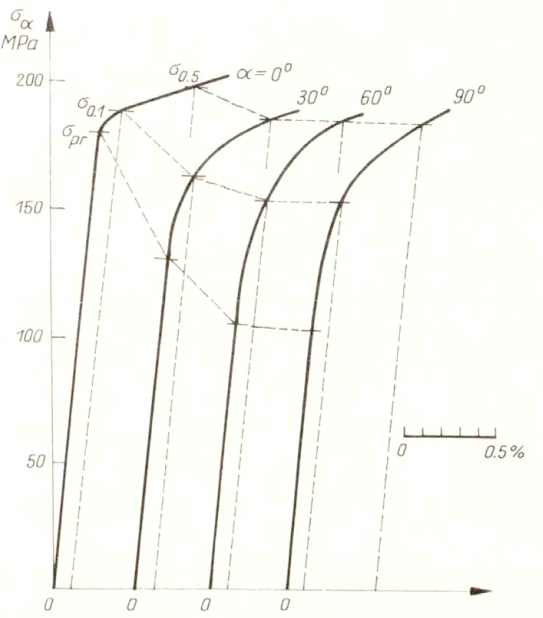

FIG. 9.

As an example, we shall discuss in brief the experimental results obtained in [16]. From a sheet of an Al-2%Mg aluminium alloy, prestressed by uniaxial tension in x-direction until 1.92 percent of permanent deformation was reached, small specimens were cut out in different directions making various angles α with the x-axis. Then all these small specimens were loaded by uniaxial tension. Initial portions of some stress-strain diagrams are shown in Fig. 9. It is also shown in the figure how the conventional yield loci were determined starting from the proportionality limit σ_{pr} to the conventional yield limit $\sigma_{0.5}$, when the permanent deformation is 0.5 percent. Having found such experimentally determined conventional yield limits σ_α for various angles α, we can calculate stress components σ_x, σ_y, τ_{xy} from the formulae

$$\sigma_x = \sigma_\alpha \cos^2 \alpha\,, \qquad \sigma_y = \sigma_\alpha \sin^2 \sigma\,, \qquad \tau_{xy} = \sigma_\alpha \sin \alpha \cos \alpha\,. \tag{4.14}$$

The limit stress states calculated in this manner can be represented in the space of stresses σ_x, σ_y, τ_{xy}. Then the corresponding curves passing through the respective points can be drawn (Fig. 10).

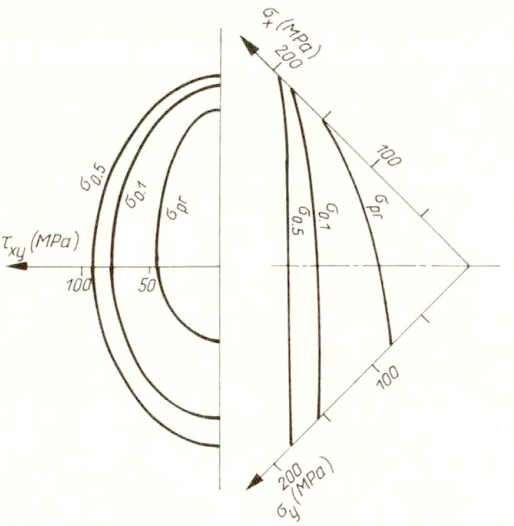

FIG. 10.

In the discussed example, when there exist three stress components only, yield condition (4.9) can be represented by a certain ellipsoid. However, the number of experimental data is not sufficient for determining all the parameters of such an ellipsoid. Nevertheless, the experimental curves shown in Fig. 10 clearly indicate that for each conventional yield limit the ellipsoid will have different dimensions and position. This simple example demonstrates how important is the proper choice of the convention concerning the definition of the yield limit, when the anisotropy coefficients are to be determined.

5. Plane stress states in anisotropic sheet metals

Plane stress state exists in a thin metal sheet when all external forces are acting in its median plane. If the coordinate axes are directed as shown in Fig. 11, we have

$$\sigma_z = \tau_{zx} = \tau_{zy} = 0 . \tag{5.1}$$

The distribution of stress components σ_x, σ_y, τ_{xy} is in general non-uniform across the thickness of the sheet, but their variations are usually insignificant. Hence they are assumed to be uniformly distributed.

Various yield conditions for anisotropic bodies discussed above reduce, for plane stress conditions, to particular forms, that are represented in the space of existing stress components σ_x, σ_y, τ_{xy} by a certain ellipsoid. Such a representation of the yield condition under plane stress states was (for isotropic bodies) used in [16]. For such bodies the yield condition concerning plane stress states takes the well-known form

$$\sigma_x^2 - \sigma_x\sigma_y + \sigma_y^2 + 3\tau_{xy}^2 = Y_0^2 . \tag{5.2}$$

This condition is represented in the stress space σ_x, σ_y, τ_{xy} by an ellipsoid (Fig. 12). One of the axes of the ellipsoid coincides with the τ_{xy}-axis, whereas the two others lie in the σ_x, σ_y-plane; they are bisectrices of the right angles between the coordinate axes. Various loading modes used in experimental investigations are represented by certain ellipses lying on the surface of the ellipsoid. For example, ellipse AB corresponds to a

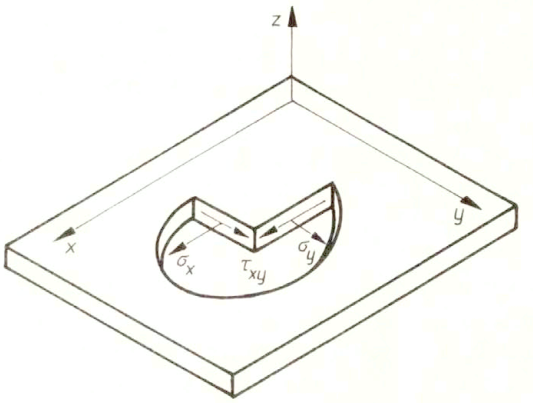

FIG. 11.

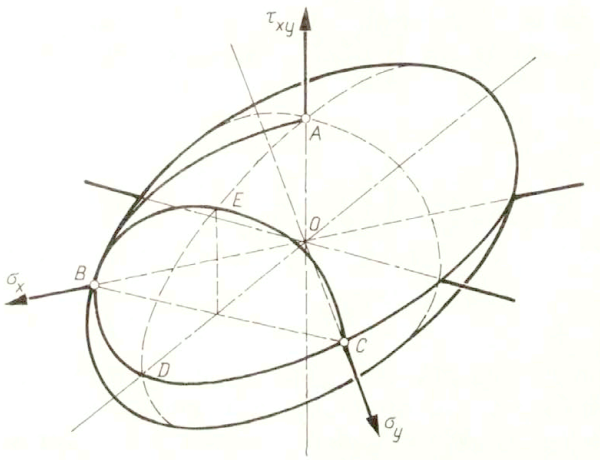

FIG. 12.

combined torsion and tension of tubular specimens. Such a loading mode was used in [13] and [15] — cf. Fig. 4. Ellipse BDC represents the states of biaxial tensile loadings.

Ellipse BEC formed by intersection of the ellipsoid with the plane $\sigma_x + \sigma_y = Y_0$ perpendicular to the σ_x, σ_y-plane, corresponds to the states of uniaxial tension in various directions with respect to the x-axis. For example, point E represents uniaxial tension in the direction making an angle of 45° with the x-axis.

We shall use such a geometrical representation of yield conditions for anisotropic materials under the conditions of plane stress states. Geometrical representation of this kind is useful when experiments for determining the anisotropy coefficients of sheet metals are programmed.

6. Yield conditions for sheet metals that do not display Bauschinger effect

We shall discuss now various cases of plastic anisotropy of sheet metals in which no Bauschinger effect is observed. When analysing such yield conditions, it is necessary to make certain assumptions concerning the uniformity of anisotropy in the direction

perpendicular to sheet's surface. The plastic deformation induced in the sheet during the rolling process is remarkably non-homogeneous across the thickness of the sheet. Such a non-homogeneity depends, among others, on the frictional conditions that exist at the interfaces between the rolls and the work-piece. Cold rolling is normally carried out with lubricated, polished rolls on material that possesses a fairly high yield stress in shear. Under these conditions, relative movement is assumed to occur between the rolls and the strip at the interfaces; this is termed the slipping friction — cf. CRANE and ALEXANDER [25].

In hot rolling, which is usually performed using rough unlubricated rolls on a very plastic hot material, the frictional drag is assumed to be large enough to attain the yield stress in shear of the rolled strip. It is then assumed that there is no relative motion at the interfaces, and the condition is termed the sticking friction.

Such a classification of frictional conditions during rolling has been repeated here after CRANE and ALEXANDER [25], who performed also the fundamental experiments concerning the distribution of deformations in rolled strips. Such experiments were performed also by MILSON and ALEXANDER [24]. Most important results of these works are discussed below.

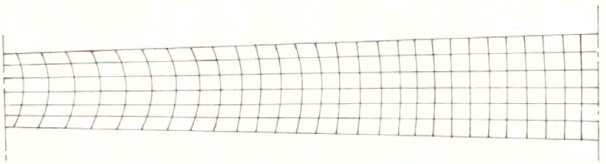

FIG. 13.

A typical distortion of an initially rectangular grid after part-rolling is shown in Fig. 13 — cf. [24]. The non-homogeneous distortion of the originally vertical lines can be clearly seen. When formulating the yield conditions for sheet metals with such induced non-homogeneous plastic strain distribution, their properties in the direction perpendicular to sheet's surface are usually averaged if the sheet is treated as a homogeneous body. Since the distortion in sheet metals is, in most cases, symmetrical with respect to the median plane, it is justified to assume that the direction normal to sheet's surface is the principal direction of anisotropy. However, not always such a symmetrical distribution of distortion occurs in rolled sheets.

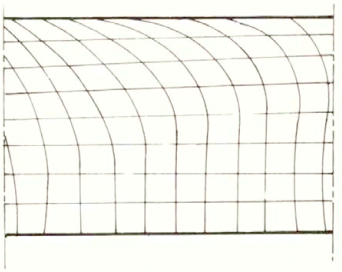

FIG. 14.

If friction at one roll surface is very different from that at the other, very asymmetric grids may be produced (Fig. 14 — cf. [25]). In such cases the averaged axis of anisotropy

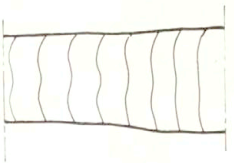

FIG. 15.

will not be normal to sheet's surface. Non-homogeneity of distortion through the thickness of the rolled strips may be connected also with multi-stage rolling. In Fig. 15 is presented the deformation of an initially rectangular grid after three stages of rolling. This figure was prepared on the basis of a photograph obtained by MCGREGOR and COFFIN [26] — cf. also [27].

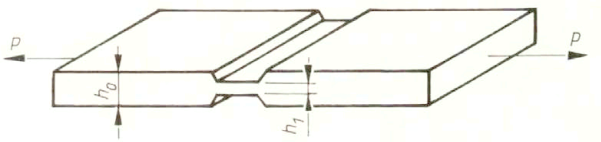

FIG. 16.

Experimental evidence of the non-uniform distribution of distortional deformation through the thickness of rolled sheets indicates that, when special test-pieces (such as that shown in Fig. 16) are prepared, we should be aware that layers of the material deformed differently from that in the vicinity of the median plane have been removed. Specimens of this kind are used for testing the sheet metals under plane strain conditions. However, the properties of the non-removed central part of sheet's material may be different from the overall properties of the whole sheet. Nevertheless, such specimens are used in experimental testing of sheet metals — cf. e.g. [42].

6.1. General form of yield condition for anisotropic sheet metals

For plane stress states the general anisotropic yield condition (2.3) may be written as

$$(6.1)\quad (k_{12}+k_{31})\sigma_x^2 - 2k_{12}\sigma_x\sigma_y + (k_{12}+k_{23})\sigma_y^2 + k_{66}\tau_{xy}^2 + 2k_{16}\sigma_x\tau_{xy} + 2k_{26}\sigma_y\tau_{xy} = 1.$$

By substituting Eqs. (2.5) and (2.6) we obtain an equivalent form of this condition, more convenient in practical interpretation of experimental results

$$(6.1')\quad \frac{1}{Y_x^2}\sigma_x^2 - \left(\frac{1}{Y_x^2}+\frac{1}{Y_y^2}-\frac{1}{Y_z^2}\right)\sigma_x\sigma_y + \frac{1}{Y_y^2}\sigma_y^2 + \frac{1}{Q^2}\tau_{xy}^2 + 2\tau_{xy}(k_{16}\sigma_x + k_{26}\sigma_y) = 1.$$

In the space of existing stress components $\sigma_x, \sigma_y, \tau_{xy}$, condition (6.1′) is represented by an ellipsoid with the central point at the origin of the coordinate system and with the symmetry axes inclined, in general, to all three coordinate axes. The dimensions and orientation of the ellipsoid are determined by the values of all six anisotropy coefficients (moduli) appearing in the condition (6.1). Experimental measurements of some of the

anisotropy coefficients is rather difficult and requires an advanced equipment. However, some of the coefficients can be measured in a relatively simple manner.

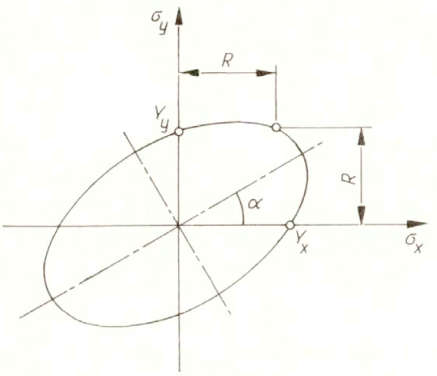

FIG. 17.

Consider at first the ellipse on the σ_x, σ_y-plane (Fig. 17) formed by intersection of the ellipsoid with the $\tau_{xy} = 0$ plane. Points on this ellipse represent various limit states of biaxial tension (compression) in the x and y directions. The equation of the ellipse can be written as

$$\frac{1}{Y_x^2}\sigma_x^2 - \left(\frac{1}{Y_x^2} + \frac{1}{Y_y^2} - \frac{1}{Y_z^2}\right)\sigma_x\sigma_y + \frac{1}{Y_y^2}\sigma_y^2 = 1\,. \tag{6.2}$$

Yield loci Y_x and Y_y can be easily measured by simple tension tests of specimens cut out in x and y directions, respectively. Certain problems arising during realization of such tests have been mentioned in Sec. 2.

The yield locus Y_z can be measured by a compression through-thickness test, with several test-pieces made to adhere to each other by using some adhesive — cf. e.g. [42, 43], or by a plane strain compression of a strip — cf. [43]. Another method of determining the value of Y_z is the equal-biaxial ($\sigma_x = \sigma_y$) test with the use of cruciform specimens. During such a test the yield stress $\sigma^p = R$ can be measured. By substituting $\sigma_x = \sigma_y = R$ to the yield condition (6.1′) we obtain

$$Y_z = R\,. \tag{6.3}$$

Tests in which the cruciform specimens are used are rather difficult to perform. A review of special testing devices was given by MIASTKOWSKI [28] and also in [29]. The main problem is to obtain the uniform stress and strain distribution in the central part of the specimen.

Still another method of measuring the yield stress Y_z is the realization of equi-biaxial tension by the hydraulic circular bulging test — cf. [33, 43], which may be applied with good approximation also for anisotropic sheet metals.

For cruciform specimens loaded by equi-biaxial tension ($\sigma_x = \sigma_y = \sigma$) general relations (2.7) for plastic strain increments reduce, after substituting Eq. (2.5), to the following simple relations:

$$
\begin{aligned}
d\varepsilon_x &= d\lambda\left(\frac{1}{Y_x^2} - \frac{1}{Y_y^2} + \frac{1}{Y_z^2}\right)\sigma\,,\\
d\varepsilon_y &= d\lambda\left(-\frac{1}{Y_x^2} + \frac{1}{Y_y^2} + \frac{1}{Y_z^2}\right)\sigma\,,\\
d\varepsilon_z &= 2d\lambda\frac{1}{Y_z^2}\sigma\,.
\end{aligned}
\tag{6.4}
$$

For example, by measuring experimentally the strain increment ratio $d\varepsilon_x/d\varepsilon_y$ we obtain a relation between the yield limit Y_z and the two remaining yield limits Y_x and Y_y, which have been previously measured during uniaxial tension tests. Such a undirect experimental procedure can provide complementary experimental information concerning anisotropic plastic properties of the sheet, and may also be used for cross-checking the values of Y_z measured by other experimental techniques.

The value of the directional yield limit Y_z measured non-directly with the use of formulae (6.4), or of the respective relations for uniaxial tension, say in x-direction

$$
\begin{aligned}
d\varepsilon_x &= 2d\lambda\frac{1}{Y_x^2}\sigma_x\,,\\
d\varepsilon_y &= -d\lambda\left(\frac{1}{Y_x^2} + \frac{1}{Y_y^2} - \frac{1}{Y_z^2}\right)\sigma_x\,,\\
d\varepsilon_z &= -d\lambda\left(\frac{1}{Y_x^2} - \frac{1}{Y_y^2} + \frac{1}{Y_z^2}\right)\sigma_x\,,
\end{aligned}
\tag{6.5}
$$

may be remarkably different from its value measured by other methods. Such a phenomenon is termed in some works (e.g. [31]) the "anomaly" of plastic behaviour of sheet metals. We shall discuss this problem later on.

The ingenious method of determining the anisotropy coefficients of sheet metals by measuring plastic strain increments during uniaxial tension tests was proposed in 1949 by KRUPKOWSKI and KAWIŃSKI [30]. Such a possibility has been mentioned also by HILL [7], who refers to the original work by Klinger and Sachs.

Experimental measurements of the remaining three anisotoropy coefficients (moduli) Q, k_{16}, k_{26}, appearing in yield condition (6.1′), would require special tests under shearing load and other tests with shearing accompanied by tension or compression. Such tests are rather difficult to perform.

6.2. Particular cases of anisotropy of non-orthotropic types

It is often observed in sheet metals that yield loci Y_x and Y_y are of the same magnitude, while yield loci measured during uniaxial tension tests on specimens cut out in directions making a certain angle with the rolling direction are different from Y_x. Such experimental observations are cited e.g. in HILL'S book [7]. This effect was also observed in numerous works, e.g. [16, 42]. This phenomenon is usually discussed in terms of the theory of plastic orthotropy. Below we shall analyse it in more general terms.

Consider a particular case of anisotropy when

$$Y_x = Y_y = Y_0 \quad \text{and} \quad k_{16} = k_{26} = k_0\,.$$

Then yield condition (6.1′) reduces to the particular form

$$\sigma_x^2 - \left[2 - \left(\frac{Y_0}{Y_z}\right)^2\right]\sigma_x\sigma_y + \sigma_y^2 + \left(\frac{Y_0}{Q}\right)^2\tau_{xy}^2 + 2k_0Y_0^2\tau_{xy}(\sigma_x + \sigma_y) = Y_0^2 . \tag{6.6}$$

In the space of stress components σ_x, σ_y, τ_{xy} yield condition (6.6) is represented by an ellipsoid shown in Fig. 18. The longer axis of the ellipsoid makes an angle β with the σ_x, σ_y-plane. The value of that angle is

$$\beta = \frac{1}{2}\operatorname{Arc\,cot}\left[\frac{1}{4k_0}\left(\frac{1}{Y_z^2} - \frac{1}{Q^2}\right)\right].$$

Projection of that axis on the σ_x, σ_y-plane coincides with the bisectrix of the right angle between the σ_x and σ_y-axes.

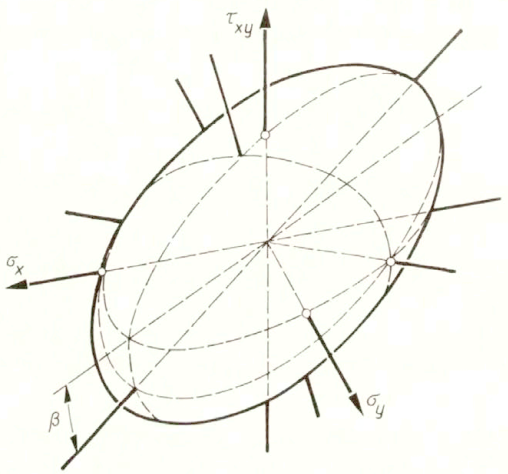

FIG. 18.

Tensile specimens cut out at the angles of $+45^\circ$ and -45° to the x-direction from a sheet obeying the yield condition (6.6) will have different yield stresses. For a specimen cut out at the angle of $+45^\circ$ we shall have $\sigma_x = \sigma_y = \tau_{xy} = \frac{1}{2}\sigma_0$, where σ_0 is the directional yield stress. From Eq. (6.6) we obtain

$$\sigma_0^+ = \frac{1}{\sqrt{\frac{1}{4}\left(\frac{1}{Y_z^2} + \frac{1}{Q^2}\right) + k_0}}. \tag{6.7}$$

For the specimen cut out at the angle of -45° we have $\sigma_x = \sigma_y = -\tau_{xy} = \frac{1}{2}\sigma_0$. Then we can write

$$\sigma_0^- = \frac{1}{\sqrt{\frac{1}{4}\left(\frac{1}{Y_z^2} + \frac{1}{Q^2}\right) - k_0}}. \tag{6.7′}$$

No experimental studies devoted to the investigation of this hypothetical effect are as yet known to the author. However, plastic deformations induced in sheet metals during

the manufacturing processes are so complex that the possibility of existence of such an effect should not be rejected without experimental confirmation. It is not excluded that a non-zero value of the coefficient k_0 may be observed in deep drawn non-circular cups, whose material was exposed to considerable shearing during the drawing operation.

6.3. Sheet metals with quasi-orthotropy

Consider the important case when $k_{16} = k_{26} = 0$. Then the yield condition (6.1′) reduces to the particular form

$$\frac{1}{Y_x^2}\sigma_x^2 - \left(\frac{1}{Y_x^2} + \frac{1}{Y_y^2} - \frac{1}{Y_z^2}\right)\sigma_x\sigma_y + \frac{1}{Y_y^2}\sigma_y^2 + \frac{1}{Q^2}\tau_{xy}^2 = 1 \tag{6.8}$$

identical with the yield condition (6.12) for sheet metals with true plastic orthotropy. Sheet metals may be considered as fully orthotropic provided certain additional conditions concerning plastic strain increments are satisfied. These additional conditions require that distortional plastic strain increments $d\varepsilon_{xz}$ and $d\varepsilon_{yz}$ should not appear when the sheet is loaded in its plane. Assuming the associated flow law (2.4) and plastic potential in the general form (2.3), these distortional strain increments are

$$\begin{aligned} d\varepsilon_{xz} &= 2d\lambda[-k_{15}\sigma_x + (k_{15} + k_{35})\sigma_y - k_{56}\tau_{xy}], \\ d\varepsilon_{yz} &= 2d\lambda[(k_{24} + k_{34})\sigma_x - k_{24}\sigma_y - k_{64}\tau_{xy}]. \end{aligned} \tag{6.9}$$

Thus a sheet metal is fully orthotropic if all six anisotropy coefficients in Eqs. (6.9) are equal to zero. It has been pointed out in Sec. 6 that, owing to complex deformation histories during the manufacturing processes, these coefficients do not always vanish. If some of them have non-zero values, the specimens cut out from the sheet may deform during the tension test in the manner similar to that shown in Fig. 19. Thus a through-thickness distortion may appear. Such a deformation of quasi-orthotropic sheets is rather difficult to measure and usually is neglected in laboratory tests. No experimental evidence of this effect is available as yet.

A particular type of quasi-orthotropy corresponds to the case when

$$Y_x = Y_y = Y_0 .$$

Then the yield condition (6.8) reduces to the well-known form

$$\sigma_x^2 - \left[2 - \left(\frac{Y_0}{Y_z}\right)^2\right]\sigma_x\sigma_y + \sigma_y^2 + \left(\frac{Y_0}{Q}\right)^2\tau_{xy}^2 = Y_0^2 , \tag{6.10}$$

identical with the yield condition (6.14) for exactly orthotropic sheet metals. However, now the sheet may suffer a through-thickness distortion even in the case when it is loaded by stresses acting in its plane.

Still another modification of yield condition (6.8) leads to the following condition:

$$\sigma_x^2 - \left[2 - \left(\frac{Y_0}{Y_z}\right)^2\right]\sigma_x\sigma_y + \sigma_y^2 + \left[4 - \left(\frac{Y_0}{Y_z}\right)^2\right]\tau_{xy}^2 = Y_0^2 , \tag{6.11}$$

which may be termed quasi-normal anisotropy. Tensile specimens cut out at arbitrary angles with respect to the x-axis will have the same yield stress equal to Y_0. Yield condition (6.11) has the same form as the yield condition (6.15) for sheet metals with normal anisotropy. However, those with quasi-normal anisotropy display through-thickness distortion when loaded in their plane.

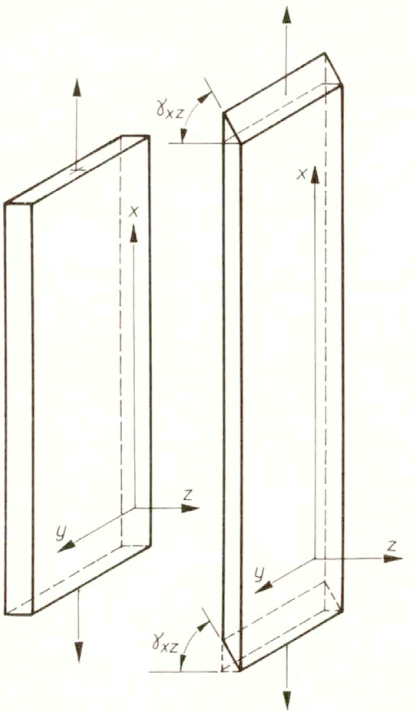

FIG. 19.

One can also distinguish quasi-isotropic sheet metals obeying yield condition (5.2), but displaying through-thickness distortion if even only one of anisotropy coefficients in expressions (6.9) has non-zero value.

6.4. Orthotropic sheet metals

Yield condition for orthotropic sheet metals is written in the following form:

$$\frac{1}{Y_x^2}\sigma_x^2 - \left(\frac{1}{Y_x^2} + \frac{1}{Y_y^2} - \frac{1}{Y_z^2}\right)\sigma_x\sigma_y + \frac{1}{Y_y^2}\sigma_y^2 + \frac{1}{Q^2}\tau_{xy}^2 = 1 \tag{6.12}$$

identical with the condition (6.8) for quasi-orthotropic sheets. However, now there is no possibility of through-thickness distortion during tension tests, because for orthotropic sheet metals all the anisotropy coefficients which are present in relations (6.9) must be equal to zero.

In the space of existing stress components σ_x, σ_y, τ_{xy} equation (6.12) is represented by an ellipsoid with the center at the origin of the reference system and with two symmetry axes lying in the σ_x, σ_y-plane (Fig. 20).

This type of anisotropy induced in a M-63 brass by previous plastic deformation has been observed, for example, by MIASTKOWSKI and SZCZEPIŃSKI [17]. In Fig. 21 are presented the yield curves for two definitions of yield stress, namely σ_{pr} and $\sigma_{0.01}$. For comparison, the initial isotropic yield curve σ_0 is also shown in the figure.

The shearing yield point of orthotropic sheet metals can be directly measured by using for example specimens of the type shown in Fig. 22. When such a specimen is loaded by

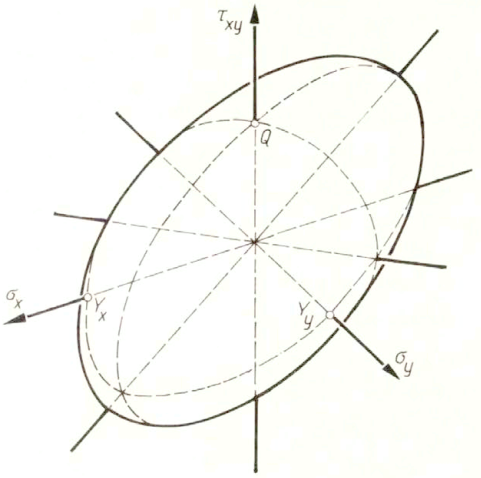

FIG. 20.

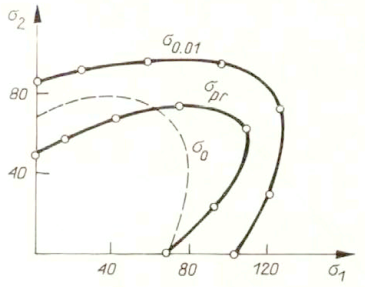

FIG. 21.

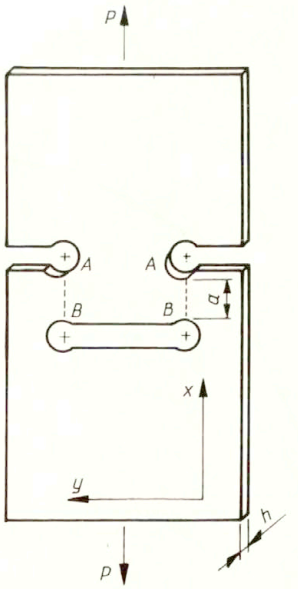

FIG. 22.

a tensile force, a state of deformation close to pure shearing develops in sections $A - B$. However, it should be noticed that interpretation of shear tests is always connected with certain difficulties. As an example, in Fig. 23 is shown the stress-elongation diagram for an ordinary tensile specimen cut out in the rolling direction from a sheet 2 mm thick of an Al-2%Mg aluminium alloy. The yield stress Y_x can easily be determined. The corresponding diagram (Fig. 24) for the specimen of the type shown in Fig. 22 cut out from the same sheet indicates that the yield stress under shear can be estimated only conventionally. These tests have been performed in [45], where also optimal shape of specimens for shearing tests has been analysed by means of methods similar to those used by ALBERTINI *et al.* [46].

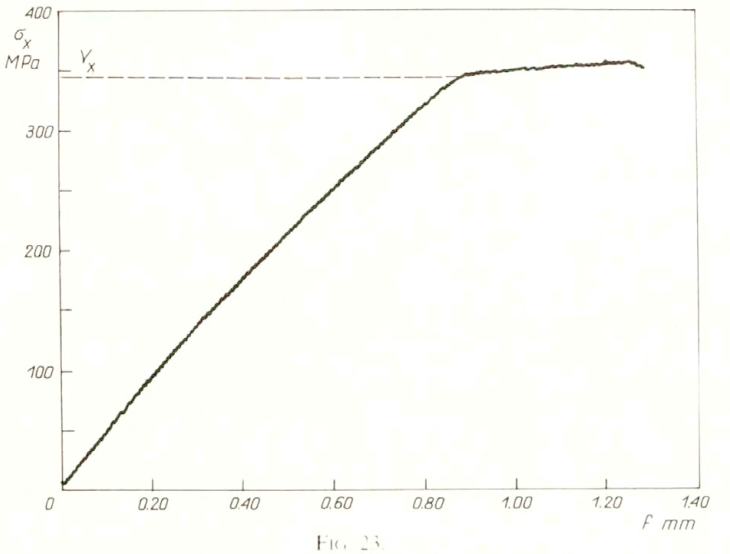

FIG. 23.

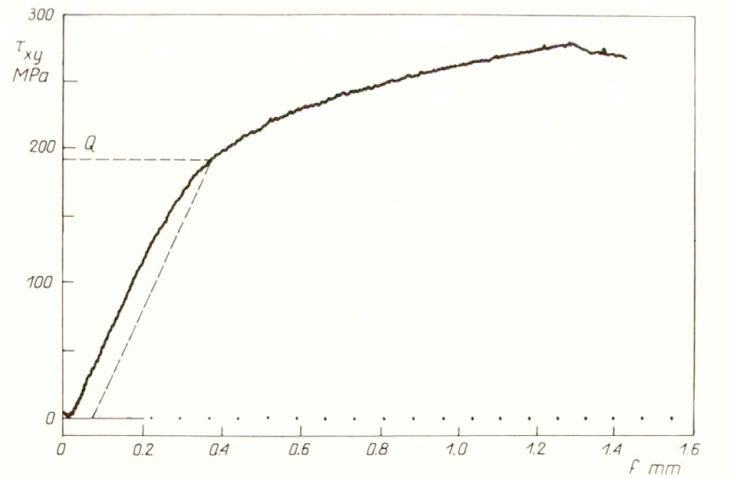

FIG. 24.

Let us notice that in both shearing zones of the specimen shown in Fig. 22 shear stresses τ_{xy} have opposite signs. It is of no practical significance in the case of the yield

condition (6.12) with quadratic terms only. Note that such specimens may also be used for sheets obeying yield consitions (6.1) or (6.6), because terms depending linearly on τ_{xy} vanish for shear test.

The value of the yield stress Q may easily be estimated in a simple indirect manner, namely by the tensile test on a specimen cut out from the sheet at the angle of 45° with respect to the x-direction. If the yield stress of such specimen equals σ_0, then Q can be calculated from the formula

$$Q = \frac{\sigma_y Y_z}{\sqrt{4Y_x^2 - \sigma_0^2}}. \tag{6.13}$$

Theoretically all four moduli of orthotropy in Eq. (6.12) could be experimentally determined by simple tension tests on specimens, each of them being cut out from the sheet at a different angle α with respect to the x-axis (cf. HILL [7]). For each specimen its yield stress should be experimentally determined. Then, by substituting relations (4.14) to (6.12), we obtain four equations with four unknowns Y_x, Y_y, Y_z, Q.

Using such indirect methods of measuring the moduli Y_z and Q, we should be aware that yield condition (6.12) describes only approximately the real deformation-induced anisotropy of sheet metals. Thus their values measured in this manner may remarkably differ from the exact values measured directly.

6.5. Particular cases of plastic orthotropy

Consider the important particular case when

$$Y_x = Y_y = Y_0.$$

Yield stresses of specimens cut out at certain angles with respect to the x-direction are assumed to be not equal to Y_0. Then the yield condition (6.12) takes the particular form

$$\sigma_x^2 - \left[2 - \left(\frac{Y_0}{Y_z}\right)^2\right]\sigma_x\sigma_y + \sigma_y^2 + \left(\frac{Y_0}{Q}\right)^2 \tau_{xy}^2 = Y_0^2 \tag{6.14}$$

identical with the yield condition (6.10) for quasi-orthotropic sheets. However, now, as in the case of the general orthotropy, all the anisotropy coefficients in Eq. (6.9) must be equal to zero.

Yield stresses Y_0 and Y_z may be estimated by tensioning uniaxially a specimen cut out from the sheet, for example in x-direction. The value of Y_0 results directly from the stress-strain diagram. The value of Y_z can be estimated non-directly by measuring plastic strain increments in the transversal direction $d\varepsilon_y$ and in the through-thickness direction $d\varepsilon_z$. Then Y_z can be calculated from the relation

$$\varkappa = \frac{d\varepsilon_y}{d\varepsilon_z} = 2\left(\frac{Y_z}{Y_0}\right)^2 - 1. \tag{6.15}$$

The yield shear stress Q may be estimated indirectly in the manner described in Sec. 6.4 by applying uniaxial tension to a specimen cut out at the angle of 45° with respect to the x-axis. Formula (6.13) holds valid also in the present case.

The value of Y_z estimated from the relation (6.15) may differ significantly from that measured directly, or by using other indirect methods. Such differences found by WOODTHROPE and PIERCE [33] for an aluminium sheet were termed the "anomaly" of

plastic properties. To eliminate this inconsistency, various non-quadratic yield criteria were proposed. They will be discussed in Sec. 6.7.

If in the yield criterion (6.14) we shall additionally assume that also $Y_z = Y_0$, then this criterion takes the simple form

$$\sigma_x^2 - \sigma_x\sigma_y + \sigma_y^2 + \left(\frac{Y_0}{Q}\right)^2 \tau_{xy}^2 = Y_0^2 \tag{6.16}$$

corresponding to the cubic orthotropy. This particular form of the yield condition may also be directly obtained from the general yield condition (3.11) for cubic orthotropy by substituting there $\sigma_z = \tau_{yz} = \tau_{zx} = 0$.

6.6. Normal anisotropy

Specimens cut out from sheet metals with normal anisotropy at any arbitrary angle have the same value of yield stress under uniaxial tension. The yield condition for sheets with such plastic properties has the following form

$$\sigma_x^2 - \left[2 - \left(\frac{Y_0}{Y_z}\right)^2\right]\sigma_x\sigma_y + \sigma_y^2 + \left[4 - \left(\frac{Y_0}{Y_z}\right)^2\right]\tau_{xy}^2 = Y_0^2, \tag{6.17}$$

identical with the yield condition (6.11) for sheet metals with the quasi-normal anisotropy. However, now the direction orthogonal to sheet's plane constitutes the principal direction of orthotropy. Yield condition (6.17) results also directly from the general yield condition (3.5′) for the so-called transversal isotropy by substituting there $\sigma_z = \tau_{yz} = \tau_{zx} = 0$.

In the space of stress components $\sigma_x, \sigma_y, \tau_{xy}$, the yield condition (6.17) is represented by an ellipsoid (Fig. 25). For $Y_z > Y_0$ the ellipsoid is more elongated in the 0-D direction than that for fully isotropic sheets (cf. Fig. 12), when $Y_z = Y_0$.

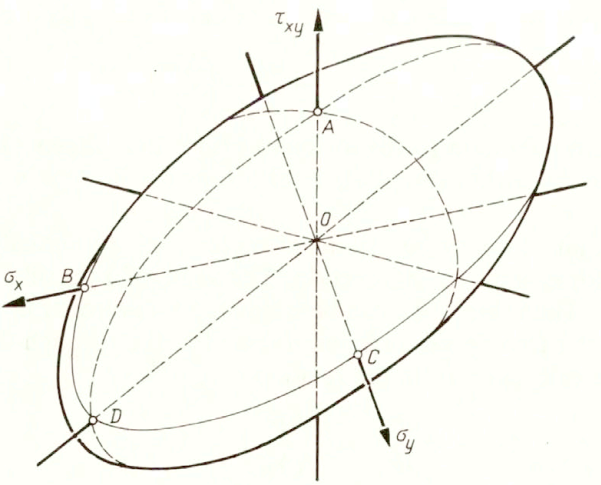

FIG. 25.

If the directions of principal stresses σ_1, σ_2 coincide with the reference axes x and y, the yield condition (6.17) is often written in the following form:

$$\sigma_y^2 - \frac{2r}{1+r}\sigma_y\sigma_2 + \sigma_2 = Y_0^2, \tag{6.18}$$

where

$$r = 2\left(\frac{Y_z}{Y_0}\right)^2 - 1 \tag{6.19}$$

is the so-called coefficient of normal anisotropy.

Comparison of Eq. (6.19) with Eq. (6.15) indicates that r can be measured as the ratio of strain increments $d\varepsilon_y/d\varepsilon_z$ in a specimen cut out from the sheet and loaded by uniaxial tension. As it was mentioned in Sec. 6.1, the idea of such measuring method was proposed by KRUPKOWSKI and KAWIŃSKI [30]. It was also proposed independently by LANKFORD *et al.* [35]. In the latter work, the following formula was recommended:

$$r = \frac{\ln(b/b_0)}{\ln(h/h_0)}, \tag{6.20}$$

where h_0 and b_0 are the initial thickness and width of the tensile specimen, respectively, and h and b are the corresponding dimensions after deformation. In [30] the coefficient of normal anisotropy was formulated as

$$K = \frac{(b_0/b)^2 - 1}{(h_0/h)^2 - 1}. \tag{6.21}$$

The main difficulty arising when such non-direct methods of measuring the anisotropy coefficients of sheet metals are used, consists in changing the anisotropy itself during the progressing deformation of the specimen tested. As an example let us analyse Fig. 10. An initially isotropic sheet metal pulled uniaxially in tension by stresses σ_x to produce a relatively small permanent deformation (about 2 percent) displays a significant anisotropy. There is a remarkable decrease of Y_y yield stress and an increase of Y_x with respect to the initial values before deformation.

Thus it can be expected that the value of the anisotropy coefficient r will be dependent on the amount of plastic deformation induced in the specimen cut out from the sheet in question. This has been experimentally demonstrated by TRUSZKOWSKI in several works, e.g. [36, 37]. To estimate the initial anisotropy of a tested sheet metal, TRUSZKOWSKI (cf. e.g. [38]) extrapolates the experimentally determined curve $r(\varepsilon)$ for the changing coefficient r to the starting point, where $\varepsilon = 0$.

For practical purposes the anisotropy coefficient r is sometimes used in the cases when the sheet material does not accurately obey the yield condition (6.18) for normal anisotropy. In some works (cf. e.g. [42, 43]) the average value of r is estimated for sheet materials for which rather the yield condition (6.12) for general orthotropy is more adequate.

6.7. Non-quadratic yield conditions for sheet metals

It was mentioned in Sec. 6.5 that experiments on certain sheet metals show that they do not obey the flow law associated with standard yield conditions. Such a phenomenon was termed the "anomaly" of plastic properties of the sheet. "Anomalies" of this kind observed in [33] and later in [42] are characterized by the inequalities

$$\varkappa = \frac{d\varepsilon_y}{d\varepsilon_z} < 1, \qquad \frac{Y_z}{Y_0} > 1.$$

Such relations are in contradiction with the relation (6.15) resulting from the flow law associated with yield conditions discussed above.

To overcome such contradictions sometimes observed HILL [31] proposed some new, the so-called non-quadratic yield conditions; in the cases when directions of principal stresses coincide with those of principal axes of orthotropy, the conditions were written as

$$(6.22)\quad F|\sigma_2-\sigma_3|^m + G|\sigma_3-\sigma_1|^m + H|\sigma_1-\sigma_2|^m + A|2\sigma_1-\sigma_2-\sigma_3|^m + B|2\sigma_2-\sigma_3-\sigma_1|^m + C|2\sigma_3-\sigma_1-\sigma_1|^m = \sigma^m,$$

where $m > 1$, and σ is a certain constant. Coefficients F, G, H are positive. Yield condition (6.22) contains seven material parameters, not counting the constant σ. For practical purposes one can assume, for a sheet metal in question, various particular forms of yield condition (6.22), by assuming that certain parameters vanish.

In [31] such particular cases were analysed for the case of transversal isotropy. E.g., by assuming, that

$$F = G = 0 \quad \text{and} \quad A = B = 0,$$

the following form of non-quadratic yield condition is obtained

$$(6.23)\qquad H|\sigma_1-\sigma_2|^m + C|2\sigma_3-\sigma_1-\sigma_2|^m = \sigma^m.$$

From the flow law associated with (6.23) we obtain for uniaxial tension by stresses σ_1 the following expression for the strain increments ratio

$$(6.24)\qquad \varkappa = \frac{d\varepsilon_2}{d\varepsilon_3} = \frac{H-C}{2C}.$$

Assuming that the direction of principal stress σ_3 coincides with the z-axis of the Cartesian coordinate system we denote, as previously, by Y_z the yield stress under uniaxial tension in z-direction, and by Y_0 — the yield stress for uniaxial tension in the x, y-plane. Then the following relations can be written:

$$(6.25)\qquad C = \left(\frac{\sigma}{2Y_z}\right)^m, \quad H = \left(\frac{\sigma}{Y_0}\right)^m - \left(\frac{\sigma}{2Y_z}\right)^m.$$

Now, instead of Eq. (6.24), we can write

$$(6.26)\qquad \varkappa = \frac{d\varepsilon_2}{d\varepsilon_3} = 2^{m-1}\left(\frac{Y_z}{Y_0}\right)^m - 1.$$

For $m = 2$ this formula takes the form (6.15).

For plane stress state, when $\sigma_3 = 0$, yield condition (6.23) reduces to the form

$$(6.27)\qquad |\sigma_1+\sigma_2|^m - \left[1-\left(\frac{2Y_z}{Y_0}\right)^m\right]|\sigma_1-\sigma_2|^m = 2Y_z^m.$$

For $m = 2$ this yield condition becomes identical with Eq. (6.17), if the latter were presented in principal stresses. Now we have an additional parameter m. If, for example, Y_z were experimentally determined, say by equi-biaxial tension test, then measuring the value of Y_0 by means of the uniaxial tension and also the strain increments ratio $\varkappa$ we could calculate from Eq. (6.26) the value of m. Thus for the non-quadratic yield condition (6.27) the problem of "anomaly" does not exist.

Since the yield condition (6.27) is formulated in principal stresses, it does not ensure the specimens cut out at various angles to have the same yield stress when they are

uniaxially pulled in tension. To secure this requirement of the transversal isotropy, a more general formulation would be necessary.

Nevertheless, the condition (6.27) has been applied in a number of investigations. The value of exponent m was estimated to vary between $m = 1.7$ and $m = 2$, depending on the material (cf. [39]). Condition (6.27) has also been used with certain modifications in some numerical solutions to various practical problems (cf. e.g. [39, 40, 42]).

A particular form of yield condition (6.22) when $A = B = C = 0$ was independently formulated by Hosford in 1979. In his next work [47] HOSFORD modified this yield condition by assuming that principal directions of stress and strain increment tensors coincide independently of whether they are parallel to the orthotropy axes or not. Bearing in mind that such an assumption may introduce certain errors, the author argues on the basis of experimental data that in real materials the mutual inclination of the two directions is rather small. Thus the errors connected with introduction of the hypothesis of transversal isotropy will be larger than those resulting from his assumption. The modified Hosford's yield criterion is

$$R_2|\sigma_1|^m + R_1|\sigma_2|^m + R_1R_2|\sigma_1 - \sigma_2|^m = R_2(R_1 + 1)Y_1^m , \tag{6.28}$$

where R_1 and R_2 are the ratios of strain increments, corresponding to $\varkappa$ determined by Eq. (6.15), but measured in the directions 1 and 2, respectively. Directional yield stress in the direction 1 is denoted by Y_1.

ZHOU WEIXIAN [48] formulated the following, more general form of the non-quadratic yield condition

$$f = F(\sigma_y^2 + 3\tau_{xy}^2)^{m/2} + G(\sigma_x^2 + 3\tau_{xy}^2)^{m/2} + H[(\sigma_x - \sigma_y)^2 + 4\tau_{xy}^2]^{m/2} + 2N(\tau_{xy}^2)^{m/2} - \frac{2}{3}(F + G + H)\sigma_i^m = 0 , \tag{6.29}$$

accounting for the influence of shear stress τ_{xy}. Here σ_i is the equivalent stress. The exponent m was estimated on the basis of experimental tests to be approximately equal to $m = 8$.

In connection with the problem of formation of the so-called "ears" in the sheet metals during the deep drawing operations, HILL [7] proposed still another form of the yield condition for plane stress states. It contains the polynomial of degree n

$$\sum A_{ijk}\sigma_x^i\sigma_y^j\tau_{xy}^k , \tag{6.30}$$

where the powers i, j, k are positive integers or zero ($i + j + k \leq n$). Note that for $n = 2$ one obtains the yield condition (6.1) resulting from the von Mises general yield function (2.1).

A particular form of this yield condition for $n = 4$ was analysed by GOTOH [43, 44]. It was found for some metals that yield curves on the σ_1, σ_2-plane differ only slightly from those resulting from the quadratic yield condition.

Owing to non-quadratic yield conditions it was possible to obtain a more accurate description of the plastic behaviour of sheet metals. However, even these conditions are not able to encompass fully all the "anomalies" (cf. also [48]) resulting from the very complex deformation pattern induced in sheet metals during the manufacturing operations.

7. Yield conditions for sheet metals with Bauschinger effect

Similarly as in the case of yield conditions discussed in Sec. 6 also now, when the Bauschinger effect is accounted for, the through-thickness averaging of plastic properties of the sheet is necessary. Experimental investigations indicate that in sheet metals delivered by the manufacturers the Bauschinger effect may be present in a clearly visible form. A distinct difference between the yield stress under tension and compression was observed for example by LITEWKA [23] in a sheet 1.5mm thick, made of an aluminium alloy PA2-M, and also in a sheet 5mm thick, made of another aluminium alloy PA4-T1. For the two materials the absolute value of the yield stress under compression was larger than that under tension in the plane of the sheet.

7.1. The case of general anisotropy

The general anisotropic yield condition (4.2) reduces for plane stress states to the following form

$$(7.1)\quad (k_{12}+k_{31})\sigma_x^2 - 2k_{12}\sigma_x\sigma_y + (k_{12}+k_{23})\sigma_y^2 + k_{66}\tau_{xy}^2 + 2k_{16}\sigma_x\tau_{xy} + 2k_{26}\sigma_y\tau_{xy} - b_{12}(\sigma_x-\sigma_y) - b_{23}\sigma_y + b_{66}\tau_{xy} = 1,$$

if relations (4.5) for the coefficients b_{ij} are assumed.

By substituting Eqs. (4.3) and (4.5), this yield condition may be written in the form more suitable for applications,

$$(7.1')\quad \frac{1}{Y_xZ_x}\sigma_x^2 - \left(\frac{1}{Y_xZ_x}+\frac{1}{Y_yZ_y}-\frac{1}{Y_zZ_z}\right)\sigma_x\sigma_y + \frac{1}{Y_yZ_y}\sigma_y^2 + k_{66}\tau_{xy}^2 - 2\tau_{xy}(k_{16}\sigma_x + k_{26}\sigma_y) + b_{66}\tau_{xy} + \left(\frac{1}{Y_x}-\frac{1}{Z_x}\right)\sigma_x + \left(\frac{1}{Y_y}-\frac{1}{Z_y}\right)\sigma_y = 1.$$

For $Y_i = Z_i (i = x, y, z)$ and, moreover, for $b_{66} = 0$ this yield condition reduces to the condition (6.1′) for sheet metals free of the Bauschinger effect.

In the σ_x, σ_y, τ_{xy}-space equation (7.1′) is represented by a certain ellipsoid with the central point shifted with respect to the origin of the reference system. The principal axes of the ellipsoid are, in a general case, inclined to the reference axes. In the yield condition (7.1′) the number of material moduli is ten, but relation (4.6) reduces that number to nine. To determine all the moduli experimentally it is necessary to make (among other tests) also the uniaxial compression tests on specimens cut out in the x and y directions. For such compression tests special devices are used — cf. e.g. DIETRICH and TURSKI [41].

The material constants (moduli) in (7.1′) can also be measured non-directly with the use of expressions for the associated plastic strain increments. For plane stress state we obtain from the general relations (4.8) the following formulae:

$$(7.2)\quad \begin{aligned} d\varepsilon_x &= d\lambda[2k_{12}(\sigma_x-\sigma_y) + 2k_{31}\sigma_x - 2k_{16}\tau_{xy} - b_{12} + b_{31}],\\ d\varepsilon_y &= d\lambda[2k_{12}(\sigma_y-\sigma_x) + 2k_{23}\sigma_y - 2k_{26}\tau_{xy} + b_{12} - b_{23}],\\ d\varepsilon_z &= d\lambda[-2k_{23}\sigma_y - 2k_{31}\sigma_x + 2(k_{16}+k_{26})\tau_{xy} + b_{23} - b_{31}]. \end{aligned}$$

For example for uniaxial tension in the x-direction we obtain, accounting for (4.3) and (4.5), the formulae for practical use

$$
\begin{aligned}
d\varepsilon_x &= d\lambda\left(\frac{2}{Y_x Z_x}\sigma_x + \frac{1}{Y_x} - \frac{1}{Z_x}\right), \\
d\varepsilon_y &= -d\lambda\left[\left(\frac{1}{Y_x Z_x} + \frac{1}{Y_y Z_y} - \frac{1}{Y_z Z_z}\right)\sigma_x - \frac{1}{Y_y} + \frac{1}{Z_y}\right], \\
d\varepsilon_z &= -d\lambda\left[\left(\frac{1}{Y_x Z_x} - \frac{1}{Y_y Z_y} + \frac{1}{Y_z Z_z}\right)\sigma_x - \frac{1}{Y_z} + \frac{1}{Z_z}\right].
\end{aligned} \tag{7.3}
$$

Similar relations can be written for uniaxial tension by stresses σ_y.

If the moduli Y_x, Z_x and Y_y, Z_y are measured directly by tension and compression tests, then the values of Y_z and Z_z can be evaluated by measuring the respective plastic strain increments. However, such non-direct measuring methods are of questionable accuracy.

7.2. Particular cases of anisotropy of sheet metals displaying Bauschinger effect

From among a large variety of possible particular yield conditions, which may be deduced from the general formulation (7.1′), we shall discuss only a few most important, for which there exists a certain experimental evidence. Unfortunately, experimental data concerning the Bauschinger effect in sheet metals are scarce. However, the few available data demonstrate that the yield conditions with terms linearly dependent on the stress components may be of practical significance.

Consider a particular form of the yield condition (7.1′) when

$$
Y_x = Y_y = Y_0, \quad Z_x = Z_y = Z_0, \quad k_{16} = k_{26} = 0.
$$

Under these assumptions the yield condition takes the following form

$$
\begin{aligned}
\sigma_x^2 - \left(2 - \frac{Y_0 Z_0}{Y_z Z_z}\right)\sigma_x\sigma_y + \sigma_y^2 + k_{66} Y_0 Z_0 \tau_{xy}^2 \\
+ b_{66} Y_0 Z_0 \tau_{xy} + (Z_0 - Y_0)(\sigma_x + \sigma_y) = Y_0 Z_0 .
\end{aligned} \tag{7.4}
$$

Let us denote the yield stress due to loading of a sheet by positively directed shear stress by Q^+, and by Q^- — the absolute value of the yield stress for the case when shear stresses are acting in the negative direction. Then we can write

$$
k_{66} = \frac{1}{Q^+ Q^-}, \qquad b_{66} = \frac{1}{Q^+} - \frac{1}{Q^-}. \tag{7.5}
$$

In the space of stress components σ_x, σ_y, τ_{xy} the yield condition (7.4) is represented by an ellipsoid shown in Fig. 26. Its central point 0* is shifted with respect to the origin 0 of the reference system.

The experimental confirmation of such a type of anisotropy in sheet metals is as yet lacking. However, anisotropy of this kind may be induced in sheet metals during deep drawing operations, when a flat blank, before entering the drawing ring of the die, may suffer considerable distortion. Thus in the drawn object the anisotropy of such a type may be present.

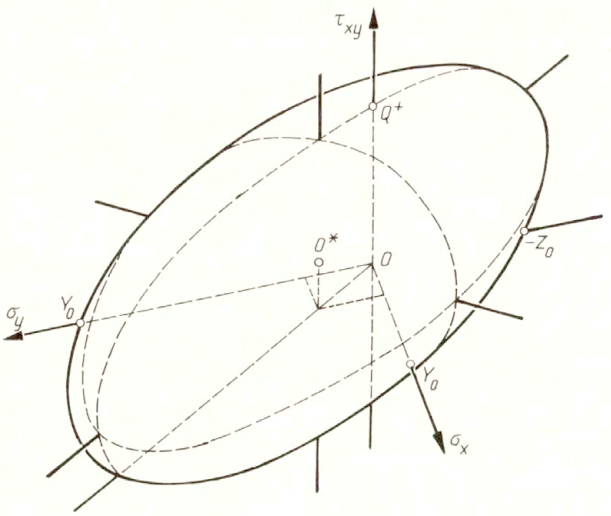

FIG. 26.

For most sheet metals it may be expected that $b_{66} = 0$. This leads to a still simpler particular form of the yield condition (7.4)

$$\sigma_x^2 - \left(2 - \frac{Y_0 Z_0}{Y_z Z_z}\right)\sigma_x\sigma_y + \sigma_y^2 + \frac{Y_0 Z_0}{Q^2}\tau_{xy}^2 + (Z_0 - Y_0)(\sigma_x + \sigma_y) = Y_0 Z_0 . \tag{7.6}$$

Now the central point of the ellipsoid is shifted in the σ_x, σ_y-plane along the bisectrix of the right angle between the axes σ_x and σ_y.

If we shall assume the yield condition in the form

$$\sigma_x^2 - \left(2 - \frac{Y_0 Z_0}{Y_z Z_z}\right)\sigma_x\sigma_y + \sigma_y^2 + \left(4 - \frac{Y_0 Z_0}{Y_z Z_z}\right)\tau_{xy}^2 + (Z_0 - Y_0)(\sigma_x + \sigma_y) = Y_0 Z_0, \tag{7.7}$$

then the yield stresses under uniaxial tension of specimens cut out from the sheet at an arbitrary angle will be of the same magnitude Y_0. The same concerns uniaxial compression, when all specimens will have the yield stress equal to Z_0.

Yield condition (7.7) corresponds to the plastic properties of sheets of an aluminium alloy PA2 and also PA4 observed by LITEWKA [22]. Yield stresses of specimens cut out in different directions under uniaxial loadings were of the same magnitude. However, Litewka noticed also another "anomaly" in these materials, because the parameter $\varkappa$ [cf. (6.15)] was different for specimens cut out in various directions. This is in contradiction with the flow law associated with the yield condition (7.7).

All the "anomalies" mentioned in this paper indicate that indirect methods of measuring the anisotropy coefficients should be used cautiously and with a certain criticism.

Acknowledgement

The author gratefully acknowledges support of the Polish Committee of Scientific Research under grant No. 3 0154 91 01.

References

1. Z. MARCINIAK, *Limit strains in the processes of sheet metals forming* [in Polish], WNT, Warszawa 1971.
2. R.V. MISES, *Mechanik der plastischen Formänderung von Kristallen*, Zeitsch. Angew. Math. Mech., **8**, 3, 161–185, 1928.
3. W. OLSZAK, W. URBANOWSKI, *The orthotropy and the non-homogeneity in the theory of plasticity* [in Polish], Arch. Mech. Stos., **8**, 1, 85–110, 1956.
4. W. OLSZAK, W. URBANOWSKI, *The plastic potential and the generalized distortion energy in the theory of non-homogeneous anisotropic elastic-plastic body*, Arch. Mech. Stos., **8**, 4, 671–694, 1956.
5. W. OLSZAK, W. URBANOWSKI, *The flow function and the yield condition for non-homogeneous orthotropic bodies*, Bull. Acad. Polon. Sci., **5**, 4, 191–203, 1957.
6. J.P. BOEHLER, L. EL AOUFI and J. RACLIN, *On experimental testing methods for anisotropic materials*, Res Mechanica, **21**, 73–95, 1987.
7. R. HILL, *The mathematical theory of plasticity*, Oxford at the Clarendon Press, 1956.
8. J.P. BOEHLER, A. SAWCZUK, *Equilibre limite des sol anisotropes*, J. de Mecanique, **9**, 1, 5–33, 1970.
9. J.P. BOEHLER and A. SAWCZUK, *On yielding of oriented solids*, Acta Mechanica, **27**, 185–206, 1977.
10. D. ALLIROT, J.P. BOEHLER and A. SAWCZUK, *Yielding and failure of transversely isotropic solids. Part I. Experiment*, Res Mechanica, **4**, 97–113, 1982.
11. J. BAUSCHINGER, *Über die Quercontraction und Dilatation bei der Längenausdehnung und Zusammendrücken prismatischer Körper*, Zivilingenieur, Leipzig, **25**, 81–124, 1879.
12. J.F. BELL, *The experimental foundations of solid mechanics*, Handbuch der Physik, Band VIa/1, Springer Verlag, 1973.
13. P.M. NAGHDI, F. ESSENBURG, W. KOFF, *An experimental study of initial and subsequent yield surfaces in plasticity*, J. Appl. Mech., **25**, 201–209, 1958.
14. J.I. JAGN, O.A. SHISHMARIEV, *On certain results of the investigation of elastic state limits of plastically deformed nickel specimens* [in Russian], Dokl. Akad. Nauk USSR, **119**, 46–48, 1958.
15. H.J. IVEY, *Plastic stress-strain relations and yield surfaces for aluminium alloys*, J. Mech. Engng. Sci., **3**, 15–31, 1961.
16. W. SZCZEPIŃSKI, *On the effect of plastic deformation on yield condition*, Arch. Mech. Stos., **15**, 275–296, 1963.
17. J. MIASTKOWSKI, W. SZCZEPIŃSKI, *An experimental study of yield surfaces of prestrained brass*, Int. J. Solids and Structures, **1**, 189–194, 1965.
18. K. IKEGAMI, *An historical perspective of the experimental study of subsequent yield surfaces for metals* [in Japanese], Japan Soc. Mat. Sci., **24**, Part 1, 491–505, Part 2, 709–719, 1975, English translation BISI 14420, Sept. 1976.
19. K. IKEGAMI, *Experimental plasticity on the anisotropy of metals*, Coll. Intern. CNRS, No. 295, 201–242, 1982.
20. G.J. DEAK, *A study on the causes of the Bauschinger effect*, Ph. D. Thesis, Massachusetts Institute of Technology, 1962.
21. T. OTA, A. SHINDO, H. FUKUOKA, *A consideration on anisotropic yield criterion*, Proc. 9th Jap. Nat. Congr. Appl. Mech., 117–120, 1959.
22. A. LITEWKA, *Non-associated flow law for plastically anisotropic aluminium alloys* [in Polish], Mech. Teor. Stos., **15**, 491–499, 1977.
23. A. LITEWKA, *Plastic flow of anisotropic aluminium alloy sheet metals*, Bull. Acad. Polon. Sci., **25**, 475–484, 1977.
24. B.E. MILSOM and J.M. ALEXANDER, *An experimental determination of the detailed distortion in hot rolling*, J. Mech. Phys. Solids, **9**, 105–113, 1961.
25. F.A.A. CRANE and J.M. ALEXANDER, *Friction in hot rolling*, J. Inst. of Metals, **91**, 188–189, 1962–63.
26. C.W. GREGOR, L.F. COFFIN, *The distribution of strains in the rolling process*, J. Appl. Mech., **10**, 1943.
27. O. PIISPANEN, R. PIISPANEN, *Die plastischen Vorgänge beim Walzen*, Bänder, Bleche, Röhre, **7**, 7, 189–193, 1966.
28. J. MIASTKOWSKI, *Experimental methods of static investigations of plastic flow of metals* [in Polish], Mech. Teor. Stos., **13**, 225–252, 1975.
29. W. SZCZEPIŃSKI, L. DIETRICH, J. MIASTKOWSKI, *Plastic properties of metals, Part I.* [in:] Experimental Methods in Mechanics of Solids, W. SZCZEPIŃSKI [Ed.], Elsevier, PWN, 1990.

30. A. KRUPKOWSKI and S. KAWIŃSKI, *The phenomenon of anisotropy in annealed polycrystalline metals*, J. Inst. of Metals, **75**, Part II, 869–880, 1949.
31. R. HILL, *Theoretical plasticity of textured aggregates*, Math. Proc. Cambridge Phil. Soc., **85**, 179–191, 1979.
32. K. MIYAUCHI, *On a simple shear deformation*, English text reprinted from Scientific Papers of the Institute of Physical and Chemical Research Rikagaku Kenkyusho, Wako-shi, Saitama, Japan, **81**, 57–67, 1987.
33. J. WOODTHROPE and R. PEARCE, *The anomalous behaviour of aluminium sheet under balanced biaxial tension*, Intern. J. Mech. Sci., **12**, 341–347, 1970.
34. Z. MARCINIAK, *Influence of the sign change of the load on the strain hardening curve of a copper test piece subject to torsion*, Arch. Mech. Stos., **6**, 743–752, 1961.
35. W.T. LANKFORD, S.G. SNYDER, J.A. BAUSCHER, *New criteria for predicting the press performance of deep drawing sheets*, Trans. ASM, **42**, 1950.
36. W. TRUSZKOWSKI, J. KŁOCH, *Application of the maximal error method for the calculation of the $r(\varepsilon)$ function*, Bull. Acad. Polon. Sci., **34**, 11–12, 691–701, 1986.
37. W. TRUSZKOWSKI, *Sur le sens physique du rapport des allongements obtenu par la methode d'extrapolation*, Memoria presentata al XIII Convegno Nazionale AIM — Milano, 1968, 17–20.
38. W. TRUSZKOWSKI, *Stress-strain relation for polycrystalline non-homogeneous anisotropic metals* [in Polish], Arch. Hutn., **28**, 4, 429–440, 1983.
39. A. PAMAR and P.B. MELLOR, *Plastic expansion of a circular hole in sheet metal subjected to biaxial tensile stress*, Intern. J. Mech. Sci., **20**, 707–720, 1978.
40. M.J. SARAN, D.J. ZHOU and R.H. WAGONER, *Numerical simulation of arbitrary sheet stampings using CFS formulation with anisotropic material models*, Proc. Third Intern. Conf. on Computational Plasticity, Barcelona 1992, Pineridge Press, 1992, 1213–1225.
41. L. DIETRICH, K. TURSKI, *A new method of compression tests of sheet metals* [in Polish], Rozpr. Inż., **26**, 1, 91–99, 1978.
42. F. MONTHEILLET, J.J. JONAS and M. BENFERRAH, *Development of anisotropy during the cold rolling of aluminium sheet*, Intern. J. Mech. Sci., **33**, 197–209, 1991.
43. M. GOTOH, *A theory of plastic anisotropy based on a yield function of fourth order (plane stress state) — I*, Intern. J. Mech. Sci., **19**, 505–512, 1977.
44. M. GOTOH, *A theory of plastic anisotropy based on a yield function of fourth order (plane stress state) — II*, Intern. J. Mech. Sci., **19**, 513–520, 1977.
45. G. SOCHA, W. SZCZEPIŃSKI, *Optimal design of a specimen for pure shear tests of sheet metals*, (in preparation).
46. C. ALBERTINI, M. MONTAGNANI, M. ZYCZKOWSKI and S. ŁACZEK, *Optimal design of a specimen for pure double shear tests*, Intern. J. Mech. Sci., **32**, 729–741, 1990.
47. W.F. HOSFORD, *Comments on anisotropic yield criteria*, Intern. J. Mech. Sci., **27**, 423–427, 1985.
48. ZHOU WEIXIAN, *A new non-quadratic orthotropic yield criterion*, Intern. J. Mech. Sci., **32**, 513–520, 1990.

POLISH ACADEMY OF SCIENCES
INSTITUTE OF FUNDAMENTAL TECHNOLOGICAL RESEARCH

Received November 2, 1992.

Arch. Mech., 45, 1, pp. 39–50, Warszawa 1993

Surface waves on thermoelastic half-spaces

M. ROMEO (GENOVA)

SURFACE PLANE waves are investigated at the boundary of a transversely isotropic thermoelastic solid half-space. Inhomogeneous wave modes are obtained by imposing a boundary radiation condition, and their dependence on the propagation direction with respect to the privileged axis of the solid is discussed. Particular homogeneous modes arise for special orientation of the surface, which do not carry temperature perturbations and are undamped.

1. Introduction

PROPAGATION of surface waves in thermoelastic solids has been recently investigated with particular attention to the attenuation of Rayleigh waves in both isotropic and anisotropic materials [1, 2, 3]. Theoretical results have been compared with available data concerning particular anisotropic solids [4] showing that only a small fraction of the observed attenuation is due to thermoelastic effects. Experimental results have also shown that wave speed, attenuation and power flux significantly depend on the particular orientation of the surface with respect to the privileged direction of the solid (see [4] and references therein). Special orientations exist which allow for high efficiency in surface wave production, and where the direction of the power flux slightly differs from that of the phase velocity. To our knowledge, the latter effects have not yet received any clear and full explanation.

A more general analysis of the admissible wave modes occurring on the boundary of a solid half-space can be performed by considering inhomogeneous waves, where planes of constant phase are not necessarily parallel to the planes of constant amplitude. Inhomogeneous waves are the natural modes in dissipative solids [5, 6] and are likely to improve the description of wave propagation in anisotropic solids [7].

In this paper we investigate the occurrence of inhomogeneous surface waves on the boundary of a thermoelastic solid half-space, focusing our attention on the influence of the material anisotropy on wave speed and attenuation. A transversely isotropic thermoelastic half-space is considered (Sec. 2) where boundary conditions are imposed for an Y-cut half-space or an arbitrary rotated-cut half-space; a linear radiation condition for the temperature is introduced in both cases. Inhomogeneous surface waves are introduced in Sec. 3 imposing some essential physical constraints, and the compatibility condition for the linear system of balance equations is derived. It is shown that three surface modes exist which satisfy the radiation boundary condition for both Y-cut and rotated-cut half-spaces. The high frequency limit is discussed in Sec. 4 using a generalized theory of heat conduction which allows for thermal waves. In Sec. 5 we show that additional surface modes may exist on Y-cut or on rotated-cut half-spaces, which carry no temperature perturbation. These modes occur for particular orientations on the Y-cut half-space or for special rotated-cut half-spaces. They are homogeneous and undamped and their speeds do not depend on frequency or on the value of the unperturbed temperature. We believe that these modes play an esential role in the high surface wave coupling, experimentally observed on particular rotated-cut specimens of anisotropic solids.

2. Basic equations

Let Σ be a half-space bounded by a plane surface S, and occupied by an elastic solid which allows for heat conduction. Assuming that the solid possesses a transversely isotropic symmetry we introduce Cartesian coordinates x_1, x_2, x_3 with x_3 directed along the privileged axis. According to linear thermoelasticity, the displacement $\mathbf{u}(\mathbf{x}, t)$ and the temperature deviation $\theta(\mathbf{x}, t)$ from the unperturbed absolute temperature θ_0 satisfy the balance equations [8, 9]

$$\rho\ddot{\mathbf{u}} = \mathbf{C}\nabla\mathbf{e} - \mathbf{H}\nabla\theta\,, \tag{2.1}$$

$$\rho C\dot{\theta} = \mathbf{K}[\nabla \otimes \nabla\theta] - \theta_0\mathbf{H}\nabla\dot{\mathbf{u}}\,. \tag{2.2}$$

As usual, ρ is the mass density, C the specific heat at constant strain and $\mathbf{e} = \operatorname{sym}(\nabla\mathbf{u})$ is the infinitesimal strain tensor. If a generalized theory of heat conduction is taken into account, the right-hand side of Eq. (2.2) and the last term in the right-hand side of Eq. (2.1) are viewed as integrals over the history of $\nabla\theta, \nabla \otimes \nabla\theta$ and $\nabla\dot{\mathbf{u}}$ [11], and consequently, for harmonic-type fields, the thermoelastic tensor $\mathbf{H}$ and the thermal conductivity tensor $\mathbf{K}$ turn out to be frequency dependent [7]. Disregarding viscosity, the isothermal elastic tensor $\mathbf{C}$ is assumed to have constant entries. These may be represented using Voigt's notation so that the non-vanishing parameters for the problem at hand are

$$\begin{aligned} &c_{11} = c_{22} := 2\mu + \lambda, \quad c_{12} := \lambda, \quad c_{13} = c_{23} := \eta - \delta\,, \\ &c_{33} := \gamma, \quad c_{44} = c_{55} := \delta, \quad c_{66} = \frac{1}{2}(c_{11} - c_{12}) = \mu\,, \\ &H_{11} = H_{22} := h, \quad H_{33} := \bar{h}, \quad K_{11} = K_{22} := \kappa, \quad K_{33} := \bar{\kappa}\,. \end{aligned} \tag{2.3}$$

Thermodynamic restrictions on the constitutive parameters imply the following inequalities (cf. [10]):

$$h, \bar{h}, \kappa, \bar{\kappa} > 0, \quad 2\mu + \lambda > 0, \quad \mu > 0,\ \delta > 0, \quad (\mu + \lambda)\gamma > (\eta - \delta)^2\,. \tag{2.4}$$

For transversely isotropic symmetries it is convenient to introduce the potentials $\chi, \overline{\psi}, \psi$ such that [10]

$$\begin{aligned} &u_\alpha = \chi_{,\alpha} + e_{\alpha\beta}\overline{\psi}_{,\beta}, \quad (\alpha, \beta = 1, 2)\,, \\ &u_3 = \psi_{,3}\,, \end{aligned} \tag{2.5}$$

where the comma denotes partial differentiation and $e_{\alpha\beta}$ is the two-dimensional alternate symbol. By means of Eqs. (2.3) and (2.5) Eqs. (2.1) and (2.2) may be written as

$$\rho\ddot{\overline{\psi}} = \mu\overline{\psi}_{,\alpha\alpha} + \delta\overline{\psi}_{,33}\,, \tag{2.6}$$

$$\rho\ddot{\chi} = (2\mu + \lambda)\chi_{,\alpha\alpha} + \delta\chi_{,33} + \eta\psi_{,33} - h\theta\,, \tag{2.7}$$

$$\rho\ddot{\psi} = \eta\chi_{,\alpha\alpha} + \gamma\psi_{,33} - \bar{h}\theta\,, \tag{2.8}$$

$$\rho C\dot{\theta} = \kappa\theta_{,\alpha\alpha} + \bar{\kappa}\theta_{,33} - \theta_0 h\dot{\chi}_{,\alpha\alpha} - \theta_0\bar{h}\dot{\psi}_{,33}\,. \tag{2.9}$$

At the boundary S of Σ we impose the usual conditions on the traction and the heat flux. Denoting by $\mathbf{n}$ the unit normal of S directed toward the solid, we have

$$(\mathbf{Ce} - \mathbf{H}\theta)\mathbf{n} = 0\,, \tag{2.10}$$

$$(\mathbf{K}\nabla\theta)\cdot\mathbf{n} = r\theta\,, \tag{2.11}$$

on S. Equation (2.11) is a linearized radiation condition where r represents a suitable heat-radiation coefficient (see also [1]). In particular, if we regard S as a black body radiating surface, we may write

$$r = 4s\theta_0^3, \tag{2.12}$$

where s is a constant which, for an ideal black body, turns out to be the Stefan–Boltzmann constant. We note that the particular case of a thermally insulated surface is obtained from Eq. (2.11) by setting $r = 0$. In the opposite situation of isothermal surfaces, Eq. (2.11) should be replaced by the condition $\theta = 0$ on S. Although we are not interested in this case here, we observe that thermoelastic surface waves are recovered on isothermal surfaces under the hypothesis of θ being discontinuous at S.

In the following we analyze separately wave propagation on surfaces parallel to the privileged axis (Y-cut half-spaces) and along the x_2-axis of surfaces arbitrarily rotated with respect to the privileged axis (rotated-cut half spaces). In both cases we assume that the real and imaginary parts of the wave vector (see Sec. 3) lie on a plane $\mathcal{P}$ perpendicular to S and parallel to the propagation direction and denote by φ the angle between $\mathcal{P}$ and the privileged direction. Having introduced the unit vectors $\mathbf{e}_1$, $\mathbf{e}_2$, $\mathbf{e}_3$, along x_1, x_2, x_3, in

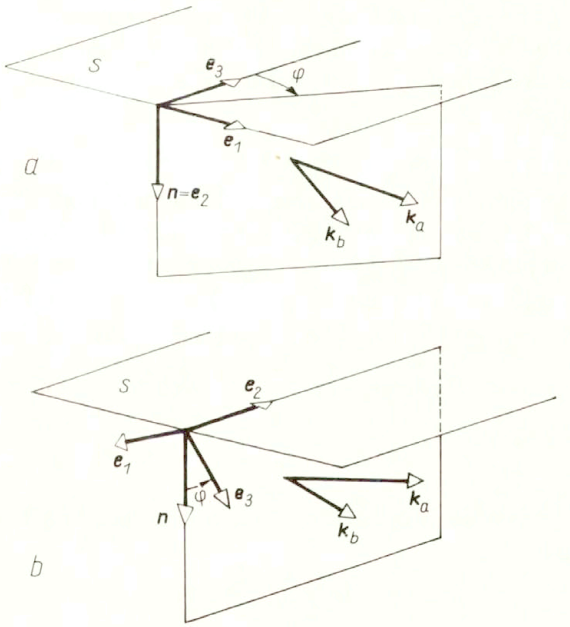

FIG. 1.

the Y-cut case, without loss of generality we can choose $\mathbf{n} = \mathbf{e}_2$ (see Fig. 1a). Equations (2.10) and (2.11) then become

$$2\chi_{,12} + \overline{\psi}_{,22} - \psi_{,11} = 0, \tag{2.13}$$

$$(2\mu + \lambda)\chi_{,22} + \lambda\chi_{,11} - 2\mu\overline{\psi}_{,12} + (\eta - \delta)\psi_{,33} - h\theta = 0, \tag{2.14}$$

$$\chi_{,23} - \overline{\psi}_{,13} + \psi_{,32} = 0, \tag{2.15}$$

$$\kappa\theta_{,2} = r\theta, \tag{2.16}$$

on $x_2 = 0$. In the rotated-cut case, we have $\mathbf{n} = (q\mathbf{e}_1 + \mathbf{e}_3/\sqrt{1 + q^2})$ where $q = \tan\varphi$

(see Fig. 1b). Equations (2.10) and (2.11) become

$$(2.17)\quad [(2\mu+\lambda)\chi_{,11}+\lambda\chi_{,22}]q+\delta\chi_{,13}+2\mu q\overline{\psi}_{,12}+\delta\overline{\psi}_{,23}+(\eta-\delta)q\psi_{,31}-h\theta q=0\,,$$

$$(2.18)\quad [2\mu\chi_{,12}+\mu(\overline{\psi}_{,22}-\overline{\psi}_{,11})]q+\delta(\chi_{,23}-\overline{\psi}_{,13}+\psi_{,32})=0\,,$$

$$(2.19)\quad \delta q(\chi_{,13}+\overline{\psi}_{,23}+\psi_{,31})+(\eta-\delta)(\chi_{,11}+\chi_{,22})+\gamma\psi_{,33}-\overline{h}\theta=0\,,$$

$$(2.20)\quad \kappa q\theta_{,1}+\overline{\kappa}\theta_{,3}=r\theta\,,$$

on $x_1 q + x_3 = 0$.

3. Thermoelastic surface waves

We consider a plane harmonic monochromatic perturbation propagating along the surface S. Denoting by ω the angular frequency, we may write the potentials χ, $\overline{\psi}$, ψ, θ as

$$(3.1)\quad (\chi,\psi,\theta)=(X,\Psi,\Theta)\exp(-i\omega t)\exp(i\mathbf{k}_L\cdot\mathbf{x})\,,$$

$$(3.2)\quad \overline{\psi}=\overline{\Psi}\exp(-i\omega t)\exp(i\mathbf{k}_T\cdot\mathbf{x})\,,$$

where, owing to Eqs. (2.6)–(2.9) and (2.5), two distinct wave numbers $\mathbf{k}_L$ and $\mathbf{k}_T$ have been introduced, respectively, for the longitudinal and the transverse parts of the displacement. Within the framework of inhomogeneous waves, $\mathbf{k}$ is a complex-valued vector, i.e. $\mathbf{k} = \mathbf{k}_a + i\mathbf{k}_b$; in components

$$(3.3)\quad k_1=\xi+i\nu,\qquad k_2=\alpha+i\beta,\qquad k_3=\zeta+i\sigma\,.$$

We require that the amplitude of a surface wave should not increase proceeding from the surface toward the solid, hence $\mathbf{k}_b$ must be inwardly directed. Moreover, since no wave is allowed to grow in amplitude during its propagation, in analogy with the isotropic case, we assume $\mathbf{k}_a\cdot\mathbf{k}_b\geq 0$ [5, 12]. Owing to Eqs. (3.3) we obtain the following constraints,

$$(3.4)\quad \mathbf{k}_b\cdot\mathbf{n}>0,\qquad \xi\nu+\alpha\beta+\zeta\sigma\geq 0\,.$$

The particular case of usual Rayleigh waves is achieved for $\mathbf{k}_a\cdot\mathbf{n}=0$ and $\mathbf{k}_a\perp\mathbf{k}_b$.

3.1. Y-cut half-space

Let us first consider a wave propagating along the surface of a Y-cut half-space ($x_2 = 0$), (see Fig. 1a). We have

$$(3.5)\quad \xi+i\nu=q(\zeta+i\sigma)\,.$$

The last factors in the right-hand side of Eqs. (3.1) and (3.2) take the form

$$(3.6)\quad \exp[i(\zeta+i\sigma)(qx_1+x_3)]\exp[i(\alpha_{L,T}+i\beta_{L,T})x_2]\,.$$

After substitution of Eqs. (3.1), (3.2) into Eqs. (2.6)–(2.9), taking into account (3.6), we obtain the following compatibility conditions:

$$(3.7)\quad K_T=1-K(1+p)\,,$$

$$(3.8)\quad [\Lambda_1\Lambda_2-a_1a_3^2(pK+K_L)]\Lambda_3-c_2[a_2^2d^2\Lambda_1K+a_1(pK+K_L)(\Lambda_2-2a_2a_3dK)]=0\,,$$

where

$$K=\left(\frac{\zeta+i\sigma}{\omega}\right)^2\frac{\delta}{\rho},\qquad K_{L,T}=\left(\frac{\alpha_{L,T}+i\beta_{L,T}}{\omega}\right)^2\frac{\mu}{\rho},\qquad p=\frac{\mu}{\delta}q^2\,,$$

and

$$A_1 = (p + a_1)K + K_L - a_1\,,$$
$$A_2 = (p + b)K + K_L - a_2\,,$$
$$A_3 = (p + b')K + K_L - c_1\,,$$

with

$$a_1 = \frac{\mu}{2\mu + \lambda}, \quad a_2 = \frac{\mu}{\delta}, \quad a_3 = \frac{\eta}{\delta}, \quad b = \frac{\gamma\mu}{\delta^2}, \quad b' = \frac{\mu\overline{\kappa}}{\delta\kappa}\,,$$

$$c_1 = i\frac{\mu C}{\omega\kappa}, \quad c_2 = i\frac{h^2\theta_0}{\rho\omega\kappa}, \quad d = \frac{\overline{h}}{h}\,.$$

Concerning the boundary conditions, we observe that Eqs. (2.6)–(2.9), which are valid within Σ, hold also at the surface S. Hence we can use Eq. (2.7) to remove θ from Eq. (2.14), letting the boundary condition (2.16) to decouple from the system (2.13)–(2.15). Using Eqs. (3.1), (3.2) and (3.6), we obtain the compatibility conditions at S.

$$K_L = -\frac{r^2\mu}{\rho\omega^2\kappa^2}, \quad \Theta \neq 0\,, \tag{3.9}$$

$$K_L = \frac{(4p^2K^2 + 4pK(K-1) - K + 1)^2}{16p^2K^2[1 - (1+p)K]}, \quad \Theta = 0\,, \tag{3.10}$$

where r is given by Eq. (2.12). Substitution of Eq. (3.9) into Eq. (3.8) yields an algebraic cubic equation for K with complex coefficients. It admits three complex roots for any value of p if the inequality

$$[(a_1 + b) - a_1a_3^2]^2 < 4a_1b \tag{3.11}$$

holds. Without any loss of generality, we assume that x_3 grows along the propagation direction, so we take $\zeta > 0$. Hence the requirements (3.4) give

$$\beta_{L,T} \geq 0, \quad (1 + q^2)\sigma + \frac{\alpha_{L,T}\beta_{L,T}}{\zeta} \geq 0\,. \tag{3.12}$$

Those roots of Eqs. (3.7), (3.8) and (3.9) which satisfy inequalities (3.12) correspond to thermoelastic inhomogeneous surface waves on Y-cut half-spaces. As to the case of surface waves propagating perpendicularly to the privileged axis, i.e. for $\varphi = \pi/2$, we observe that the potentials χ, $\overline{\psi}$, ψ, θ may be regarded as independent of x_3. Then, the compatibility condition of the system (2.6)–(2.9) splits into

$$K_T = 1 - K'\,, \tag{3.13}$$

$$(K' + K_L)^2 - (a_1 + c_1 + a_1c_2)(K' + K_L) + a_1c_1 = 0\,, \tag{3.14}$$

where

$$K' = \left(\frac{\xi + i\nu}{\omega}\right)^2\frac{\mu}{\rho}\,.$$

Together with Eq. (3.9), Eq. (3.14) gives two modes which correspond to inhomogeneous surface waves propagating along the x_1-axis.

3.2 Rotated-cut half-spaces

Let us consider a surface wave propagating along the x_2-axis on a surface S whose normal makes an angle φ with the privileged axis (see Fig. 1b). Equation (3.5) holds as well in this case, and the wave fields have the following **x**-dependence

$$(\chi, \psi, \theta) = (X, \Psi, \theta)\exp[i(\alpha + i\beta)x_2]\exp[i(\zeta_L + i\sigma_L)(qx_1 + x_3)],$$
$$\overline{\psi} = \overline{\Psi}\exp[i(\alpha + i\beta)x_2]\exp[i(\zeta_T + i\sigma_T)(qx_1 + x_3)].$$

If we re-define the quantities K and $K_{L,T}$ as

$$K = \left(\frac{\alpha + i\beta}{\omega}\right)^2 \frac{\mu}{\rho}, \qquad K_{L,T} = \left(\frac{\zeta_{L,T} + i\sigma_{L,T}}{\omega}\right)^2 \frac{\delta}{\rho},$$

the propagation condition obtained from Eqs. (2.6)–(2.9) may be derived directly from Eqs. (3.7) and (3.8) by simply exchanging K for K_T in Eq. (3.7) and K for K_L in Eq. (3.8). The resulting equations are

$$K_T = \frac{1 - K}{1 + p}, \tag{3.15}$$

$$K^3 + \Gamma_2 K^2 + \Gamma_1 K + \Gamma_0 = 0, \tag{3.16}$$

where

$$\Gamma_2 = \overline{A}_1 + \overline{A}_2 + \overline{A}_3 - a_1 a_3^2 K_L - a_1 c_2,$$
$$\Gamma_1 = \overline{A}_1\overline{A}_2 + \overline{A}_1\overline{A}_3 + \overline{A}_2\overline{A}_3 - a_1 a_3^2 K_L(pK_L + \overline{A}_3) - c_2[a_1(pK_L + \overline{A}_2) + a_2 d K_L(a_2 d - 2a_1 a_3)],$$
$$\Gamma_0 = \overline{A}_1\overline{A}_2\overline{A}_3 - a_1 a_3^2 p K_L^2 \overline{A}_3 - c_2 K_L(a_1 p\overline{A}_2 + a_2^2 d^2 \overline{A}_1 - 2a_1 a_2 a_3 p d K_L),$$

with

$$\overline{A}_1 = (p + a_1)K_L - a_1,$$
$$\overline{A}_2 = (p + b)K_L - a_2,$$
$$\overline{A}_3 = (p + b')K_L - c_1.$$

The boundary conditions for the case at hand are Eqs. (2.17)–(2.20). In analogy with the previous analysis, we account for the continuity of the wave fields at S, using Eqs. (2.7) and (2.8) to remove θ from Eqs. (2.17) and (2.19). The resulting compatibility conditions at S are

$$K_L = -\frac{a_2}{(p + b')^2}\frac{r^2\mu}{\rho\omega^2\kappa^2}, \qquad \Theta \neq 0, \tag{3.17}$$

$$K_L = \frac{p^2(p + 1)(K - a_2)^2(2K - 1)^4}{K^2(1 - K)[(K - a_2)(2p + 1)^2 - (p + K)]^2}, \qquad \Theta = 0. \tag{3.18}$$

From Eqs. (3.17) and (3.16) we obtain again a cubic equation for K which admits three complex roots for any value of $p > 0$. Posing $\alpha > 0$, the requirements (3.4) yield

$$\sigma_{L,T} > 0, \qquad \beta + (q^2 + 1)\frac{\zeta_{L,T}\sigma_{L,T}}{\alpha} \geq 0. \tag{3.19}$$

The roots of Eqs. (3.15), (3.16) and (3.17) which satisfy inequalities (3.19) correspond to inhomogeneous thermoelastic surface waves on rotated-cut half-spaces. We finally remark

that for thermally insulated surfaces, $r = 0$ and consequently $K_L = 0$. Then Eq. (3.16) reduces to the equation

$$K^3 - (a_1 + a_2 + c_1 + a_1c_2)K^2 + (a_1a_2 + a_1c_1 + a_2c_1 + a_1a_2c_2)K - a_1a_2c_1 = 0, \tag{3.20}$$

the roots of which are evidently independent of p.

4. High freqencies

Having recourse to a generalized theory of heat conduction we observe that the thermal conductivities κ, $\overline{\kappa}$ and the thermoelastic coefficients h, $\overline{h}$ are frequency-dependent quantities. In particular, following [7] we have

$$(\kappa, \overline{\kappa}) = (\kappa_0, \overline{\kappa}_0)\frac{1}{1 - i\omega\tau_\kappa}, \qquad (h, \overline{h}) = (h_0, \overline{h}_0)\frac{1}{1 - i\omega\tau_h}, \tag{4.1}$$

where τ_κ and τ_h are suitable relaxation times. Consequently, the parameters b' and d are frequency-independent, while c_1 and c_2 are complex-valued functions of ω. We briefly sketch here the behaviour of the solutions obtained in the previous sections when $\omega \gg \tau_\kappa^{-1}, \tau_h^{-1}$. In this case we have

$$c_1 \to \frac{\mu C \tau_\kappa}{\kappa_0} := c_{01}, \qquad c_2 \to 0. \tag{4.2}$$

Consider first the Y-cut insulated half-spaces by taking $K_L = 0$ and using (4.2). Equation (3.8) yields then

$$A_3 = 0, \tag{4.3}$$

$$A_1A_2 - a_1a_3^2pK^2 = 0. \tag{4.4}$$

From Eq. (4.3) we obtain

$$K = \frac{c_{01}}{p + b'}.$$

This solution corresponds to a Rayleigh wave if $K_T < 0$. Owing to Eq. (3.7), this is true for any value of $p > 0$ if $\tau_\kappa > \max\left(\frac{\kappa_0}{\mu C}, \frac{\overline{\kappa}_0}{\delta C}\right)$. It is easy to show that Eq. (4.4) admits two real and positive solutions for K with any $p > 0$, but, in this case, the condition $K_T < 0$ is not satisfied for every $p > 0$. In particular, for $p = 0$ we obtain

$$K = 1, \qquad K = \frac{a_2}{b}. \tag{4.5}$$

The first result implies $K_T = 0$, the second one gives $K_T < 0$ if $\gamma < \delta$. The case $\varphi = \pi/2$ for insulated Y-cut half-spaces can be derived by Eq. (3.14). We have

$$K' = a_1, \qquad K' = c_{01}. \tag{4.6}$$

The first of Eq. (4.6) corresponds to a purely homogeneous elastic wave since, owing to Eqs. (3.13) and (2.4), $K_T > 0$. The second of Eqs. (4.6) yields $K_T < 0$ only if $\tau_\kappa > \frac{\kappa_0}{\mu C}$.

As regards rotated-cut insulated half-spaces, Eq. (3.20) gives, for $\varphi \neq \pi/2$,

$$K = a_1, \qquad K = a_2, \qquad K = c_{01}, \tag{4.7}$$

independently of the value of p. The second of (4.7) gives rise to a Rayleigh wave if and only if $\delta < \mu$.

5. Elastic modes on thermoelastic half-spaces

We are interested here in those particular solutions of Eqs. (3.8) and (3.16) which meet the boundary conditions (3.10) and (3.18), respectively. They apply for $\Theta = 0$, i.e. in absence of temperature perturbations. Concerning Y-cut half-spaces, for $\theta = 0$, Eq. (3.8) must be replaced by the compatibility conditions

$$K_L = a_2 + (a_2 a_3 d - p - b)K\,, \tag{5.1}$$

$$AK^2 + BK + E = 0\,, \tag{5.2}$$

where

$$A = (p + a_1)(p + b) - a_1 a_3^2 p\,,$$
$$B = (p + b)(K_L - a_1) + (p + a_1)(K_L - a_2) - a_1 a_3^2 K_L\,,$$
$$E = (K_L - a_1)(K_L - a_2)\,.$$

Substituting Eq. (5.1) into (5.2) we obtain one real solution for K which turns out to be independent of p,

$$K = a_2 \frac{a_1 a_3 - (a_2 - a_1)d}{a_1 a_2 d + (a_2 d - a_1 a_3)(a_2 a_3 d - b)} := \overline{K}\,. \tag{5.3}$$

The boundary condition (3.10) implies an additional constraint on this solution. Substituting Eqs. (5.1) and (5.3) into (3.10) we obtain an algebraic equation for p with real coefficients

$$D_3 p^3 + D_2 p^2 + D_1 p + D_0 = 0\,, \tag{5.4}$$

where

$$D_3 = 16\overline{K}^3[a_2 + (a_2 a_3 d - b + 1)\overline{K} - 1]\,,$$
$$D_2 = 16\overline{K}^2(\overline{K} - 1)\left[a_2 + (a_2 a_3 d - b + 1)\overline{K} - \frac{3}{2}\right]\,,$$
$$D_1 = -8\overline{K}(\overline{K} - 1)^2\,,$$
$$D_0 = (\overline{K} - 1)^2\,.$$

Owing to Eqs. (5.1), (5.3) and (3.7), K_L and K_T turn out to be real. Moreover, from Eq. (3.10) we observe that K_L and K_T are negative for any value of $p \geq 0$ if and only if $\overline{K} > 1$. Hence, any non-negative solution p_Y of Eq. (5.4) yields a privileged direction along which elastic homogeneous (undamped) Rayleigh waves can propagate if $\overline{K} > 1$. Instead, a solution $p_Y \geq 0$ of Eq. (5.4) with $\overline{K} \leq 0$ corresponds to a particular orientation of the plane $\mathcal{P}$ on which a purely elatic mode can propagate within the solid along the x_2-axis. For $0 < \overline{K} \leq 1$ one of these two modes can occur depending on the value obtained for p_Y.

As to the rotated-cut half-space, we observe that, in absence of temperature perturbations, the compatibility conditions can be obtained directly from Eq. (5.1) and (5.3) by simply exchanging K with K_L. Solving for K and K_L and substituting into the boundary condition (3.18), we arrive at an algebraic equation of the ninth order in p with real coefficients. For brevity we don't write it explicitly but note that it admits at least one real solution p_{rot}. If $p_{\text{rot}} \geq 0$ and $K_L < 0$, Eq. (3.18) gives $K > 1$ and, in turn, from Eq. (3.15) $K_T < 0$. Such a solution represents a particular rotated-cut half-space on which an elastic homogeneous Rayleigh wave can propagate without damping. If $K_L > 0$

we obtain $K < 1$ and $K_T > 0$ and the corresponding rotated-cut half-space admits an elastic homogeneous mode propagating within the solid along the normal to S. We finally remark that, owing to (4.1) and the definition of d, the solutions of Eq. (5.4) are independent of the frequency and temperature θ_0.

6. Numerical results and concluding remarks

In order to illustrate the previous results we have determined some of the main surface wave properties by numerical computation. In particular we are interested in the wave speed v and the wave attenuation Ω for the modes corresponding to solutions of Eqs. (3.8) and (3.16). To this end we observe that, according to Eq. (2.12), for a solid-vacuum boundary at room temperature, the terms containing K_L in Eqs. (3.8) and (3.16) turn out to be negligible. A preliminary numerical computation of v and Ω has confirmed this view allowing us to restrict attention to thermally insulated surfaces by putting $r = 0$. Denoting by k_s the projection on S of the real part of the wave vector and observing that $\mathbf{k}_L$ and $\mathbf{k}_T$ have common values of k_s, we may write the surface wave speed as

$$v = \frac{\omega}{k_s}. \tag{6.1}$$

As to the wave attenuation Ω we note that, in view of Eq. (3.1) and (3.3), the wave amplitude decays from $\mathbf{x} = \bar{\mathbf{x}}$ to $\mathbf{x} = \bar{\mathbf{x}} + \Delta\mathbf{x}$ by a factor $\exp(-\omega|\Delta\mathbf{x}|)$, where, since $K_L = 0$,

$$\Omega = \begin{cases} \sqrt{1+q^2\sigma} + \dfrac{\alpha_T\beta_T}{\zeta\sqrt{1+q^2}}, & \text{for } Y\text{-cut h} - \text{s}, \\ \beta + (1+q^2)\dfrac{\alpha_T\beta_T}{\alpha}, & \text{for rotated-cut h} - \text{s}. \end{cases} \tag{6.2}$$

Obviously, the quantities defined in Eqs. (6.2) are subject to the conditions $(3.12)_2$ and $(3.19)_2$, respectively.

Table 1. Thermomechanical properties of zinc [13].

μ	63.25 GPa	α_0	129	$(\times 10^{-7})\,°\text{K}^{-1}$
λ	36.5 "	$\overline{\alpha}_0$	645	$(\times 10^{-7})\,°\text{K}^{-1}$
η	92 "	$\kappa \cong \overline{\kappa}$	102	W/m °K
δ	39 "	C	389	J/Kg °K
γ	63.5 "	ρ	7135	Kg/m^3

Our results have been applied to a half-space made of zinc. The thermomechanical properties at $\theta_0 = 300°\text{K}$ are summarized in Table 1 (cf. [13] and references therein). As usual, the thermoelastic constants h and $\overline{h}$ are evaluated via the thermal expansion coefficients α_0 and $\overline{\alpha}_0$. Using the present notations we have

$$h = 2(\mu + \lambda)\alpha_0 + (\eta - \delta)\overline{\alpha}_0,$$
$$\overline{h} = 2(\eta - \delta)\alpha_0 + \gamma\overline{\alpha}_0.$$

According to [14] the relaxation times τ_κ and τ_h are taken to be equal to $\kappa_0/\mu C$; namely $\tau_\kappa = \tau_h = 10^{-12}$ s. Inequalities (2.4) are evidently satisfied by the parameters of Ta-

ble 1. It is easy to verify that also the condition (3.11) is fulfilled. This implies that Eq. (3.8) admits three complex roots for any value of p. Two of these roots yield thermoelastic modes that satisfy inequalities (3.12) while, for the third root, Ω turns out to be negative for any $p > 0$. The corresponding values of v and Ω, expressed in m/s and db/cm, respectively, are given in Fig. 2 and Fig. 3, against the angle φ. Equation (3.20) admits again three complex roots, one of which yields $\Omega < 0$, the remaining two modes are practically undamped and their speeds are independent of φ. Their value are given in Table 2. We remark that our results give wave attenuations of the same order of magnitude as those calculated in [3] for a $LiNbO_3$ half-space, whose material symmetry is similar to that of zinc.

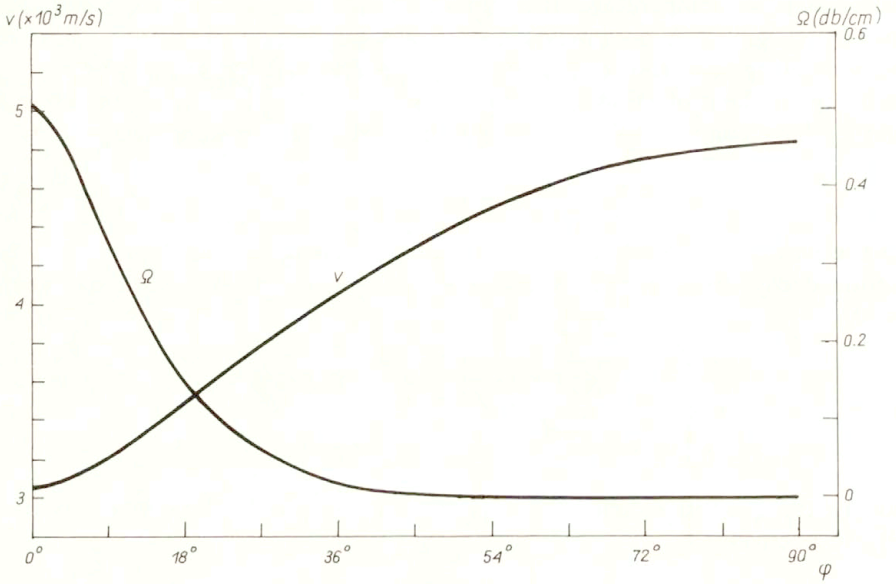

FIG. 2.

Table 2. Speeds and attenuations in rotated-cut half-spaces.

	v (m/s)	Ω (db/cm)
mode 1	4836	< 0.056
mode 2	2338	0

Concerning the wave modes described in Sec. 5, we note that $\overline{K}$, as defined in Eq. (5.3), turns out to be negative, and consequently, K_L and K_T are positive. Equation (5.4) has only one real positive root corresponding to a particular angle φ_Y, while the analogous solution for the case of the rotated-cut half-space gives one real positive solution for p corresponding to an angle φ_{rot}. The results, shown in Table 3, allow us to conclude that, independently of the frequency and of the value of θ_0, two special elastic modes are of particular importance for a thermoelastic transversely isotropic half-space. The first one corresponds to an elastic bulk wave propagating perpendicularly to the surface of

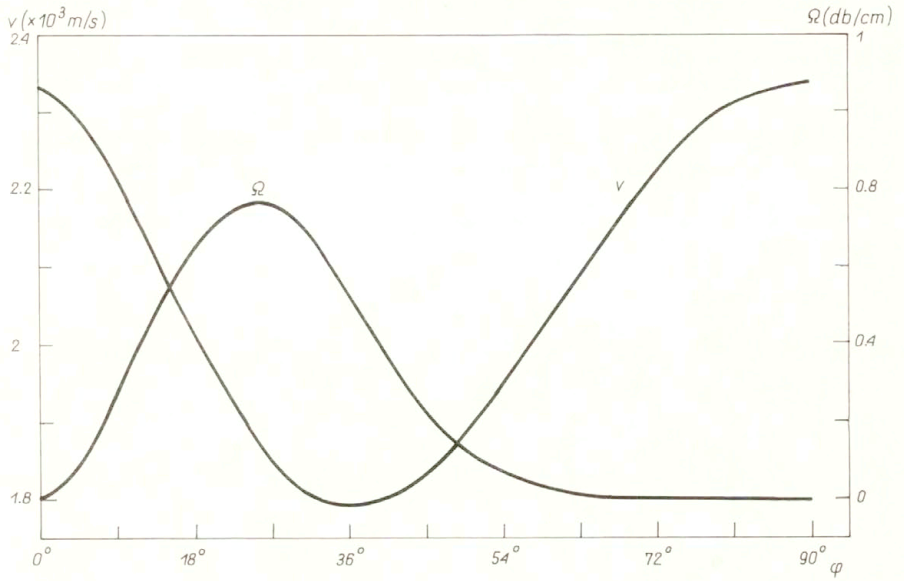

FIG. 3.

the Y-cut half-space. The second one corresponds to a homogeneous Rayleigh wave that propagates on the surface of a φ_{rot}-rotated half-space. Both waves don't carry temperature perturbations and turn out to be undamped.

Table 1. Particular elastic modes on thermoelastic half-spaces.

Y-cut	p_Y	φ_Y	K	K_L	K_T
	8.542	66.45°	−0.323	4.109	4.084
rotated-cut	p_{rot}	φ_{rot}	K	K_L	K_T
	1.216	40.88°	4.109	−0.323	−1.403

References

1. P. CHADWICK and D.W. WINDLE, *Propagation of Rayleigh waves along isothermal and insulated boundaries*, Proc. R. Soc. Lond., **A280**, 44–71, 1964.
2. G.K. JURCZYK and P.G. KLEMENS, *Thermoelastic attenuation of Rayleigh waves*, J. Appl. Phys., **58**, 7, 2593–2598, 1985.
3. A.P. MAYER, *Thermoelastic attenuation of surface acoustic waves*, Int. J. Engng Sci., **28**, 1073–1082, 1990.
4. A.J. SLOBODNIK Jr, P.H. CARR and A.J. BUDREAU, *Microwave frequency acoustic surface-wave loss mechanisms on $LiNbO_3$*, J. Appl. Phys., **41**, 11, 4380–4387, 1970.
5. G. CAVIGLIA, A. MORRO and E. PAGANI, *Inhomogeneous waves in viscoelastic media*, Wave Motion, **12**, 143–159, 1990.
6. G. CAVIGLIA and A. MORRO, *Surface waves at a fluid-viscoelastic solid interface*, Eur. J. Mech., A., Solids, **9**, 1–13, 1990.
7. M. ROMEO, *Inhomogeneous waves in transversely isotropic dielectrics*, Acta Mechanica, **97**, 51–61, 1993.
8. D.S. CHANDRASEKHARAIAH, *A generalized linear thermo-elasticity theory for piezoelectric media*, Acta Mech., **71**, 39–49, 1988.
9. A.C. ERINGEN and G.A. MAUGIN, *Continuum electrodynamics*, Springer, Berlin, Heidelberg, New York, Tokyo 1990.

10. D.S. CHANDRASEKHARAIAH and H.R. KESHAVAN, *Thermoelastic plane waves in a transversely isotropic body*, Acta Mech., **87**, 11–22, 1991.
11. D.D. JOSEPH, and L. PREZIOSI, *Heat waves*, Rev. Mod. Phys., **61**, 41–73, 1989.
12. P.K. CURRIE, M.A. HAYES and P.M. O'LEARY, *Viscoelastic Rayleigh waves*, Quart. Appl. Math., **35**, 35–53, 1977.
13. M. DELANNOY-COURTIS, N. TOUPANCE and J. BOISTEL DE BELLOY, *Temperature dependence of elastic moduli for non-cubic solids: application to cadmium, magnesium and zinc*, J. Phys. D., Appl. Phys., **23**, 1695–1702, 1990.
14. A.J. RUDGERS, *Analysis of thermoacoustic wave propagation in elastic media*, J. Acoust. Soc. Am., **88**, 1078–1094, 1990.

D.I.B.E. UNIVERSITA', GENOVA, ITALY.

Received September 2, 1992.

Arch. Mech., 45, 1, pp. 51–64, Warszawa 1993

Macroscopic modelling of pollutant transport in porous media(*)

J.-L. AURIAULT (GRENOBLE) and J. LEWANDOWSKA (GDAŃSK)

A RIGOROUS MODEL for pollutant transport in porous media has been developed by means of the double scale asymptotic development technique [3, 7]. It has been assumed that the microscopic equations, governing the pore-scale processes of diffusion, advection and adsorption, are known. The application of the homogenisation method has permitted the replacement of the real heterogeneous medium by the macroscopic equivalent continuum characterised by the macroscopic equivalent dispersion tensor and the macroscopic governing equations for the average concentration field. The investigations of three characteristic cases that correspond to different macroscopic models, have been carried out. The most general case concerns the modelling of flow in the presence of strong advection as well as diffusion and adsorption. The expression for the dispersion-adsorption coefficient in terms of the given microscale parameters and geometry has been derived. As an example, a flow of a pollutant in a layered porous medium has been considered. The different forms of the dispersion tensor in relation to the order of magnitude of the dimensionless parameters has been presented.

Notations

a_s	the specific surface of the porous medium,
$c(\mathbf{x}, \mathbf{y}, t)$	the concentration of the pollutant,
D_{ij}	the molecular diffusion tensor,
D^{*}_{ij}	the macroscopic (or effective) diffusion tensor,
D^{**}_{ij}	the macroscopic (or effective) dispersion tensor,
D^{***}_{ij}	the macroscopic (or effective) dispersion-adsorption tensor,
ERV	the elementary representative volume,
K_d	the distribution coefficient or the partitioning coefficient,
l	a characteristic length of the ERV or the periodic cell,
L	a characteristic marcoscopic length,
n	the porosity,
N_i	the unit outward vector normal to Γ,
Q_l, P_l, Pe_l, P, Q, Pe	the dimensionless numbers,
R_d	the coefficient of retardation or the retardation factor,
S_p	the total surface of the solid in the cell,
t	the time variable,
v_i	the advective velocity,
$\mathbf{x}$	the macroscopic (or slow) space variable,
$\mathbf{y}$	the microscopic (or fast) space variable,
α	the parameter of adsorption,
ε	the homogenisation parameter,
ϱ	the bulk density of the dry medium,
Ω_s	the solid volume in the periodic cell,
Ω_l	the volume of pores in the periodic cell,
Γ	the boundary between Ω_S and Ω_l,
$\lvert\Omega\rvert$	the total volume of the periodic cell,

(*) The paper contains the material which was communicated during the 29th Annual Technical Meeting of the Society of Engineering Science, University of California, San Diego, September 14–16, 1992

$|\Omega_l|$ the volume of pores in the cell,
χ_i, χ_i^1, χ_i^2 the local vectorial fields.

1. Introduction

THE POLLUTANT transport in porous media represents an important engineering problem of environmental protection. Although the mechanism of pollutant transport in the microscale, it is in the scale of pores, has been well established, it is practically impossible to solve the full equations for the complex microscale geometry. In order to overcome these difficulties, the idea to replace the real heterogeneous medium by the macroscopic equivalent continuum has been developed.

There are many methods available in the literature to derive the macroscopic (effective) governing equations and the macroscopic (effective) transport properties. In the paper the double scale asymptotic development technique [3, 7] will be applied to determine the macroscopic model of diffusion, advection and adsorption phenomena. The methodology followed in this paper has been presented in details in [1].

2. Phenomenological approach

Within the framework of the phenomenological approach the medium is investigated in the scale of a sample, called macroscale, directly [2, 8, 6].

At each point of the medium the vectorial field of the velocity and the scalar field of the concentration (the mass of the pollutant in a unit volume of the fluid) are introduced. It is assumed that the phenomena that contribute to the distribution of pollutant in a porous medium are: advection, diffusion, dispersion and adsorption. At each point of the space the macroscopic flux of the pollutant, as the quantity averaged over the representative volume in the vicinity of the given point, is defined. The component fluxes are the following:

- The advective flux $(\overline{c}, \overline{\mathbf{v}})$, where $\overline{\mathbf{v}}$ is the average velocity of Darcy.
- The dispersive flux due to the variations of the velocity in the pores, expressed by the Fick's law $(-\mathbf{D} \cdot \nabla \overline{c})$. $\mathbf{D}$ is the coefficient of mechanical dispersion given by the formula

$$D_{ij} = a_{ijkm} \frac{\overline{v}_k \overline{v}_m}{v}, \qquad \overline{v} = |\overline{\mathbf{v}}|, \tag{2.1}$$

where the fourth order tensor $\mathbf{a}$ reveals the microscopic configuration of the interface solid-fluid. In the case of isotropic porous medium the components a_{ijkm} may be written in terms of two parameters a_L (called the longitudinal dispersivity) and a_T (called the transversal dispersivity)

$$a_{ijkm} = a_T \delta_{ij} \delta_{km} + \frac{a_L + a_T}{2} (\delta_{ik}\delta_{jm} + \delta_{im}\delta_{jk}). \tag{2.2}$$

Applying the above equation, the following formula is obtained:

$$D_{ij} = a_T \overline{v} \delta_{ij} + (a_L - a_T) \overline{v}_i \overline{v}_j / \overline{v}. \tag{2.3}$$

If one of the Cartesian axes coincides with the direction of the average velocity, then

the dispersion matrix at this point is

$$\mathbf{D} = \begin{vmatrix} a_L\overline{v} & 0 & 0 \\ 0 & a_T\overline{v} & 0 \\ 0 & 0 & a_T\overline{v} \end{vmatrix}. \tag{2.4}$$

This matrix is evidently anisotropic.

• The average pollutant flux related to the molecular diffusion $(-\mathbf{D}_d^* \cdot \nabla\overline{c})$, where $\mathbf{D}_d^* = \mathbf{T}^* D_d$ is the coefficient of effective molecular diffusion, and $\mathbf{T}^*$ is the second order symmetrical tensor called the tortuosity tensor. For the isotropic medium it reduces to

$$T_{ij}^* = \frac{\vartheta_w^s}{\vartheta_w}\delta_{ij}, \tag{2.5}$$

where

$$\vartheta_w^s = \frac{S_{ww}}{S_0} \quad \text{and} \quad \vartheta_w = \frac{U_{0w}}{U_0}. \tag{2.6}$$

S_{ww} denotes the water-water portion (of the total S_0) of the bounding surface of the representative volume (ERV) and U_{0w} means the volume occupied by water within the total volume U_0 of the ERV. The total flux of the pollutant is the sum of the flux components

$$q_{c,\text{total}} = \vartheta_w(\overline{c}\,\overline{\mathbf{v}} - \mathbf{D}_h \cdot \nabla\overline{c}), \tag{2.7}$$

where $\mathbf{D}_h = \mathbf{D} + \mathbf{D}_d^*$ is the coefficient of the hydrodynamic dispersion.

• The mass balance equation gives the macroscopic phenomenological description of the problem in function of the concentration $\overline{c} = \overline{c}(\mathbf{x}, t)$

$$nR_d\frac{\partial\overline{c}}{\partial t} = -\nabla \cdot n(\overline{c}\,\overline{\mathbf{v}} - \mathbf{D}_h \cdot \nabla\overline{c}), \tag{2.8}$$

where R_d is the retardation coefficient ($R_d > 1$).

This is the traditional form of the pollutant transport equation for the saturated porous medium, commonly used in the engineering practice.

3. Homogenisation by the asymptotic development method

The derivation of the macroscopic model will be accomplished by the application of the homogenisation method which is based on the double scale asymptotic expansions [3, 7]. The general idea of the homogenisation process consists in the passage from the description of the phenomenon at the microscale (the local scale) where the governing equations are given, to the equivalent macroscopic boundary value problem that provides the „averaged" behaviour of the medium. The proposed approach is rigorous in the sense that the macroscopic quantities depend solely on the microscopic transport parameters and the geometrical properties of the medium.

3.1. General description [1]

The basic assumption of the method is the existence of an elementary representative volume (ERV) of the medium, small when compared with the macroscopic volume. The above condition, which is equivalent to the separation of scales, must be valid for both the geometry and the physical quantities. In the periodic medium the ERV represents

the periodic cell. Let l be a characteristic length of the ERV or the periodic cell, and L is a characteristic macroscopic length. The separation of scales yields

$$\frac{l}{L} = \varepsilon \ll 1 . \tag{3.1}$$

The two characteristic lengths l and L introduce two dimensionless space variables $\mathbf{X}/l$ and $\mathbf{X}/L$ where $\mathbf{X}$ is a physical space variable. Each quantity Φ does depend a priori on these two dimensionless space variables. In practice two space variables $\mathbf{x}$ and $\mathbf{y} = \mathbf{x}/\varepsilon$ are used instead because of their more physical meanings. The variable $\mathbf{x}$ is the macroscopic (or slow) space variable and $\mathbf{y}$ is the microscopic (or fast) space variable. Two equivalent descriptions are then possible

$$\Phi = \Phi(\mathbf{x}, \mathbf{y}), \quad \mathbf{y} = \mathbf{x}/\varepsilon , \quad \text{the macroscopic point of view,}$$

$$\Phi = \Phi(\mathbf{x}, \mathbf{y}), \quad \mathbf{x} = \varepsilon \mathbf{y} , \quad \text{the microscopic point of view.}$$

If $\langle \Phi \rangle$ means the average of the quantity Φ, the following relation is generally valid:

$$\Phi = O(\langle \Phi \rangle) , \tag{3.2}$$

where the symbol $O(\cdot)$ denotes the order of magnitude of the quantity $< \Phi >$ with respect to ε

$$\Phi = O(\langle \Phi \rangle) \quad \text{if} \quad \varepsilon \ll (\Phi / \langle \Phi \rangle) \ll \varepsilon^{-1} . \tag{3.3}$$

The separation of scales for Φ implies that (see Fig. 1)

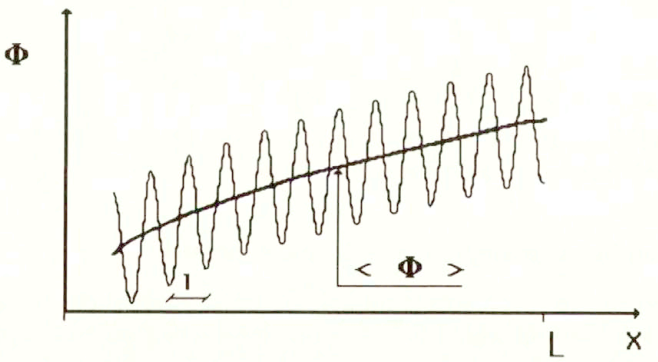

FIG. 1.

$$\frac{\partial \Phi}{\partial \mathbf{y}} = O\left(\frac{\partial \langle \Phi \rangle}{\partial \mathbf{x}} \right) \tag{3.4}$$

i.e. the local gradient of Φ is of the same order of magnitude as the macroscopic gradient of $\langle \Phi \rangle$. Further, from Eq. (3.2) it is deduced that

$$\frac{\partial \Phi}{\partial \mathbf{y}} = O\left(\frac{\partial \Phi}{\partial \mathbf{x}} \right) . \tag{3.5}$$

Equation (3.4) and Fig. 2 show that the variations of $\langle \Phi \rangle$ against $\mathbf{x}$ over a length $O(l)$ are small and zero in the limiting case of $\varepsilon \to 0$. It means that the quantity Φ is $\mathbf{y}$-stationary,

i.e. its average is invariant under a local translation of the order l. A similar property holds when the micro-structure is periodic, the elementary representative volume being replaced by the periodic cell. In this case Φ is **y**-periodic.

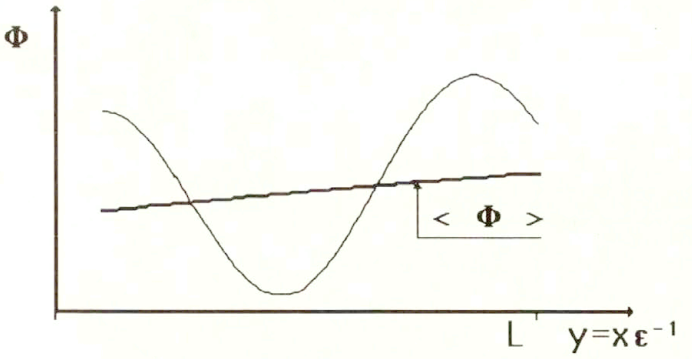

FIG. 2.

In the process of homogenisation the unknowns are presented in the form of asymptotic expansions with the small parameter ε playing the fundamental role

$$\Phi = \Phi(\mathbf{x}, \mathbf{y}) = \Phi^0(\mathbf{x}, \mathbf{y}) + \varepsilon^1 \Phi^1(\mathbf{x}, \mathbf{y}) + \varepsilon^2 \Phi^2(\mathbf{x}, \mathbf{y}) + \ldots . \tag{3.6}$$

The perfect homogenisation is obtained for $\varepsilon \to 0$. Since in practice ε takes small but finite value, the macroscopic equivalent description, which gives the equation for Φ^0, represents an approximation of the real behaviour with the precision in terms of ε.

The stationariness or the periodicity implies the **y**-stationarity or **y**-periodicity of Φ^i. If the unknowns can be found in the form (3.6) where Φ^i are **y**-stationary or **y**-periodic, then the homogenisation is possible. If not, the medium and the phenomenon considered are not homogenizable.

3.2. Microscopic equations

In the analysis a rigid saturated porous periodic medium will be considered (Fig. 3). The following notations are introduced: Ω_S — the solid volume in the periodic cell, Ω_l — the pores volume occupied by the incompressible fluid, Γ — the boundary between Ω_S and Ω_l, Ω_S and Ω_l are to be connected. The solid part Ω_S is assumed to be undeformable. In the problem considered the scale l represents the size of the pores, whereas the scale L reveals the dimension of the sample.

The physical processes of molecular diffusion, advection and adsorption are described by the following microscale equations:

$$\frac{\partial c}{\partial t} + \frac{\partial}{\partial y_i}\left(- D_{ij} \frac{\partial c}{\partial y_j} + v_i c \right) = 0 , \tag{3.7}$$

$$- N_i \left(D_{ij} \frac{\partial c}{\partial y_j} \right) = \alpha \frac{\partial c}{\partial t} \quad \text{on } \Gamma , \tag{3.8}$$

where D_{ij} is the molecular diffusion tensor, t is the time variable and N_i is the unit vector normal to Γ. The coefficient α denotes the adsorption parameter (α positive).

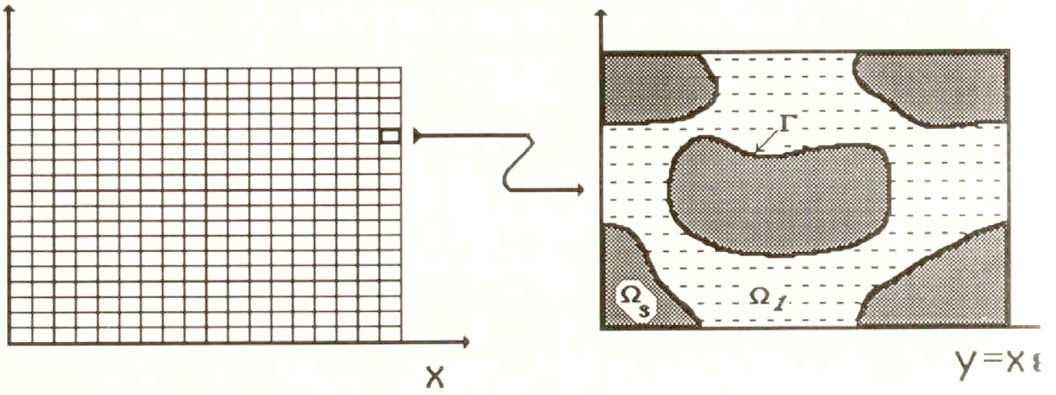

FIG. 3.

It represents a length which characterises the kinematics of the adsorption phenomenon. It is not related to the thickness of the adsorbed layer. For the sake of simplicity of the presentation it is assumed that the adsorption is instantaneous, reversible and linear (the linear equilibrium isotherm) but similar results may be obtained for the nonlinear equilibrium isotherms.

The study is based on the assumption that the microscopic velocity vector $\mathbf{v}$ satisfies the Stokes equation

$$\mu \frac{\partial^2 v_i}{\partial y_j \partial y_j} - \frac{\partial p}{\partial y_i} = 0 \tag{3.9}$$

together with the incompressibility condition

$$\frac{\partial v_i}{\partial y_i} = 0 \tag{3.10}$$

and the no-slip condition on the solid surface

$$\mathbf{v} = 0 \quad \text{on } \Gamma . \tag{3.11}$$

The above system of equations shows that the advective motion is independent of the diffusion and adsorption phenomena. Therefore, the macroscopic description of the advection (Darcy law), which has been already presented in the earlier contributions, for example [1], will be directly used in the analysis. Note also that for the sake of simplicity we assume the thickness of the adsorbed layer and the inter-particle distance as sufficiently small compared to the pore size l (to assure the validity of the continuous description (3.7)–(3.11)).

The problem may be formulated as follows:

Supposing that the microscopic equations governing the combined processes of the pollutant diffusion, advection and adsorption are known, determine the macroscopic transport equation and the effective macroscopic material properties for the equivalent continuous medium.

3.3. Normalisation

In the process of homogenisation all the variables will be normalised with respect to the characteristic length l. Therefore, it can be said that the microscopic point of view is adopted [1]. Owing to the normalisation, all the quantities appearing in the equations will be $O(1)$ and the method of homogenisation can be applied properly.

Equations (3.7) and (3.8) comprise three dimensionless numbers P_l, Q_l and Pe_l that will measure the relative influence of the different components, representing different phenomena incorporated into the analysis

$$\mathrm{Pe}_l = \frac{\left|\frac{\partial}{\partial y_i}(v_i c)\right|}{\left|\frac{\partial}{\partial y_i}\left(D_{ij}\frac{\partial c}{\partial y_j}\right)\right|} \quad \text{(the Peclet number)}, \tag{3.12}$$

$$Q_l = \frac{\left|\alpha\frac{\partial c}{\partial t}\right|}{\left|N_i\left(D_{ij}\frac{\partial c}{\partial y_j}\right)\right|} \quad \text{(the Damköhler number)}, \tag{3.13}$$

$$P_l = \frac{\left|\frac{\partial c}{\partial t}\right|}{\left|\frac{\partial}{\partial y_i}\left(D_{ij}\frac{\partial c}{\partial y_j}\right)\right|}. \tag{3.14}$$

3.4. Homogenisation

Due to the separation of scales the concentration field c is the function of three variables

$$c(\mathbf{x}, \mathbf{y}, t),$$

where $\mathbf{x} = (x_1, x_2, x_3)$ is the macroscopic space variable, $\mathbf{y} = (y_1, y_2, y_3)$ is the microscopic space variable and t means the time variable.

When following the homogenisation technique, it is assumed that the concentration c can be presented in the form of an asymptotic expansion

$$c(\mathbf{x}, \mathbf{y}, t) = c^0(\mathbf{x}, \mathbf{y}, t) + \varepsilon^1 c^1(\mathbf{x}, \mathbf{y}, t) + \varepsilon^2 c^2(\mathbf{x}, \mathbf{y}, t) + \ldots, \tag{3.15}$$

where the components $c^i(\mathbf{x}, \mathbf{y}, t)$ are $\mathbf{y}$-periodic and the variable $\mathbf{x}$ is expressed by the variable $\mathbf{y}$, i.e. $\mathbf{x} = \varepsilon\mathbf{y}$. The latter implies that the gradient operator will be $\left(\frac{\partial}{\partial \mathbf{y}} + \varepsilon\frac{\partial}{\partial \mathbf{x}}\right)$.

An expansion similar to Eq. (3.15) is used also with respect to the velocity vector $\mathbf{v}$.

The methodology of the homogenisation consists in application of the asymptotic development (3.15) in Eqs. (3.7) and (3.8). The comparison of the terms of the same powers of ε will yield the successive descriptions in the form of the systems of differential equations to be analysed and solved.

When applied to the advective motion, the process leads to the Darcy law expressed

in the form [1]

$$\langle v_i^0 \rangle = -K_{ij} \frac{\partial p^0}{\partial x_j}, \tag{3.16}$$

where the pore scale velocity $\mathbf{v}^0$ of a fluid filtrating in the porous medium is

$$v_i^0 = -k_{ij} \frac{\partial p^0}{\partial x_j}, \tag{3.17}$$

$\mathbf{k}$ denotes the tensor depending on the local space variable $\mathbf{y}$, and $\mathbf{K}$ is the permeability tensor defined as the volume average

$$K_{ij} = \langle k_{ij} \rangle = \frac{1}{|\Omega|} \int_{\Omega_l} k_{ij} \, d\Omega . \tag{3.18}$$

The second result of homogenisation with respect to the advection problem is the volume balance equation [1]

$$\frac{\partial}{\partial x_i} \langle v_i^0 \rangle = 0, \tag{3.19}$$

where

$$\langle v_i^0 \rangle = \frac{1}{|\Omega|} \int_{\Omega_l} v_i^0 \, d\Omega . \tag{3.20}$$

In the next sections three characteristic cases, corresponding to different orders of magnitude of the dimensionless numbers Q_l, P_l and Pe_l, will be examined.

3.5. The case of $P_l = O(\varepsilon^2)$, $Q_l = O(\varepsilon^2)$ and $\mathrm{Pe}_l = O(\varepsilon^1)$

The concentration c satisfies the normalised local advection-diffusion-adsorption equation

$$\varepsilon^2 \frac{\partial c}{\partial t} + \frac{\partial}{\partial y_i} \left(- D_{ij} \frac{\partial c}{\partial y_j} + \varepsilon v_i c \right) = 0 \tag{3.21}$$

with the boundary condition imposed on the solid-liquid interface

$$-N_i \left(D_{ij} \frac{\partial c}{\partial y_j} \right) = \varepsilon^2 \alpha \frac{\partial c}{\partial t} \quad \text{on } \Gamma . \tag{3.22}$$

Despite the same notations used, all the quantities appearing in Eqs. (3.21) and (3.22) are dimensionless now. Hence, the terms standing by ε^2, ε^1 and ε^0 are of the order 1, i.e. $O(1)$.

The analysis of the above problem followed the methodology presented by AURIAULT [1]. The macroscopic governing equation obtained has the final form

$$R_d \frac{\partial c^0}{\partial t} - \frac{\partial}{\partial x_i} \left(D_{ij}^* \frac{\partial c^0}{\partial x_j} \right) + \frac{\partial}{\partial x_j} (c^0 \langle v_i^0 \rangle) = 0, \tag{3.23}$$

where the effective diffusion tensor D_{ij}^* is defined as

$$D_{ij}^* = \frac{1}{|\Omega|} \int_{\Omega_l} D_{ik} \left(I_{kj} + \frac{\partial \chi_j}{\partial y_k} \right) d\Omega . \tag{3.24}$$

The local linear boundary value problem to determine the vectorial field χ_i depends on the geometrical properties of the cell and takes the form

$$-\frac{\partial}{\partial y_i}\left[D_{ij}\left(I_{jk}+\frac{\partial \chi_k}{\partial y_j}\right)\right]=0, \tag{3.25}$$

$$-N_i\left[D_{ij}\left(I_{jk}+\frac{\partial \chi_k}{\partial y_j}\right)\right]=0 \quad \text{on } \Gamma, \tag{3.26}$$

where $\chi_i = \chi_i(\mathbf{y})$ is $\mathbf{y}$-periodic and

$$\langle \chi \rangle = \frac{1}{|\Omega|}\int_{\Omega_l} \chi \, d\Omega = 0. \tag{3.27}$$

It can be shown that the tensor $\mathbf{D}^*$ is symmetric and positive definite. From Eq. (3.24) it is seen that the tensor $\mathbf{D}^*$ has a contribution from the molecular diffusion and the geometry of the periodic cell. It does not contain the advective term though this term appears in the differential governing equation.

The coefficient R_d (the retardation factor) in expression (3.23) is found to be related to the adsorption parameter by the following formula

$$R_d = \frac{|\Omega_l| + \alpha S_p}{|\Omega|}. \tag{3.28}$$

3.6. The case of $P_l = O(\varepsilon^2)$, $Q_l = O(\varepsilon^2)$ and $\mathrm{Pe}_l = O(\varepsilon^0)$

In this section the relative magnitude of the microscopic advection will be increased with respect to the preceeding case. The homogenisation procedure will be repeated to investigate the form of the macroscopic equation and the definitions of the effective parameters. The normalised equations (3.7) and (3.8) take the following forms

$$\varepsilon^2\frac{\partial c}{\partial t}+\frac{\partial}{\partial y_i}\left(-D_{ij}\frac{\partial c}{\partial y_j}+v_i c\right)=0, \tag{3.29}$$

$$-N_i\left(D_{ij}\frac{\partial c}{\partial y_j}\right)=\varepsilon^2\alpha\frac{\partial c}{\partial t} \quad \text{on } \Gamma. \tag{3.30}$$

The process of homogenisation leads to two succeeding order macroscopic governing equations that give the approximation of the real pollutant behaviour within an error $O(\varepsilon)$

$$\frac{\partial}{\partial x_i}(\langle v_i^0\rangle c^0) = O(\varepsilon), \tag{3.31}$$

$$R_d\frac{\partial c^0}{\partial t}-\frac{\partial}{\partial x_i}\left(D_{ij}^{**}\frac{\partial c^0}{\partial x_j}\right)+\frac{\partial}{\partial x_i}(\langle v_i^1\rangle c^0+\langle v_i^0\rangle \bar{c}^1)=O(\varepsilon), \tag{3.32}$$

where tensor $\mathbf{D}^{**}$ is the macroscopic dispersion tensor defined as

$$D_{ij}^{**}=\frac{1}{|\Omega|}\int_{\Omega_l} D_{ik}\left(I_{kj}+\frac{\partial \chi_j^1}{\partial y_k}\right)d\Omega+\frac{\partial p^0}{\partial x_k}\frac{1}{|\Omega|}\int_{\Omega_l} k_{ik}\chi_j^1\, d\Omega. \tag{3.33}$$

The vectorial field χ_i^1 is in this case the solution of the following cell problem:

$$-\frac{\partial}{\partial y_i}\left[D_{ij}\left(I_{jk}+\frac{\partial \chi_k^1}{\partial y_j}\right)\right]+v_i^0\frac{\partial \chi_k^1}{\partial y_i}=n^{-1}\langle v_k^0\rangle - v_k^0\,, \tag{3.34}$$

$$-N_i\left[D_{ij}\left(I_{jk}+\frac{\partial \chi_k^1}{\partial y_j}\right)\right]=0 \quad \text{on } \Gamma\,, \tag{3.35}$$

where

$$\begin{aligned} &\chi_i^1=\chi_i^1(\mathbf{y}) \quad \text{is } \mathbf{y}\text{-periodic}\,,\\ &\langle \chi^1\rangle=\frac{1}{|\Omega|}\int\limits_{\Omega_l}\chi^1\,d\Omega=0\,. \end{aligned} \tag{3.36}$$

Remark that the presence of $\mathbf{v}^0$ in Eqs. (3.34)–(3.35) makes the vector χ_i depend on the macroscopic gradient of pressure.

It can be shown that the dispersion tensor $\mathbf{D}^{**}$ is positive definite but in general case non-symmetric. The expression (3.33) consists of two components which both depend on the macroscopic gradient of pressure and therefore can be said to represent the dispersive character. In general, it is then impossible to separate in $\mathbf{D}^{**}$ the purely diffusive component and the hydrodynamical contribution [2].

In order to derive the differential equation governing the average concentration $\langle c\rangle$, Eq. (3.31) is added to Eq. (3.32) multiplied by ε. After some transformations the final form of the dispersion equation is obtained. It gives the macroscopic model approximation within an error $O(\varepsilon^2)$

$$\varepsilon R_d\frac{\partial\langle c\rangle}{\partial t}-\varepsilon\frac{\partial}{\partial x_i}\left(D_{ij}^{**}\frac{\partial\langle c\rangle}{\partial x_j}\right)+\frac{\partial}{\partial x_i}(\langle v_i\rangle\langle c\rangle)=O(\varepsilon^2)\,. \tag{3.37}$$

Note that the dispersive term as well as the transient term are of the order ε in the macroscopic equation (3.37).

3.7. The case of $P_l = O(\varepsilon^1)$, $Q_l = O(\varepsilon^1)$ and $\mathrm{Pe}_l = O(\varepsilon^0)$

To see the competitive influence of advection with respect to the other phenomena, the case considered in the Sec. 3.6 will be taken once again, but the parameters P_l and Q_l will be increased each by one order of magnitude. The equations to be investigated are

$$\varepsilon\frac{\partial c}{\partial t}+\frac{\partial}{\partial y_i}\left(-D_{ij}\frac{\partial c}{\partial y_j}+v_i c\right)=0\,, \tag{3.38}$$

$$-N_i\left(D_{ij}\frac{\partial c}{\partial y_j}\right)=\varepsilon\alpha\frac{\partial c}{\partial t} \quad \text{on } \Gamma\,. \tag{3.39}$$

The homogenisation procedure applied to this problem gives for the first order approximation the macroscopic governing equation which does not contain the diffusive term. Instead, it consists of the transient term related to the microscopic transient term as well as the adsorption and the advection terms

$$R_d\frac{\partial c^0}{\partial t}+\frac{\partial}{\partial x_i}(\langle v_i^0\rangle c^0)=0\,. \tag{3.40}$$

The next order approximation of the macroscopic equation is obtained in the form

$$R_d\frac{\partial\langle c^1\rangle}{\partial t} - \frac{\partial\langle c^0\rangle}{\partial t}\frac{\partial}{\partial x_i}(\alpha\langle\chi_i^2\rangle_\Gamma) + \frac{\partial}{\partial x_i}(\langle v_i^1\rangle\langle c^0\rangle + \langle v_i^0\rangle\langle c^1\rangle) - \frac{\partial}{\partial x_i}(D_{ij}^{***})\frac{\partial\langle c^0\rangle}{\partial x_j} = 0\,, \tag{3.41}$$

where the symbol $\langle\ \rangle_\Gamma$ means

$$\langle\chi_i^2\rangle_\Gamma = \frac{1}{|\Omega|}\int_\Gamma \chi_i^2\, dS\,. \tag{3.42}$$

Remark that the second term in the expression (3.41) represents the additional adsorption contribution defined as the interaction between the macroscopic gradient of the temporal changes of the averaged concentration field $\langle c^0\rangle$ and the surface integral of the microscopic vectorial field $\langle\chi_i^2\rangle_\Gamma$. If the quantities α and $\langle\chi_i^2\rangle_\Gamma$ are assumed to be x-independent, then the classical macroscopic dispersion equation is obtained.

The tensor $\mathbf{D}^{***}$ is expressed as

$$D_{ij}^{***} = \frac{1}{|\Omega|}\int_{\Omega_l}\left\{D_{ik}\left(I_{kj} + \frac{\partial\chi_j^2}{\partial y_k}\right) - v_i^0\chi_j^2 + v_j^0\frac{\alpha}{R_d}\langle\chi_i^2\rangle_\Gamma\right\} d\Omega\,. \tag{3.43}$$

Note that $\mathbf{D}^{***}$ depends on the adsorption coefficient α and therefore may be called the dispersion-adsorption coefficient. It can be shown that $\mathbf{D}^{***}$ is positive definite but in general case nonsymmetric.

The local boundary value problem for determining the vectorial field χ^2 is the following:

$$-\frac{\partial}{\partial y_i}\left[D_{ij}\left(I_{jk} + \frac{\partial\chi_k^2}{\partial y_j}\right)\right] + v_i^0\frac{\partial\chi_k^2}{\partial y_i} = \langle v_k^0\rangle^* - v_k^0\,, \tag{3.44}$$

$$-N_i\left[D_{ij}\left(I_{jk} + \frac{\partial\chi_k^2}{\partial y_j}\right)\right] = -\alpha\langle v_k^0\rangle^* \quad \text{on } \Gamma\,, \tag{3.45}$$

where $\chi_i^2 = \chi_i^2(\mathbf{y})$ is $\mathbf{y}$-periodic

$$\langle\chi^2\rangle = \frac{1}{|\Omega|}\int_{\Omega_l}\chi^2\, d\Omega = 0\,. \tag{3.46}$$

Remark that χ^2 depends this time not only on the advection but also on the adsorption phenomenon. Moreover, in this case the pollutant is transported with the velocity $\langle\mathbf{v}\rangle^*$ equal to the effective fluid velocity divided by the retardation factor.

Finally, the equation governing the average concentration $\langle c\rangle$ can be determined by adding Eq. (3.40) to Eq. (3.41) multiplied by ε.

$$R_d^*\frac{\partial\langle c\rangle}{\partial t} - \varepsilon\frac{\partial}{\partial x_i}\left(D_{ij}^{***}\frac{\partial\langle c\rangle}{\partial x_j}\right) + \frac{\partial}{\partial x_i}(\langle v_i\rangle\langle c\rangle) = O(\varepsilon^2)\,, \tag{3.47}$$

where

$$R_d^* = R_d - \varepsilon\frac{\partial}{\partial x_i}(\alpha\langle\chi_i^2\rangle_\Gamma)\,. \tag{3.48}$$

If Eq. (3.47) is compared with Eq. (3.37), it can be concluded that the increase by one in the order of magnitude of parameters P_l and Q_l causes that the transient term $R_d^* \dfrac{\partial \langle c \rangle}{\partial t}$ in the macroscopic equation becomes of the order one.

4. Example

As an example, a layered medium showed in Fig. 4 will be analysed. The medium is composed of the horizontal impermeable layers forming the spatially periodic structure. Note that the pores are not connected. The unidirectional flow of a solvent with velocity vector parallel to the y_1-axis (the horizontal direction) will be considered. It is assumed that the solute particles diffuse in the solvent and undergo adsorption on the surface.

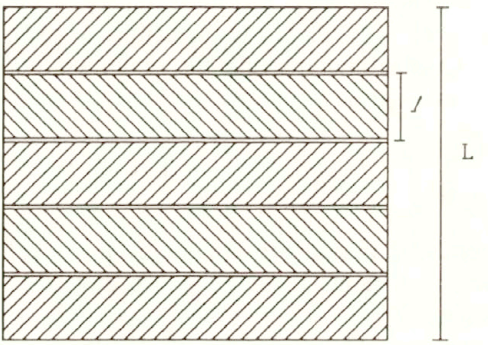

FIG. 4.

Three different forms of the dispersion tensor in relation to the order of magnitude of the dimensionless parameters P_l, Q_l and Pe_l were obtained.

CASE $P_l = O(\varepsilon^2)$, $Q_l = O(\varepsilon^2)$, $\mathrm{Pe}_l = O(\varepsilon^1)$,

$$\mathbf{D}^* = \begin{vmatrix} n\,D & 0 & 0 \\ 0 & 0 & 0 \\ 0 & 0 & n\,D \end{vmatrix}. \tag{4.1}$$

CASE $P_l = O(\varepsilon^2)$, $Q_l = O(\varepsilon^2)$, $\mathrm{Pe}_l = O(\varepsilon^0)$,

$$\mathbf{D}^{**} = \begin{vmatrix} D_{11}^{**} & 0 & 0 \\ 0 & 0 & 0 \\ 0 & 0 & n\,D \end{vmatrix}, \tag{4.2}$$

$$D_{11}^{**} = \frac{h}{H} D \left[1 + \frac{1}{2\,3\,5\,7} (\mathrm{Pe})^2 \right]. \tag{4.3}$$

It should be noted that this tensor represents the classical Taylor dispersion coefficient.

CASE $P_l = O(\varepsilon^1)$, $Q_l = O(\varepsilon^1)$, $\mathrm{Pe}_l = O(\varepsilon^0)$

$$\mathbf{D}^{***} = \begin{vmatrix} D_{11}^{***} & 0 & 0 \\ 0 & 0 & 0 \\ 0 & 0 & n\,D \end{vmatrix}, \tag{4.4}$$

$$D_{11}^{***} = \frac{h}{H} D \left[1 + \frac{1}{2357} (\mathrm{Pe})^2 \frac{1 + 18\,\mathrm{Da} + 102(\mathrm{Da})^2}{(1 + 2\,\mathrm{Da})^2} \right], \tag{4.5}$$

where the Peclet number and the Damköhler number are written as

$$\mathrm{Pe} = \frac{\langle v_1^0 \rangle \frac{H}{h} h}{D}, \tag{4.6}$$

$$\mathrm{Da} = \frac{Q_l}{P_l} = \frac{\alpha}{h}, \tag{4.7}$$

and $n = h/H$ means the porosity.

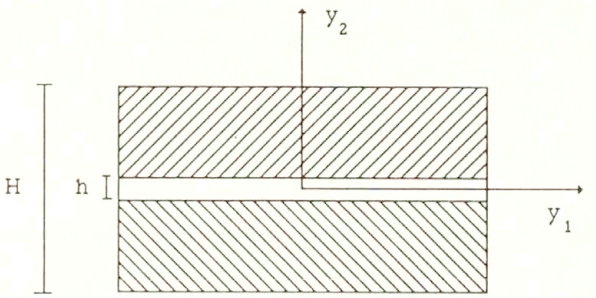

FIG. 5. The periodic cell.

The formula (4.5) contains the effect of adsorption. It corresponds to the result derived by DUNGAN, SHAPIRO and BRENNER [5]. They used a variant of a Taylor–Aris method-of-moments scheme [4] to study convective-diffusive transport of chemically reactive solute for a general model of multiphase system composed of ordered or disordered particles of arbitrary shapes and sizes. However, in the method proposed in this paper no assumption is made on the form of the macroscopic equation.

Remark that if $Q_l = O(\varepsilon^1)$ tends to $Q_l = O(\varepsilon^2)$, the contribution to the longitudinal dispersion from adsorption vanishes and $\mathbf{D}^{***} = \mathbf{D}^{**}$.

5. Conclusions

Expressions for the macroscopic dispersion tensors and the macroscopic governing equations were derived by the double scale asymptotic development method. The proposed approach is rigorous in the mathematical sense. The complete macroscopic laws were obtained without any a priori assumptions as to their character. The derivation is made entirely on the basis of the governing equations valid on the local level where the medium is heterogeneous. It should be noted that the method allows to examine a whole class of transport processes in heterogeneous media with respect to different dominating phenomena. It is interesting to remark that the three investigated cases reveal a characteristic length of adsorption α of the same order of magnitude as the pore size l. This conclusion comes from the following:

$$\frac{Q_l}{P_l} = \frac{\alpha}{l} = O(1).$$

In result the adsorption effects survive the macroscopisation process.

As an example, the case of unidirectional flow of a pollutant in a spatially periodic porous medium has been considered. The classical formula for Taylor dispersivity between parallel plates in the absence of adsorption has been rederived. The adsorption-dispersion tensor in the case of strong advection, diffusion and adsorption has been shown to correspond to the one given by DUNGAN *et al.*, [5].

Acknowledgement

This research was performed in the framework of the cooperation agreement between the Institut de Mécanique de Grenoble (now Sols, Solides, Structures Laboratory), France and the Geotechnical Department of the Gdańsk University of Technology, Poland. The work presented in this paper was supported by the grant from the Ministère de la Recherche et de la Technologie, France, followed by the grant from the Région Rhône–Alpes (the TEMPRA program) — to the second author.

References

1. J. L. AURIAULT, *Heterogeneous medium. Is an equivalent macroscopic description possible?*, Int. J. Engng. Sci., **29**, 7, 785–795, 1991.
2. J. BEAR and A. VERRUIJT, *Modelling ground water flow and pollution*, D. Reidel Publ. Comp., 1987.
3. A. BENSOUSSAN, J. L. LIONS and G. PAPANICOLAOU, *Asymptotic analysis for periodic structures*, North-Holland, 1979.
4. H. BRENNER and M. ADLER, *Dispersion resulting from flow through spatially periodic porous media*, II. Surface and inter-particle transport, Phil. Trans. R. Soc. Lond., **A 307**, 149–200, 1982.
5. S. R. DUNGAN, M. SHAPIRO and H. BRENNER, *Convective-diffusive-reactive Taylor dispersion processes in particulate multiphase systems*, Proc. R. Soc. Lond., **A 429**, 639–671, 1990.
6. V. N. NIKOLAEVSKI, *Convective diffusion in porous media*, J. Appl. Mech. (PMM), **23**, 6, 1042–1050, 1959.
7. E. SANCHEZ-PALENCIA, *Non-homogeneous media and vibration theory*, Lecture Note in Physics, 127, Springer-Verlag, Berlin 1980.
8. A. E. SCHEIDEGGER, *General theory of dispersion in porous media*, J. Geophys. Res., **66**, 3273–3278, 1961.

SOLS, SOLIDES, STRUCTURES, IMG,
DOMAINE UNIVERSITARE, GRENOBLE, FRANCE
AND
GEOTECHNICAL DEPARTMENT
GDAŃSK UNIVERSITY OF TECHNOLOGY, GDAŃSK.

Received October 7, 1992.

Arch. Mech., 45, 1, pp. 65–75, Warszawa 1993

Nonlinear torsional vibration analysis of the drive systems using one-dimensional elastic waves

R. BOGACZ and T. SZOLC (WARSZAWA)

IN THE PAPER nonlinear transient and steady-state torsional vibrations of the drive systems are investigated. Considerations are performed using discrete-continuous models consisting of rigid bodies of constant and variable mass moments of inertia connected with each other by means of cylindrical elastic elements with continuously distributed parameters as well as by means of massless nonlinear torsional springs. An application of the d'Alembert solutions of the wave motion equations leads to appropriate systems of linear and nonlinear ordinary differential equations with a "shifted" argument. The shifted argument enables us to solve these systems of equations numerically in an appropriate sequence which, in comparison with coupled ordinary differential equations for analogous discrete models, essentially increases numerical efficiency and accuracy of the proposed method. In the numerical examples some nonlinear effects due to variation of mass moments of inertia, elastic coupling with nonlinear characteristics, dry friction in the clutch and due to a nonlinear character of damping are considered.

1. Introduction

TORSIONAL vibrations of the drive systems of machines and motor-vehicles driven by the internal combustion reciprocating engines or by the electric motors are usually a source of severe dynamic loads of shaft segments, couplings, gears and other elements. Because of this reason, possibly accurate analysis of torsional vibrations of the drive systems is extremely important for design optimization and to guarantee the system quality and reliability. This problem was considered so far by many authors using various methods in theoretical and practical aspects [1–3]. An analysis of torsional vibrations belongs now to routine practices during designing processes of the considered mechanical systems, where in majority of cases the calculations are based on linear models [1]. But an urge to obtain more and more accurate results of investigations makes the linear theory of torsional vibrations insufficient. The drive systems of machines and motor vehicles are characterized by nonlinear effects due to variations of mass moments of inertia of the reciprocating parts of the system, elastic couplings with nonlinear characteristics, dry friction in clutches and vibration absorbers, backlashes in the gear stages and joints, variation of the gear mesh stiffness as well as due to a nonlinear character of damping [2, 3]. For the nonlinear torsional vibration analysis the considered drive systems are usually represented by discrete mechanical models, motion of which is described by appropriate systems of ordinary differential equations. Determination of drive system's transient or steady-state nonlinear torsional response usually reduces to computer simulations in the form of a direct integration of the equations of motion [2, 3]. Although very many advanced numerical methods have been developed so far, such computer simulations for relatively long time of calculations with a sufficiently small integration step still require a big computation effort. Moreover, there are some problems with numerical stability and accuracy.

In order to overcome the difficulties mentioned above, in the paper an alternative method is proposed. This method is based on a discrete-continuous (hybrid) model of the drive system, for which the torsional wave propagation theory is applied for vibra-

tion analysis. This approach was applied in [4, 5] for crank mechanisms of the internal combustion reciprocating engines as well as in [6, 7] for the rotor machines.

2. Assumptions and formulation of the problem

In the paper the subject of considerations is the drive system of a machine driven by the internal combustion reciprocating engine. This system consists of elements of the engine crank mechanism, flywheel, dry friction clutch with elastic coupling, gear stages, Cardan universal joints, l rigid couplings and the machine rotor, connected with each other by means of shaft segments. The discrete model of such system is a combination of $n + 2m + l + 2$ rigid bodies of constant and variable mass moments of inertia $\overline{I}_i$, $i = 1, 2, \ldots, n + m + l + 2$, representing, respectively, masses of the engine auxiliary drive elements, n crank assemblies, flywheel, coupling halfs, gear wheels, joint elements and the driven machine rotor. These rigid bodies are connected by massless torsional springs of constant stiffnesses k_j, $j = 1, 2, \ldots, n + m + l + 1$, representing shaft segments as well as by means of m massless torsional springs of variable stiffnesses h_k, $k = n + 2, n + 3, \ldots, n + m + 1$, representing torsional flexibilities of the elastic coupling, gear stage meshings and Cardan universal joints, Fig. 1. It is assumed that the mass

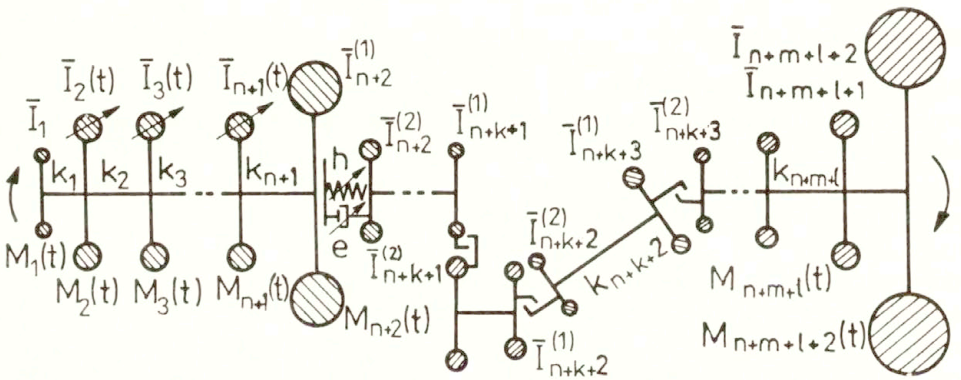

FIG. 1. Discrete model of the drive system.

moments of inertia $\overline{I}_j(\phi_j(t))$, $j = 2, 3, \ldots, n + 1$, of the rigid bodies corresponding to the engine crank assemblies, where t denotes time and ϕ_j — the j-th rigid body instantaneous angular displacement, are described by well known functions [2]. Internal and external damping in the system is represented by a linear model of the viscous type except the elastic coupling and the gear stages, for which nonlinear damping terms are introduced [2]. The considered system is excited to vibrations by the external torques $M_j(t)$, $j = 2, 3, \ldots, n + 1$, due to engine gas and inertia forces, as well as by constant or variable passive external torques $M_k(t)$, $k = 1, n + 2, n + 3, \ldots, n + m + l + 2$.

Equations of motion for this model are the following well known linear and nonlinear simultaneous ordinary differential equations [2, 3]:

$$
\begin{aligned}
(2.1)\quad & \overline{I}_1\ddot{\phi}_1(t) + d_1\dot{\phi}_1(t) - c_1[\dot{\phi}_2(t) - \dot{\phi}_1(t)] - k_1[\phi_2(t) - \phi_1(t)] = M_1(t)\,,\\
& \overline{I}_i(\phi_1)\ddot{\phi}_i(t) + [d_i + 0.5\dot{\phi}_i(t)L_i(\phi_i)]\dot{\phi}_i(t) + c_{i-1}[\dot{\phi}_i(t) - \dot{\phi}_{i-1}(t)] - c_i[\dot{\phi}_{i+1}(t) - \dot{\phi}_i(t)]\\
& \quad + k_{i-1}[\phi_i(t) - \phi_{i-1}(t)] - k_i[\phi_{i+1}(t) - \phi_i(t)] = M_i(t), \qquad i = 2, 3, \ldots, n + 1\,,
\end{aligned}
$$

$$
\begin{aligned}
(2.1)\quad & \bar{I}_k^{(1)}\ddot{\phi}_k^{(1)}(t) + d_k^{(1)}\dot{\phi}_k^{(1)}(t) + c_{k-1}[\dot{\phi}_k^{(1)}(t) - \dot{\phi}_{k-1}^{(2)}(t)] + \alpha_k e_k(\Delta\phi_k(t))[\alpha_k\dot{\phi}_k^{(1)}(t) \\
[\text{cont.}]\quad & - \beta_k\dot{\phi}_k^{(2)}(t)] + k_{k-1}[\phi_k^{(1)}(t) - \phi_{k-1}^{(2)}(t)] + \alpha_k h_k(\Delta\phi_k(t))[\alpha_k\phi_k^{(1)}(t) - \beta_k\phi_k^{(2)}(t)] \\
& = M_k^{(1)}(t), \\
& \bar{I}_k^{(2)}\ddot{\phi}_k^{(2)}(t) + d_k^{(2)}\dot{\phi}_k^{2}(t) - c_k[\dot{\phi}_{k+1}^{(1)}(t) - \dot{\phi}_k^{(2)}(t)] - \beta_k e_k(\Delta\phi_k(t))[\alpha_k\dot{\phi}_k^{(1)}(t) - \beta_k\dot{\phi}_k^{(2)}(t)] \\
& - k_k[\phi_{k+1}^{(1)}(t) - \phi_k^{(2)}(t)] - \beta_k h_k(\Delta\phi_k(t))[\alpha_k\phi_k^{(1)}(t) - \beta_k\phi_k^{(2)}(t)] = M_k^{(2)}(t), \\
& k = n+2, n+3, \ldots, n+m+1, \\
& \bar{I}_j\ddot{\phi}_j(t) + d_j\dot{\phi}_j(t) + c_{j-1}[\dot{\phi}_j(t) - \dot{\phi}_{j-1}(t)] - c_j[\dot{\phi}_{j+1}(t) - \dot{\phi}_j(t)] \\
& + k_{j-1}[\phi_j(t) - \phi_{j-1}(t)] - k_j[\phi_{j+1}(t) - \phi_j(t)] = M_j(t), \\
& j = n+m+2, n+m+3, \ldots, n+m+l+1, \\
& \bar{I}_{nml2}\ddot{\phi}_{nml2}(t) + d_{nml2}\dot{\phi}_{nml2}(t) + c_{nml1}(t)[\dot{\phi}_{nml1}(t) - \dot{\phi}_{nml2}(t)] \\
& + k_{nml1}[\phi_{nml1}(t) - \phi_{nml2}(t)] = M_{nml2}(t),
\end{aligned}
$$

where $L_i(\phi_i(t)) = d\bar{I}_i(\phi_i(t))/d(\phi_i(t))$, $i = 2, 3, \ldots, n+1$, $\Delta\phi_k(t) = \alpha_k\phi_k^{(1)}(t) - \beta_k\phi_k^{(2)}(t)$, $k = n+2, n+3, \ldots, n+m+1$, and d_j, c_l are, respectively, constant external and internal damping coefficients, $j = 1, 2, \ldots, n+m+l+2$, $l = 1, 2, \ldots, n+m+l+1$. However, functions $e_k(\Delta\phi_k(t))$ and $h_k(\Delta\phi_k(t))$ denote nonlinear damping and stiffness coefficients, respectively, for the elastic coupling, gear stages and joints. Coefficients α_k and β_k are radii of the driving and driven gear wheels, respectively, for the case of gear stages. However, for the elastic coupling, friction clutch and for the Cardan universal joints α_k and β_k are equal to unity. Superscripts (1) and (2) are assigned to respective quantities corresponding to the driving and driven elements in the system, and $nml2 = n+m+l+2$, $nml1 = n+m+l+1$.

The above system of equations can be solved numerically using various direct integration methods. The most advantageous for this purpose seem to be the Runge–Kutta, Newmark, Hamming or the Taylor method [2, 3].

In order to avoid the mentioned numerical difficulties connected with integration of Eqs. (2.1), for the considered drive system an alternative discrete-continuous (hybrid) model is introduced. This model consists of the same number of rigid bodies like the discrete one, but the shaft segments of constant torsional flexibilities are represented by torsionally deformable cylindrical elastic elements with continuously distributed parameters of lengths l_i and identical stiffness values k_i, $i = 1, 2, \ldots, n+m+l+1$, Fig. 2. Only torsional flexibilities of the elastic coupling, gear stage meshings and the Cardan universal joints are represented by the massless springs of the same variable stiffnesses h_j, $j = n+2, n+3, \ldots, n+m+1$. The external torques as well as the variable components of the mass moments of inertia are described by identical functions as those in the case of discrete model. Moreover, in the hybrid model also external and internal damping is assumed in the form of analogous concentrated linear and nonlinear damping moments imposed on extreme cross-sections of the continuous elastic elements [4–8]. These moments due to external, internal and nonlinear damping are characterized by the same coefficients d_j, c_l and e_k, $j = 1, 2, \ldots, n+m+l+2$, $l = 1, 2, \ldots, n+m+l+1$, $k = n+2, n+3, \ldots, n+m+1$, respectively, as in the case of discrete model. The constant components of mass moments of inertia of the hybrid model rigid bodies are

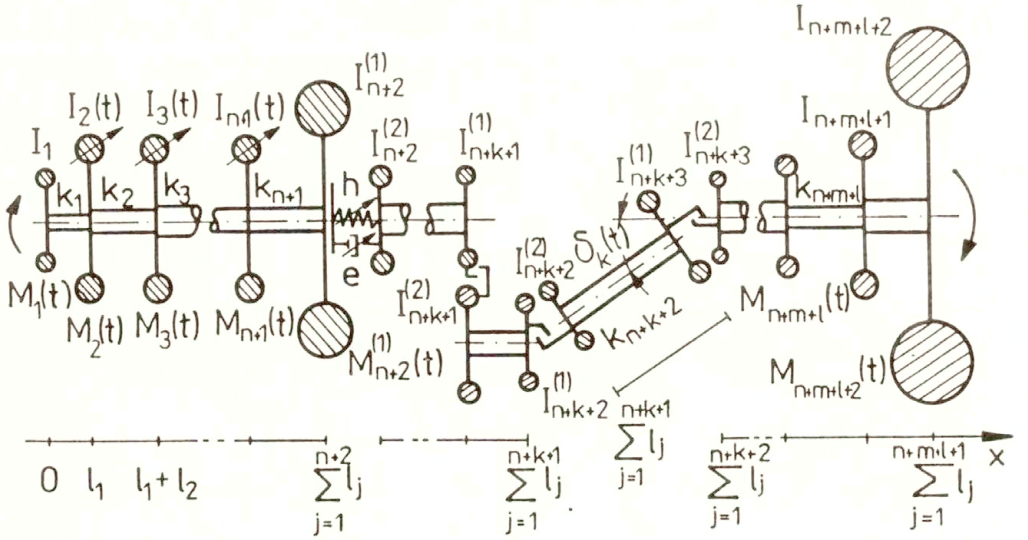

FIG. 2. Discrete-continuous model of the drive system.

determined using the proper parameter identification procedure [6] in order to keep the total mass moment of inertia of the system unchanged and, for the assumed stiffness and damping coefficients k_i, d_j, c_l with sufficiently small l_i, to obtain possibly small differences of the corresponding first natural frequencies and mode shape functions of linearized free vibrations in comparison with those of the discrete model.

Equations of motion for angular displacements of the elastic element's cross-sections of the hybrid model are the classical wave equations

$$a^2\Theta_{i,xx}(x,t) - \Theta_{i,tt}(x,t) = 0, \quad i = 1,2,\ldots,n+m+l+1, \tag{2.2}$$

where $a^2 = G/\rho$ and x is a spatial coordinate parallel to the system rotation axis, Fig. 2. These equations are solved with following boundary conditions

$$I_1\Theta_{1,tt} + d_1\Theta_{1,t} - c_1l_1\Theta_{1,xt} - k_1l_1\Theta_{1,x} = M_1(t), \quad \text{for} \quad x = 0,$$

$$I_i(\Theta_i)\Theta_{i,tt} + [d_i + 0.5\Theta_{i,t}L_i(\Theta_i)]\Theta_{i,t} + c_{i-1}l_{i-1}\Theta_{i-1,xt} - c_il_i\Theta_{i,xt}$$
$$+k_{i-1}l_{i-1}\Theta_{i-1,x} - k_il_i\Theta_{i,x} = M_i(t), \quad \Theta_{i-1} = \Theta_i, \quad i = 2,3,\ldots,n+1,$$
$$\text{for} \quad x = \sum_{j=1}^{i-1} l_j,$$

$$I_k^{(1)}\Theta_{k-1,tt} + d_k^{(1)}\Theta_{k-1,t} + c_{k-1}l_{k-1}\Theta_{k-1,xt} + \alpha_k e_k(\Delta\Theta_k(t))[\alpha_k\Theta_{k-1,t} - \beta_k\Theta_{k,t}]$$
$$+ k_{k-1}l_{k-1}\Theta_{k-1,x} + \alpha_k h_k(\Delta\Theta_k(t))[\alpha_k\Theta_{k-1} - \beta_k\Theta_k] = M_k^{(1)}(t), \tag{2.3}$$

$$I_k^{(2)}\Theta_{k,tt} + d_k^{(2)}\Theta_{k,t} - c_kl_k\Theta_{k,xt} - \beta_k e_k(\Delta\Theta(t))[\alpha_k\Theta_{k-1,t} - \beta_k\Theta_{k,t}]$$
$$-k_kl_k\Theta_{k,x} - \beta_k h_k(\Delta\Theta_k(t))[\alpha_k\Theta_{k-1} - \beta_k\Theta_k] = M_k^{(2)}(t),$$

$$\Delta\Theta_k(t) = \alpha_k\Theta_{k-1} - \beta_k\Theta_k, \quad \text{for} \quad x = \sum_{j=1}^{k-1} l_j, \quad k = n+2, n+3, \ldots, n+m+1,$$

$$I_j\Theta_{j,tt} + d_j\Theta_{j,t} + c_{j-1}l_{j-1}\Theta_{j-1,xt} - c_jl_j\Theta_{j,xt} + k_{j-1}l_{j-1}\Theta_{j-1,x} - k_jl_j\Theta_{j,x} = M_j(t),$$

$$\Theta_{j-1} = \Theta_j, \quad j = n+m+2, n+m+3, \ldots, nml1, \quad \text{for} \quad x = \sum_{i=1}^{j-1} l_i,$$

(2.3) [cont.]

$$I_{nml2}\Theta_{nml1,tt} + d_{nml2}\Theta_{nml1,t} + c_{nml1}l_{nml1}\Theta_{nml1,xt} + k_{nml1}l_{nml1}\Theta_{nml1,x} = M_{nml2}(t), \quad \text{for} \quad x = \sum_{j=1}^{nml1} l_j,$$

where the subscripts after commas denote partial differentiations (notice the analogy between the appropriate terms in the dynamic boundary conditions (2.3) and in the motion equations (2.1) for the discrete model). Solutions of Eqs. (2.2) are sought in the form of d'Alembert wave solutions

$$\begin{aligned}
\Theta_1(x,t) &= f_1(at - x + l_1) + g_1(at + x - l_1),\\
\Theta_i(x,t) &= f_i(at - x + \sum_{j=1}^{i-1} l_j) + g_i(at + x - \sum_{j=1}^{i-1} l_j), \quad i = 2,3,\ldots,n+1,\\
\Theta_k(x,t) &= f_k(at - x + \sum_{j=1}^{n-1} l_j) + g_k(at + x - \sum_{j=1}^{n-1} l_j - 2\sum_{j=n}^{k-1} l_j),\\
&\qquad k = n+2, n+3, \ldots, n+m+l+1.
\end{aligned} \tag{2.4}$$

The functions f_i and g_i in Eqs. (2.4) represent torsional waves propagating in the elastic elements as a result of the external torque applied. They are determined by the boundary and initial conditions [4–8]. Thus, substituting Eqs. (2.4) into the boundary conditions (2.3) leads to the following system of linear and nonlinear ordinary differential equations with a "shifted" argument z for the functions f_i and g_i, $i = 1, 2, \ldots, n+m+l+1$,

$$\begin{aligned}
&r_{21}f''_1(z) + r_{11}f'_1(z) = M_1(z) + s_{21}g''_1(z - 2l_1) + s_{11}g'_1(z - 2l_1),\\
&r_{2,nml2}g''_{nml1}(z) + r_{1,nml2}g'_{nml1}(z) = M_{nml2}(z) + s_{2,nml2}f''_{nml1}(z - 2l_{nml1})\\
&\qquad + s_{1,nml2}f'_{nml1}(z - 2l_{nml1}),\\
&g'_i(z) = -f'_i(z - 2l_i) + f'_{i+1}(z - l_i) + g'_{i+1}(z - l_i), \quad i = 2,3,\ldots,n,\\
&g'_j(z) = -f'_j(z - 2l_j) + f'_{j+1}(z - 2l_j) + g'_{j+1}(z - 2l_j),\\
&\qquad j = n+m+1, n+m+2, \ldots, n+m+l,\\
&r_{22}(z)f''_2(z) + r_{12}(z)f'_2(z) = M_2(z) + s_{22}(z)g''_2(z) + s_{12}(z)g'_2(z) + t_{22}f''_1(z)\\
&\qquad + t_{12}f'_1(z),\\
&r_{2i}(z)f''_i(z) + r_{1i}(z)f'_i(z) = M_i(z) + s_{2i}(z)g''_i(z) + s_{1i}(z)g'_i(z) + t_{2i}f''_{i-1}(z - l_{i-1})\\
&\qquad + t_{1i}f'_{i-1}(z - l_{i-1}), \; i = 3,4,\ldots,n+1,\\
&\begin{bmatrix} p_{2,k-1} & 0 \\ 0 & r_{2,k} \end{bmatrix} \begin{bmatrix} g''_{k-1}(z + 2l_{k-1}) \\ f''_k(z) \end{bmatrix} + \begin{bmatrix} p_{1,k-1}(z) & -\alpha_k\beta_k e_k(\Delta_k(z)) \\ -\alpha_k\beta_k e_k(\Delta_k(z)) & r_{1,k}(z) \end{bmatrix}\\
&\begin{bmatrix} g'_{k-1}(z + 2l_{k-1}) \\ f'_k(z) \end{bmatrix} + \begin{bmatrix} \alpha_k^2 h_k(\Delta_k(z)) & -\alpha_k\beta_k h_k(\Delta_k(z)) \\ -\alpha_k\beta_k h_k(\Delta_k(z)) & \beta_k^2 h_k(\Delta_k(z)) \end{bmatrix} \begin{bmatrix} g_{k-1}(z + 2l_{k-1}) \\ f_k(z) \end{bmatrix}\\
&\qquad = \begin{bmatrix} M_k^{(1)}(z) + u_{2,k-1}f''_{k-1}(z) \\ M_k^{(2)}(z) + s_{2,k}g''_k(z) \end{bmatrix}
\end{aligned} \tag{2.5}$$

$$
\begin{aligned}
(2.5)_{[\text{cont.}]}\quad & +u_{1,k-1}(z)f'_{k-1}(z)+\alpha_k\beta_k e_k(\Delta_k(z))g'_k(z)+\alpha_k h_k(\Delta_k(z))[\beta_k g_k(z)-\alpha_k f_{k-1}(z)] \\
& +s_{1k}(z)g'_k(z)+\alpha_k\beta_k e_k(\Delta_k(z))f'_{k-1}(z)-\beta_k h_k(\Delta_k(z))[\beta_k g_k(z)-\alpha_k f_{k-1}(z)]\Big]
\end{aligned}
$$

$$
\Delta_k(z)=\alpha_k[f_{k-1}(z)+g_{k-1}(z+2l_{k-1})]-\beta_k[f_k(z)+g_k(z)],
$$

$$
k=n+2,n+3,\ldots,n+m+1,
$$

$$
r_{2j}f''_j(z)+r_{1j}f'_j(z)=M_j(z)+s_{2j}g''_j(z)+s_{1j}g'_j(z)+t_{2j}f''_{j-1}(z)+t_{1j}f'_{j-1}(z),
$$

$$
j=n+m+2,n+m+3,\ldots,n+m+l+1,
$$

$$
g'_1(z)=-f'_1(z)+f'_2(z)+g'_2(z),
$$

where

$$
r_{21}=c_1l_1+aI_1,\ r_{11}=l_s(k_1l_1+ad_1)/a,\quad s_{21}=c_1l_1-aI_1,\quad s_{11}=l_s(k_1l_1-ad_1)/a,
$$

$$
r_{2,nml2}=c_{nml1}l_{nml1}+aI_{nml2},\quad r_{1,nml2}=l_s(k_{nml1}l_{nml1}+ad_{nml2})/a,
$$

$$
s_{2,nml2}=c_{nml1}l_{nml1}-aI_{nml2},\quad s_{1,nml2}=l_s(k_{nml1}l_{nml1}-ad_{nml2})/a,
$$

$$
r_{2i}(z)=c_il_i+c_{i-1}l_{i-1}+aI_i(z),\quad r_{1i}(z)=l_s[k_il_i+k_{i-1}l_{i-1}+a(d_i+\Omega_i(z)L_i(z))]/a,
$$

$$
s_{2i}(z)=c_il_i-c_{i-1}l_{i-1}-aI_i(z),\quad s_{1i}(z)=l_s[k_il_i-k_{i-1}l_{i-1}-a(d_i+\Omega_i(z)L_i(z))]/a,
$$

$$
t_{2i}=2c_{i-1}l_{i-1},\quad t_{1i}=2k_{i-1}l_{i-1}l_s/a,\quad \Omega_i(z)=0.5[f'_i(z)+g'_i(z)],
$$

$$
i=2,3,\ldots,n+1,n+m+2,n+m+3,\ldots,n+m+l+1,
$$

$$
p_{2,k-1}=c_{k-1}l_{k-1}+aI_k^{(1)},\quad p_{1,k-1}(z)=l_s[k_{k-1}l_{k-1}+a(d_k^{(1)}+\alpha_k^2e_k(\Delta_k(z)))]/a,
$$

$$
u_{2,k-1}=c_{k-1}l_{k-1}-aI_k^{(1)},\quad u_{1,k-1}(z)=l_s[k_{k-1}l_{k-1}-a(d_k^{(1)}-\alpha_k^2e_k(\Delta_k(z)))]/a,
$$

$$
r_{2,k}=c_kl_k+aI_k^{(2)},\quad r_{1,k}(z)=l_s[k_kl_k+a(d_k^{(2)}+\beta_k^2e_k(\Delta_k(z)))]/a,
$$

$$
s_{2,k}=c_kl_k-aI_k^{(2)},\quad s_{1,k}(z)=l_s[k_kl_k-a(d_k^{(2)}-\beta_k^2e_k(\Delta_k(z)))]/a,
$$

$$
k=n+2,n+3,\ldots,n+m+1
$$

and l_s is an arbitrary value. Using the Newmark method to solve Eqs. (2.5) together with Eqs. (2.4), one obtains a system transient or steady-state dynamic response in the form of tangential stresses, torques, angular velocities and displacements of arbitrary cross-sections of the hybrid model elastic elements. The "shifted" argument in Eqs. (2.5), which is a consequence of the wave interpretation of torsional vibrations, makes their right-hand sides always known in each computation step. Thus, contrary to coupled equations (2.1) for the discrete model, it is possible to solve equations (2.5) successively, one after another, in the presented order. This feature very essentially simplifies the numerical procedure making it much more efficient, stable and accurate, which will be confirmed by numerical examples.

3. Numerical results

The proposed wave method of torsional vibration analysis was compared with the traditional ones based on the discrete model. Numerical calculations were performed for systems consisting only of the crank mechanisms of 4 and 6 cylinder in-line engines, i.e. for $n=4$ or $n=6$ and for $m=l=0$, in steady-state operating conditions. Figure 3a presents plots of dynamic angular displacements of the crankshaft's free end of the 4-cylinder Diesel engine of the automobile type in resonant operating conditions. However, Fig. 3b presents plots of tangential stresses in the 7-th journal of the crankshaft of the

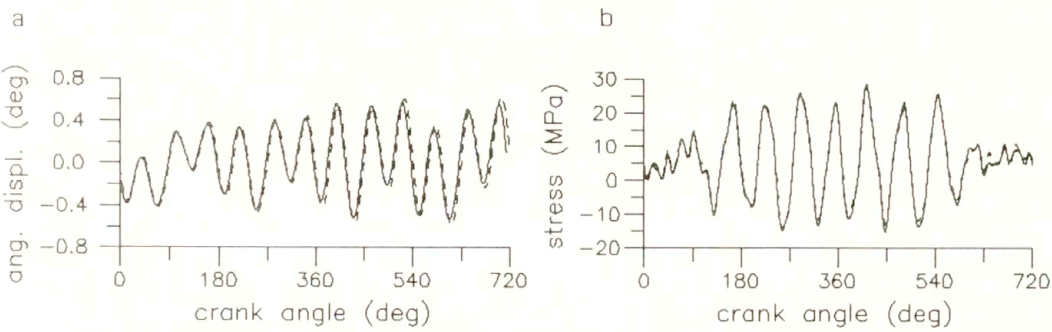

FIG. 3. Steady state response of the crank mechanisms of (a) 4-cylinder and (b) 6-cylinder engine using the wave (—) and the Hamming (- - -) method.

6-cylinder medium-speed Diesel engine at nominal operating conditions. The obtained results of steady-state vibrations for the crank mechanisms of the engines mentioned above, where for the discrete model the Hamming method was applied, are characterized by very similar plot shapes. For the investigated cases the greatest discrepancies of extreme values did not exceed 6–8%. But the wave method requires about 2.5–3.0 times shorter computation time with an excellent numerical stability, contrary to the Hamming method. For the same cases the Runge–Kutta and the Taylor methods are characterized by better stability than the Hamming method, but they require much longer computation time [4].

For the linear hybrid model, where the variable mass moments of inertia of the reciprocating parts of the engine were represented by their average values, the wave method was also compared with the well known Fourier method [1] for 24 and 36 harmonics. Then, discrepancies of results for steady-state vibrations are greater and reach 40%, particularly for more "peaky" torsional responses. Figure 4 presents exemplary plots of tangential stresses in the 5-th crankshaft journal of the 4-cylinder carburettor engine of the automobile type. For resonant operating conditions at the rotational speed 4250 [rpm], where the curves of system response are characterized by fluent "quasi-sinusoidal" shapes, the wave and the Fourier method yield quite similar results, Fig. 4a. However, for non-resonant operating conditions at the speed 2000 [rpm], where the system response is more "peaky", essential discrepancies of results take place, Fig. 4b. The peaks yielded by means of the Fourier method are smoothed in comparison with those obtained by the wave method and the hybrid model. Thus, one may expect that the wave approach is more accurate. Moreover, it should be noticed that, for the compared models of the 4- and 6-cylinder engine crank mechanisms, computation times for the wave method and the Fourier method were comparable.

From the above comparisons it follows, that the wave method based on the hybrid mechanical model is characterized by the greatest numerical efficiency, and very good stability as well as a numerical accuracy of this method seems to be higher. Because of these advantages, the proposed approach is most convenient for relatively long in time nonlinear transient vibration analyses. As an example, a run-up simulation was performed for the drive system of a machine driven by the 6-cylinder in line Diesel engine by means of the elastic coupling and two rigid couplings, i.e. for $n = 6$, $m = 1$ and $l = 2$. The characteristic of the elastic coupling was assumed to be linear or progressive and degressive hyperbolic sinusoidal. But the damping coefficient $\epsilon_8(\Delta\Theta_8(t))$

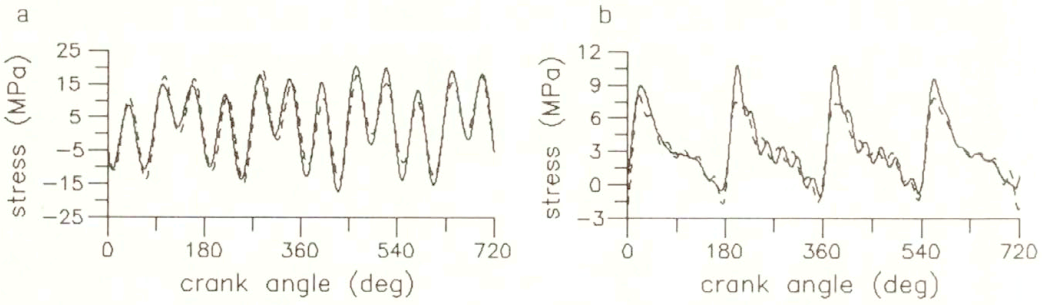

FIG. 4. Tangential stresses obtained by means of the wave (—) and the Fourier (- - -) method for (a) resonant and (b) non-resonant operating conditions.

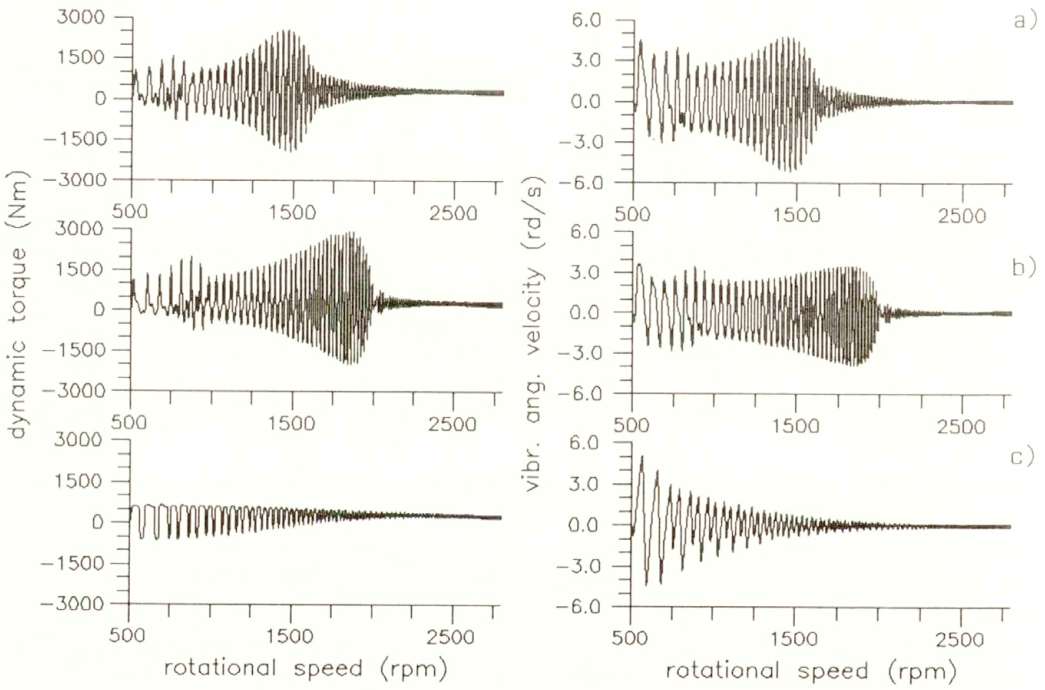

FIG. 5. System transient response for various coupling characteristics.

was described by the constant or parabolic function [2]. This system was accelerated from the average rotational speed 500 [rpm] to the nominal speed equal to 2800 [rpm]. Figure 5a presents plots of the system response for constant h_8 and e_8 in the form of dynamic torque transmitted by the drive-shaft segment (8), and in the form of vibratory angular velocity of the machine rotor. However, Figs. 5b and c present plots of the mentioned quantities for variable h_8 and e_8, where Fig. 5b corresponds to the progressive coupling characteristic and Fig. 5c corresponds to the degressive one. Plots in Fig. 5a are characterized by relatively fluent increase and decrease of local extremes occurring during a passage through the resonance zone. For the progressive characteristic of the coupling and the variable damping coefficient e_8 one obtains greater extreme values of the dynamic

torque and smaller extreme values of the angular velocity than those for constant h_8 and e_8, Fig. 5b. Moreover, in this case the transient response of the system reaches maximum at higher value of the shaft average rotational speed, and then decays rapidly. However, for the degressive coupling characteristic and variable e_8 the system response increases rapidly to reach a maximum at smaller value of the rotational speed than in the case of constant h_8 and e_8, Fig. 5c. The extreme values of the torque are much smaller, but peaks of the angular velocity are slightly greater only at the beginning of the run-up. From this exemplary comparison it follows, that the elastic coupling with degressive characteristic seems to be optimum for the drive system considered.

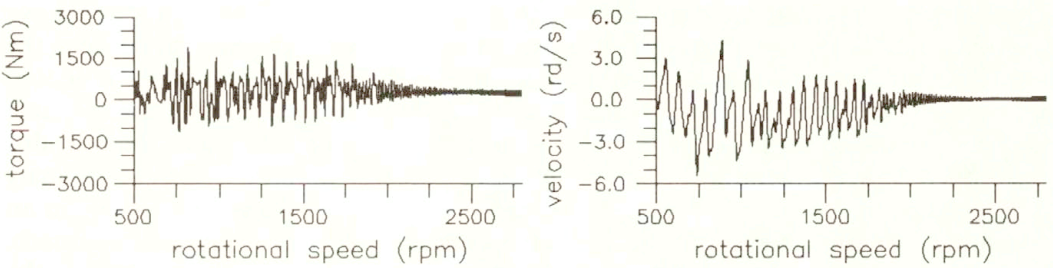

FIG. 6. Transient response of the system with the friction clutch of the overload type.

In the case of coupling with progressive characteristic, in order to minimize the extreme values of the drive shaft transient response, a dry friction clutch of the overload type was applied [2], Fig. 2. The dry friction characteristic of the clutch was assumed according to the Coulomb model [2]. This clutch was expected to transmit maximal torque, the value of which did not exceed 1.5 of the maximal average torque produced by the engine. For this case Fig. 6 presents plots of the dynamic torque in the drive shaft and of the vibratory angular velocity of the machine rotor. A character of the obtained curves is completely different than that of the curves in Fig. 5b. The overload friction clutch in the drive system caused an essential decrease of extreme values of the dynamic torque transmitted by the drive shaft.

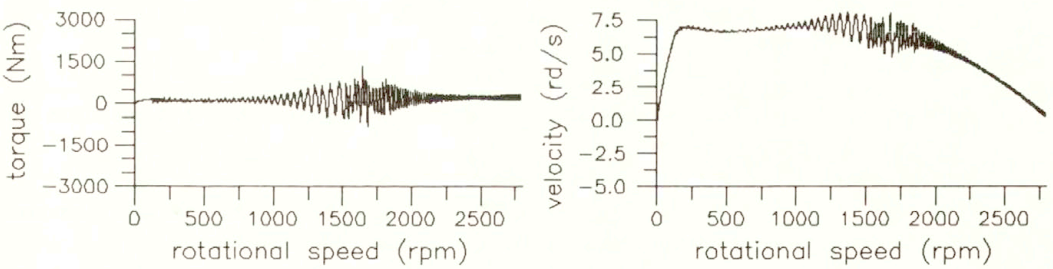

FIG. 7. Transient response due to run-up of the system with friction clutch of the disengaging type.

During run-up of the machine the smallest values of the dynamic torque in the drive shaft were obtained, when the machine was started from its rest, i.e. from null rotational speed, by means of the disengaging friction clutch. Figure 7 presents plots of the dynamic torque in the drive shaft and of the vibratory angular velocity of the machine rotor, where

the initial average rotational speed of the engine shaft was 500 [rpm] and then the system was accelerated to the common nominal speed 2800 [rpm], and where a duration of the clutch fluent engaging was equal to 1.5 [s]. In this case fluctuations of the machine rotor vibratory angular velocity were also characterized by the smallest local amplitudes in comparison with the previous cases presented in Figs. 5 and 6.

4. Final remarks

In the presented paper nonlinear torsional vibrations of the drive system were investigated. For this purpose a discrete-continuous (hybrid) model and the torsional wave propagation theory were applied. In the performed considerations, for the proposed wave approach and for the methods applied so far, the analogies were emphasized between the respective mechanical and mathematical models. Nevertheless, because of a continuous distribution of mass in the elastic elements representing the shaft segments, one can state that the discrete-continuous mechanical model better corresponds to reality than the discrete one. Moreover, the wave interpretation of torsional vibrations leads to ordinary differential equations with a "shifted" argument, which one can solve successively in an appropriate order. This feature of the mathematical model of the proposed approach, in comparison with the classical methods based on the discrete model described by the coupled ordinary differential equations, causes an essential increase of the numerical efficiency of the presented procedure, as well as yields a very good numerical stability, which was confirmed by the numerical examples. Also the numerical accuracy of this method seems to be higher than the accuracy of the methods based on the discrete model applied so far. Thus, the wave method can be particularly advantageous (from the practical standpoint) for nonlinear transient vibration analyses for relatively long time spans.

For example, the presented procedure enabled us to investigate an influence of the elastic coupling characteristic on the transient torsional response of the drive system due to run-up. Moreover, an application of this method made it possible to select an appropriate type of the friction clutch for the considered drive system in order to obtain minimal extreme values of the transmitted dynamic torques and the smallest fluctuations of angular velocity of the driven machine rotor.

References

1. S. DOUGHTY, *Steady-state torsional response with viscous damping*, Trans. ASME, J. Vibr. Acous. Stress and Rel. in Design, **107**, pp. 123–127, 1985.
2. A. LASCHET, *Simulation von Antriebssystemen*, Springer-Verlag 1988.
3. B.F. EVANS, A.J. SMALLEY, H.R. SIMONS, *Startup of synchronous motor drive trains: the application of transient torsional analysis to cumulative fatigue assessment*, Trans. ASME, No. 85-DET-122.
4. W. NADOLSKI, A. PIELORZ, *Dynamic investigation of the main journals of two-cylinder engine crankshaft with damping*, Intern. J. Mech. Sci., **25**, 12, pp. 887–898, 1983.
5. T. SZOLC, *Modelling of the crank mechanisms of internal combustion engines using torsional elastic waves*, Doct. Dissert., Inst. of Fundamental Technological Research, Warsaw 1985 [in Polish].
6. R. BOGACZ, H. IRRETIER and T. SZOLC, *Analysis of transient torsional vibrations of the rotor machine using a hybrid model*, Proc. of the 3rd Int. Conf. on Rotordynamics, IFToMM, Eds du CNRS, pp. 207–211, Lyon 1990.

7. R. BOGACZ, T. SZOLC, H. IRRETIER, *An application of torsional wave analysis to turbogenerator rotor shaft response*, Trans. ASME, J. Vibr. and Acoust., **114**, pp. 149–153, 1992.
8. W. NADOLSKI, *Application of wave method in investigations of single gear transmission*, Ingenieur-Archiv, **58**, pp. 329–338, 1988.

POLISH ACADEMY OF SCIENCES
INSTITUTE OF FUNDAMENTAL TECHNOLOGICAL RESEARCH

Received November 9, 1992.

Arch. Mech., 45, 1, pp. 77–91, Warszawa 1993

On the compatibility conditions in the fluid-fluid saturated porous solid contact problems

M. CIESZKO and J. KUBIK (POZNAŃ)

COMPATIBILITY CONDITIONS for macroscopic mechanical fields at the material discontinuity surface formed by the permeable boundary of a fluid-saturated porous solid being in contact with flowing viscous bulk fluid are considered. The conditions are derived by means of the standard discontinuity analysis applied to the general balance equations for mass, linear momentum and mechanical energy. Within the saturated porous solid region the macroscopic description of immiscible porous solid-fluid mixture is applied, while in the bulk fluid region the governing equation are those of Newtonian fluid mechanics. It has been shown that at the surface of porous skeleton there exists a dissipation of mechanical energy due to the fluid viscosity, for which the constitutive relation is proposed. It has been proved that this dissipation directly influences the form of linear compatibility conditions for the tangential components of the relative fluid velocities, and that the condition postulated by BEAVERS and JOSEPH [2] is a special case of the condition obtained in the paper.

1. Introduction

IN PROBLEMS of fluid flow through porous solids with permeable boundary it is necessary to describe the flow conditions to be imposed at the interface between regions of a fluid flow in a porous skeleton and the adjacent bulk fluid flow. There exists a number of works which describe coupled fluid motions satisfying the Navier–Stokes equations in the bulk fluid, some averaged or semi-empirical equations (typically Darcy's law) within the porous material and propose the matching conditions at the common boundaries (see ref. in [1]).

The classical conditions at the permeable boundary are, for a viscous fluid, the continuity of the fluid pressure and the normal velocity across the surface, and vanishing of the tangential velocity at the surface of the bulk fluid.

Though the adherence condition is valid at an impermeable surface, it is not valid at the permeable boundary where there exists a migration of fluid particles across such boundary.

Experiments done by Beavers and Joseph, [2], have shown that the zero tangential fluid velocity is not adequate. Therefore, instead of the adherence condition, these authors introduced a slip velocity condition in the following form:

$$\left.\frac{du}{dy}\right|_{y=0} = \beta(u_B - q)\,. \tag{1.1}$$

In Eq. (1.1) u_B is the slip velocity of the bulk fluid at the permeable boundary B, and q is the filter velocity of a fluid flowing through the permeable skeleton (Fig. 1). Parameter β is a material constant characterizing the skeleton pore structure within the boundary region and does not depend on the fluid viscosity.

It should be pointed out, that both experimental and theoretical work was done (see [3–7]) to establish the validity of such a condition without obtaining a concluding answer.

The main purpose of this work is to establish conditions (say Compatibility Conditions) matching macroscopic mechanical fields at the contact surface between fluid-saturated porous solid and the adjacent bulk fluid.

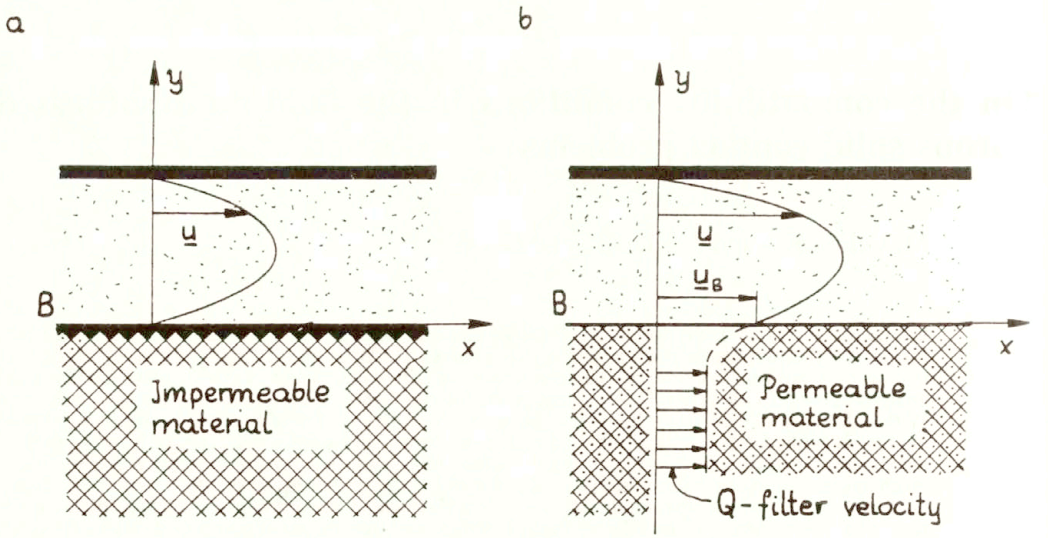

FIG. 1. Velocity profile for the rectilinear flow in a horizontal channel with impermeable (a) and permeable (b) lower wall.

Our approach is based on the description of two-component immiscible mixture, which is the most adequate model to discuss transport processes across the permeable boundary of fluid-solid composition being in contact with bulk fluid.

Such a model motivates the use of independent velocity fields for each component and, therefore, allows to define the material discontinuity surface (contact surface).

In our analysis fields describing macroscopic mechanical phenomena in bodies occupying two adjacent regions being in contact will be considered as compatible if they satisfy the balance equations for mass, linear momentum and mechanical energy at the contact surface of these regions. Consequently, general compatibility conditions are identified with the balance equations at the contact surface.

In the paper we derive the local form of compatibility conditions using standard discontinuity analysis. The obtained conditions allowed us to prove that the macroscopic relative fluid velocities (for both the bulk and free pore fluid) with respect to porous skeleton are discontinuous at the permeable contact surface. This justified the existence of dissipation of mechanical energy at such surface due to the fluid viscosity, for which the constitutive relation is proposed. Special attention was paid to the analysis of linear compatibility conditions. It has been shown that the form of linear conditions for the tangential components of the relative fluid velocities is directly connected with the existence of fluid energy dissipation at the surface of porous skeleton. It has been found, moreover, that the condition postulated by Beavers and Joseph is the special case of the conditions obtained in the paper.

2. Macroscopic balance equations for the basic mechanical quantities at the surface of discontinuity. Compatibility conditions for mechanical fields

We consider a deformable system (see Fig. 2) composed of a fluid saturated porous solid (Region I) being in contact with a bulk fluid (Region II) at the permeable boundary

σ. The σ-surface is a material singular surface. The viscous fluid filling pores and the bulk fluid are physically the same.

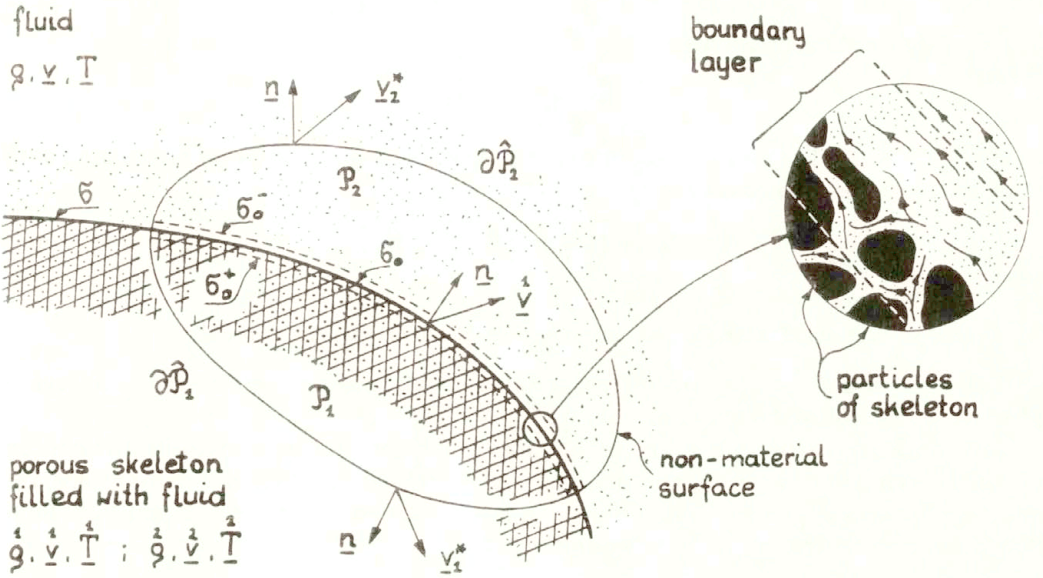

FIG. 2. Contact surface between fluid-saturated porous skeleton and bulk fluid.

The problem is to establish compatibility conditions at the contact surface σ for the macroscopic mechanical fields describing deformation and flow phenomena in both regions. We assume that the motion of bulk fluid and its local state is defined by the particle velocity, $\mathbf{v}$, density ϱ and stress tensor $\mathbf{T}$ that satisfy the dynamic equations for viscous fluid (see e.g. [8]).

The mechanical macro-behaviour of porous solid filled with fluid is described by continuum immiscible mixture theory [9], in which geometrical pore structure is characterized by two macro-parameters. In the case of isotropic pore structure they are: the volume porosity, f_v, and the structural permeability parameter λ ($\lambda \leq f_v$), [10].

The quantity f_v represents the fluid volume fraction and λ reflects the pore architecture and is the measure of inhomogeneity of the fluid micro-velocity field in its relative flow.

It should be pointed out that, within the two-parametric theory, the fluid-saturated porous solid can be considered as composed of two physical components or two virtual components, [11]. For physical components, which are simply porous skeleton ($|^s$) and fluid ($|^f$), the local velocities $\mathbf{v}^s$ and $\mathbf{v}^f$ and partial densities $\overline{\varrho}^s$ and $\overline{\varrho}^f$ are understood as the local volume average quantities.

In the case of virtual components resulting from kinematic division of fluid-porous solid mixture, the first one is the skeleton and the fluid associated with it, of partial density $\overset{1}{\varrho} = \overline{\varrho}^s + (1-\kappa)\overline{\varrho}^f$ and moving at the skeleton velocity $\overset{1}{\mathbf{v}}$. The other is the free fluid of partial density $\overset{2}{\varrho} = \kappa\overline{\varrho}^f$ moving at its own velocity $\overset{2}{\mathbf{v}}$, where

$$\overset{1}{\mathbf{v}} = \mathbf{v}^s, \qquad \overset{2}{\mathbf{v}} = \mathbf{v}^s + \frac{1}{\kappa}(\mathbf{v}^f - \mathbf{v}^s), \qquad \kappa = \lambda / f_v .$$

Partial stress vectors $\overset{1}{\mathbf{t}}$ and $\overset{2}{\mathbf{t}}$ for virtual components are related with those for physical components ($\mathbf{t}^s$ and $\mathbf{t}^f$) as follows

$$\mathbf{t}^1 = \mathbf{t}^s + (1-\kappa)\mathbf{t}^f, \qquad \mathbf{t}^2 = \kappa \mathbf{t}^f .$$

They satisfy the Cauchy theorem

$$\overset{k}{\mathbf{t}} = \overset{k}{\mathbf{T}} \cdot \mathbf{n}, \qquad (k = 1,2),$$

where $\overset{k}{\mathbf{T}}$ $(k = 1,2)$ are the stress tensors of the virtual components and are related with stresses for physical components by

$$\overset{1}{\mathbf{T}} = \mathbf{T}^s + (1-\kappa)\mathbf{T}^f, \qquad \overset{2}{\mathbf{T}} = \kappa \mathbf{T}^f .$$

2.1. General balance equation for a region containing the material discontinuity σ-surface

Let φ be any scalar-, vector- or tensor-valued field function prescribed in the region of space occupied by the material system shown in Fig. 2.

We consider general integral balance equation for quantity φ in an arbitrarily chosen region P bounded by a closed non-material surface ∂P and containing the σ-surface, i.e. interface between regions of a fluid flow in a porous skeleton and the adjacent bulk fluid flow. This can be written in the following form:

$$\frac{d}{dt}\int_P \varphi \, d\nu = \int_{\partial P} \hat{\vartheta}(\mathbf{n})\, ds + \int_P \vartheta^* \, d\nu + \int_{\sigma_0} \vartheta_\sigma \, ds , \tag{2.1}$$

where

$$\sigma_0 = \sigma \cap P .$$

In the above equation, the first term on the RHS stands for the total flux of φ into the region P across ∂P, the second term represents the total production of φ within P, and the third term is the total production of φ in the part of σ-surface included in P.

In order to derive the local form of balance equation for quantity φ on the σ-surface we consider the region P to be divided by this surface into two disjoint parts P_1 and P_2, where

$$P_1 \cup P_2 = P . \tag{2.2}$$

These subregions are bounded by the closed surfaces ∂P_1 and ∂P_2, respectively, which are

$$\partial P_1 = \sigma_0^+ \cup \partial \hat{P}_1, \qquad \partial P_2 = \sigma_0^- \cup \partial \hat{P}_2 , \tag{2.3}$$

where $\partial \hat{P}_1$ and $\partial \hat{P}_2$ are disjoint parts of ∂P divided by the σ-surface so that

$$\partial \hat{P}_1 \cup \partial \hat{P}_2 = \partial P . \tag{2.4}$$

Quantities σ_0^+ and σ_0^- stand for the + side and the − side of the surface σ_0, respectively[1].

In our consideration $\mathbf{n}$ is a unit vector normal to the surfaces bounding particular regions and is externally oriented. For the σ-surface external orientation is assumed to be related with the region occupied by porous skeleton.

---

[1] From the microscopic point of view σ^+ and σ^- form two different surfaces demarcating the boundary contact layer of both media.

Taking relations (2.2)–(2.4) and applying the theorem on the time derivative of time-dependent volume integral, [12], Eq. (2.1) becomes

$$(2.5)\qquad \int_P \frac{\partial \varphi}{\partial t}\,dv + \int_{\partial \widehat{P}_1} \varphi \mathbf{v}_1^* \cdot \mathbf{n}\,ds + \int_{\partial \widehat{P}_2} \varphi \mathbf{v}_2^* \cdot \mathbf{n}\,ds + \int_{\sigma_0^+} \varphi^+ \overset{1}{\mathbf{v}} \cdot \mathbf{n}\,ds - \int_{\sigma_0^-} \varphi^- \overset{1}{\mathbf{v}} \cdot \mathbf{n}\,ds$$
$$= \int_{\partial \widehat{P}_1} \widehat{\vartheta} \cdot \mathbf{n}\,ds + \int_{\partial \widehat{P}_2} \widehat{\vartheta} \cdot \mathbf{n}\,ds + \int_P \vartheta^*\,dv + \int_{\sigma_0} \vartheta_\sigma\,ds\,,$$

where $\mathbf{v}_1^*$ and $\mathbf{v}_2^*$ are velocities of surfaces $\partial \widehat{\mathcal{P}}_1$ and $\partial \widehat{\mathcal{P}}_2$, respectively, $\overset{1}{\mathbf{v}}$ represents the velocity of porous skeleton particles which form material discontinuity surface σ. Quantities φ^+ and φ^- denote the values of φ on the surfaces σ_0^+ and σ_0^-, respectively.

In derivation of Eq. (2.5) the linearity condition for the flux $\widehat{\vartheta}(\mathbf{n})$ with respect to the normal vector $\mathbf{n}$ was used, i.e.

$$\widehat{\vartheta}(\mathbf{n}) = \widehat{\mathfrak{s}} \cdot \mathbf{n}\,,$$

where the order of tensorial quantity $\widehat{\mathfrak{s}}$ depends on the character of the balanced quantity φ.

Since Eq. (2.5) is valid for arbitrarily chosen region P, it should be also valid for the particular case when the volume of P tends to zero preserving, however, the area of σ_0-surface (Fig. 3).

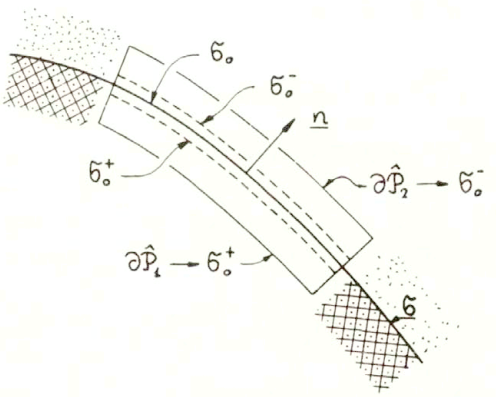

FIG. 3. Scheme of transition from 3-D to 2-D balance region.

In such a case, and under the additional assumptions that quantities $\partial\varphi/\partial t$ and ϑ^* are continuous in P_1 and P_2, the volume integrals in Eq. (2.5) tend to zero and the formula gets finally the form

$$(2.6)\qquad -\int_{\sigma_0^+} \varphi^+ \mathbf{v}_1^* \cdot \mathbf{n}\,ds + \int_{\sigma_0^-} \varphi^- \mathbf{v}_2^* \cdot \mathbf{n}\,ds + \int_{\sigma_0^+} \varphi^+ \overset{1}{\mathbf{v}} \cdot \mathbf{n}\,ds - \int_{\sigma_0^-} \varphi^- \overset{1}{\mathbf{v}} \cdot \mathbf{n}\,ds$$
$$= -\int_{\sigma_0^+} \widehat{\vartheta}^+ \cdot \mathbf{n}\,ds + \int_{\sigma_0^-} \widehat{\vartheta}^- \cdot \mathbf{n}\,ds + \int_{\sigma_0} \vartheta_\sigma\,ds\,.$$

Since the surfaces σ_0, σ_0^+ and σ_0^- coincide and are arbitrary, from Eq. (2.6) it follows that

$$\varphi^-(\mathbf{v}_2^* - \overset{1}{\mathbf{v}}) \cdot \mathbf{n} - \varphi^+(\mathbf{v}_1^* - \overset{1}{\mathbf{v}}) \cdot \mathbf{n} = (\vartheta^- - \vartheta^+) \cdot \mathbf{n} + \vartheta_\sigma . \tag{2.7}$$

It is the general form of the local balance equation for quantity φ on the interface between a fluid-saturated porous solid and an adjacent bulk fluid. This equation is, at the same time, the general compatibility condition at the contact surface σ for mechanical fields in both regions. In applying the condition (2.7) the important thing is the identification of φ^+, φ^-, ϑ^+ and ϑ^- with the particular balanced quantities compatible with the motion definition of the surfaces $\partial\widehat{\mathcal{P}}_1$ and $\partial\widehat{\mathcal{P}}_2$ which approach σ_0^+ and σ_0^-, respectively, ($\vartheta^+ \cdot \mathbf{n}$ is the flux of φ across $\partial\widehat{\mathcal{P}}_1$, and $\vartheta^- \cdot \mathbf{n}$ is the flux of φ across $\partial\widehat{\mathcal{P}}_2$). If we identify the points of surface $\partial\widehat{\mathcal{P}}_1 \to \sigma_0^+$ with the particles of porous skeleton, and the points of surface $\partial\widehat{\mathcal{P}}_2 \to \sigma_0^-$ with particles of bulk fluid, we have

$$\mathbf{v}_1^* = \overset{1}{\mathbf{v}}, \qquad \mathbf{v}_2^* = \mathbf{v},$$

and then Eq. (2.7) takes form

$$\varphi^-(\mathbf{v} - \overset{1}{\mathbf{v}}) \cdot \mathbf{n} = (\vartheta^- - \vartheta^+) \cdot \mathbf{n} + \vartheta_\sigma . \tag{2.8}$$

The above equation will be used in derivation of the balance equations for mass, linear momentum and total mechanical energy at the discontinuity surface σ.

2.2. Balance of mass

On the assumption that at the σ-surface there is no source of mass ($\vartheta_\sigma \equiv 0$), it is evident that the condition (2.8) for the skeleton and the associated fluid (the first virtual component) is satisfied identically.

In the case of fluid phase we find that on the positive side of σ there is a free fluid (the second virtual component), and on the negative side of σ there is a bulk fluid. Therefore we have:

$$\varphi^- \equiv \varrho, \qquad \widehat{\vartheta}^- \cdot \mathbf{n} \equiv 0, \qquad \widehat{\vartheta}^+ \cdot \mathbf{n} \equiv -\overset{2}{\varrho}(\overset{2}{\mathbf{v}} - \overset{1}{\mathbf{v}}) \cdot \mathbf{n}, \tag{2.9}$$

where the "$-$" sign in the term $(2.9)_3$ results from the fact that the direction of fluid flux is opposite to the normal vector $\mathbf{n}$. Using Eqs. (2.9) the balance equation (2.8) for the mass of fluid takes the form

$$\varrho \mathbf{u} \cdot \mathbf{n} = \overset{2}{\varrho}\,\overset{2}{\mathbf{u}} \cdot \mathbf{n}, \tag{2.10}$$

where

$$\mathbf{u} = \mathbf{v} - \overset{1}{\mathbf{v}}, \qquad \overset{2}{\mathbf{u}} = \overset{2}{\mathbf{v}} - \overset{1}{\mathbf{v}}$$

are velocities of bulk and free fluid flow relative to σ-surface, respectively.

Equation (2.10) is the first compatibility condition on the interface between regions of fluid-saturated porous skeleton and the adjacent bulk fluid. This condition proves that the normal component of the relative fluid mass flux across permeable boundary of the porous skeleton is continuous.

2.3. Balance of linear momentum

It is evident that the force interaction at σ-surface exists between the bulk fluid and the both virtual components of fluid-saturated porous solid; therefore the balance of linear momentum has to be formulated jointly for these three components of the system under consideration.

In such a case, quantities of general balance equation (2.8) can be specified as follows:

$$\varphi^{-} \equiv \varrho \mathbf{v}, \qquad \hat{\vartheta}^{-} \cdot \mathbf{n} \equiv \mathbf{t}, \tag{2.11}$$
$$\hat{\vartheta}^{+} \cdot \mathbf{n} \equiv (\overset{1}{\mathbf{t}} + \overset{2}{\mathbf{t}}) - \overset{2}{\varrho}\,\overset{2}{\mathbf{v}}(\overset{2}{\mathbf{v}} - \overset{1}{\mathbf{v}}) \cdot \mathbf{n},$$

where $\mathbf{t}$, $\overset{1}{\mathbf{t}}$ and $\overset{2}{\mathbf{t}}$ are stress vectors for the bulk fluid, the first and the second virtual components of the saturated porous medium, respectively. In the expression $(2.11)_3$ the "+" sign at stress vectors and "−" sign at the momentum flux due to the mass transport results from the convention for increase (decrease) of the momentum in the balance region.

In the analysis we assume that there is no external surface force on the σ-surface, thus the surface momentum production is equal to zero, i.e.

$$\vartheta_\sigma \equiv \vartheta_\sigma \equiv \mathbf{0}. \tag{2.12}$$

Taking Eqs. (2.11) and (2.12) into account and using Eq. (2.10), the Eq. (2.8) for the momentum balance at σ-surface takes the form

$$\varrho \mathbf{u} \cdot \mathbf{n}(\mathbf{u} - \overset{2}{\mathbf{u}}) = \mathbf{t} - (\overset{1}{\mathbf{t}} + \overset{2}{\mathbf{t}}), \tag{2.13}$$

which is the second compatibility condition for the macroscopic mechanical fields.

2.4. Balance of mechanical energy

First, we recall that on the discontinuity σ-surface three components of the system interact with each other. Thus, similarly as in the case of balance of linear momentum, the balance of total mechanical energy has to be formulated jointly for all three components.

In this case the specification of φ^{-}, $\hat{\vartheta}^{-}$, and $\hat{\vartheta}^{+}$ in Eq. (2.8), gives

$$\varphi^{-} \equiv \varrho\left(\frac{1}{2}\mathbf{v} \cdot \mathbf{v} + e^{\mathrm{bf}}\right), \qquad \hat{\vartheta}^{-} \cdot \mathbf{n} \equiv \mathbf{t} \cdot \mathbf{v}, \tag{2.14}$$
$$\hat{\vartheta}^{+} \cdot \mathbf{n} \equiv \overset{1}{\mathbf{t}} \cdot \overset{1}{\mathbf{v}} + \overset{2}{\mathbf{t}} \cdot \overset{2}{\mathbf{v}} - \overset{2}{\varrho}\left(\frac{1}{2}\overset{2}{\mathbf{v}} \cdot \overset{2}{\mathbf{v}} + e^{\mathrm{pf}}\right)(\overset{2}{\mathbf{v}} - \overset{1}{\mathbf{v}}) \cdot \mathbf{n},$$

where e^{bf} and e^{pf} stands for the internal energy of the bulk fluid and pore fluid, respectively [2].

The absence of the external surface force on the σ-surface assumed in the previous section eliminates the possibility of existence of the mechanical energy source at this surface. However, as it will be shown later, at the σ-surface a sink of the mechanical energy may exist due to dissipation caused by fluid viscosity.

Therefore we may write

$$\vartheta_\sigma \equiv -\vartheta_e. \tag{2.15}$$

[2] For the barotropic fluid these quantities are uniquely determined by effective pressure of the fluid.

Making use of the expressions (2.14) and (2.15) and taking Eqs. (2.10) and (2.13) into account, the general equation (2.8) for the balance of mechanical energy on the σ-surface gets the form

$$\varrho \mathbf{u} \cdot \mathbf{n} \left[\frac{1}{2} (\mathbf{u}^2 - (\overset{2}{\mathbf{u}})^2) + e^{\mathrm{bf}} - e^{\mathrm{pf}} \right] = \mathbf{t} \cdot \mathbf{u} - \overset{2}{\mathbf{t}} \cdot \overset{2}{\mathbf{u}} - \vartheta_\sigma \,. \tag{2.16}$$

Equation (2.16) is the third compatibility condition for mechanical fields on the interface between regions of a fluid flow in a porous skeleton and the adjacent bulk fluid flow. It can be effectively used after the specification of ϑ_σ-function.

3. Dissipation of the mechanical energy at the σ-surface

We will show here that at the discontinuity surface σ all the three macroscopic velocity fields of the constituents of the considered system are in pairs discontinuous. These discontinuities, together with the assumption that the pore and bulk fluid are viscous, motivate the existence of a sink of mechanical energy on the σ-surface.

3.1. Discontinuities of the velocity fields

The normal components of macroscopic velocities of particular constituents of the system under consideration are confined by the mass continuity equation for the fluid phase. Equation (2.10), after the use of the inequality

$$\varrho_- = \varrho \neq \overset{2}{\varrho} = \lambda \varrho_+ \qquad (0 < \lambda \leq f_v \leq 1)$$

shows that the normal component of the relative velocity of fluid flow through the surface of porous skeleton is not continuous, i.e.

$$0 \neq \mathbf{u} \cdot \mathbf{n} \neq \overset{2}{\mathbf{u}} \cdot \mathbf{n} \neq 0$$

or equivalently

$$\mathbf{v} \cdot \mathbf{n} \neq \overset{1}{\mathbf{v}} \cdot \mathbf{n} \neq \overset{2}{\mathbf{v}} \cdot \mathbf{n} \,. \tag{3.1}$$

The inequality (3.1) proves that in general case the normal velocity components describing a motion of particular constituents of the system differ from each other on the discontinuity surface σ. Similar conclusion for tangential components of these velocities can be derived basing on the linear momentum balance (2.13), and the balance of total mechanical energy (2.16) when the experimental results, that of BEAVERS and JOSEPH [2], are used.

Rewriting the Eqs. (2.13) and (2.16) in the form corresponding to the fluid flow along the σ-surface ($\mathbf{u} \cdot \mathbf{n} = \overset{2}{\mathbf{u}} \cdot \mathbf{n} = 0$) and disregarding in this step the function ϑ_σ, from Eq. (2.13) we have

$$\mathbf{t}_\tau = \overset{1}{\mathbf{t}}_\tau + \overset{2}{\mathbf{t}}_\tau \,, \tag{3.2}$$

and from Eq. (2.16) we obtain

$$\mathbf{t}_\tau \cdot \mathbf{u}_\tau = \overset{2}{\mathbf{t}}_\tau \cdot \overset{2}{\mathbf{u}}_\tau \,, \tag{3.3}$$

where the subscript τ indicates vector components tangential to the σ-surface.

In the case when a fluid in the system is non-viscous, the conditions (3.2) and (3.3) do not impose any restriction on the tangential velocities $\mathbf{u}_\tau$ and $\overset{2}{\mathbf{u}}_\tau$, since the lack of the tangential force interactions, i.e.

$$\mathbf{t}_\tau = \overset{2}{\mathbf{t}}_\tau = \overset{1}{\mathbf{t}}_\tau = 0,$$

ensures these conditions to be satisfied identically, irrespective of the values of velocities $\mathbf{u}_\tau$ and $\overset{2}{\mathbf{u}}_\tau$.

For the viscous fluid, however, all the tangential stresses are not zero, and the conditions (3.2) and (3.3) constrain both the values of tangential stresses as well as the tangential velocities $\mathbf{u}_\tau$ and $\overset{2}{\mathbf{u}}_\tau$.

Taking into account the Beavers and Joseph experimental results for viscous fluid flow along permeable boundary [2] which proves that the tangential component of the bulk fluid velocity is nonzero, i.e.

$$\mathbf{u}_\tau \neq \mathbf{0}, \tag{3.4}$$

from Eqs. (3.2) and (3.3) we conclude that

$$\overset{2}{\mathbf{u}}_\tau \neq \mathbf{0}. \tag{3.5}$$

and also

$$\mathbf{u}_\tau \neq \overset{2}{\mathbf{u}}_\tau. \tag{3.6}$$

The inequalities (3.4)–(3.6) rewritten in the form

$$\mathbf{v}_\tau \neq \overset{1}{\mathbf{v}}_\tau \neq \overset{2}{\mathbf{v}}_\tau \tag{3.7}$$

show that the tangential components of velocities of particular constituents of the system differ from each other on the σ-discontinuity surface.

The above considerations allow us to state that at the σ-surface the velocity fields of virtual components of the fluid-saturated porous solid $(\overset{1}{\mathbf{v}}, \overset{2}{\mathbf{v}})$ and the bulk fluid $(\mathbf{v})$ are discontinuous in pairs. It concerns both the normal and tangential components of the velocity vectors.

The existence of relative motion of the constituents on the σ-discontinuity surface results in the viscous friction between the constituents responsible for the dissipation of mechanical energy.

It should be pointed out here that the dissipation process takes place on the σ-surface unlike the well known volume dissipation appearing in viscous bulk fluid. Thus the function ϑ_e requires a separate constitutive postulate.

3.2. The constitutive postulate for the dissipation function

In the previous section we have stated that the dissipation of mechanical energy on the σ-surface results from the discontinuity of velocity fields of particular constituents of the system. Therefore, on the assumption that the pore structure of permeable matrix is isotropic, it is reasonable to assume that the constitutive function for the sink of the mechanical energy ϑ_e will depend on velocities $\mathbf{v}$, $\overset{1}{\mathbf{v}}$, $\overset{2}{\mathbf{v}}$ and, additionally, on the σ-surface

orientation defined by the normal vector $\mathbf{n}$. We write

$$\vartheta_e = \overline{\vartheta}_e(\mathbf{v}, \overset{1}{\mathbf{v}}, \overset{2}{\mathbf{v}}, \mathbf{n}). \tag{3.8}$$

A common requirement for constitutive function is to satisfy the objectivity condition. Moreover, it is evident that $\overline{\vartheta}_e$, for arbitrarily chosen nonzero values of $\mathbf{v}$, $\overset{1}{\mathbf{v}}$ and $\overset{2}{\mathbf{v}}$, should be a positive defined function, i.e.

$$\overline{\vartheta}_e(\mathbf{v}, \overset{1}{\mathbf{v}}, \overset{2}{\mathbf{v}}, \mathbf{n}) > 0 \tag{3.9}$$

and in the case of no fluid flow ($\mathbf{v} = \overset{1}{\mathbf{v}} = \overset{2}{\mathbf{v}} = \mathbf{0}$) it should satisfy the following condition

$$\overline{\vartheta}_e(\mathbf{0}, \mathbf{0}, \mathbf{0}, \mathbf{n}) = 0. \tag{3.10}$$

The inequality (3.9) results from the entropy production principle [13], due to the dissipation of mechanical energy on the σ-surface.

The objectivity condition, [12], when applied to Eq. (3.8) shows that $\overline{\vartheta}_e$ depends only on the relative velocities and vector $\mathbf{n}$. We may write

$$\vartheta_e = \overline{\vartheta}'_e(\mathbf{u}, \overset{2}{\mathbf{u}}, \mathbf{n}), \tag{3.11}$$

where

$$\mathbf{u} = \mathbf{v} - \overset{1}{\mathbf{v}}, \qquad \overset{2}{\mathbf{u}} = \overset{2}{\mathbf{v}} - \overset{1}{\mathbf{v}}.$$

Moreover, the function $\overline{\vartheta}'_e$ is the isotropic scalar-valued vector function, i.e. for any orthogonal tensor $\mathbf{Q}(\mathbf{Q}^T = \mathbf{Q}^{-1})$ and all vectors $\mathbf{u}$, $\overset{2}{\mathbf{u}}$ and $\mathbf{n}$, the condition

$$\overline{\vartheta}'_e(\mathbf{Qu}, \mathbf{Q}\overset{2}{\mathbf{u}}, \mathbf{Qn}) = \overline{\vartheta}'_e(\mathbf{u}, \overset{2}{\mathbf{u}}, \mathbf{n}) \tag{3.12}$$

is satisfied.

According to the Cauchy representation theorem for the isotropic scalar-valued functions, [12], we find that $\overline{\vartheta}'_e(\mathbf{u}, \overset{2}{\mathbf{u}}, \mathbf{n})$ can be regarded as a function of five scalar products

$$I: \quad \mathbf{u}\cdot\mathbf{u}, \quad \mathbf{u}\cdot\overset{2}{\mathbf{u}}, \quad \overset{2}{\mathbf{u}}\cdot\overset{2}{\mathbf{u}}, \quad \mathbf{u}\cdot\mathbf{n}, \quad \overset{2}{\mathbf{u}}\cdot\mathbf{n}.$$

Then the relation (3.11) takes form

$$\overline{\vartheta}'_e(\mathbf{u}, \overset{2}{\mathbf{u}}, \mathbf{n}) \equiv \overline{\vartheta}''_e(\mathbf{u}\cdot\mathbf{u}, \mathbf{u}\cdot\overset{2}{\mathbf{u}}, \overset{2}{\mathbf{u}}\cdot\overset{2}{\mathbf{u}}, \mathbf{u}\cdot\mathbf{n}, \overset{2}{\mathbf{u}}\cdot\mathbf{n}) \equiv \overline{\vartheta}''_e(I), \tag{3.13}$$

and for any $\overline{\vartheta}''_e$ the condition (3.12) is satisfied identically. Now, taking the compatibility condition (2.10) into account, the number of arguments in Eq. (3.13) can be reduced by one, and we obtain

$$\vartheta_e = \overline{\vartheta}^*_e(\mathbf{u}\cdot\mathbf{u}, \mathbf{u}\cdot\overset{2}{\mathbf{u}}, \overset{2}{\mathbf{u}}\cdot\overset{2}{\mathbf{u}}, \mathbf{u}\cdot\mathbf{n}). \tag{3.14}$$

After decomposition of $\mathbf{u}$ and $\overset{2}{\mathbf{u}}$ into their normal and tangential components, that is

$$\mathbf{u}_n = (\mathbf{u}\cdot\mathbf{n})\mathbf{n}, \qquad \mathbf{u}_\tau = \mathbf{u} - \mathbf{u}_n, \qquad \overset{2}{\mathbf{u}}_\tau = \overset{2}{\mathbf{u}} - (\overset{2}{\mathbf{u}}\cdot\mathbf{n})\mathbf{n}, \tag{3.15}$$

we get the following representation

$$\vartheta_e = \hat{\vartheta}_e(\mathbf{u}_\tau^2, \mathbf{u}_\tau\cdot\overset{2}{\mathbf{u}}_\tau, \overset{2}{\mathbf{u}}_\tau\cdot\overset{2}{\mathbf{u}}_\tau, \mathbf{u}\cdot\mathbf{n}) \tag{3.16}$$

where, according to (3.9) and (3.10), the function $\hat{\vartheta}_e$ has to satisfy conditions:

$$\hat{\vartheta}_e(\mathbf{u}_\tau^2, \mathbf{u}_\tau \cdot \overset{2}{\mathbf{u}}_\tau, \overset{2}{\mathbf{u}}_\tau \cdot \overset{2}{\mathbf{u}}_\tau, \mathbf{u} \cdot \mathbf{n}) > 0, \tag{3.17}$$

$$\hat{\vartheta}_e(\mathbf{0}, \mathbf{0}, \mathbf{0}, \mathbf{0}) = 0. \tag{3.18}$$

The relation (3.16) is a general form of the constitutive equation for the dissipation of the mechanical energy at the interface between regions of a fluid flow in a porous skeleton and the adjacent bulk fluid flow. The only constraints for the function $\hat{\vartheta}_e$ are conditions (3.17) and (3.18).

The form of constitutive function (3.16) is fully equivalent to Eq. (3.14), but the interpretation of Eq. (3.16) is easier due to the fact that the decomposition of fluid flow into the normal and tangential parts with respect to the σ-surface is compatible with internal symmetry of the system.

Since in general case the function $\hat{\vartheta}_e$ may not be an even function of the argument $\mathbf{u} \cdot \mathbf{n}$, then from Eq. (3.16) it follows that the dissipation of mechanical energy during fluid flow out or into the porous skeleton may reach different values. However, if velocities $\mathbf{u}_\tau$, $\overset{2}{\mathbf{u}}_\tau$ and $\mathbf{u} \cdot \mathbf{n}$ are small, conditions (3.17) and (3.18) ensure that $\hat{\vartheta}_e$ is an even function of the argument $\mathbf{u} \cdot \mathbf{n}$.

It results from the fact that when the function $\hat{\vartheta}_e$ satisfies (3.17) and (3.18) and its derivatives are continuous at $\mathbf{u} = \overset{2}{\mathbf{u}} = \mathbf{0}$, it has also a minimum there.

In such a case the dissipation function can be proposed in the quadratic form

$$\vartheta_e = \alpha_1 \overset{2}{\mathbf{u}}_\tau - 2\alpha_2 \mathbf{u}_\tau \cdot \overset{2}{\mathbf{u}}_\tau + \alpha_3 \overset{2}{\mathbf{u}}_\tau^2 + \varepsilon(\mathbf{u} \cdot \mathbf{n})^2, \tag{3.19}$$

where α_1, α_2, α_3 and ε are constant coefficients. Considering particular cases of fluid flow (tangential and normal to the σ-surface) it can be shown that the constitutive relation (3.19) will have a minimum at $\mathbf{u} = \overset{2}{\mathbf{u}} = \mathbf{0}$ when constant coefficients satisfy the following inequalities:

$$\alpha_1 > 0, \quad \alpha_3 > 0, \quad \alpha_2^2 < \alpha_1 \alpha_3, \quad \varepsilon > 0. \tag{3.20}$$

4. Linear compatibility conditions

The general equations (2.10), (2.13) and (2.15) together with the dissipation function (3.16) form the set of compatibility conditions for mechanical fields on the discontinuity σ-surface.

We take these equations to establish the linear form of compatibility conditions which play an important role in a large number of linear problems of porous media.

The linear compatibility conditions for stress vectors of particular constituents of the system can be derived directly from the balance equation of linear momentum (2.13) disregarding the nonlinear terms of its LHS. These conditions written for the normal and tangential stress components are

$$t_n = \overset{1}{t}_n + \overset{2}{t}_n, \tag{4.1}$$

$$\mathbf{t}_\tau = \overset{1}{\mathbf{t}}_\tau + \overset{2}{\mathbf{t}}_\tau, \tag{4.2}$$

where

$$( )_n = (\_) \cdot \mathbf{n}, \qquad (\_)_\tau = (\_) - ( )_n \cdot \mathbf{n}.$$

From Eqs. (4.1) and (4.2) it follows that in linear interactions between the bulk fluid and the saturated porous solid the force exerted by the bulk fluid on permeable boundary is equilibrated by forces occurring in both constituents of saturated porous solid.

The immediate linearization of the balance equation (2.15) for total mechanical energy on the σ-surface, in contradistinction to the balance of linear momentum (2.13), is not possible. We can arrive, however, at linear relations under some assumptions. After the use of Eqs. (2.10) and (3.19) and disregarding the LHS of Eq. (2.15), we obtain

$$\left[\varrho\left(\frac{t_n}{\varrho} - \frac{\overset{2}{t}_n}{\overset{2}{\varrho}}\right) - \varepsilon u_n\right] u_n = \overset{2}{\mathbf{t}}_\tau \cdot \overset{2}{\mathbf{u}}_\tau - \mathbf{t}_\tau \cdot \mathbf{u}_\tau - \alpha_1 \mathbf{u}_\tau^2 + 2\alpha_2 \mathbf{u}_\tau \cdot \overset{2}{\mathbf{u}}_\tau - \alpha_3 \overset{2}{\mathbf{u}}{}^2_\tau . \tag{4.3}$$

In the above equation the components of stress vectors of bulk and free fluid are related with the corresponding relative velocities.

Since, in the linear case, the normal and tangential components of any vector field are mutually independent, Eq. (4.3) will be satisfied if its both sides are identically equal to zero. According to the relations

$$\varrho = \varrho^-, \qquad \overset{2}{\varrho} = \lambda \varrho^+, \qquad t_n = -p^-, \qquad \overset{2}{t}_n = -\lambda p^+ \tag{4.4}$$

from Eq. (4.3) we get

$$\varrho^- \left(\frac{p^+}{\varrho^+} - \frac{p^-}{\varrho^-}\right) = \varepsilon u_n , \tag{4.5}$$

$$\overset{2}{\mathbf{t}}_\tau \cdot \overset{2}{\mathbf{u}}_\tau - \mathbf{t}_\tau \cdot \mathbf{u}_\tau - \alpha_1 \mathbf{u}_\tau^2 + 2\alpha_2 \mathbf{u}_\tau \cdot \overset{2}{\mathbf{u}}_\tau - \alpha_3 \overset{2}{\mathbf{u}}{}^2_\tau = 0 , \tag{4.6}$$

where superscripts + and − denote values of quantities on the positive and negative side of σ-surface, respectively.

Now, assuming the tangential forces $\mathbf{t}_\tau$ and $\overset{2}{\mathbf{t}}_\tau$ to be linearly dependent on the relative velocities $\mathbf{u}_\tau$ and $\overset{2}{\mathbf{u}}_\tau$, we can separate Eq. (4.6) into two independent equations

$$\mathbf{t}_\tau = \alpha_1 \mathbf{u}_\tau - \alpha_2' \overset{2}{\mathbf{u}}_\tau , \tag{4.7}$$

$$-\overset{2}{\mathbf{t}}_\tau = \alpha_3 \overset{2}{\mathbf{u}}_\tau - \alpha_2'' \mathbf{u}_\tau , \tag{4.8}$$

in which

$$\alpha_2' + \alpha_2'' = 2\alpha_2 . \tag{4.9}$$

In order to obtain the linear form of Eq. (4.5) we assume that the fluid is barotropic, i.e.

$$p = p(\varrho) \tag{4.10}$$

and fluid densities ϱ^+ and ϱ^- differ from its equilibrium density ϱ_0 in such a way that the following relation is satisfied

$$p^+ - p^- = \alpha_0^2(\varrho^+ - \varrho^-) , \tag{4.11}$$

where

$$\alpha_0 = \left(\frac{dp}{d\varrho}\right)^{\frac{1}{2}}\Big|_{\varrho=\varrho_0}$$

is the velocity of disturbances propagating in an undisturbed region of the bulk fluid.

Under the above assumptions, from Eq. (4.5) we obtain the linear compatibility condition

$$p^+ - p^- = \frac{\varepsilon}{1-(p_0/\varrho_0)\alpha_0^2} u_n \,. \tag{4.12}$$

It relates the fluid pressure on both sides of the σ-surface and the normal component of relative fluid velocity.

In the case when the RHS of Eq. (4.12) can be omitted, the condition (4.12) reduces to the classical one reflecting the fluid pressure continuity

$$p^+ = p^- = p \,. \tag{4.13}$$

Assumptions (4.10) and (4.11) and condition (4.12) allow the linearization of the fluid mass balance equation (2.10) at the σ-surface. As a consequence, we obtain the compatibility condition for normal components of fluid flow across the σ-surface

$$u_n = \lambda \overset{2}{u}_n \tag{4.14}$$

in which the proportionality coefficient is the pore structure parameter λ.

Equations (4.7) and (4.8) are the next two linear compatibility conditions. They define the dependence of tangential components of the vector stresses for bulk and free fluid on the corresponding tangential velocities.

Their functional form is directly related to the dissipation of the mechanical energy of fluid due to viscosity at the surface in the boundary layer of porous solid.

Conditions (4.7) and (4.8), when fluid viscosity μ and permeability of porous skeleton k are explicitly introduced, can be written as follows:

$$\mathbf{t}_\tau = \frac{\mu}{\sqrt{k}}(\lambda_1 \mathbf{u}_\tau - \lambda_2' \overset{2}{\mathbf{u}}_\tau) \,, \tag{4.15}$$

$$-\overset{2}{\mathbf{t}}_\tau = \frac{\mu}{\sqrt{k}}(\lambda_3 \overset{2}{\mathbf{u}}_\tau - \lambda_2'' \mathbf{u}_\tau) \,, \tag{4.16}$$

where coefficients λ_1, λ_2', λ_2'', $(\lambda_2' + \lambda_2'' = 2\lambda_2)$ and λ_3 are nondimensional constant quantities.

Taking into account the fact that tangential stresses in bulk and free fluid are related with their corresponding velocity gradients via the constitutive equations, the compatibility conditions (4.15) and (4.16) can be transformed to the form of conditions for the velocities only.

Considering a one-dimensional rectilinear fluid flow along a plane surface of porous solid, we have

$$\mathbf{t}_\tau = -\mu \frac{\partial u_\tau}{\partial x}\boldsymbol{\tau} \,, \tag{4.17}$$

$$\overset{2}{\mathbf{t}}_\tau = \mu^* \frac{\partial \overset{2}{u}_\tau}{\partial x}\boldsymbol{\tau} \,,$$

$$(\,)_\tau = (\,)\cdot\boldsymbol{\tau} \,, \tag{4.18}$$

where $\boldsymbol{\tau}$ is the unit vector tangential to the σ-surface indicating the direction of fluid flow. The coordinate x is directed along the vector $\mathbf{n}$ normal to the σ-surface. In Eq. (4.17) the "—" sign results from the fact that vector $\mathbf{n}$ is oriented internally to the region of bulk fluid.

The coefficient μ^* stands for the effective viscosity of a fluid filling the porous skeleton corresponding to the coefficient introduced by BRINKMAN [14]. In such a case, from Eqs. (4.15) and (4.16) we obtain

$$-\frac{\partial u_\tau}{\partial x}\boldsymbol{\tau} = \frac{1}{\sqrt{k}}(\lambda_1 \mathbf{u}_\tau - \lambda_2' \overset{2}{\mathbf{u}}_\tau), \tag{4.19}$$

$$-\frac{\mu^*}{\mu}\frac{\partial \overset{2}{u}_\tau}{\partial x}\boldsymbol{\tau} = \frac{1}{\sqrt{k}}(\lambda_3 \overset{2}{\mathbf{u}}_\tau - \lambda_2'' \mathbf{u}_\tau). \tag{4.20}$$

Taking the above results into account, and the linear relationship between volume discharge and velocity $\overset{2}{\mathbf{u}}_\tau$ of fluid flow through porous skeleton, we find that the Beavers–Joseph postulate (1.1) is a particular case of the condition (4.19).

5. Final remarks

The problem of compatibility conditions for macroscopic mechanical fields at the contact surface between the fluid-saturated porous solid and the bulk fluid have been considered on the grounds of standard discontinuity analysis.

General form of these conditions is obtained as the balance equations for mass, linear momentum and mechanical energy formulated at the discontinuity surface.

The analysis of the compatibility conditions derived proves the existence of discontinuity of the macroscopic relative fluid velocities (free and bulk fluid) and justifies the existence of the mechanical energy dissipation at the contact surface due to the fluid viscosity. The proposed quadratic form of the dissipation function introduces to the considered description of the contact problem certain new parameters characterising the permeable boundary layer of porous skeleton. Their relations with the skeleton pore structure characteristics require further theoretical and experimental investigations.

It has been shown that the slip condition postulated by Beavers and Joseph for the relative bulk fluid velocity is the special case of the linearized conditions obtained in this paper.

References

1. D.D. JOSEPH and L.N. TAO, *Lubrication of a porous bearing Stokes' solution*, J. Appl. Mech. Trans. ASME, 753–760, 1966.
2. G.S. BEAVERS and D.D. JOSEPH, *Boundary conditions at a naturally permeable wall*, J. Fluid Mech., **30**, 197–207, 1967.
3. G.I. TAYLOR, *A model for the boundary condition of a porous material. Part I*, J. Fluid Mech., **49**, 319–326, 1971.
4. S. RICHARDSON, *A model for the boundary condition of a porous material. Part II*, J. Fluid Mech., **49**, 327–336, 1971.
5. P.G. SAFFMAN, *On the boundary condition at the surface of a porous medium*, Studies in Appl. Mech., **L**, 2, 1971.
6. T. LEVY, E. SANCHEZ-PALENCIA, *On the boundary conditions for fluid flow in porous media*, Int. J. Engng. Sci., **13**, 923–940, 1975.

7. J. KOPLIK, H. LEVINE and A. SEE, *Viscosity renormalization in the Brinkman equation*, Phys. Fluids, **26**, 10, 1983.
8. L.D. LANDAU and E.M. LIFSHIC, *Hydromechanics* [in Russian], Nauka, Moskva 1986.
9. J. KUBIK, *On the internal coupling in dynamic equations of fluid-saturated porous solid*, Int. J. Engng Sci., **24**, 6, 981–989, 1986.
10. J. KUBIK, *A macroscopic description of geometrical pore structure of porous solid*, Int. J. Engng Sci., **24**, 6, 971–980, 1986.
11. J. KUBIK, *Pore structure in dynamic behaviour of saturated materials*, Transport in Porous Media, **9**, 15–24, 1992.
12. D.C. LEIGH, *Nonlinear continuum mechanics*, McGraw-Hill Book Company, New York 1968.
13. K. WILMAŃSKI, *Phenomenological thermodynamics*, [in:] Engineering Mechanics. Vol. 1. Foundations of Mechanica, [in Polish], PWN, Warszawa 1985.
14. H.C. BRINKMAN, *A calculation of the viscous force exerted by a flowing fluid on a dense swarm of particles*, Appl. Sci. Res., **A1**, 27–34, 1947.

POLISH ACADEMY OF SCIENCES
INSTITUTE OF FUNDAMENTAL TECHNOLOGICAL RESEARCH.

Received December 7, 1992.

Arch. Mech., 45, 1, pp. 93–105, Warszawa 1993

Underlying algebraic and gauge structures of the theory of disclinations

C. MALYSHEV (ST.-PETERSBURG)

THE MAIN PURPOSE of the paper is to derive the group of gauge transformations of the theory of disclinations with the help of the Schaefer's motor calculus. The Lie algebraic aspect of the problem under consideration is specially emphasized. The first part of the paper deals with the representation of the algebra $iso(3) = t(3) \dot{+} so(3, \mathbb{R})$ (motor algebra) by the Schaefer's differential operators, the elements of $iso(3)$-valued exterior calculus are suggested. The second part of the paper contains the derivation of the group of gauge transformations of the defect theory. It is shown that the theory of disclinations is a particular case of the gauge model with noncompact Abelian gauge group.

1. Introduction

IT IS REMARKABLE that the gauge field formalism turns out to be useful not only in the physics of fundamental interactions, as it was intended, but also in the description of defects in solids [1–3]. The meaning of this assertion becomes especially transparent if one takes into account the energy scales characterizing these two fields of physics.

The main purpose of this paper is to deduce over again the group of gauge transformations of the theory of disclinations which was successively developed by R. DEWIT in the series of papers [4, 5]. This group of gauge transformations was derived for the first time in the Refs. [6, 7] under the influence of the idea concerning close analogy between the pure dislocation theory and the Maxwell's electrodynamics, both being considered as the Abelian gauge models. We shall denote this group of transformations as the GLE-group (abbreviating the names of the authors [6, 7]).

The theory of disclinations (another equivalent name is the defect theory) is based on the incompatible theory of elasticity, and it describes both the rotational and translational defects in solids, i.e. disclinations and dislocations. The algebraic structure of the theory of disclinations non-typical for the Abelian gauge approach is connected with the existence of two different types of the defect densities, and it is provided by the form of the corresponding continuity equations. These equations are connected naturally (as it will be shown below) with the Lie algebra $iso(3) = t(3) \dot{+} so(3, \mathbb{R})$, where $so(3, \mathbb{R})$ and $t(3)$ are the Lie algebras of the special ortogonal rotation Lie group $SO(3, \mathbb{R})$ and translation Lie group $T(3)$, respectively, and $\dot{+}$ denotes semi-direct sum of algebras [8]. But it is known that the algebraic structure of any gauge model is stipulated by the gauge group choice and it is an important ingredient of the machinery of gauging in general. As to the analogy discussed in Refs. [6, 7] and to the original strategy of derivation of the GLE-group, namely the choice of the gauge group and, consequently, the pure algebraic aspect of the problem were missing there, and so the following question was left open: why the theory of disclinations admits two different types of defects, i.e. disclinations and dislocations? Some attempts to clarify this question will be made in the present work with the help of the motor calculus proposed by H. SCHAEFER [9, 10].

The monographs [1, 2] contain the recent attempts to develop the gauge model, both of dislocations and disclinations, in the way proposed by C.N. YANG and R. MILLS [11]. The gauging of the group $ISO(3) = T(3) \dot{+} SO(3, \mathbb{R})$ ($\dot{+}$ denotes semi-direct product of groups [8]) [1, 2] again shows us the important role of the corresponding Lie algebra $iso(3)$. So just the same algebras lie behind the basic geometric constructions in the defect theory [4, 5], on the one hand, and in the model [1, 2], on the other. This coincidence helps us to get an alternative way of deriving the GLE-group and explains the relations between the approaches of the Refs. [4, 5] and [1, 2]. It is possible that the wievpoint developed here can stimulate a more profound explanation of the problem concerning the embedding of such a reliable model as the theory of disclinations in some extended non-Abelian gauge models.

As to the general notions concerning the physics and mathematics of gauge fields, for the needs of this work it is sufficient to restrict ourselves only to Refs. [12–14]. A brief, but quite instructive insight into the pure mathematical aspects of gauge field formalism is given in [15].

This paper is written in four sections. Section 2 is devoted to some mathematical preliminaries concerning the representation of the algebra $iso(3)$ by Schaefer's differential operators. We shall develop the so-called $iso(3)$-valued exterior calculus which gives the most adequate tool to investigate the gauge properties of the theory of disclinations. Section 3 deals with the derivation of the GLE-group's transformation law. Special emphasis will be laid on the close similarity (from the geometrical viewpoint) between the defect theory and the Abelian gauge model without monopoles. The discussion in Sec. 4 concludes the paper. Some auxiliary information about the difference between the Abelian gauge models with compact and non-compact gauge group can be found in the Appendix.

Let us note that the consideration in this paper is restricted only by three spatial dimensions (it implies a static defects distribution). In the non-relativistic limit time and space coordinates play quite different roles, both physically and geometrically, and so the case of moving defects requires a separate consideration.

The following notations will be adopted here. The Latin indices denote 1, 2, 3; repeated indices imply summation. The symbol := denotes equality by definition, $\circ$ — the composition of two formal operators, $\in$ and $\ni$ are the belonging signs, ϵ^{abc} is the Levi–Civita tensor ($\epsilon^{123} = 1$).

2. The representation of the algebra $iso(3)$ by Schaefer's differential operators. Schaefer's exterior calculus

The group of rigid motions of three-dimentional Euclidean space E^3 is the Lie group $ISO(3) = T(3) \circledS SO(3, \mathbb{R})$, and the corresponding Lie algebra is $iso(3) = t(3) \dot{+} so(3, \mathbb{R})$. Let us denote by $\{\gamma_a\}$ and $\{\mathbf{e}_a\}$ the bases of the three-dimensional algebras $so(3, \mathbb{R})$ (it consists of skew-symmetric real matrices of the third order) and $t(3)$, respectively. Arbitrary elements of these algebras look as follows:

$$\begin{aligned} \lambda &= \lambda_a \gamma_a \in so(3, \mathbb{R}), \\ \eta &= \eta_a \mathbf{e}_a \in t(3), \end{aligned} \tag{2.1}$$

where λ_a and η_a are real numbers, γ_a are the matrices with elements $(\gamma_a)_{bc} \equiv \epsilon^{bac}$, and $\mathbf{e}_a$ are the columns with a unit in the a-th line (otherwise zero). The algebraic composition

laws for $so(3,\mathbb{R})$ and $t(3)$ are given by the following commutation relations

$$[\gamma_a, \gamma_b] = C^k_{ab}\gamma_k, \qquad [\mathbf{e}_a, \mathbf{e}_b] = 0\,, \tag{2.2}$$

where C^k_{ab} are the structural constants, and $[\cdot,\cdot]$ is the Lie bracket. For the case of $so(3,\mathbb{R})$ we have $C^k_{ab} \equiv \epsilon^{kab}$.

The algebra $iso(3)$ is the six-dimensional algebra defined by the following Lie brackets:

$$\begin{aligned} [\![M_a, M_b]\!] &= \epsilon^{cab} M_c\,, \\ [\![P_a\ , M_b]\!] &= \epsilon^{cab} P_c\,, \\ [\![P_a\ , P_b\ ]\!] &= 0\,, \end{aligned} \tag{2.3}$$

where P_a generates translation along the a-th axis, and M_a generates rotation around the a-th axis; $[\![\cdot,\cdot]\!]$ is here the Lie bracket for $iso(3)$. The formulas $(2.3)_1$, $(2.3)_3$ coincide with the expressions (2.2) and, namely, the bracket $(2.3)_2$ defines the semi-direct sum of $t(3)$ and $so(3,\mathbb{R})$, giving $iso(3)$.

It is convenient to represent the elements of $iso(3)$ by square matrices of the fourth order with the block structure as follows:

$$iso(3) \ni \widetilde{\lambda} := \begin{bmatrix} \lambda & \eta \\ 0 & 0 \end{bmatrix}\,, \tag{2.4}$$

where λ and η are given by Eqs. (2.1). The usefulness of the matrix representation (2.4) is due to the possibility of expressing an arbitrary infinitesimal rigid motion of $E^2_3 \ni \mathbf{x}$

$$\mathbf{x} \to \mathbf{x} + \boldsymbol{\lambda} \times \mathbf{x} + \boldsymbol{\eta}$$

via the matrix multiplication as follows

$$\begin{bmatrix} \mathbf{x} \\ 1 \end{bmatrix} \to [\mathbf{1}_4 + \widetilde{\lambda}] \begin{bmatrix} \mathbf{x} \\ 1 \end{bmatrix} = \begin{bmatrix} \mathbf{x} + \boldsymbol{\lambda} \times \mathbf{x} + \boldsymbol{\eta} \\ 1 \end{bmatrix}\,,$$

where $\mathbf{1}_4$ is the unit matrix, and the equality

$$[\lambda \mathbf{x}]_b = \lambda_a (\gamma_a)_{bc} x_c = (\boldsymbol{\lambda} \times \mathbf{x})_b \tag{2.5}$$

is used. Furthermore, taking

$$M_a = \begin{bmatrix} \gamma_a & 0 \\ 0 & 0 \end{bmatrix} \quad \text{and} \quad P_a = \begin{bmatrix} 0 & \mathbf{e}_a \\ 0 & 0 \end{bmatrix}$$

it is easy to get all the Lie brackets (2.3) by direct computation of the matrix commutators

$$[\![\widetilde{\lambda}_1, \widetilde{\lambda}_2]\!] = \widetilde{\lambda}_1 \widetilde{\lambda}_2 - \widetilde{\lambda}_2 \widetilde{\lambda}_1\,.$$

The Lie bracket for $iso(3)$ can be expressed *via* the Lie bracket for $so(3,\mathbb{R})$ with the help of the matrix representation (2.4). One gets

$$[\![\widetilde{\lambda}_1, \widetilde{\lambda}_2]\!] = \begin{bmatrix} [\lambda_1, \lambda_2] & \lambda_1 \eta_2 - \lambda_2 \eta_1 \\ 0 & 0 \end{bmatrix}\,. \tag{2.6}$$

Using Eq. (2.5) it is possible to rewrite the bracket $[\lambda_1, \lambda_2]$ in the following way: $[\lambda_1, \lambda_2] = (\boldsymbol{\lambda}_1 \times \boldsymbol{\lambda}_2)_a \gamma_a$, what permits, in turn, to convert Eq. (2.6) into another form:

$$[\![\widetilde{\lambda}_1, \widetilde{\lambda}_2]\!] = \begin{bmatrix} (\boldsymbol{\lambda}_1 \times \boldsymbol{\lambda}_2)_a \gamma_a & \boldsymbol{\lambda}_1 \times \boldsymbol{\eta}_2 - \boldsymbol{\lambda}_2 \times \boldsymbol{\eta}_1 \\ 0 & 0 \end{bmatrix}\,. \tag{2.7}$$

Now it is easy to see that the R.H.S. of Eq. (2.7) is nothing else but the rule of motor multiplication of two formal 6-vectors (motors) as follows:

$$\tilde{\lambda}_1 \circ \tilde{\lambda}_2 \equiv \begin{bmatrix} \lambda_1 \\ \eta_1 \end{bmatrix} \circ \begin{bmatrix} \lambda_2 \\ \eta_2 \end{bmatrix} := \begin{bmatrix} \lambda_1 \times \lambda_2 \\ \lambda_1 \times \eta_2 - \lambda_2 \times \eta_1 \end{bmatrix} . \tag{2.8}$$

The notion of a motor and the rule of motor multiplication of two motors (2.8) were introduced in theoretical mechanics by R. MISES [16]. Following the terminology of the Ref. [16], λ is the vector part and η is the moment part of the motor $\tilde{\lambda} = \begin{bmatrix} \lambda \\ \eta \end{bmatrix}$.

The change of the so-called reduction point [16] due to a constant shift $\mathbf{x} \to \mathbf{x} + \mathbf{y}$ results in the following replacement rule for the motor $\tilde{\lambda}$:

$$\begin{bmatrix} \lambda \\ \eta \end{bmatrix} \to \begin{bmatrix} \lambda \\ \eta - \lambda \times \mathbf{y} \end{bmatrix} . \tag{2.9}$$

Thus, from Eqs. (2.6)–(2.8) the main observation of the present section follows: the R. Mises motors are simply elements of $iso(3)$ endowed with the replacement rule (2.9) and the motor multiplication Eq. (2.8) is nothing else but the corresponding Lie bracket Eq. (2.6) for two elements of $iso(3)$.

Now it is appropriate to consider briefly two representations of the algebra $iso(3)$ which are isomorphic to the natural matrix representation:

$$M_a = \begin{bmatrix} \gamma_a & 0 \\ 0 & 0 \end{bmatrix}, \qquad P_b = \begin{bmatrix} 0 & \mathbf{e}_b \\ 0 & 0 \end{bmatrix} .$$

Let us introduce the space of differentiable scalar functions $D_S \ni f(\mathbf{x})$, $\mathbf{x} \in E^3$ and let us consider two differential operators acting on elements of D_S : $\partial_a := \partial/\partial x_a$ and $(\mathbf{x} \times \partial)_a := \epsilon^{abc} x_b \partial_c$. These operators generate infinitesimal changes of the functions $f \in D_S$ under the replacement of variable $\mathbf{x}$:

$$\begin{aligned} &\mathbf{x} \to \mathbf{x} + d\varphi \times \mathbf{x} + d\mathbf{x} , \\ &f \to f + (d\mathbf{x} \cdot \partial) f + d\varphi \cdot (\mathbf{x} \times \partial) f . \end{aligned} \tag{2.10}$$

It is easy to check that the operators $P_a = \partial_a$ and $M_a = (\mathbf{x} \times \partial)_a$ satisfy the following algebra:

$$\begin{aligned} [\![M_a, M_b]\!] &= \epsilon^{acb} M_c , \\ [\![P_a , M_b]\!] &= \epsilon^{acb} P_c , \\ [\![P_a , P_b]\!] &= 0 , \end{aligned} \tag{2.11}$$

and give us the well-known representation of $iso(3)$. The bases $\{\gamma_a, \mathbf{e}_b\}$ and $\{(\mathbf{x} \times \partial)_a, \partial_b\}$ are dual ones because they generate the changes in the two dual spaces: E^3 and D_S.

In order to get another representation of $iso(3)$, let us define the space D_M of motor-valued functions

$$\tilde{\lambda}(\mathbf{x}) = \begin{bmatrix} \lambda(\mathbf{x}) \\ \eta(\mathbf{x}) \end{bmatrix} ,$$

where $\lambda(\mathbf{x})$ and $\eta(\mathbf{x})$ are differentiable vector-valued functions. It is possible to call $\lambda(\mathbf{x})$ and $\eta(\mathbf{x})$, respectively, rotation and displacement fields acting on the vector $\mathbf{x}$ as follows:

$$\mathbf{x} \to \mathbf{x} + \delta(\mathbf{x}), \qquad \delta(\mathbf{x}) := \lambda(\mathbf{x}) \times \mathbf{x} + \eta(\mathbf{x}) . \tag{2.12}$$

Let us compare the terms $\delta(\mathbf{x})$ (2.12) for the two neighbouring points $\mathbf{x}$ and $\mathbf{x} + d\mathbf{x}$. One gets

$$\delta(\mathbf{x} + d\mathbf{x}) = \delta(\mathbf{x}) + dx_a[\partial_a\lambda \times \mathbf{x} + \partial_a\eta + \lambda \times \mathbf{e}_a]\,. \tag{2.13}$$

Starting from Eq. (2.13) one can introduce a new differential operator ∂_a^{Sh} — the so-called Schaefer's derivative — acting on elements of D_M:

$$\partial_a^{Sh}\widetilde{\lambda}(\mathbf{x}) := \begin{bmatrix} \partial_a\lambda \\ \partial_a\eta + \lambda \times \mathbf{e}_a \end{bmatrix}. \tag{2.14}$$

The operator ∂_a^{Sh} Eq. (2.14) generates infinitesimal variations of $iso(3)$-valued functions $\widetilde{\lambda}(\mathbf{x})$ as follows:

$$\widetilde{\lambda}(\mathbf{x} + d\mathbf{x}) = \widetilde{\lambda}(\mathbf{x}) + (d\mathbf{x} \cdot \partial^{Sh})\widetilde{\lambda}(\mathbf{x})\,. \tag{2.15}$$

It is important that Eq. (2.15) is the operator equation: action of the L.H.S. of Eq. (2.15) on the vector $\begin{bmatrix} \mathbf{x} + d\mathbf{x} \\ 1 \end{bmatrix}$, and of the R.H.S. of Eq. (2.15) — on the vector $\begin{bmatrix} \mathbf{x} \\ 1 \end{bmatrix}$ yields the ordinary equality, leading to Eq. (2.13). The operator ∂_a^{Sh} Eq. (2.14) was introduced by H. SCHAEFER [9, 10] in order to construct the description of a Cosserat continuum.

Following the clear analogy with the case of scalar functions, let us define the operator $(\mathbf{x} \times \partial)_a^{Sh}$ generating rotations of elements of D_M:

$$(\mathbf{x} \times \partial)_a^{Sh}\widetilde{\lambda}(\mathbf{x}) := \begin{bmatrix} (\mathbf{x} \times \partial)_a\lambda \\ (\mathbf{x} \times \partial)_a\eta + \lambda \times (\mathbf{e}_a \times \mathbf{x}) \end{bmatrix}. \tag{2.16}$$

Substituting $M_a = (\mathbf{x} \times \partial)_a^{Sh}$ and $P_a = \partial_a^{Sh}$ into Eq. (2.11) one concludes that the Schaefer's operators (2.14), (2.16) form together a representation of $iso(3)$.

With the help of the matrix representation (2.4) one can rewrite the formulas (2.14), (2.16) as follows:

$$\partial_a^{Sh}\widetilde{\lambda} = \partial_a\widetilde{\lambda} + [\![\widetilde{\lambda}, \mathbf{e}_a]\!]\,,$$
$$(\mathbf{x} \times \partial)_a^{Sh}\widetilde{\lambda} = (\mathbf{x} \times \partial)_a\widetilde{\lambda} + [\![\widetilde{\lambda}, \mathbf{e}_a \times \mathbf{x}]\!]\,,$$

where the vectors $\mathbf{e}_a$ and $\mathbf{e}_a \times \mathbf{x}$ are also written in the matrix representation:

$$\begin{bmatrix} 0 & \mathbf{e}_a \\ 0 & 0 \end{bmatrix}, \quad \begin{bmatrix} 0 & \mathbf{e}_a \times \mathbf{x} \\ 0 & 0 \end{bmatrix}.$$

The algebra $iso(3)$ can be viewed as an additive Abelian group (vector space) and this is why it is possible to construct the formalism of "motor-valued" ($iso(3)$-valued) exterior calculus. As to the standard notions of exterior calculus see, for example, [15, 17]; the short remark is given also in [18].

Let us introduce the linear infinite-dimensional spaces $\overset{(n)}{\Omega}(E^3)$ consisting of $iso(3)$-valued differential n-forms $\overset{(n)}{\omega}(\mathbf{x})$ defined on E^3:

$$\overset{(n)}{\omega}(\mathbf{x}) \in \overset{(n)}{\Omega}(E^3)\,,$$

where $n = 0, 1, 2, 3$. The forms of higher orders are trivially zero on E^3. One has the

following explicit expressions for $\overset{(n)}{\omega}(\mathbf{x})$:

$$\overset{(0)}{\omega}(\mathbf{x}) := \widetilde{\lambda}(\mathbf{x}) = \begin{bmatrix} \lambda & \eta \\ 0 & 0 \end{bmatrix}, \quad \overset{(1)}{\omega}(\mathbf{x}) := \widetilde{\lambda}_a(\mathbf{x}) dx_a = \begin{bmatrix} \lambda_a & \eta_a \\ 0 & 0 \end{bmatrix} dx_a,$$

$$\overset{(2)}{\omega}(\mathbf{x}) := (1/2!)\widetilde{\lambda}_{ab}(\mathbf{x}) dx_a \wedge dx_b = (1/2!) \begin{bmatrix} \lambda_{ab} & \eta_{ab} \\ 0 & 0 \end{bmatrix} dx_a \wedge dx_b,$$

$$\overset{(3)}{\omega}(\mathbf{x}) := (1/3!)\widetilde{\lambda}_{abc}(\mathbf{x}) dx_a \wedge dx_b \wedge dx_c$$

$$= (1/3!) \begin{bmatrix} \lambda_{abc} & \eta_{abc} \\ 0 & 0 \end{bmatrix} dx_a \wedge dx_b \wedge dx_c,$$

where $\lambda_{i_1 \ldots i_n}$, $\eta_{i_1 \ldots i_n}$ are skew-symmetric with respect to $i_1, \ldots, i_n$, and $\wedge$ denotes an exterior product. Now let us introduce the Schaefer's exterior derivative operator $d^{Sh} := dx_a \wedge \partial_a^{Sh}$ acting on $\overset{(n)}{\omega}(\mathbf{x})$ as follows:

$$d^{Sh} \overset{(n)}{\omega} = d \overset{(n)}{\omega} + (-1)^n [\![\overset{(n)}{\omega}, d\mathbf{x}]\!], \tag{2.17}$$

where d is the standard exterior derivative and $d\mathbf{x}$ is the one-form in matrix representation (2.4). Calculating the second term in Eq. (2.17) one has to multiply the forms $\overset{(n)}{\omega}(\mathbf{x})$ and $d\mathbf{x}$ externally.

It is clear from the definition (2.17) that d^{Sh} increases the order of n-form $\overset{(n)}{\omega}$: $\overset{(n)}{\Omega}(E^3) \xrightarrow{d^{Sh}} \overset{(n+1)}{\Omega}(E^3)$. One can establish also that d^{Sh} is the nilpotent operator: $d^{Sh} \circ d^{Sh} = 0$. We shall say that n-form $\overset{(n)}{\omega}$ is the exact differential form if $\overset{(n)}{\omega} = d^{Sh} \overset{(n-1)}{\omega}$, and $\overset{(n)}{\omega}$ is the closed differential form if $d^{Sh} \overset{(n)}{\omega} = 0$. Due to nilpotency property of d^{Sh} one can find the following sequence of homeomorphisms is exact [17]:

$$\overset{(0)}{\Omega}(E^3) \xrightarrow{d^{Sh}} \overset{(1)}{\Omega}(E^3) \xrightarrow{d^{Sh}} \overset{(2)}{\Omega}(E^3) \xrightarrow{d^{Sh}} \overset{(3)}{\Omega}(E^3).$$

In the next section we shall consider the gauge properties of the theory of disclinations. The most natural way to do it is to take into consideration the elements of the $iso(3)$-valued exterior calculus introduced above.

3. The "toy principle" of gauge invariance and the gauge structure of the theory of disclinations

Now one can proceeds to the direct consideration of the gauge properties of the theory of disclinations. To begin with, one has to postulate the principle of local gauge invariance of some Lagrangian (following, as usually, the standard YANG-MILLS approach [11]). In this work the general principle of gauge invariance will be replaced by the requirement of the local gauge covariance of the appropriate derivative operator. A condition of such kind might be called the "toy principle". Here it is natural to confine ourselves only to the "toy principle" because it is sufficient to deduce the group of gauge transformations of the model in question. On the other hand, application of concrete Lagrangians and analysis of the dynamics generated by them are outside the scope of this paper. As to the derivative operator, we shall consider here the Schaefer's exterior derivative (2.17).

Let us consider an arbitrary $iso(3)$-valued field

$$\widetilde{v}(\mathbf{x}) := \begin{bmatrix} \mathbf{v}_1(\mathbf{x}) \\ \mathbf{v}_2(\mathbf{x}) \end{bmatrix} \equiv \begin{bmatrix} \boldsymbol{\omega}(\mathbf{x}) \\ \mathbf{u}(\mathbf{x}) \end{bmatrix} . \quad (1)$$

The algebra $iso(3)$, as an Abelian additive group, acts on $\widetilde{v}(\mathbf{x})$ by the shifts

$$\widetilde{v}(\mathbf{x}) \rightarrow \widetilde{v}(\mathbf{x}) + \overline{\delta}\widetilde{v}_0 , \tag{3.1}$$

where it is proposed to adopt the following rule of calculating the term $\overline{\delta}\widetilde{v}_0$:

$$\overline{\delta}\widetilde{v}_0 := \begin{bmatrix} \boldsymbol{\omega}_0 + (1/2)(\partial \times \mathbf{u}_0) \\ \mathbf{u}_0 \end{bmatrix} . \tag{3.2}$$

For constant vectors $\boldsymbol{\omega}_0$ and $\mathbf{u}_0$ the formula (3.2) gives the usual additive transformation of the field $\widetilde{v}(\mathbf{x})$. It is not the case for the $\mathbf{x}$-dependent functions $\boldsymbol{\omega}_0(\mathbf{x})$, $\mathbf{u}_0(\mathbf{x})$. The rule (3.2) implies that one takes into account both the direct rotational contribution $\boldsymbol{\omega}_0$ and the rotational contribution $(1/2)(\partial \times \mathbf{u}_0)$ from the displacement field $\mathbf{u}_0$ to the vectorial part of the field $\widetilde{v}(\mathbf{x})$. Now one gets the following variation of the exterior derivative $d^{Sh}\widetilde{v}(\mathbf{x})$ Eq. (2.17) under the replacement (3.1)–(3.2)

$$(\overline{\delta} \circ d^{Sh})\widetilde{v}(\mathbf{x}) = \begin{bmatrix} 0 \\ \boldsymbol{\omega}_0 \times d\mathbf{x} \end{bmatrix} . \tag{3.3}$$

Let us identify the vector part of $d^{Sh}\widetilde{v}(\mathbf{x})$ with a bend-twist one-form [4, 5, 7]. The coefficients of the moment part of $d^{Sh}\widetilde{v}(\mathbf{x})$ after symmetrization give us the strain tensor components. After the transformation (3.1)–(3.2) both the bend-twist tensor and the strain tensor remains unchanged because the coefficients of the one-form $\boldsymbol{\omega}_0 \times d\mathbf{x}$ are antisymmetric.

Now let us assume the shifts (3.1)–(3.2) are inhomogeneous. Then one gets, instead of Eq. (3.3),

$$(\overline{\delta} \circ d^{Sh})\widetilde{v}_0(\mathbf{x}) = d^{Sh}\begin{bmatrix} \boldsymbol{\omega}_0 \\ \mathbf{u}_0 \end{bmatrix} + d^{Sh}\begin{bmatrix} (1/2)\partial \times \mathbf{u}_0 \\ 0 \end{bmatrix} = \begin{bmatrix} d\boldsymbol{\omega}_0 + (1/2)d(\partial \times \mathbf{u}_0) \\ d\mathbf{u}_0 \end{bmatrix} + \begin{bmatrix} 0 \\ \boldsymbol{\omega}_0 \times d\mathbf{x} + (1/2)(\partial \times \mathbf{u}_0) \times d\mathbf{x} \end{bmatrix} . \tag{3.4}$$

Following the standard strategy of the gauge approach let us define the "compensated derivative" $D^{Sh} := d^{Sh} + \mathcal{A}^{Sh}$ in such way that the inhomogeneous replacement (3.1)–(3.2) will contribute to the moment part of $(\overline{\delta} \circ D^{Sh})\widetilde{v}(\mathbf{x})$ only antisymmetric terms (like in Eq. (3.3) for the case of homogeneous shift). It is just the requirement of the "toy principle" of local gauge covariance of the derivative D^{Sh}. It is clear from Eq. (3.4) that one-form $\mathcal{A}^{Sh}$ should have the following structure:

$$\mathcal{A}^{Sh} := \begin{bmatrix} \varphi^* \\ \beta^* \end{bmatrix}, \qquad \begin{aligned} \varphi^* &:= (1/2)d(\mathbf{e}_c \times \beta_c) + \varphi , \\ \beta^* &:= \beta_a dx_a , \qquad \varphi := \varphi_a dx_a . \end{aligned} \tag{3.5}$$

The compensating shift is generated by the transformations

$$\beta^* \rightarrow \beta^* - d\mathbf{u}_0, \qquad \varphi \rightarrow \varphi - d\boldsymbol{\omega}_0 \tag{3.6}$$

(1) We shall use further the Mises notations (columns) for the $iso(3)$-valued n-forms, bearing in mind the correspondence between motors and matrices (2.4) when calculating the Lie brackets. It is convenient to do so in order to "avoid" formally the zeros in the fourth line of matrices (2.4).

giving, after substitution into Eq. (3.5), the result

$$\mathcal{A}^{Sh} \to \mathcal{A}^{Sh} - \begin{bmatrix} d\omega_0 + (1/2)d(\partial \times \mathbf{u}_0) \\ d\mathbf{u}_0 \end{bmatrix} . \tag{3.7}$$

It is evident that the shift (3.7) possesses the required property.

It is appropriate to put the gauge transformation rule (3.7) into a slightly extended form

$$\mathcal{A}^{Sh} \to \mathcal{A}^{Sh} - d^{Sh} \begin{bmatrix} \omega_0 \\ \mathbf{u}_0 \end{bmatrix} - d^{Sh} \begin{bmatrix} (1/2)\partial \times \mathbf{u}_0 \\ 0 \end{bmatrix} . \tag{3.8}$$

The point here is as follows: both transformations (3.7) and (3.8) generate the same replacement rules

$$\begin{gathered} \varphi^* \to \varphi^* - d\omega_0 - (1/2)d(\partial \times \mathbf{u}_0), \\ \operatorname{Sym} \beta_a \to \operatorname{Sym} \beta_a - (1/2)(\partial_a (u_0)_b + \partial_b (u_0)_a), \end{gathered} \tag{3.9}$$

where Sym implies symmetrization of the coefficients of the one-form β^* (symmetrizing the distortion one-form coefficients one gets the strain tensor components). The rules (3.9) at $\omega_0 = \text{const}$ are just the gauge transformation for the bend-twist and the strain tensors derived in [7], i.e. the GLE-group.

One-form $\mathcal{A}^{Sh}$ is an $iso(3)$-valued one-form looking like an Abelian connection one-form. Then the two-form

$$\mathcal{F} = (1/2!) \begin{bmatrix} \mathbf{A}_{ab} \\ \mathbf{B}_{ab} \end{bmatrix} dx_a \wedge dx_b \equiv \begin{bmatrix} \mathbf{A} \\ \mathbf{B} \end{bmatrix} := d^{Sh} \mathcal{A}^{Sh} \tag{3.10}$$

should play the role of the curvature two-form of the Abelian connection $\mathcal{A}^{Sh}$, and

$$d^{Sh} \mathcal{F} = 0 \tag{3.11}$$

is the analogue of the Bianchi identity (see Eqs. (A.1), (A.3) in the Appendix). From the electromagnetic analogy viewpoint, $\mathcal{F}$ is the strength of the field $\mathcal{A}^{Sh}$ and Eq. (3.11) is a kind of the first Maxwell's equation forbidding the presence of monopoles. The corresponding bundle over E^3 turns out to be topologically trivial. The two-form $\mathcal{F}$ Eq. (3.10) is gauge-invariant under the transformation (3.8) due to nilpotency of the operator d^{Sh}.

Let us express the components of the form $\mathcal{F}$ by the fields φ_a, β_a Eq. (3.5),

$$\mathcal{F} = d \begin{bmatrix} \varphi^* \\ \beta^* \end{bmatrix} - \left[\!\!\left[\begin{bmatrix} \varphi^* \\ \beta^* \end{bmatrix}, d\mathbf{x} \right]\!\!\right] ,$$

or

$$\mathcal{F} = \begin{bmatrix} d\varphi^* \\ d\beta^* + \varphi^* \overset{\times}{\wedge} d\mathbf{x} \end{bmatrix} , \tag{3.12}$$

where

$$\varphi^* \overset{\times}{\wedge} d\mathbf{x} := (1/2!)(\varphi_b^* \times \mathbf{e}_a - \varphi_a^* \times \mathbf{e}_b) dx_a \wedge dx_b .$$

The coefficients of the form $\mathcal{F}$ Eq. (3.10) can be written as follows:

$$\begin{aligned} A_{ab}^k &= \partial_a \varphi_{bk} - \partial_b \varphi_{ak} , \\ B_{ab}^k &= \partial_a e_{bk} - \partial_b e_{ak} + \epsilon^{kca} \varphi_{bc} - \epsilon^{kcb} \varphi_{ac} , \end{aligned} \tag{3.13}$$

where $e_{bk} = (1/2)(\beta_{bk} + \beta_{kb})$. The coefficient-functions A_{ab}^k and B_{ab}^k are just the disclination and dislocation densities of the theory of disclinations [4, 5]. It can be made

more obvious by introducing the one-form $*\mathcal{F}$ dual to $\mathcal{F}$ as follows:

$$*\mathcal{F} = \begin{bmatrix} \theta_a \\ \alpha_a \end{bmatrix} dx_a, \qquad \begin{bmatrix} \theta_a \\ \alpha_a \end{bmatrix} := (1/2)\epsilon^{acd} \begin{bmatrix} \mathbf{A}_{cd} \\ \mathbf{B}_{cd} \end{bmatrix} . \tag{3.14}$$

The coefficients θ_a and α_a are the disclination and dislocation densities of the defect theory [4, 5].

The Bianchi identity (3.11) has the following explicit form:

$$\partial_a^{Sh} \begin{bmatrix} \mathbf{A}_{bc} \\ \mathbf{B}_{bc} \end{bmatrix} + \partial_c^{Sh} \begin{bmatrix} \mathbf{A}_{ab} \\ \mathbf{B}_{ab} \end{bmatrix} + \partial_b^{Sh} \begin{bmatrix} \mathbf{A}_{ca} \\ \mathbf{B}_{ca} \end{bmatrix} = 0 , \tag{3.15}$$

or

$$\partial_a \theta_{ab} = 0, \qquad \partial_a \alpha_{ab} - \epsilon^{bcd} \theta_{cd} = 0 , \tag{3.16}$$

where

$$\begin{bmatrix} \theta_{ab} \\ \alpha_{ab} \end{bmatrix} \equiv \begin{bmatrix} \theta_a \\ \alpha_a \end{bmatrix} .$$

The Eqs. (3.16) are the continuity equations of the theory of disclinations, and being written in the form Eq. (3.15) they show us the algebraic (related to $iso(3)$) nature. The Eq. (3.11) (without indices) directly characterizes the defect theory as an example of Abelian gauge model without monopoles.

Before concluding the section let us compare the Eqs. (3.9) with the corresponding equations of the Ref. [18], where the approach of the Refs. [6, 7] was formulated on the basis of the "usual" (scalar-valued) exterior calculus. First of all it is necessary to establish the correspondence between the definitions of the defect densities here (given by Eqs. (3.12)–(3.14)) and in [18]. In the Ref. [18] the disclination density three-form θ and the dislocation density two-form α are defined in the following way:

$$\begin{aligned} \theta &= d\kappa , \\ \alpha &= d\beta + \kappa , \end{aligned} \tag{3.17}$$

where β is a distortion one-form, and κ is a bend-twist two-form. Let us identify the Eq. $(3.17)_2$ with the equation

$$\mathbf{B} = d\beta^* + \varphi^* \overset{\times}{\wedge} d\mathbf{x}$$

(see Eqs. (3.10), (3.12)) because both of them define the dislocation density two-form. This comparison gives us the explicit expression for the two-form κ

$$\kappa \equiv \varphi^* \overset{\times}{\wedge} d\mathbf{x} . \tag{3.18}$$

Let us apply the exterior derivative operator d to both sides of Eq. (3.18) in order to compare the two definitions of disclination density, given by Eq. $(3.17)_1$ and (3.12)–(3.14). The result is as follows:

$$\mathbf{e}_a \times \theta_a = \theta_E \quad \text{or} \quad \epsilon^{abc} \theta_{bc} = (\theta_E)_a . \tag{3.19}$$

Here θ_E denotes the disclination density three-form (i.e. zero form) in the sense of Ref. [18]. Strictly speaking, the Eq. (3.19) shows us that the disclination densities do not coincide with each other, and so both the definitions can not be transformed into each other by means of the exterior calculus only. Nevertheless, we shall compare the corresponding formulae for the gauge transformations groups.

In the Ref. [18] the group of gauge transformations is defined by the replacements

$$\beta \to \beta + d\mathbf{h} - \mathbf{g}, \tag{3.20}$$
$$\kappa \to \kappa + d\mathbf{g},$$

preserving the form-invariance of the Eqs. (3.17). Here $\mathbf{g}$ is an arbitrary one-form and $d\mathbf{h}$ is an arbitrary exact one-form. One can identify the term $d\mathbf{h}$ in $(3.20)_1$ with the term $-d\mathbf{u}_0$ in Eq. (3.7). Moreover, taking into account (3.18) the unique way to get the replacement rule $(3.20)_2$ consists in performing the following transformation of the one-form φ^*:

$$\begin{array}{c} \varphi^* \to \varphi^* - d\omega_0 \\ \Downarrow \\ \kappa \to \kappa - d\omega_0 \overset{\times}{\wedge} d\mathbf{x} = \kappa + d(\omega_0 \times d\mathbf{x}). \end{array} \tag{3.21}$$

One gets from Eqs. (3.21) and $(3.20)_2$ that

$$\mathbf{g} = \omega_0 \times d\mathbf{x}$$

and so the shift $\mathbf{g}$ Eq. $(3.20)_1$ is also contained in the moment part of the transformation (3.8).

Finally one can conclude that the transformation (3.20) overlap partially the transformation rule (3.8) $\left(\text{except the shift } (1/2)d^{Sh}\begin{bmatrix} \partial \times \mathbf{u}_0 \\ 0 \end{bmatrix}\right)$. On the other hand, the gauge transformation GLE [7] does not contain the shift $d^{Sh}\begin{bmatrix} \omega_0 \\ 0 \end{bmatrix}$. So the transformation rule (3.8) includes both the results of the Refs. [7] and [18]. The approach given here, involving Schaefer's exterior calculus and some modification of the arguments of the Ref. [11], leads to the required gauge transformation group (3.9) in a more formal and expedient way.

4. Discussion and conclusions

Let us summarize the main results of the preceding considerations.

The main idea following from Sec. 2 is as follows: the motor algebra introduced by R. MISES [16] is nothing else but the Lie algebra $iso(3)$ corresponding to the Lie group $ISO(3) = T(3) \rtimes SO(3, \mathbb{R})$ which is used now to formulate the non-Abelian gauge model of defects in solids [1, 2]. Such viewpoint suggests the representation of the algebra $iso(3)$ by the tools of the motor calculus: the Schaefer's differential operators, acting on the space of differentiable $iso(3)$-valued functions, form indeed such a representation. The algebra $iso(3)$ can be considered as a six-parameter additive Abelian group (i.e. as a six-dimensional linear vector space provided with the additional operation of Lie multiplication), and it allows us to introduce a notion of the $iso(3)$-valued exterior calculus. In spite of the fact that a close picture has been established in the original SCHAEFER'S papers [9, 10], the pure Lie algebraic structure of the corresponding formulae related to the representation of $iso(3)$ has not been achieved there. For example, the operator d^{Sh} Eq. (2.17) is treated here without involving the formalism of affine connections [10], but pure algebraically with the help of the Lie bracket for $iso(3)$.

The next Sec. 3 contains the investigation of the gauge properties of the theory of disclinations [4, 5] by means of the formulae of the Sec. 2. Postulating the "toy principle" of gauge invariance one gets the group of gauge transformations of the defect theory.

The replacement rule (3.8) (leading to the gauge transformation group (3.9)) combines the corresponding results of the Refs. [6, 7, 18] in the sense that one can deduce from Eq. (3.8) all the concrete gauge transformation formulas suggested in these references. The approach given here makes it evident that the algebra $iso(3)$ plays the role of the six-dimensional Abelian gauge group in the theory of disclinations. Furthermore the two types of the defect densities (disclination and dislocation ones) arise in the model in question due to the Lie algebraic structure of $iso(3)$ itself, what is shown by the above considerations. Both the expressions of the defect densities in terms of the bend-twist and strain fields (3.13) and the continuity equations (3.16) take the form of the "$iso(3)$-valued" Abelian electrodynamics without monopoles (compare Eqs. (3.10) and (3.11), with the corresponding formulas given in Appendix). Hence the disclination and dislocation singular lines get the status of Dirac strings for the case of monopole being at spatial infinity in E^3. As it is explained in the Appendix, the given gauge model corresponds to the trivial bundle over E^3 with vanishing first Chern class $[C_1] = 0$. As to more complicated generalization, the singular dislocation lines can not be attached to monopoles but only to the dislocation lines (as it is clear from Eq. (3.16)) due to noncompactness of the translation subgroup — it is a well-known fact. But the disclination lines can admit some monopole-like sources if it "compactifies" any subalgebra of $so(3, \mathbb{R}) \subset iso(3)$ up to a one-parameter rotation group $SO(2)$.

The gauge properties of the theory of disclinations turn out to be related to the pure mathematical problems of exactness and closeness of the corresponding differential forms. The exterior calculus language is the adequate mathematical reformulation of the Abelian gauge problems and the theory of disclinations is a special example of such kind.

The given approach leads to the following questions. For example, is it possible to introduce the non-Abelian generalization of the defect theory in order to smooth the singular defect's cores — as it happens for the Hooft–Polyakov solution of the Georgi–Glashow gauge model ([12], Chapter 15)? Or, how to reduce the general Cartan equations of some non-Abelian gauge model to the simple equation $\mathcal{F} = d^{Sh}\mathcal{A}^{Sh}$ in order to identify unambiguously the disclination and dislocation densities? Anyway, a more detailed study of these problems deserves further investigation.

Appendix

Several facts concerning the Abelian gauge fields.

The classical Maxwell's electrodynamics and the quantum Dirac's electrodynamics are particular but most important examples of the Abelian gauge models. They correspond to the two possible choices of the Abelian gauge group $G : G = U(1) \approx SO(2) \approx S^1$ is the compact group (Dirac's electrodynamics) or $G = T(1) \approx \mathbb{R}$ is the non-compact one (Maxwell's electrodynamics). Here the symbol $\approx$ denotes isomorphism, S^1 is a one-dimensional sphere, $\mathbb{R}$ is a set of real numbers; $T(1)$ is a one-parameter translation group, $U(1)$ is a one-dimensional unitary group, and $SO(2)$ is a rotation group [8].

Let us consider a smooth oriented three-manifold M endowed with some Euclidean metric. Let G be an Abelian gauge group and $\mathcal{G}$ its Lie algebra. One can pick a G-bundle E over M (in particular E may be a trivial bundle) by introducing a $\mathcal{G}$-valued connection one-form A which defines the parallel transport law on M. The corresponding curvature two-form F looks as follows

$$F = dA\,, \tag{A.1}$$

where d is the exterior differentiation operator. The form F (A.1) is the gauge invariant under the transformation rule

$$A \to A + df \tag{A.2}$$

due to the nilpotency property of the operator d : $d \circ d = 0$. The two-form F is defined by (A.1) unambiguously on the whole M and usually one identifies F as a physical quantity with field's A strength. Obviously the following Bianchi identity holds

$$dF = 0\,. \tag{A.3}$$

The form F defines an element of the second group of cohomologies $H^2(M)$ of the manifold M. The corresponding class of cohomologies is the first Chern class $[C_1]$.

The bundle E is topologically trivial if and only if the first Chern class vanishes: $[C_1] = 0$. The following question arises: when an arbitrary closed scalar two-form F is a curvature form of some Abelian bundle? The answer is the following:

a) for $G = U(1)$ the necessary and sufficient condition is $[C_1] \approx 2\pi\mathbb{Z}$;

b) for $G = T(1)$ the necessary and sufficient condition is $[C_1] = 0$;

(here $\mathbb{Z}$ implies the ring of integers). From the physical viewpoint the condition $[C_1] = 0$ means the absence of monopoles in the case of a non-compact Abelian gauge group.

More detailed information about the gauge field formalism can be found in the cited literature and in the references therein.

Acknowledgement

The author would like to thank Professor V.N. POPOV for reading the manuscript and for the discussions.

References

1. A. KADIC and D.G.B. EDELEN, *A gauge theory of dislocations and disclinations*, Lecture Notes in Physics No.174, Springer, Berlin 1983.
2. D.G.B. EDELEN and D.C. LAGOUDAS, *Gauge theory and defects in solids*, North-Holland, Amsterdam 1988.
3. *Gauge theories in mechanics*, pp. 233–294 [in:] Trends in Applications of Pure Mathematics to Mechanics, [Eds.] E. KRÖNER and K. KIRCHGÄSSNER, Lecture Notes in Physics No. 249, Springer, Berlin 1986.
4. R. DE WIT, *Linear theory of static disclination*, [in:] Fundamental Aspects of Dislocation, [Eds.] J.A. SIMMONS, R. DE WIT and R. BULLOUGH, Nat. Bur. Stand. US, Spec. Publ., 651–673, 1970.
5. R. DE WIT, *Theory of disclinations. II. Continuous and discrete disclinations in anisotropic elasticity*, J. Res. Nat. Bur. Stand. US, **77A**, 1, 49-100, 1973; *III. Continuous and discrete disclination in isotropic elasticity*, J. Res. Nat. Bur. Stand. US, **77A**, 3, 359–368, 1973; *IV. Straight disclinations*, J. Res. Nat. Bur. Stand. US, **77A**, 5, 607–658, 1973.
6. A.A. GOLEBIEWSKA-LASOTA, *Dislocations and gauge invariance*, Int. J. Engng. Sci., **17**, 3, 329–333, 1979.
7. A.A. GOLEBIEWSKA-LASOTA and D.G.B. EDELEN, *On the gauge transformations admitted by the equations of defect dynamics*, Int. J. Engng. Sci., 17, 3, 335–339, 1979.
8. A.O. BARUT and R. RĄCZKA, *Theory of group representations and applications*, vol. 1, 2. PWN-Polish Scientific Publ., Warszawa 1980.
9. H. SCHAEFER, *Analysis der Motorfelder in Cosserat-Kontinuum*, ZAMM, **47**, 5, 319–328, 1967; H. SCHAEFER, *Das Cosserat-Kontinuum*, ZAMM, **47**, 8, 485–498, 1967.
10. H. SCHAEFER, *The basic affine connection in a Cosserat continuum*, pp. 57–62, [in:] Mechanics of Generalized Continua, IUTAM Symposium, [Ed.] K. KRÖNER, Springer, Berlin 1968.
11. C.N. YANG and R. MILLS, *Conservation of isotropic spin and isotopic gauge invariance*, Phys. Rev., **96**, 1, 191–195, 1954.
12. TA-PEI CHENG and LING-FONG LI, *Gauge theory of elementary particle physics*, Clarendon Press, Oxford 1984.

13. E.W. MIELKE, *Geometrodynamics of gauge fields*, Akademie-Verlag, Berlin 1987.
14. R.B. MARATHE and G. MARTUCCI, *The geometry of gauge fields*, J. Geom. Phys., **6**, 1, 1–107, 1989.
15. M.B. GREEN, J.H. SCHWARZ and E. WITTEN, *Superstring theory*, vol. 2, Cambridge University Press, New York 1988.
16. R. v. MISES, *Motorrechnung, ein neues Hilfsmittel der Mechanik*, ZAMM, **4**, 2, 155–181, 1924.
17. R. BOTT and L.W. TU, *Differential forms in algebraic topology*, Springer, New York 1987.
18. D.G.B. EDELEN, *On a closure of the governing equations of defect dynamics and the resulting theory of the plastic state*, Int. J. Engng Sci., **17**, 4, 441–464, 1979.

RUSSIAN ACADEMY OF SCIENCES
ST.-PETERSBURG BRANCH OF V.A. STEKLOV MATHEMATICAL INSTITUTE,
ST.-PETERSBURG, RUSSIA.

Received December 7, 1992.

Arch. Mech., 45, 1, pp. 107–119, Warszawa 1993

Kink-shaped solitary waves in viscoelastic material: Selected properties

A. BLINOWSKI (WARSZAWA)

IT IS SHOWN that, for a wide class of nonlinear viscoelastic media, the propagation velocity of kink-shaped stationary solitary wave, as well as the total dissipation rate associated with such a wave motion, do not depend on the viscous properties of the material and can be found in terms of boundary value conditions and the elastic characteristics without solving the equation of motion, which may include unknown viscous constitutive characteristics. Moreover, their values are equal to the corresponding values, obtained for the case of shock propagation in inviscid material (provided the wave amplitude and the elastic potentials are the same). Thermodynamic restrictions imposed on the kink-shaped wave propagation schemes are briefly discussed. For a simple wave motion scheme, the viscous wave profile is effectively found.

1. Introduction

RECENTLY, ([1, 2]) the present author considered, in the framework of the small deformation approach, Eimer's bimodular material modeling the cracked media. If such a material is additionally endowed with the linear viscous properties, then a quasi-stationary solution of the wave propagation problem with diffused shock profile can be obtained. It turned out, that both the propagation velocity of such a wave and its total dissipation rate do not depend on the viscosity and (as one could expect in this situation) are equal to the corresponding values obtained from the considerations on the shock front propagation in purely elastic material.

It was natural to suspect that these particular results are valid also for much more general situations that those considered in the mentioned paper.

It is not possible to mention here even a small part of the vast literature devoted to the problem of viscous shock propagation, thus we shall point out a few papers only. The textbook example of the complete solution of the initial-value problem of discontinuity evolution for the Burgers equation[1] describing the wave, asymptotically tending to the quasi-stationary solitary kink, should be mentioned here [3]. This result points out, that it could be worthwhile to study the quasi-stationary solitary kink waves in infinite viscoelastic media as the asymptotic forms of the real solutions of the initial-value problems. Despite the huge variety of the papers devoted to these and related problems, still many authors find it possible to contribute some new elements to the knowledge of the problem (e.g., quite recently, the paper by GOODING and BALES [4], see also the references quoted in [4]).

The author cannot point out, however, any paper, containing sufficiently general results, from which the effects observed for Eimer's material can be derived as a particular case.

In the present paper the author, using very simple, but quite general, purely mechanical model, will try to disclose some general features of the problem, which apply also to the particular case of Eimer's material.

---

[1] (1) I.e. $u_t + uu_x = \nu u_{xx}$.

It should be underlined here that the problem under consideration is by no means of purely academic interest only. It is a well known fact that, in the course of numeric calculations of the shock wave propagation processes, some (usually artificial) viscous properties must be introduced into the algorithm in order to suppress the numeric instabilities. On the other hand, if the old, but still effective, classical analytic model of the discontinuity propagation is employed, then the real material viscous properties are disregarded. Thus it seems to be worthwhile to learn, at least qualitatively (but not only), how the viscous properties affect the global characteristics of the wave motion.

2. Preliminaries

Since we shall consider one-dimensional deformations only, it will be convenient to introduce a simplified scalar notation corresponding to the tensorial symbols in three-dimensional nonlinear mechanics of continua. Thus we shall denote by

$$x = x(X, t)$$

the current (Eulerian) coordinate of the material particle whose (Lagrangian) coordinate in the reference configuration was X. We denote also:

$$\text{(2.1)} \qquad \begin{aligned} &(1) \quad F \equiv \frac{\partial x(X,t)}{\partial X}, \qquad (3) \quad \varepsilon \equiv F - 1, \\ &(2) \quad v \equiv \frac{\partial x(X,t)}{\partial t}, \qquad (4) \quad \varrho \equiv \frac{\varrho_0}{F}, \end{aligned}$$

where ϱ_0 denotes the density in reference configuration. It is obvious that ϱ is the current density (in the symbolic notation we can express the one-dimensional mass conservation law as follows: $\varrho dx = \varrho_0 dX$). From Eq. $(2.1)_4$ using another well-known expression for mass conservation law (in one-dimensional form):

$$\text{(2.2)} \qquad \dot{\varrho} = -\varrho \partial v / \partial x \,,$$

where the dot stands for the material time-derivative: $\dot{\varrho} \equiv \partial \varrho(X,t)/\partial t$, we obtain at once:

$$\text{(2.3)} \qquad \dot{F} = F \partial v / \partial x \,.$$

For the further considerations we confine our attention to the quasi-stationary field, describing waves travelling into right-hand side direction with constant velocity without change of its shape. Thus for $x(X,t)$ we can write:

$$\text{(2.4)} \qquad x(X,t) = X + u(x(X,t) - Ut) + x_0 + v_0 t \,,$$

where U, x_0 and v_0 are some constants, the choice of the last two of them is merely a matter of choice of the frame of reference; for the time being, we shall assume them to vanish. According to the definition $(2.1)_1$ and $(2.1)_2$, using Eq. (2.4), one obtains:

$$\text{(2.5)} \qquad F = \frac{\partial X}{\partial X} + \frac{du}{d(x - Ut)} \frac{\partial [x(X,t) - Ut]}{\partial X} = 1 + u' F \,,$$

where "prime" stands for $d/d\xi$, $\xi \equiv x - Ut$. For velocity we obtain:

$$\text{(2.6)} \qquad v = \frac{du}{d(x - Ut)} \frac{\partial [x(X,t) - Ut]}{\partial t} = u'(v - U) \,.$$

Eliminating u' from Eqs. (2.5) and (2.6) we obtain the following relation between F and v:

$$v = U(1 - F), \tag{2.7}$$

hence

$$\frac{\partial v}{\partial x} = v' = -UF', \tag{2.8}$$

and

$$\dot{v} = -U\dot{F} = -UF\frac{\partial v}{\partial x} = U^2FF'. \tag{2.9}$$

3. Basic assumptions and constitutive relations

We shall consider a class of viscoelastic materials exhibiting the following behavior:

a. The total stress can be subdivided into two parts:

$$\sigma = \sigma_{\text{el}} + \sigma_{\text{inel}}, \tag{3.1}$$

where we assume that:

- the first term depends only on the present state of deformation (strain ε),

$$\sigma_{\text{el}} = \sigma_{\text{el}}(\varepsilon). \tag{3.2}$$

- σ_{inel} (which can be a function of deformation and velocity gradients of any order) vanishes in absence of velocity gradients.

Since we consider one-dimensional processes only, by σ we denote in Eqs. (3.1) and (3.2) the normal component of Cauchy stress tensor. One-dimensionality of our problem makes it possible to represent all functions of deformation ε as functions of density ϱ (we have $\varrho = \varrho_0/(\varepsilon + 1)$).

b. The total energy density (per unit mass) is equal to the sum of the elastic potential, which depends on the strain (density) only, and kinetic energy density, thus the total energy E (per unit cross-section) of the portion of medium contained between the planes $x = a$ and $x = b$ can be expressed as follows:

$$E = \int_a^b \varrho\left(w(\varrho) + \frac{v^2}{2}\right) dx, \tag{3.3}$$

thus we have constricted our field of interests to the purely mechanical theory. The energy density $w(\varrho)$ can be considered, depending on the problem under consideration, as Gibbs or Helmholz free energy density. Let us consider now the total mechanical energy dissipation rate D in the material interval $\langle A, B\rangle$, defined as the difference between the external force power and the total energy growth rate

$$D = \sigma v\Big|_a^b - \frac{d}{dt}\int_a^b \varrho\left(w + \frac{v^2}{2}\right) dx, \tag{3.4}$$

where $a = x(A, t)$, $b = x(B, t)$. Taking into account, that $\varrho dx = \varrho_0 dX$, we can rewrite Eq. (3.4) as follows:

$$D = \int_A^B \left[\frac{\partial}{\partial X}(\sigma v) - \varrho_0\left(\frac{dw}{d\varepsilon}\dot{\varepsilon} + v\dot{v}\right)\right] dX. \tag{3.5}$$

Recalling that $\dot{\varepsilon} = \dot{F} = F dv/dx$ and $d/dX = F d/dx$, we can write

$$D = \int_A^B \left[F\left(\frac{\partial \sigma}{\partial x} - \varrho \dot{v} \right) v + F\left(\sigma - \varrho_0 \frac{dw}{d\varepsilon} \right) \frac{\partial v}{\partial x} \right] dX . \tag{3.6}$$

In virtue of the equation of motion, the first term in parenthesis vanishes; if the material were elastic then the second term would also vanish, thus for consistency of the model, the following constitutive relation should be valid:

$$\sigma_{\mathrm{el}}(\varepsilon) = \varrho_0 \frac{dw(\varepsilon)}{d\varepsilon} = -\varrho^2 \frac{dw(\varrho)}{d\varrho} \tag{3.7}$$

(the second equality follows from the relation $\varrho(1 + \varepsilon) = \varrho_0$).

Thus we finally obtain the following familiar expression for the dissipation rate D:

$$D = \int_A^B F \sigma_{\mathrm{inel}} \frac{\partial v}{\partial x} dX = \int_a^b \sigma_{\mathrm{inel}} \frac{\partial v}{\partial x} dx . \tag{3.8}$$

4. Kink-shaped quasi-stationary wave profiles

Among all possible quasi-stationary solutions in infinite regions we shall consider only localized solutions, i.e. we shall require vanishing of the strain gradients in infinities (in virtue of Eq. (2.7) also velocity gradients should vanish then).

We shall start from the equation of motion in the absence of body forces expressed in terms of Cauchy stress,

$$\frac{\partial \sigma}{\partial x} = \varrho \dot{v} . \tag{4.1}$$

Using relations (2.1) (d) and (2.9) we can reduce Eq. (4.1) to the following ordinary nonlinear differential equation:

$$\Sigma'(\xi) - \varrho_0 U^2 \varepsilon'(\xi) = 0 , \tag{4.2}$$

where, as it has been already mentioned, "prime" denotes differentiation with respect to $\xi \equiv x - Ut$, and

$$\Sigma(\xi) = \sigma_{\mathrm{el}}[\varepsilon(\xi)] + \sigma_{\mathrm{inel}}[\varepsilon(\xi), \varepsilon'(\xi)]$$

is an expression for the stress as the function of ξ, while σ_{el} and σ_{inel} are known functions of the strain and its derivative.

The inelastic stress σ_{inel} depends on the strain derivative ε' since it depends on the velocity gradient which, in turn, for quasi-stationary solution, can be expressed through ε' (compare Eq. (2.8)).

Equation (4.2) in fact constitutes a cornerstone of all our considerations, the remaining reasoning is merely a matter of skills in the formula transformations.

Integrating Eq. (4.2) (we assume of course $\varrho_0 = \mathrm{const}$), we obtain at once

$$\Sigma(\varepsilon, \varepsilon') - \varrho_0 U^2 \varepsilon = C , \tag{4.3}$$

where C is an integration constant, $\varepsilon = \varepsilon(\xi)$.[2]

[2] For the sake of simplicity we confined our considerations to the dependence of inelastic stress on the first velocity gradient; one can easily see that taking into account the higher gradients does not change the consideration.

This yields immediately

$$\sigma_{-\infty} - \varrho_0 U^2 \varepsilon_{-\infty} = \sigma_{\infty} - \varrho_0 U^2 \varepsilon_{\infty} . \tag{4.4}$$

Solving algebraic equation (4.4) with respect to U^2 one obtains:

$$U^2 = \frac{\sigma_{-\infty} - \sigma_{\infty}}{\varrho_0(\varepsilon_{-\infty} - \varepsilon_{\infty})} , \tag{4.5}_1$$

or, in terms of densities

$$U^2 = \frac{\sigma_{-\infty} - \sigma_{\infty}}{\varrho_{\infty} - \varrho_{-\infty}} \frac{\varrho_{-\infty}\varrho_{\infty}}{\varrho_0^2} . \tag{4.5}_2$$

Two important facts should be mentioned here:

The first — according to our assumptions, the inelastic stress vanishes at infinities, thus relations $(4.5)_1$, $(4.5)_2$ express propagation velocity U entirely in terms of strains (densities) at infinities and elastic properties of the material *independently of its inelastic properties*.

The second — taking arbitrarily $v_0 = 0$ in Eq. (2.4) we assumed tacitly (compare Eq. (2.7)) that the medium in local reference configuration is at rest; the point is that, for certain processes, it can happen that no part of the material remains in the local reference configuration (e.g. for the case of wave propagation through the pre-stressed material). Thus, rather the difference between the material velocity and propagation velocity than merely the propagation velocity has the physical meaning.

Using Eqs. (2.7) and $(2.1)_4$ we obtain immediately

$$(v - U)^2 = U^2 \frac{\varrho_0^2}{\varrho^2} . \tag{4.6}$$

Substituting Eqs. (4.5) into the last relation we obtain:

$$(v - U)^2 = \frac{\sigma_{-\infty} - \sigma_{\infty}}{\varrho_{\infty} - \varrho_{-\infty}} \frac{\varrho_{-\infty}\varrho_{\infty}}{\varrho^2} . \tag{4.7}$$

Relation (4.7) is valid for any choice of the frame of reference, it should be satisfied for any values of time and space coordinates, thus for infinities we obtain:

$$\begin{aligned} (v_{-\infty} - U)^2 &= \frac{\sigma_{-\infty} - \sigma_{\infty}}{\varrho_{\infty} - \varrho_{-\infty}} \frac{\varrho_{\infty}}{\varrho_{-\infty}} , \\ (v_{\infty} - U)^2 &= \frac{\sigma_{-\infty} - \sigma_{\infty}}{\varrho_{\infty} - \varrho_{-\infty}} \frac{\varrho_{-\infty}}{\varrho_{\infty}} . \end{aligned} \tag{4.8}$$

The first remark, concerning relation (4.5), remains valid for Eqs. (4.8) as well. These relations will be useful for the discussion of the limit behavior of the solution for vanishing viscosity.

As a matter of fact, we have not solved Eq. (4.2), up to this point, nevertheless, we were able to find the effective relation between the boundary values at infinities and the propagation velocity. It turns out that also the total dissipation rate can be found at this stage of considerations. To this end we use relation (4.3) and express inelastic part of stress as follows:

$$\sigma_{\text{inel}} = C + \varrho_0 U^2 \varepsilon - \varrho_0 \frac{dw}{d\varepsilon} . \tag{4.9}$$

Substituting the last expression into relation (3.8) and expressing dv/dx through ε', in the case of infinite region one obtains

$$(4.10) \qquad D = -U \int_{-\infty}^{\infty} \left(C + \varrho_0 U^2 \varepsilon - \varrho_0 \frac{dw}{d\varepsilon} \right) \varepsilon' \, d\xi = -U \left(C\varepsilon + \frac{1}{2} \varrho_0 U^2 \varepsilon^2 - \varrho_0 w \right) \Big|_{-\infty}^{\infty}.$$

Expressing C in terms of the boundary values in infinities (compare Eqs. (4.3) and (4.4)) as follows:

$$(4.11) \qquad C = \frac{1}{2} \left[\varrho_0 \left(\frac{dw}{d\varepsilon}\Big|_{-\infty} + \frac{dw}{d\varepsilon}\Big|_{\infty} \right) - \varrho_0 U^2 (\varepsilon_{-\infty} + \varepsilon_{\infty}) \right],$$

and substituting this expressions into Eq. (4.10), we arrive at the following expression for the total dissipation rate:

$$(4.12)_1 \qquad D = U \varrho_0 \left[(w_{\infty} - w_{-\infty}) - \frac{1}{2} \left(\frac{dw}{d\varepsilon}\Big|_{\infty} + \frac{dw}{d\varepsilon}\Big|_{-\infty} \right) (\varepsilon_{\infty} - \varepsilon_{-\infty}) \right].$$

Equivalent expression in terms of densities assumes the following form:

$$(4.12)_2 \qquad D = U \varrho_0 \left[(w_{\infty} - w_{-\infty}) + \frac{1}{2\varrho_{-\infty}\varrho_{\infty}} (\sigma_{\infty} + \sigma_{-\infty})(\varrho_{\infty} - \varrho_{-\infty}) \right],$$

where stress values at infinities can be expressed in terms of densities only: $\sigma_{\pm\infty} = -(\varrho^2 dw/d\varrho)|_{\pm\infty}$. Expressions $(4.12)_1$, $(4.12)_2$ are valid in the particular frame of reference, for which the medium in the local reference configuration rests. Using relations (4.5) one obtains frame-independent expressions for the dissipation rate, we quote them for completeness:

$$(4.12)_3 \qquad D = \sqrt{\frac{\sigma_{-\infty} - \sigma_{\infty}}{(\varepsilon_{-\infty} - \varepsilon_{\infty})} \varrho_0} \times \left[(w_{\infty} - w_{-\infty}) - \frac{1}{2} \left(\frac{dw}{d\varepsilon}\Big|_{\infty} + \frac{dw}{d\varepsilon}\Big|_{-\infty} \right) (\varepsilon_{\infty} - \varepsilon_{-\infty}) \right],$$

or, in terms of densities:

$$(4.12)_4 \qquad D = \sqrt{\frac{\sigma_{-\infty} - \sigma_{\infty}}{(\varepsilon_{-\infty} - \varepsilon_{\infty})} \varrho_0} \times \left[(w_{\infty} - w_{-\infty}) + \frac{1}{2\varrho_{-\infty}\varrho_{\infty}} (\sigma_{\infty} + \sigma_{-\infty})(\varrho_{\infty} - \varrho_{-\infty}) \right].$$

It is quite evident that also these relations do not include any inelastic terms. Therefore the total *viscous* dissipation is determined entirely in terms of the boundary values at infinities and the *elastic* properties of the material. The above result is valid of course under the assumption of the asymptotically vanishing inelastic stresses in infinities.

5. Discussion of the results, some particular cases

5.1. Asymptotic behavior of the solution for decreasing viscosity

The first item which should be discussed here is the asymptotic behavior of the solutions for vanishing viscosity. At the first glance the problem is trivial: if both: the

propagation velocity and the total dissipation rate do not depend on the viscous properties, then the limit transition yields a nonsense — the presence of viscous dissipation in inviscid material. As a matter of fact, the problem is not so simple: the point is that, in the nonlinear elasticity, as a rule, the continuous solution for constant velocity wave does not exist. Starting with a purely mechanical model and using the standard consideration of the shock propagation theory, we can easily obtain (see Appendix 1) the following expressions for the discontinuity propagation velocity and the total dissipation rate:

$$(v_- - U)^2 = \frac{\sigma_- - \sigma_+}{\varrho_+ - \varrho_-}\frac{\varrho_+}{\varrho_-},$$

$$(v_+ - U)^2 = \frac{\sigma_- - \sigma_+}{\varrho_+ - \varrho_-}\frac{\varrho_-}{\varrho_+}, \tag{5.1}$$

$$D = \sqrt{\frac{\sigma_- - \sigma_+}{\varrho_+ - \varrho_-}\varrho_-\varrho_+}\left[(w_+ - w_-) + \frac{1}{2\varrho_-\varrho_+}(\sigma_+ + \sigma_-)(\varrho_+ - \varrho_-)\right], \tag{5.2}$$

where subscripts "plus" and "minus" denote limit values taken at the right and left-hand sides of the discontinuity surface.

We had obtained previously essentially the same expressions for the quantities under consideration for the viscous wave case, the only difference consisting in replacing the values at infinity with the values at interface. Moreover, we were able, like in the previous case, to find an effective expression for the dissipation rate, despite the fact that even the dissipation mechanism at the shock front was not specified. One can see that there is no contradiction and the limit transition is correct. For completeness one should show, how the slope of the density (strain) profile changes with decreasing viscosity, tending to infinity for inviscid material. We shall discuss this problem later.

5.2. Restrictions imposed by demanding the positive dissipation

The problem of positiveness of the *total* dissipation rate and the restrictions imposed by this condition on the existence and direction of propagation of the kink-shaped quasi-stationary wave has obviously exactly the same solution, as that derived for the case of shock wave propagation in inviscid materials. It is not clear, however, (at least to the author) if the *local* (i.e. required to be fulfilled for any finite interval) condition of the positiveness of the dissipation rate imposes some additional restrictions.

The detailed discussion of the restrictions imposed by the local and total dissipation rate seems to be worthwhile, we shall however omit this topic in the present paper. We shall only point out some geometric interpretation of the expression which can be obtained from Eq. $(4.12)_1$, namely:

$$(w_\infty - w_{-\infty}) - \frac{1}{2}\left(\left.\frac{dw}{d\varepsilon}\right|_\infty + \left.\frac{dw}{d\varepsilon}\right|_{-\infty}\right)(\varepsilon_\infty - \varepsilon_{-\infty}) \geq 0\,. \tag{5.3}$$

Deriving Eq. (5.3) from Eq. $(4.12)_1$ we have assumed that U is positive i.e. we are considering the wave propagating into the right-hand direction. Assuming that elastic stress vanishes in the reference configuration, and that, in agreement with Eq. $(4.5)_1$, σ is an

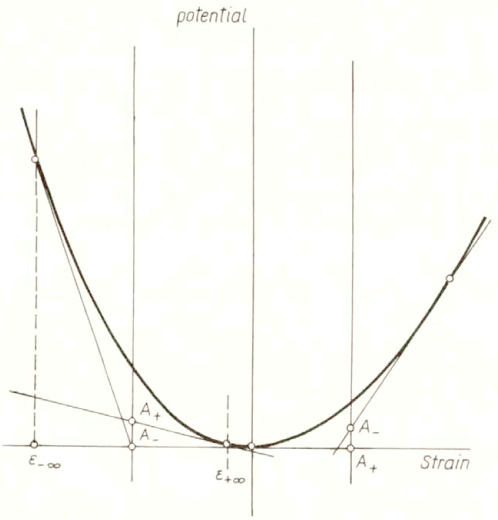

FIG. 1. Examples of thermodynamically admissible (left) and forbidden (right) wave-propagation schemes. Elastic potential was assumed in the form: $w(\varepsilon) = c_{11}^2\varepsilon^2/2(\varepsilon + 1)$.

increasing function of ε, and remembering also that for ε tending to -1 the density tends to infinity, we can qualitatively plot the potential as the function of strain ε as in Fig. 1. We can rewrite now inequality (5.3) in a following form:

$$w_{-\infty} + \frac{1}{2}\frac{dw}{d\varepsilon}\bigg|_{-\infty}(\varepsilon_\infty - \varepsilon_{-\infty}) \leq w_\infty - \frac{1}{2}\frac{dw}{d\varepsilon}\bigg|_{\infty}(\varepsilon_\infty - \varepsilon_{-\infty}). \tag{5.4}$$

Let us consider e.g. the propagation of the compression wave across the pre-compressed material: $\varepsilon_{-\infty} < \varepsilon_\infty < 0$, and $dw/d\varepsilon < 0$ for both values of ε. Let us draw now the vertical line $\varepsilon = (\varepsilon_{-\infty} + \varepsilon_\infty)/2$ and two other lines tangent to the graph of the function $w(\varepsilon)$ at the points $\varepsilon_{-\infty}$ and ε_∞ (compare Fig. 1). Let us denote the point of intersection of the vertical line $\varepsilon = (\varepsilon_{-\infty} + \varepsilon_\infty)/2$ and the tangent line drawn through the point $\varepsilon_{-\infty}$ by A_-, and the other point of intersection by A_+. It is not difficult to notice now that the value of the left-hand side term of inequality (5.4) is equal to the vertical coordinate of the point A_-, while the right-hand side describes the position of the point A_+. One can see that inequality (5.4) claims, that the point A_+ should lie above the point A_-; it is exactly what we indeed observe. Thus the condition of positive value of the total dissipation rate does not exclude the considered case.

Let us consider now another example — rarefaction wave propagating over the initially unstressed material: $\varepsilon_{-\infty} > 0$, $\varepsilon_\infty = 0$, $dw/d\varepsilon > 0$ for $\varepsilon = \varepsilon_{-\infty}$ and $dw/d\varepsilon = 0$ for $\varepsilon = \varepsilon_\infty$. In this case (5.4) reduces to the following form:

$$w_{-\infty} - \frac{1}{2}\frac{dw}{d\varepsilon}\bigg|_{-\infty}\varepsilon_{-\infty} \leq 0\,. \tag{5.5}$$

In terms of geometry it means that vertical coordinate of the point A_- should be negative, which is not the case; as a consequence, the considered wave-propagation scheme is forbidden.

For certain situations, simple analytic wave propagation conditions can be specified. Let us represent, for example, the elastic potential density $w(\varrho)$ in a following form:

$$w(\varrho) = \frac{1}{2}c_0^2\left(\frac{\varrho}{\varrho_0} - 1\right)^2 f\left(\frac{\varrho}{\varrho_0}\right). \tag{5.6}$$

Using relation $(4.12)_4$ one can easily prove, that propagation of compression wave of arbitrary amplitude across the unstressed material does not contradict the condition of positive value of the total dissipation rate, provided the first derivative of the product $\varrho^2 f(\varrho/\varrho_0)$ is positive[3].

5.3. Problem solution in quadratures

If the expression for inelastic stress is linear with respect to the velocity gradient

$$\sigma_{\text{inel}} = \overline{\mu}(\varepsilon)\frac{dv}{dx}, \tag{5.7}_1$$

or, in our case,

$$\sigma_{\text{inel}} = -U\overline{\mu}(\varepsilon)\varepsilon', \tag{5.7}_2$$

then the solution for strain profile can be obtained in quadratures.

Substituting Eqs. (5.7) into Eq. (4.3) one obtains

$$\varrho_0\frac{dw(\varepsilon)}{d\varepsilon} - \varrho_0 U^2\varepsilon - C = U\overline{\mu}(\varepsilon)\varepsilon' \tag{5.8}$$

or

$$\frac{d\xi}{d\varepsilon} = \frac{U\overline{\mu}(\varepsilon)}{\varrho_0\dfrac{dw(\varepsilon)}{d\varepsilon} - \varrho_0 U^2\varepsilon - C}. \tag{5.9}$$

The denominator of the right-hand side term is equal to zero both for $\varepsilon = \varepsilon_{-\infty}$ and for $\varepsilon = \varepsilon_{\infty}$, thus if it tends to zero quickly enough to provide the divergence of the integral at both ends of the interval $\langle \varepsilon_{-\infty}, \varepsilon_{\infty} \rangle$ and, moreover, is not equal to zero at any point inside the interval, then the function $\xi(\varepsilon)$ exists, is monotonic and assumes all values from the interval $(-\infty, \infty)$. Thus the inverse function $\varepsilon(\xi) = \varepsilon(x - Ut)$ exists, is monotonic and assumes proper values at infinities. A particular case of analytic solution is shown in Appendix 2.

Let us notice at last, that in the expression (5.9) the denominator depends only on the boundary conditions and on the elastic properties of the material, thus with decreasing viscosity the slope of the function $\xi(\varepsilon)$ tends to zero, which means that the slope of the inverse function $\varepsilon(\xi)$ tends to infinity and the wave profile tends to the inviscid shock front.

This completes our present considerations, some topics being left for the future investigations. At conclusion, the author would like to present very simple consideration which, as a matter of fact, proves in a few lines the main results of the present paper, i.e. the independence of the propagation velocity and the total dissipation rate of the inelastic properties of the material.

---

[3] Taking w and σ equal to zero at plus infinity and substituting potential function (5.6) into Eq. (4.12) one obtains at minus infinity (i.e. for any $\varrho > \varrho_0$) the following inequality: $2f + \varrho df/d\varrho > 0$; multiplying this expression by ϱ we obtain at once $d(\varrho^2 f)/d\varrho > 0$.

5.4. Similarity considerations

For simplicity we confine our considerations to the case of constant viscosity (which is, however, not necessary at all). Let us expand for better explanation the elastic potential into the power series

$$w(\varrho) = \frac{1}{2}c_0^2\left(\frac{\varrho}{\varrho_0} - 1\right)^2\left[1 + \sum_{n=1}^{\infty} E_n\left(\frac{\varrho}{\varrho_0}\right)^n\right]. \tag{5.10}$$

It is evident that all coefficients E_n are dimensionless, thus if one prescribes the boundary conditions in infinities in terms of strains or dimensionless densities ϱ/ϱ_0, then the whole problem contains only three dimensional parameters:

sound velocity $$[c_0] = \left[\frac{\mathrm{m}}{\mathrm{s}}\right],$$

initial density $$[\varrho_0] = \left[\frac{\mathrm{kg}}{\mathrm{m}^3}\right],$$

viscosity $$[\overline{\mu}] = \left[\frac{\mathrm{kg}}{\mathrm{m\,s}}\right].$$

This system of dimensional quantities is independent and complete, thus we can built the following characteristic quantities:

characteristic length $$l_0 = \frac{\overline{\mu}}{\varrho_0 c_0},$$

characteristic time $$t_0 = \frac{\overline{\mu}}{\varrho_0 c_0^2},$$

characteristic mass $$m_0 = \frac{\overline{\mu}^3}{\varrho_0^2 c_0^3}.$$

For the total dissipation rate (per unit cross-section) and for the propagation velocity we have following dimensional relations:

$$[D] = \left[\frac{\mathrm{kg}}{\mathrm{s}^3}\right] = \left[\frac{m_0}{t_0^3}\right] = [\varrho_0 c_0^3], \tag{5.11}$$

$$[U] = \left[\frac{\mathrm{m}}{\mathrm{s}}\right] = \left[\frac{l_0}{t_0}\right] = [c_0]. \tag{5.12}$$

Thus, according to π-theorem (c.f. [5]), any formulae for D and U should assume the following form:

$$D = \varrho_0 c_0^3 f(\pi_1, \ldots, \pi_n), \tag{5.13}$$

$$U = c_0 g(\pi_1, \ldots, \pi_n), \tag{5.14}$$

where $f(\cdot)$, $g(\cdot)$ are some functions and π_i $(i = 1, \ldots, n)$ are dimensionless parameters of the problem. Since the set of dimensional quantities is independent, one cannot built any dimensionless parameter including $\overline{\mu}$, and therefore both U and D cannot depend on $\overline{\mu}$.

Appendix 1

We shall start from the following form of Rankine–Hugoniot conditions

$$\varrho_-(U - v_-) - \varrho_+(U - v_+) = 0\,, \tag{I.1}$$

$$\varrho_- v_-(U - v_-) - \varrho_+ v_+(U - v_+) = \sigma_+ - \sigma_-\,, \tag{I.2}$$

(compare [1, 2]). Multiplying the first expression by U and subtracting the second one we arrive at the following equation:

$$\varrho_-(U - v_-)^2 - \varrho_+(U - v_+)^2 = \sigma_- - \sigma_+\,. \tag{I.3}$$

From Eq. (I.1) one obtains:

$$\varrho_-^2(U - v_-)^2 - \varrho_+^2(U - v_+)^2 = 0\,. \tag{I.4}$$

Solving Eqs. (I.3) and (I.4) with respect to $(U - v_-)^2$ and $(U - v_+)^2$ one arrives at Eq. (5.1).

To determine the total dissipation rate for the medium contained between two material planes: $x = a(A,t) < y(t)$ and $x = b(B,t) > y(t)$, where A and B are material coordinates, $y(t)$ denoting the current position of the discontinuity, we write:

$$D = -\sigma_a v_a + \sigma_b v_b - \frac{d}{dt}\left[\int_{a(A,t)}^{y(t)} \left(\varrho w + \frac{1}{2}\varrho v^2\right) dx + \int_{y(t)}^{b(A,t)} \left(\varrho w + \frac{1}{2}\varrho v^2\right) dx\right]. \tag{I.5}$$

Differentiating with respect to time and remembering that $d(\varrho dx)/dt = 0$, we arrive at the following expression:

$$\begin{aligned} D = -\sigma_a v_a + \sigma_b v_b - U\left(\varrho_- w_- + \frac{1}{2}\varrho_- v_-^2\right) + v_a\left(\varrho_a w_a + \frac{1}{2}\varrho_a v_a^2\right) \\ - v_b\left(\varrho_b w_b + \frac{1}{2}\varrho_b v_b^2\right) + U\left(\varrho_+ w_+ + \frac{1}{2}\varrho_+ v_+^2\right) \\ - \left[\int_{a(A,t)}^{y(t)} (\varrho \dot{w} + \varrho v \dot{v}) dx + \int_{y(t)}^{b(A,t)} (\varrho \dot{w} + \varrho v \dot{v}) dx\right], \end{aligned} \tag{I.6}$$

where $v_a = \dot{a}(A,t)$, $v_b = \dot{b}(B,t)$ are velocities in a and b, $U = dy(t)/dt$. Substituting $d\sigma/dx$ for $\varrho \dot{v}$, $-\sigma/\varrho$ for $\varrho dw/d\varrho$ and $-\varrho dv/dx$ for $\dot{\varrho}$, we obtain:

$$\varrho \dot{w} + \varrho v \dot{v} = \frac{d}{dx}(\sigma v)\,. \tag{I.7}$$

Performing integration and the limit transitions: $a \to y$, $b \to y$ (no dissipation at the continuity regions!) we obtain the following almost evident expression, which we probably had to propose at once without derivation:

$$\begin{aligned} D = -\sigma_- v_- + \sigma_+ v_+ - (U - v_-)\left(\varrho_- w_- + \frac{1}{2}\varrho_- v_-^2\right) \\ + (U - v_+)\left(\varrho_+ w_+ + \frac{1}{2}\varrho_+ v_+^2\right). \end{aligned} \tag{I.9}$$

Now, to complete the derivation we have to eliminate unknown values of v_- and v_+, to this end we should (a) add Eq. (I.2), multiplied by U, to Eq. (I.9) (side by side);

(b) make use of relation (I.1) and (c) recall the following identity:

$$v_- U - v_+ U - v_-^2/2 + v_+^2/2 = [(U - v_+)^2 - (U - v_-)^2]/2 . \tag{I.10}$$

If we do this, we shall obtain the following expression:

$$D = (U - v_\pm)\varrho_\pm \left(\frac{1}{2}(U - v_+)^2 - \frac{1}{2}(U - v_-)^2 + \frac{\sigma_-}{\varrho_-} - \frac{\sigma_+}{\varrho_+} \right), \tag{I.11}$$

where, instead of double sign, either plus or minus can be taken. Substitution of relations $(5.1)_1$ and $(5.1)_2$ into Eq. (I.11) readily produces Eq. (5.2).

Appendix 2

EXAMPLE

Relation (5.9) can be rewritten in the following form

$$\xi(\varrho) = U\varrho_0 \int \frac{\overline{\mu}(\varrho)}{\varrho^4 \dfrac{dw}{d\varrho} + C_1\varrho^2 + U^2\varrho_0^2\varrho} d\varrho + C_2 , \tag{II.1}$$

where C_1 can be expressed in terms of the boundary conditions at infinities:

$$C_1 = \frac{\varrho_{-\infty}^3 \left.\dfrac{dw}{d\varrho}\right|_{-\infty} - \varrho_\infty^3 \left.\dfrac{dw}{d\varrho}\right|_\infty}{\varrho_\infty - \varrho_{-\infty}} . \tag{II.2}$$

Probably the simplest form of potential described by Eq. (5.6) can be obtained by taking ϱ_0/ϱ for $f(\varrho/\varrho_0)$[4]. If we also assume $\overline{\mu}$ = const, then we obtain the following expression for ξ as the function of dimensionless density $\overline{\varrho} = \varrho/\varrho_0$:

$$\xi(\overline{\varrho}) = \frac{\sqrt{2\overline{\mu}}}{c_0\varrho_0} \sqrt{\overline{\varrho}_{-\infty}\overline{\varrho}_\infty(\overline{\varrho}_{-\infty} + \overline{\varrho}_\infty)} \times \int \frac{d\overline{\varrho}}{\overline{\varrho}(\overline{\varrho} - \overline{\varrho}_{-\infty})(\overline{\varrho} - \overline{\varrho}_\infty)(\overline{\varrho} + \overline{\varrho}_\infty + \overline{\varrho}_{-\infty})} + C_2 . \tag{II.3}$$

Fixing the frame of reference by taking $C_2 = 0$, we finally obtain the following implicit expression for wave profile $\xi(\overline{\varrho})$:

$$\exp(\beta\xi) = \overline{\varrho}^{\alpha_1}(\overline{\varrho}_{-\infty} - \overline{\varrho})^{\alpha_2}(\overline{\varrho} - \overline{\varrho}_\infty)^{\alpha_3}(\overline{\varrho} + \overline{\varrho}_\infty + \overline{\varrho}_{-\infty})^{\alpha_4} , \tag{II.4}$$

where

$$\beta = \frac{\varrho_0 c_0}{\sqrt{2\overline{\mu}}} \sqrt{\overline{\varrho}_{-\infty}\overline{\varrho}_\infty(\overline{\varrho}_\infty + \overline{\varrho}_{-\infty})},$$

$$\alpha_1 = \frac{1}{\overline{\varrho}_{-\infty}\overline{\varrho}_\infty(\overline{\varrho}_{-\infty} + \overline{\varrho}_\infty)}, \qquad \alpha_2 = \frac{1}{\overline{\varrho}_{-\infty}(\overline{\varrho}_{-\infty} - \overline{\varrho}_\infty)(\overline{\varrho}_\infty + 2\overline{\varrho}_{-\infty})} , \tag{II.5}$$

$$\alpha_3 = \frac{1}{\overline{\varrho}_\infty(\overline{\varrho}_\infty - \overline{\varrho}_{-\infty})(\overline{\varrho}_{-\infty} + 2\overline{\varrho}_\infty)},$$

$$\alpha_4 = \frac{-1}{(\overline{\varrho}_\infty + \varrho_{-\infty})(\overline{\varrho}_\infty + 2\overline{\varrho}_{-\infty})(\overline{\varrho}_{-\infty} + 2\overline{\varrho}_\infty)} .$$

[4] This is the same potential as that depicted in terms of strain in the Fig. 1. Possible pathological behavior of such a potential in the vicinity of zero density is far out of the scope of the present considerations.

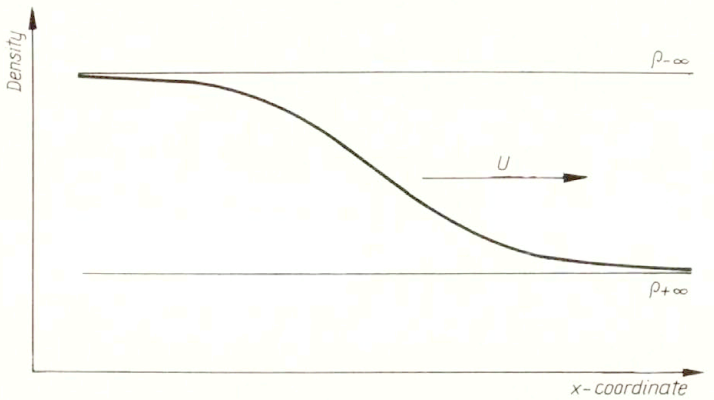

FIG. 2. An example of wave profile (mass density versus coordinate) for the constant viscosity coefficient and the elastic potential density $w(\varrho) = c_0^2 \varrho_0 (\varrho/\varrho_0 - 1)2\varrho$.

Density profile described by the implicit relation (II.4) is shown in Fig. 2.

References

1. A. BLINOWSKI, *Small amplitude wave propagation in the Eimer's cracked material (The instructive case of irremovable nonlinearity)*, Arch. Mech., **44**, 3, pp. 152–169, 1992.
2. A. BLINOWSKI, *On the mechanical energy dissipation in small deformation elasticity and the simple analytic expression for the viscous kink-shaped solitary wave*, Arch. Mech., **44**, 5–6, pp. 615–620, 1992.
3. S.A. GABOV, *Introduction into the theory of non-linear waves* [in Russian], pp. 130–134, Moscow University Publishing House, Moscow 1988.
4. R.J. GOODING, G.S. BALES, *Boosted kink-type solitary waves in nonlinear elastic media*, Physica D, Nonlinear Phenomena, **55**, Nos. 3&4, March 1992.
5. J. RYCHLEWSKI, *Dimensions and similarity* [in Polish], PWN, Warszawa 1992.

POLISH ACADEMY OF SCIENCES
INSTITUTE OF FUNDAMENTAL TECHNOLOGICAL RESEARCH.

Received January 13, 1993.

Arch. Mech., 45, 1, pp. 121–134, Warszawa 1993

Hodograph method in plane MHD non-Newtonian fluid flows

I. ADLURI (WHEELING)

EQUATIONS of steady flow of a conducting non-Newtonian fluid of finite electrical conductivity are transformed to the hodograph plane by using the Legendre transform function of the stream-function when the velocity field is orthogonal to the magnetic field everywhere in the plane of flow. Three theorems are stated, some flow problems of physical importance are investigated and exact solutions are obtained in each case.

1. Introduction

TRANSFORMATION techniques are some of the powerful methods of solving systems of nonlinear partial differential equations governing the steady plane flows. One of these techniques is a hodograph transformation which has been widely used in continuum mechanics. AMES [1] presented an excellent survey of this method and its applications in various other fields. CHANDNA *et al.* [2–8] applied the hodograph and Legendre transformations to investigate steady plane viscous flows, non-Newtonian flows and constantly inclined, aligned, transverse and orthogonal MHD non-Newtonian flows. In recent years, the interest in problems of non-Newtonian fluid flows has grown considerably because of an extensive use of these fluids in chemical processes in industries, food and construction engineering, petroleum production, power engineering and commercial applications. Since electrical conductivity is finite for most liquid metals and for many electrically conducting non-Newtonian as well as many other second grade fluids to which single fluid model can be applied, accounting for finite electrical conductivity makes the flow problem realistic and attractive both from a mathematical and a physical point of view.

The present paper deals with application of the hodograph transformation to obtain exact solutions of the nonlinear partial differential equations governing the steady plane flow of a power-law non-Newtonian fluid of finite electrical conductivity in the presence of an orthogonal magnetic field.

First, equations governing the flow are transformed to the hodograph plane interchanging the role of independent variables x, y and the components of the velocity vector field u, v; then, by introducing a Legendre transform function of the streamfunction, all equations in the hodograph plane are expressed in terms of this transform function. Results are summarized in the form of theorems and finally, the following flow problems are studied as applications of these theorems:

a) vortex flows,

b) radial flows,

c) spiral flows.

Exact solutions are obtained for vortex and radial flows and it is proved that a spiral flow cannot exist in an orthogonal non-Newtonian power-law fluid of finite electrical conductivity.

2. Equations of motion

The flow of a steady plane electrically conducting non-Newtonian fluid of finite electrical conductivity which obeys the Ostwaald–de Waele power-law model

$$\tau_{ij} = 2K[2D_{kl}D_{kl}]^{(n-1)/2}D_{ij},$$

where

$$D_{ij} = \frac{1}{2}\left(\frac{\partial u_i}{\partial x_j} + \frac{\partial u_j}{\partial x_i}\right),$$

is governed by

$$\frac{\partial u}{\partial x} + \frac{\partial v}{\partial y} = 0 \qquad \text{(continuity)}, \tag{2.1}$$

$$\begin{aligned} \frac{\partial F}{\partial x} &= \varrho v w + K\left\{\frac{2\partial}{\partial x}\left(I\frac{\partial u}{\partial x}\right) + \frac{\partial}{\partial y}\left[I\left(\frac{\partial u}{\partial y} + \frac{\partial v}{\partial x}\right)\right]\right\} - \mu_e j H_2, \\ \frac{\partial F}{\partial y} &= -\varrho u w + K\left\{\frac{\partial}{\partial x}\left[I\left(\frac{\partial u}{\partial y} + \frac{\partial v}{\partial x}\right)\right] + \frac{2\partial}{\partial y}\left(I\frac{\partial v}{\partial y}\right)\right\} + \mu_e j H_1, \end{aligned} \tag{2.2}$$

(linear momentum),

$$\begin{aligned} uH_2 - vH_1 &= \frac{1}{\mu_e\sigma}j + A, && \text{(diffusion)}, \\ \frac{\partial H_1}{\partial x} + \frac{\partial H_2}{\partial y} &= 0, && \text{(solenoidal)}, \\ j &= \frac{\partial H_2}{\partial x} - \frac{\partial H_1}{\partial y}, && \text{(current density)}, \\ w &= \frac{\partial v}{\partial x} - \frac{\partial u}{\partial y}, && \text{(vorticity)}. \end{aligned} \tag{2.3}$$

Here τ_{ij} denotes the strain rate tensor, $u(x, y)$, $v(x, y)$ are the components of the velocity vector $\mathbf{V}$, $H_1(x, y)$, $H_2(x, y)$ are the components of the magnetic field $\mathbf{H}$, p is the pressure, ϱ is the fluid density, μ_e is the magnetic permeability, σ is the electrical conductivity, K is the consistency index coefficient, A is an arbitrary constant obtained from the integration of the diffusion equation

$$\begin{aligned} \nabla \times (\mathbf{V} \times \mathbf{H} - \frac{1}{\mu_e\sigma}\nabla \times \mathbf{H}) &= \mathbf{0}, \\ I = \left[2\left(\frac{\partial u}{\partial x}\right)^2 + 2\left(\frac{\partial v}{\partial y}\right)^2 + \left(\frac{\partial u}{\partial y} + \frac{\partial v}{\partial x}\right)^2\right]^{(n-1)/2} & \end{aligned} \tag{2.4}$$

is the Ostwaald–de Waele parameter and

$$F(x, y) = \frac{1}{2}\varrho(u^2 + v^2) + p. \tag{2.5}$$

Equations (2.1)–(2.3) form a system of seven partial differential equations in seven unknown functions u, v, H_1, H_2, j, w and F.

We consider a plane flow in which the velocity vector is orthogonal to magnetic field everywhere in the plane of flow, that is

$$\mathbf{H} = \mathbf{k} \times \lambda(x, y)\mathbf{V}, \tag{2.6}$$

where $\mathbf{k}$ is the unit vector normal to the plane of flow and $\lambda(x, y)$ is a scalar function.

Using Eq. (2.6), Equations (2.2) and (2.3) can be expressed as follows:

$$\frac{\partial F}{\partial x} = \varrho v w + K\left\{\frac{w\partial I}{\partial y} - \frac{I\partial w}{\partial y} + 2\left(\frac{\partial u}{\partial x}\frac{\partial I}{\partial x} + \frac{\partial u}{\partial y}\frac{\partial I}{\partial y}\right)\right\} - \mu_e j\lambda u\,, \tag{2.7}$$

$$\frac{\partial F}{\partial y} = -\varrho u w - K\left\{\frac{w\partial I}{\partial x} - \frac{I\partial w}{\partial x} + 2\left(\frac{\partial v}{\partial x}\frac{\partial I}{\partial x} + \frac{\partial v}{\partial y}\frac{\partial I}{\partial y}\right)\right\} - \mu_e j\lambda v\,, \tag{2.8}$$

$$\lambda(u^2 + v^2) = \frac{1}{\mu_e \sigma} j + A\,, \tag{2.9}$$

$$-\lambda w + \frac{u\partial\lambda}{\partial y} - \frac{v\partial\lambda}{\partial x} = 0\,, \tag{2.10}$$

$$j = \frac{u\partial\lambda}{\partial x} + \frac{v\partial\lambda}{\partial y}\,. \tag{2.11}$$

3. Equations in the hodograph plane

Let the flow variables $u(x, y)$, $v(x, y)$ be such that, in the region of flow, the Jacobian

$$J(x, y) = \frac{\partial(u, v)}{\partial(x, y)} \neq 0\,.$$

Considering x, y as functions of u and v, we can derive the following relations:

$$\frac{\partial u}{\partial x} = \frac{J\partial y}{\partial v}, \quad \frac{\partial u}{\partial y} = -\frac{J\partial x}{\partial v}, \quad \frac{\partial v}{\partial x} = -\frac{J\partial y}{\partial u}, \quad \frac{\partial v}{\partial y} = \frac{J\partial x}{\partial u}, \tag{3.1}$$

$$J(x, y) = \frac{\partial(u, v)}{\partial(x, y)} = \left[\frac{\partial(x, y)}{\partial(u, v)}\right]^{-1} = \overline{J}(u, v), \tag{3.2}$$

$$\begin{aligned} \frac{\partial g}{\partial x} &= \frac{\partial(g, y)}{\partial(x, y)} = \frac{J\partial(\overline{g}, y)}{\partial(u, v)} = \overline{J}\frac{\partial(\overline{g}, y)}{\partial(u, v)}, \\ \frac{\partial g}{\partial y} &= -\frac{\partial(g, x)}{\partial(x, y)} = J\frac{\partial(x, \overline{g})}{\partial(u, v)} = \overline{J}\frac{\partial(x, \overline{g})}{\partial(u, v)}, \end{aligned} \tag{3.3}$$

where $g = g(x, y) = g(x(u, v), y(u, v)) = \overline{g}(u, v)$ is any continuously differentiable function.

Using these relations in Eqs. (2.1)–(2.4) and (2.7)–(2.11), we obtain the following system of partial differential equations in the (u, v)-plane:

$$\frac{\partial x}{\partial u} + \frac{\partial y}{\partial v} = 0, \tag{3.4}$$

$$\overline{J}\frac{\partial(\overline{F}, y)}{\partial(u, v)} = \varrho v\overline{w} + K\overline{J}\left\{\overline{w}Q_1 - \overline{I}P_1 + 2\overline{J}\left(Q_2\frac{\partial y}{\partial v} - Q_1\frac{\partial x}{\partial v}\right)\right\} - \mu_e\overline{j}\,\overline{\lambda}u, \tag{3.5}$$

$$\overline{J}\frac{\partial(x, \overline{F})}{\partial(u, v)} = -\varrho u\overline{w} - K\overline{J}\left\{\overline{w}Q_2 - \overline{I}P_2 + 2\overline{J}\left(Q_2\frac{\partial y}{\partial u} - Q_1\frac{\partial x}{\partial u}\right)\right\} - \mu_e\overline{j}\,\overline{\lambda}v, \tag{3.6}$$

$$\overline{\lambda}(u^2 + v^2) = \frac{1}{\mu_e\sigma}\overline{j} + A, \tag{3.7}$$

$$-\overline{\lambda}\overline{w} + \overline{J}\left\{u\frac{\partial(x,\overline{\lambda})}{\partial(u,v)} - v\frac{\partial(\overline{\lambda},y)}{\partial(u,v)}\right\} = 0, \tag{3.8}$$

$$\overline{j} = \overline{J}\left\{u\frac{\partial(\overline{\lambda},y)}{\partial(u,v)} + v\frac{\partial(x,\overline{\lambda})}{\partial(u,v)}\right\}, \tag{3.9}$$

$$\overline{w} = \overline{J}\left(\frac{\partial x}{\partial v} - \frac{\partial y}{\partial u}\right), \tag{3.10}$$

$$\overline{I} = (\overline{J})^{(n-1)}\left\{2\left(\frac{\partial x}{\partial u}\right)^2 + 2\left(\frac{\partial y}{\partial v}\right)^2 + \left(\frac{\partial x}{\partial v} + \frac{\partial y}{\partial u}\right)^2\right\}^{(n-1)/2}, \tag{3.11}$$

where

$$\overline{J} = \left[\frac{\partial(x,y)}{\partial(u,v)}\right]^{-1}, \quad P_1(u,v) = \frac{\partial(x,\overline{w})}{\partial(u,v)}, \quad P_2(u,v) = \frac{\partial(\overline{w},y)}{\partial(u,v)},$$
$$Q_1(u,v) = \frac{\partial(x,\overline{I})}{\partial(u,v)}, \quad Q_2(u,v) = \frac{\partial(\overline{I},y)}{\partial(u,v)}. \tag{3.12}$$

Equations (3.4)–(3.11) are a system of eight equations in seven unknown functions $x(u,v)$, $y(u,v)$, $\overline{w}(u,v)$, $\overline{\lambda}(u,v)$, $j(u,v)$, $\overline{F}(u,v)$ and $\overline{I}(u,v)$. Once these functions are determined, we can find $u(x,y)$, $v(x,y)$, $w(x,y)$, $\lambda(x,y)$, $j(x,y)$ and $F(x,y)$ which are solutions of Eqs. (2.1)–(2.3).

4. Equations in Legendre transformation function and $\overline{\lambda}(u,v)$

The equation of continuity (2.1) implies the existence of a streamfunction $\psi(x,y)$, so that

$$d\psi = -v\,dx + u\,dy, \quad \frac{\partial\psi}{\partial x} = -v, \quad \frac{\partial\psi}{\partial y} = u, \tag{4.1}$$

and Eq. (3.4) implies the existence of a function $L(u,v)$ called the Legendre transformation function of the streamfunction $\psi(x,y)$, such that

$$dL = -y\,du + x\,dv, \quad \frac{\partial L}{\partial u} = -y, \quad \frac{\partial L}{\partial v} = x. \tag{4.2}$$

Functions $L(u,v)$ and $\psi(x,y)$ are related by

$$L(u,v) = vx - uy + \psi(x,y). \tag{4.3}$$

Using Eq. (4.3), equations (3.5)–(3.12) can be rewritten in terms of $L(u,v)$ as follows:

$$\overline{J}\frac{\partial\left(\frac{\partial L}{\partial u},\overline{F}\right)}{\partial(u,v)} = \varrho v\overline{w} + K\overline{J}(\overline{w}Q_1 - \overline{I}P_1 - 2\overline{J}R_1) - \mu_e\overline{j}\,\overline{\lambda}u, \tag{4.4}$$

$$\overline{J}\frac{\partial\left(\frac{\partial L}{\partial v},\overline{F}\right)}{\partial(u,v)} = -\varrho u\overline{w} - K\overline{J}(\overline{w}Q_2 - \overline{I}P_2 - 2\overline{J}R_2) - \mu_e\overline{j}\,\overline{\lambda}v, \tag{4.5}$$

$$\overline{\lambda}(u^2+v^2) = \frac{1}{\mu_e\sigma}\overline{j} + A, \tag{4.6}$$

$$-\overline{\lambda}\overline{w}+\overline{J}\left\{u\frac{\partial\left(\frac{\partial L}{\partial v},\overline{\lambda}\right)}{\partial(u,v)}-v\frac{\partial\left(\frac{\partial L}{\partial u},\overline{\lambda}\right)}{\partial(u,v)}\right\}=0, \tag{4.7}$$

$$\overline{j}=\overline{J}\left\{u\frac{\partial\left(\frac{\partial L}{\partial u},\overline{\lambda}\right)}{\partial(u,v)}+v\frac{\partial\left(\frac{\partial L}{\partial v},\overline{\lambda}\right)}{\partial(u,v)}\right\}, \tag{4.8}$$

$$\overline{w}=\overline{J}\left(\frac{\partial^2 L}{\partial v^2}+\frac{\partial^2 L}{\partial u^2}\right), \tag{4.9}$$

where

$$\overline{J}=\left[\frac{\partial^2 L}{\partial v^2}\frac{\partial^2 L}{\partial u^2}-\left(\frac{\partial^2 L}{\partial u\partial v}\right)^2\right]^{-1}, \tag{4.10}$$

$$\overline{I}=(\overline{J})^{(n-1)}\left\{\left(\frac{\partial^2 L}{\partial u^2}-\frac{\partial^2 L}{\partial v^2}\right)^2+4\left(\frac{\partial^2 L}{\partial u\partial v}\right)^2\right\}^{(n-1)/2}, \tag{4.11}$$

$$P_1=P_1(u,v)=\frac{\partial\left(\frac{\partial L}{\partial v},\overline{w}\right)}{\partial(u,v)},\qquad P_2=P_2(u,v)=\frac{\partial\left(\frac{\partial L}{\partial u},\overline{w}\right)}{\partial(u,v)},$$

$$Q_1=Q_1(u,v)=\frac{\partial\left(\frac{\partial L}{\partial v},\overline{I}\right)}{\partial(u,v)},\qquad Q_2=Q_2(u,v)=\frac{\partial\left(\frac{\partial L}{\partial u},\overline{I}\right)}{\partial(u,v)}, \tag{4.12}$$

$$R_1=R_1(u,v)=Q_1\frac{\partial^2 L}{\partial v^2}+Q_2\frac{\partial^2 L}{\partial u\partial v},$$

$$R_2=R_2(u,v)=Q_1\frac{\partial^2 L}{\partial u\partial v}+Q_2\frac{\partial^2 L}{\partial u^2}.$$

To eliminate $\overline{F}(u,v)$ from Eqs. (4.4) and (4.5), we use the integrability condition

$$\left(\overline{J}\frac{\partial^2 L}{\partial u\partial v}\frac{\partial}{\partial v}-\overline{J}\frac{\partial^2 L}{\partial v^2}\frac{\partial}{\partial u}\right)\left(\overline{J}\frac{\partial\left(\frac{\partial L}{\partial u},\overline{F}\right)}{\partial(u,v)}\right)$$

$$=\left(\overline{J}\frac{\partial^2 L}{\partial u^2}\frac{\partial}{\partial v}-\overline{J}\frac{\partial^2 L}{\partial u\partial v}\frac{\partial}{\partial u}\right)\left(\overline{J}\frac{\partial\left(\frac{\partial L,\overline{F}}{\partial v}\right)}{\partial(u,v)}\right)$$

and get

$$\varrho(vP_1+uP_2)+K\{\overline{w}W_1+\overline{J}(P_1Q_1+P_2Q_2)-\overline{I}W_2-\overline{J}W_3-2\overline{J}^2W_4-4\overline{J}W_5\}$$

$$+\mu_e\left\{\overline{\lambda}\,\overline{J}\left(\frac{\partial^2 L}{\partial u^2}+\frac{\partial^2 L}{\partial v^2}\right)+\frac{v\partial\left(\frac{\partial L}{\partial u},\overline{\lambda}\,\overline{J}\right)}{\partial(u,v)}-\frac{u\partial\left(\frac{\partial L}{\partial v},\overline{\lambda}\,\overline{j}\right)}{\partial(u,v)}\right\}=0, \tag{4.13}$$

where

$$
\begin{aligned}
W_1 &= W_1(u,v) = \frac{\partial\left(\frac{\partial L}{\partial v}, \overline{J}Q_1\right)}{\partial(u,v)} + \frac{\partial\left(\frac{\partial L}{\partial u}, \overline{J}Q_2\right)}{\partial(u,v)},\\
W_2 &= W_2(u,v) = \frac{\partial\left(\frac{\partial L}{\partial v}, \overline{J}P_1\right)}{\partial(u,v)} + \frac{\partial\left(\frac{\partial L}{\partial u}, \overline{J}P_2\right)}{\partial(u,v)},\\
W_3 &= W_3(u,v) = P_1\frac{\partial\left(\frac{\partial L}{\partial v}, \overline{I}\right)}{\partial(u,v)} + P_2\frac{\partial\left(\frac{\partial L}{\partial u}, \overline{I}\right)}{\partial(u,v)},\\
W_4 &= W_4(u,v) = \frac{\partial\left(\frac{\partial L}{\partial v}, R_1\right)}{\partial(u,v)} + \frac{\partial\left(\frac{\partial L}{\partial u}, R_2\right)}{\partial(u,v)},\\
W_5 &= W_5(u,v) = R_1\frac{\partial\left(\frac{\partial L}{\partial v}, \overline{J}\right)}{\partial(u,v)} + R_2\frac{\partial\left(\frac{\partial L}{\partial u}, \overline{J}\right)}{\partial(u,v)}.
\end{aligned} \tag{4.14}
$$

Using Eqs. (4.6) and (4.7), equation (4.13) can be simplified to

$$
\begin{aligned}
&\varrho(vP_1 + uP_2) + K\{\overline{w}W_1 + \overline{J}(P_1Q_1 + P_2Q_2) - \overline{I}W_2 - \overline{J}W_3 - 2\overline{J}^2W_4 - 4W_5\overline{J}\}\\
&\quad + \mu_e^2\sigma\overline{\lambda}\left\{v\frac{\partial\left(\frac{\partial L}{\partial u}, \overline{\lambda}(u^2+v^2)\right)}{\partial(u,v)} - u\frac{\partial\left(\frac{\partial L}{\partial v}, \overline{\lambda}(u^2+v^2)\right)}{\partial(u,v)}\right\} = 0.
\end{aligned} \tag{4.15}
$$

Eliminating $\overline{j}$ from Eqs. (4.6) and (4.8), we get

$$
\mu_e\sigma\{\overline{\lambda}(u^2+v^2) - A\} = \overline{J}\left\{u\frac{\partial\left(\frac{\partial L}{\partial u}, \overline{\lambda}\right)}{\partial(u,v)} + v\frac{\partial\left(\frac{\partial L}{\partial v}, \overline{\lambda}\right)}{\partial(u,v)}\right\}. \tag{4.16}
$$

From Eq. (4.7), (4.15) and (4.16), we obtain the following theorem:

THEOREM 1. *If $L(u,v)$ is the Legendre transform function of a streamfunction of a steady plane orthogonal flow of a power-law non-Newtonian fluid of finite electrical conductivity and $\overline{\lambda}(u,v)$ is the transformed proportionality function, then $L(u,v)$ and $\overline{\lambda}(u,v)$ must satisfy equations* (4, 7), (4.15) *and* (4.16) *where $\overline{w}$, $\overline{I}$, $\overline{J}$, $\overline{j}$, P_1, P_2, Q_1, Q_2, R_1, R_2 and W are given by Eqs.* (4.8)–(4.12) *and* (4.14).

We determine $L(u,v)$ and $\overline{\lambda}(u,v)$, the velocity components, $\overline{J}$ and $\overline{I}$ by solving Eqs. (4.8)–(4.12), (4.15) and (4.16), and $u(x,y)$, $v(x,y)$ to obtain $\lambda(x,y)$ and other flow variables in the physical plane.

To find $L(u,v)$ and $\overline{\lambda}(u,v)$, we write Eqs. (4.8)–(4.12), (4.15) and (4.16) in polar coordinates (q,θ) in the hodograph plane.

Let

$$
u = q\cos\theta, \qquad v = q\sin\theta,
$$
$$
q^2 = u^2 + v^2, \qquad \theta = \tan^{-1}(v/u).
$$

Using the chain rule of partial differentiation, we can derive the following relations:

$$\frac{\partial f}{\partial u} = \cos\theta\frac{\partial f}{\partial q} - \frac{\sin\theta}{q}\frac{\partial f}{\partial\theta}, \qquad \frac{\partial f}{\partial v} = \sin\theta\frac{\partial f}{\partial q} + \frac{\cos\theta}{q}\frac{\partial f}{\partial\theta},$$

$$\frac{\partial(f,h)}{\partial(u,v)} = \frac{\partial(f^*,h^*)}{\partial(q,\theta)}\cdot\frac{\partial(q,\theta)}{\partial(u,v)} = \frac{1}{q}\frac{\partial(f^*,h^*)}{\partial(q,\theta)},$$

where $f(u,v) = f^*(q,\theta)$, $h(u,v) = h^*(q,\theta)$ are any continuously differentiable functions.

Using these relations, Eqs. (4.15), (4.7), (4.16), (4.14) and (4.8)–(4.12) can be transformed, respectively, into the following form:

(4.17)
$$\varrho q(P_1^*\sin\theta + P_2^*\cos\theta) + K\{w^*, W_1^* + J^*(P_1^*Q_1^* + P_2^*Q_2^*) - I^*W_2^* - J^*W_3^* - 2J^2W_4^* - 4J^*W_5^*\} + \mu_e^2\sigma\lambda^*\left\{\sin\theta\frac{\partial\left(\cos\theta\frac{\partial L^*}{\partial q} - \frac{\sin\theta}{q}\frac{\partial L^*}{\partial\theta}, \lambda^*q^2\right)}{\partial(q,\theta)} - \cos\theta\frac{\partial\left(\sin\theta\frac{\partial L^*}{\partial q} + \frac{\cos\theta}{q}\frac{\partial L^*}{\partial\theta}, \lambda^*q^2\right)}{\partial(q,\theta)}\right\} = 0,$$

(4.18)
$$\lambda^*w^* = J^*\left\{\cos\theta\frac{\partial\left(\sin\theta\frac{\partial L^*}{\partial q} + \frac{\cos\theta}{q}\frac{\partial L^*}{\partial\theta}, \lambda^*\right)}{\partial(q,\theta)} - \sin\theta\frac{\partial\left(\cos\theta\frac{\partial L^*}{\partial q} - \frac{\sin\theta}{q}\frac{\partial L^*}{\partial\theta}, \lambda^*\right)}{\partial(q,\theta)}\right\},$$

(4.19)
$$\mu_e\sigma(\lambda^*q^2 - A) = J^*\left\{\cos\theta\frac{\partial\left(\cos\frac{\partial L^*}{\partial q} - \frac{\sin\theta}{q}\frac{\partial L^*}{\partial\theta}, \lambda^*\right)}{\partial(q,\theta)} + \sin\theta\frac{\partial\left(\sin\theta\frac{\partial L^*}{\partial q} + \frac{\cos\theta}{q}\frac{\partial L^*}{\partial\theta}, \lambda^*\right)}{\partial(q,\theta)}\right\},$$

$$W_1^* = \frac{1}{q}\left\{\frac{\partial\left(\sin\theta\frac{\partial L^*}{\partial q} + \frac{\cos\theta}{q}\frac{\partial L^*}{\partial\theta}, J^*Q_1^*\right)}{\partial(q,\theta)} + \frac{\partial\left(\cos\theta\frac{\partial L^*}{\partial q} - \frac{\sin\theta}{q}\frac{\partial L^*}{\partial\theta}, J^*Q_2^*\right)}{\partial(q,\theta)}\right\},$$

(4.20)
$$W_2^* = \frac{1}{q}\left\{\frac{\partial\left(\sin\theta\frac{\partial L^*}{\partial q} + \frac{\cos\theta}{q}\frac{\partial L^*}{\partial\theta}, J^*P_1^*\right)}{\partial(q,\theta)} + \frac{\partial\left(\cos\theta\frac{\partial L^*}{\partial q} - \frac{\sin\theta}{q}\frac{\partial L^*}{\partial\theta}, J^*P_2^*\right)}{\partial(q,\theta)}\right\},$$

(4.20) [cont.)

$$W_3^* = \frac{1}{q}\left\{ P_1^* \frac{\partial\left(\sin\theta\frac{\partial L^*}{\partial q} + \frac{\cos\theta}{q}\frac{\partial L^*}{\partial\theta}, I^*\right)}{\partial(q,\theta)} + P_2^* \frac{\partial\left(\cos\theta\frac{\partial L^*}{\partial q} - \frac{\sin\theta}{q}\frac{\partial L^*}{\partial\theta}, I^*\right)}{\partial(q,\theta)}\right\},$$

$$W_4^* = \frac{1}{q}\left\{ \frac{\partial\left(\sin\theta\frac{\partial L^*}{\partial q} + \frac{\cos\theta}{q}\frac{\partial L^*}{\partial\theta}, R_1^*\right)}{\partial(q,\theta)} + \frac{\partial\left(\cos\theta\frac{\partial L^*}{\partial q} - \frac{\sin\theta}{q}\frac{\partial L^*}{\partial\theta}, R_2^*\right)}{\partial(q,\theta)}\right\},$$

$$W_5^* = \frac{1}{q}\left\{ R_1^* \frac{\partial\left(\sin\theta\frac{\partial L^*}{\partial q} + \frac{\cos\theta}{q}\frac{\partial L^*}{\partial\theta}, J^*\right)}{\partial(q,\theta)} + R_2^* \frac{\partial\left(\cos\theta\frac{\partial L^*}{\partial q} - \frac{\sin\theta}{q}\frac{\partial L^*}{\partial\theta}, J^*\right)}{\partial(q,\theta)}\right\},$$

(4.21)

$$j^* = \mu_e\sigma(\lambda^* q^2 - A),$$

$$W^* = J^*\left(\frac{\partial L^*}{\partial q^2} + \frac{1}{q}\frac{\partial L^*}{\partial q} + \frac{1}{q^2}\frac{\partial^2 L^*}{\partial\theta^2}\right),$$

$$J^* = q^4\left\{ q^2\frac{\partial^2 L^*}{\partial q^2}\left(q\frac{\partial L^*}{\partial q} + \frac{\partial^2 L^*}{\partial\theta^2}\right) - \left(\frac{\partial L^*}{\partial\theta} - q\frac{\partial^2 L^*}{\partial q\partial\theta}\right)^2\right\}^{-1},$$

$$I^* = (J^*)^{n-1}\left\{ \left(\frac{\partial^2 L^*}{\partial q^2} - \frac{1}{q}\frac{\partial L^*}{\partial q} - \frac{1}{q^2}\frac{\partial^2 L^*}{\partial\theta^2}\right)^2 + \frac{4}{q^4}\left(\frac{\partial L^*}{\partial\theta} - q\frac{\partial^2 L^*}{\partial q\partial\theta}\right)^2\right\}^{(n-1)/2},$$

(4.22)

$$P_1^* = \frac{1}{q}\frac{\partial\left(\sin\theta\frac{\partial L^*}{\partial q} + \frac{\cos\theta}{q}\frac{\partial L^*}{\partial\theta}, w^*\right)}{\partial(q,\theta)},$$

$$P_2^* = \frac{1}{q}\frac{\partial\left(\cos\theta\frac{\partial L^*}{\partial q} - \frac{\sin\theta}{q}\frac{\partial L^*}{\partial\theta}, w^*\right)}{\partial(q,\theta)},$$

$$Q_1^* = \frac{1}{q}\frac{\partial\left(\sin\theta\frac{\partial L^*}{\partial q} + \frac{\cos\theta}{q}\frac{\partial L^*}{\partial\theta}, I^*\right)}{\partial(q,\theta)},$$

(4.22) [cont.)
$$Q_2^* = \frac{1}{q}\frac{\partial\left(\cos\theta\dfrac{\partial L^*}{\partial q} - \dfrac{\sin\theta}{q}\dfrac{\partial L}{\partial\theta}, I^*\right)}{\partial(q,\theta)},$$

(4.23)
$$R_1^* = Q_1^*\left(\sin^2\theta\frac{\partial^2 L^*}{\partial q^2} + \frac{\cos^2\theta}{q}\frac{\partial L^*}{\partial q} - \frac{\sin 2\theta}{q^2}\frac{\partial L^*}{\partial\theta} + \frac{\sin 2\theta}{q}\frac{\partial^2 L^*}{\partial q\partial\theta} + \frac{\cos^2\theta}{q^2}\frac{\partial^2 L^*}{\partial\theta^2}\right) + Q_2^*\left(\sin\theta\cos\theta\frac{\partial^2 L^*}{\partial q^2} - \frac{\sin\theta\cos\theta}{q}\frac{\partial L^*}{\partial q} - \frac{\cos 2\theta}{q^2}\frac{\partial L^*}{\partial\theta} + \frac{\cos 2\theta}{q}\frac{\partial^2 L^*}{\partial q\partial\theta} - \frac{\sin\theta\cos\theta}{q^2}\frac{\partial^2 L^*}{\partial\theta^2}\right),$$

$$R_2^* = Q_1^*\left(\sin\theta\cos\theta\frac{\partial^2 L^*}{\partial q^2} - \frac{\sin\theta\cos\theta}{q}\frac{\partial L^*}{\partial q} - \frac{\cos 2\theta}{q^2}\frac{\partial L^*}{\partial\theta} + \frac{\cos 2\theta}{q}\frac{\partial^2 L^*}{\partial q\partial\theta} - \frac{\sin\theta\cos\theta}{q^2}\frac{\partial^2 L^*}{\partial\theta^2}\right) + Q_2^*\left(\cos^2\theta\frac{\partial^2 L^*}{\partial q^2} + \frac{\sin^2\theta}{q}\frac{\partial L^*}{\partial q} + \frac{\sin 2\theta}{q^2}\frac{\partial L^*}{\partial\theta} - \frac{\sin 2\theta}{q}\frac{\partial^2 L^*}{\partial q\partial\theta} + \frac{\sin^2\theta}{q^2}\frac{\partial^2 L^*}{\partial\theta^2}\right).$$

Once $L^*(q,\theta)$ and $\lambda^*(q,\theta)$ are found, we can use the relations

(4.24)
$$x = \sin\theta\frac{\partial L^*}{\partial q} + \frac{\cos\theta}{q}\frac{\partial L^*}{\partial\theta},$$
$$y = \frac{\sin\theta}{q}\frac{\partial L^*}{\partial\theta} - \cos\theta\frac{\partial L^*}{\partial q}$$

to find the velocity components, $\lambda(x,y)$ and other flow variables in the physical plane.

5. Applications

In this section we investigate the vortex, radial, and spiral flow problems as applications of Theorem 1 stated in the previous section.

5.1. Vortex flow

Let

(5.1)
$$L^*(q,\theta) = G(q), \quad G'(q) \neq 0, \quad G''(q) \neq 0$$

be the Legendre transformation, where prime denotes differentiation with respect to q.

Using Eq. (5.1) in Eqs. (4.17)–(4.24), we get

(5.2)
$$\frac{K}{q}\left\{w^*\left[I^* + G'\left(\frac{I^{*\prime}}{G''}\right)'\right] - I^*\left[w^{*\prime} + G'\left(\frac{w^{*\prime}}{G''}\right)'\right] - \frac{2J^{*2}}{q^3}(3G'^2G''I^{*\prime} - 2G'^3I^{*\prime} + G'^3qI^{*\prime}) - \frac{4G'^3I^{*\prime}J^*J^{*\prime}}{q^2}\right\} + \mu_e^2\sigma G'\lambda^*\frac{\partial(\lambda^*q^2)}{\partial q} = 0,$$

(5.3)
$$\frac{\partial\lambda^*}{\partial q} + \lambda^*\left(\frac{G''}{G'} + \frac{1}{q}\right) = 0,$$

$$\frac{\partial \lambda^*}{\partial \theta} = \mu_e \sigma G' \left(q\lambda^* - \frac{A}{q} \right), \tag{5.4}$$

$$J^* = \frac{q}{G'G''},$$

$$w^* = \frac{qG'' + G'}{G'G''}, \tag{5.5}$$

$$I^* = \left(\frac{qG'' - G'}{G'G''} \right)^{(n-1)}.$$

Solving Eq. (5.3), we obtain

$$\lambda^* = \frac{\alpha(\theta)}{qG'},$$

where $\alpha(\theta)$ is an arbitrary function of θ.

Since J^*, w^*, I^* and their derivatives are functions of q, from Eq. (5.2) it follows that $\alpha(\theta)$ is an arbitrary constant and λ is a function of q only.

Letting $\alpha(\theta) = \alpha_1$, we can express λ^* as

$$\lambda^* = \frac{\alpha_1}{qG'}, \tag{5.6}$$

where α_1 is an arbitrary constant.

Employing Eqs. (5.6) in (5.4), we obtain

$$\lambda^* = \frac{A}{q^2}. \tag{5.7}$$

From Eqs. (5.6) and (5.7) it follows that

$$G'(q) = \frac{\alpha_1}{A} q \tag{5.8}$$

which on integration yields

$$G(q) = \frac{\alpha_1}{2A} q^2 + \alpha_2, \tag{5.9}$$

where α_2 is an arbitrary constant.

Substituting Eq. (5.9) in Eq. (5.5), we get

$$J^* = \frac{A^2}{\alpha_1^2}, \qquad w^* = \frac{2A}{\alpha_1}, \qquad I^* = 0. \tag{5.10}$$

Using Eqs. (5.9) and (5.10), we find that Eq. (5.2) is satisfied identically. Therefore

$$L^*(q, \theta) = G(q) = \frac{\alpha_1}{2A} q^2 + \alpha_2, \qquad A \neq 0 \tag{5.11}$$

is a Legendre transform function of the streamfunction in polar coordinates in the hodograph plane and can be written in the u, v-coordinates as

$$L(u, v) = \frac{\alpha_1}{2A} (u^2 + v^2) + \alpha_2. \tag{5.12}$$

Using Eq. (5.12) in Eq. (4.2), we obtain the velocity components in the following form:

$$u(x, y) = -\frac{Ay}{\alpha_1}, \qquad v(x, y) = \frac{Ax}{\alpha_1}. \tag{5.13}$$

Substituting these in Eq. (5.7), we get

$$\lambda(x, y) = \frac{\alpha_1^2}{A(x^2 + y^2)}. \tag{5.14}$$

Employing Eqs. (5.13) and (5.14) in Eq. (2.5) to Eq. (2.8), we obtain

$$\mathbf{H}(x, y) = \left(-\frac{\alpha_1 x}{x^2 + y^2}, -\frac{\alpha_1 y}{x^2 + y^2}\right), \tag{5.15}$$

$$p(x, y) = \frac{\varrho A^2}{2\alpha_1^2}(x^2 + y^2) + \pi_1, \tag{5.16}$$

where π_1 is an arbitrary constant.

As a result, we can formulate the following theorem:

THEOREM 2. *If $L^*(q, \theta) = G(q)$ is the Legendre transform function of a streamfunction for a steady plane orthogonal flow of a non-Newtonian power-law fluid of finite electrical conductivity, then the flow in the physical plane is a vortex flow given by Eq.* (5.13) *to Eq.* (5.16).

5.2. Radial flow

Let

$$L^*(q, \theta) = A_1\theta + B_1, \tag{5.17}$$

where $A_1 \neq 0$, and B_1 are arbitrary constants.

In this case we get

$$\begin{aligned} &J^* = -\frac{q^4}{A_1^2}, \qquad w^* = 0, \qquad P_1^* = 0, \qquad P_2^* = 0, \\ &I^* = \frac{2^{(n-1)}q^{2(n-1)}}{A_1^{(n-1)}}, \qquad W_2^* = W_3^* = W_4^* = W_5^* = 0. \end{aligned} \tag{5.18}$$

Using Eqs. (5.17) and (5.18) in Eqs. (4.18) and (4.19), we obtain

$$\frac{\partial \lambda^*}{\partial \theta} = 0, \tag{5.19}$$

$$\frac{\partial \lambda^*}{\partial q} + \frac{A_1\mu_e\sigma\lambda^*}{q} = \frac{AA_1\mu_e\sigma}{q^3}. \tag{5.20}$$

Equation (5.19) implies that λ^* is a function of q alone. Solving the linear equation (5.20), we get

$$\lambda^*(q) = \begin{cases} \dfrac{AA_1\mu_e\sigma}{(A_1\mu_e\sigma - 2)}\dfrac{1}{q^2} + \alpha_3 q^{-A_1\mu_e\sigma} & \text{if } A_1 \neq \dfrac{2}{\mu_e\sigma}, \\ \dfrac{2A}{q^2}\ln q + \dfrac{\alpha_4}{q^2} & \text{if } A_1 = \dfrac{2}{\mu_e\sigma}, \end{cases} \tag{5.21}$$

where α_3 and α_4 are arbitrary constants.

As in the previous application, Eq. (4.17) is satisfied identically. Proceeding as before, we obtain the flow variables in the following form

(i) $A_1 \neq \dfrac{2}{\mu_e \sigma}$

$$u(x,y) = \frac{A_1 x}{(x^2+y^2)}, \qquad v(x,y) = \frac{A_1 y}{(x^2+y^2)},$$

$$\mathbf{H}(x,y) = \left(\frac{A A_1 \mu_e \delta}{(A_1\mu_e\sigma - 2)} q^{-2} + \alpha_3 q^{-A_1\mu_e\sigma}\right)\left(-\frac{A_1 y}{(x^2+y^2)}, \frac{A_1 x}{(x^2+y^2)}\right),$$

$$j = \frac{2A\mu_e\sigma}{(A_1\mu_e\sigma - 2)} + \mu_e\sigma\alpha_3 q^{2-A_1\mu_e\sigma},$$

$$p(x,y) = 2^{(n-1)} K \frac{(n-1)}{n} - \frac{1}{2}\varrho q^2 - A_1\mu_e\left\{\frac{A^2 A_1^2 \mu_e^2 \sigma^2}{(A_1\mu_e\sigma - 2)^2} q^{-2} + \frac{A\alpha_3(A_1\mu_e\sigma + 2)}{A_1(A_1\mu_e\sigma - 2)} q^{-A_1\mu_e\sigma} + \frac{\mu_e\sigma\alpha_3^2}{2(A_1\mu_e\sigma - 1)} q^{-2(A_1\mu_e\sigma - 1)}\right\} + \pi_2,$$

where

$$q^2 = \frac{A_1^2}{(x^2+y^2)}. \tag{5.22}$$

(ii) $A_1 = \dfrac{2}{\mu_e\sigma}$

$$u(x,y) = \frac{2x}{\mu_e\sigma(x+y^2)}, \qquad v(x,y) = \frac{2y}{\mu_e\sigma(x^2+y^2)},$$

$$\mathbf{H}(x,y) = \left(\frac{2A}{q^2}\ln q + \mu_e\sigma\alpha_4\right)\left(\frac{-2y}{\mu_e\sigma(x^2+y^2)}, \frac{2x}{\mu_e\sigma(x^2+y^2)}\right),$$

$$j(x,y) = A\mu_e\sigma(2\ln q - 1) + \mu_e\sigma\alpha_4,$$

$$p(x,y) = 2^{(n-1)} K \frac{(n-1)}{n} - \frac{1}{2}\varrho q^2 - A_1\mu_e\left\{\frac{A^2\mu_e\sigma}{q^2}[2(\ln q)^2 + 2\ln q + 1]\right.$$

$$\left. + 2A\mu_e\sigma(A - \alpha_4)[(\ln q)^2 + 2\ln q + 2] + A\mu_e\sigma(A - \alpha_4)(\ln q)^2 - \frac{\mu_e\sigma\alpha_4}{2q^2}(A - \alpha_4)\right\} + \pi_3,$$

where

$$q^2 = \frac{4}{\mu_e^2\sigma^2(x^2+y^2)}, \tag{5.23}$$

and π_2 and π_3 are arbitrary constants.

THEOREM 3. *If $L^*(q,\theta) = A_1\theta + B_1$ is the Legendre transform function of a streamfunction of a steady plane orthogonal flow of a non-Newtonian power-law fluid of finite electrical conductivity, then the flow in the physical plane is a radial flow and flow variables are given by Eq.* (5.21) *to* (5.23).

5.3. Spiral flow

In this case let

$$L^*(q,\theta) = c_1 \ln q + c_2\theta, \qquad c_1 \neq 0, c_2 \neq 0, \tag{5.24}$$

where c_1 and c_2 are arbitrary constants.

Proceeding as in the previous applications, we get

$$
\begin{aligned}
&I^* = \frac{2^{n-1}}{(c_1^2 + c_2^2)^{(n-1)/2}} q^{(2n-3)}, \\
&J^* = -\frac{q^4}{(c_1^2 + c_2^2)}, \qquad w^* = 0, \qquad P_1^* = 0, \qquad P_2^* = 0, \\
&Q_1^* = -\frac{I^*}{q^2}(c_1 \cos\theta - c_2 \sin\theta), \qquad Q_2^* = \frac{I^*}{q^2}(c_1 \sin\theta + c_2 \cos\theta), \\
&R_1^* = -\frac{I^{*\prime}}{q^4}(c_1^2 + c_2^2)\cos\theta, \qquad R_2^* = \frac{I^{*\prime}}{q^4}(c_1^2 + c_2^2)\sin\theta, \\
&W_1^* = 0, \qquad W_2^* = 0, \qquad W_3^* = 0, \\
&W_4^* = \frac{c_1}{q^4}(c_1^2 + c_2^2)\left(I^{*\prime\prime} - \frac{5I^{*\prime}}{q}\right), \qquad W_5^* = -c_1 \frac{(c_1^2 + c_2^2)}{q^6} I^{*\prime} J^{*\prime}.
\end{aligned} \tag{5.25}
$$

Employing Eq. (5.24) and (5.25) in Eq. (4.17), (4.18), we obtain

$$
\frac{2^{n+2} K (n-1)(n-8)}{(c_1^2 + c_2^2)^{(n+1)/2}} q^{2n-2} = \mu_e^2 \sigma \lambda^* \left\{ 2c_1 \lambda^* + c_1 \frac{q \partial \lambda^*}{\partial q} + c_2 \frac{\partial \lambda^*}{\partial \theta} \right\}, \tag{5.26}
$$

$$
c_1 q \frac{\partial \lambda^*}{\partial q} + c_2 \frac{\partial \lambda^*}{\partial \theta} = 0, \tag{5.27}
$$

$$
\mu_e \sigma (\lambda^* q^2 - A) = \frac{q^4}{(c_1^2 + c_2^2)} \left\{ \frac{c_1}{q^2} \frac{\partial \lambda^*}{\partial \theta} - \frac{c_2}{q} \frac{\partial \lambda^*}{\partial q} \right\}. \tag{5.28}
$$

From the above system of equations it follows that

$$
\lambda^* = 0, \tag{5.29}
$$

which is a trivial solution. Therefore, in a steady plane flow of an orthogonal non-Newtonian power-law fluid of finite electrical conductivity the spiral is not possible. However, the spiral flow can exist in a nonconducting steady plane flow of an incompressible viscous fluid or a non-Newtonian power-law fluid for which $n = 8$.

References

1. W. F. AMES, *Non-linear partial differential equations*, Academic Press, New York 1989.
2. O. P. CHANDNA, R. M. BARRON and A. C. SMITH, *Rotational plane steady flow of viscous fluid*, SIAM J. Appl. Math., **42**, 1323–1336, 1982.
3. A. M. SIDDIQUI, Q. M. KALONI and O. P. CHANDNA, *Hodograph transformation methods in non-Newtonian fluid flows*, J. Engng Math., **19**, 203–216, 1985.
4. O. P. CHANDNA and P. V. NGUYEN, *Hodograph method in non-Newtonian MHD transverse fluid flows*, J. Engng. Math., **23**, 119–139, 1989.
5. P. V. NGUYEN and O. P. CHANDNA, *Hodograph study of non-Newtonian MHD aligned steady plane flows*, Int. J. Math. and Math. Sci., **13**, 93–114, 1990.
6. O. P. CHANDNA and P. V. NGUYEN, *Hodograph transformation method and solution in aligned MHD plane flows*, Int. J. Engng. Sci., **28**, 973–987, 1990.

7. O. P. CHANDNA and P. V. NGUYEN, *Hodographic study of MHD constantly inclined fluid flows*, Int. J. Engng. Sci., **30**, 69–82, 1992.
8. P. V. NGUYEN and O. P. CHANDNA, *Hodograph method in MHD orthogonal fluid flows*, Int. J. Math. and Math. Sci., **15**, 149–160, 1992.

WHEELING JESUIT COLLEGE, WHEELING, WEST VIRGINIA, USA.

Received January 18, 1993.

Arch. Mech., 45, 1, pp. 135–155, Warszawa 1993

Thermomechanical behavior of polycrystalline shape memory alloys Cu-Zn-Al

CH. LEXCELLENT and P. VACHER (BESANCON)

IN A WIDE TEMPERATURE interval, on either side of transformation temperature, tension-unloading tests ($1\% \ldots 4\%$) enable the separation of the pseudoelastic and plastic strains. During these mechanical tests, resistivity measurements allow the evolution of the martensite fraction x to be followed (at loading and unloading). This measurement is complemented by acoustic emission recordings. The strain ε^{PE} seems to be proportional to x used as an internal variable. In order to be operational, the model should be completed by the introduction of an orientation parameter which accounts for the nature of the martensite formed.

Notations

$\alpha = \begin{cases} 1 & \text{austenite,} \\ 2 & \text{martensite,} \end{cases}$

$\varepsilon_{(\alpha)}$ uniaxial strain of phase (α),

ε uniaxial total strain,

ε^{PE} uniaxial pseudoelastic strain,

ε_c^{el} uniaxial classical elastic strain,

ε^{pl} uniaxial plastic strain,

x weight fraction of martensite,

$1 - x$ weight fraction of austenite,

$u_0^{*(\alpha)}$ specific internal energy of phase (α),

$s_0^{*(\alpha)}$ specific internal entropy of phase (α),

$\overline{u}_0$ specific configurational energy,

$\overline{s}_0$ specific configurational entropy,

τ uniaxial Kirchhoff stress,

$\tau_{(\alpha)}$ uniaxial Kirchhoff stress of phase (α),

σ uniaxial Cauchy stress,

$\sigma_{(\alpha)}$ uniaxial Cauchy stress of phase (α),

ϱ mass density,

E_M, $E_{(1)}$ martensite Young modulus,

E_A, $E_{(2)}$ austenite Young modulus,

M_s, (M_F) martensite start (finish) temperature at stress-free state,

$A_s (A_F)$ austenite start (finish) temperature at stress-free state,

s specific entropy,

T temperature,

c_v specific heat at constant volume,

γ pseudoelastic strain obtained in tensile test after complete phase transformation $(A \rightleftarrows M)$,

α_0 thermal expansion coefficient,

r resistivity,

$X_e(N)$ training stress (at cycle N),

$\langle x \rangle = \begin{cases} x & \text{if } x \geq 0, \\ 0 & \text{if } x < 0. \end{cases}$

1. Introduction

GIVEN THE NUMEROUS possible technological applications, the interest in studying the thermomechanical properties of shape memory alloys and their modelization, no longer, needs to be justified. It is primarily a matter of introducing the effect of a martensite transformation, induced under stress, into the elastoplastic behavior laws.

Here, the mechanical behavior of polycrystalline Cu-Zn-Al alloys is studied in the neighbourhood of the transformation temperatures (under zero external stress), that is to say, initially in a martensitic phase ($T < M_F$) or in a austenitic phase ($T > A_F$). When an alloy, at a temperature T, is subjected to a stress field σ, several strain modes can be activated.

a. If $T \leq M_F$ the phase is always martensitic. Following the classical elastic strain, a pseudoplastic strain occurs corresponding to the orientation of the martensite variants due to the effect of σ.

b. If T is slightly greater than $M_s (0 \leq (T - M_s) < 30°)$, then it is the case of the pure transformation associated with a thermoelastic martensitic transformation (at least in this case where $\varepsilon \leq 2\%$) [1] (ε represents the total strain).

c. As the difference $(T - M_s)$ increases, the stress necessary to induce the martensitic transformation approaches that which is necessary to initiate plastic strain by gliding in the β-phase and an interference between the transformation and the plastic strain can occur.

d. At temperatures much higher than $M_s ((T - M_s)$ of the order of 200°C for the alloy in question), only a plastic strain of the β-phase occurs [2].

Taking simultaneously into account the cases b, c and d, we obtain the complex problem of coupled transformation plasticity. Work in this field has been done by ONODERA and TAMURA [3] and ROMERO and AHLERS [4] for shape memory alloys and DENIS, SJOSTROM and SIMON [5] and LEBLOND, MOTTET and DEVAUX [6] for steels.

In order to analyze the coupled transformation plasticity in a wide temperature interval ($-100° \leq (T - M_s) \leq 220$°C), tension-unloading tests (systematic unloading at $1\%, 2\%, \ldots, 4\%$) have been performed by assuming the classical separation: (classical elasticity and pseudoelasticity) + (plasticity). During these tests, electrical resistivity measurements are used to indicate the volume fraction x of martensite which is present. Finally, acoustic emission recordings allow the evolution of x to be followed as a function of the applied stress.

The present study includes:

i. A description of the experimental procedure of the tensile tests and, in particular, the measurements of resistivity under stress and acoustic emission.

ii. An evaluation of the obtained experimental results.

2. Experimental procedure and results

2.1. Experimental procedure

2.1.1. Material — thermal treatment — mechanical tests. The two shape memory alloys, fabricated by the company "Trefimétaux", have the following weight composition and transformation points (resistivity measurements under zero stress):

% weight		Cu	Zn	Al	Zr	Mg	Fe	P	M_F °C	M_S	A_S	A_F
R205	Al	67.93	28.07	4.00	275PPM	231PPM	60PPM	< 20PPM	−110.5	−98	−94	−91
R150	A2	67.56	28.45	3.99	"	"	"	"	−148	−137	−136	−133

For $T \geq A_F$, the desired metallurgical state is the β-monophase austenitic state. In order to obtain this condition, a standard heat treatment has been chosen of 10 min. at 850°C in air, followed by a water quench. Note that the amount of aluminium in the alloy is sufficient to produce a fine layer of impermeable alumina which protects the sample from rapid corrosion or from dezincification [7]. Following the treatment, a metallurgical examination indicates a single phase (austenitic β-phase) with an average grain size of $\delta = 300\ \mu$. The machined samples have a gauge length of 25 mm and a total length of 75 mm. The rectangular cross-section is 10 mm wide and 0.6 mm thick for A1 and 3 mm thick for A2.

The tests are performed on an "Instron" tensile machine. It consists in uniaxial tension-unloading tests, with systematic reloading at $1\%, 2\%, \ldots, 4\%$:

i) an imposed strain rate of $\Delta l = kt$,

ii) an imposed force rate of $F = Kt$.

2.1.2. Measurement of electrical resistance. The use of this technique is based on the simple idea which says that every change of phase inside a material leads to a variation of its physical properties. For shape memory alloys, the variation of electrical resistivity of a sample, during the transformation, is one of the physical variables which is easily measurable; moreover, this variable shows well the change of the structure.

The total transformation from austenite into martensite of a copper SMA leads to an increase of resistivity by 25%.

From the resistivity values of austenite and martensite, and if we use the mixture law in case of two mixed phases, we are able to determine:

i) the four transformation temperatures, which are characteristics for the material (M_F, M_S, A_S, A_F) and the associated hysteresis loop (free stress, variable temperature),

ii) the volume fraction of martensite which exists at any time, during an isothermal loading-unloading tensile test.

A test steady current i is applied to the sample (here: $i = 4A$). We have to measure the voltage U applied to the sample, so we can determine the resistance R.

The resistivity measurement is not easy in our case, and it is almost zero ($r = 10^{-7}\Omega$m for a copper SMA).

The measuring instruments have to be very sensitive and without parasites. Therefore, we use the "four wires" method. The current goes between two welded wires (Laser weld), which are situated at both ends of the sample. We measure the voltage between the two wires at the intermediate positions. This method enables us to suppress the error due to the resistance of the wires.

During a tensile test, the resistance varies like:

$$R(t) = r(t)\frac{l(t)}{S(t)}. \tag{2.1}$$

If we suppose to have small strains and the volume variation of an austenite domain giving martensite is less than 0.5%, we can find the resistivity r of the alloy from the formula (form the voltage U)

$$\frac{r}{r_{0a}} \simeq \frac{U}{U_0}(1 - (1 + 2\nu)\varepsilon), \qquad \text{with } \nu = 0.5. \tag{2.2}$$

$r_{0a}(r_{0m})$ is the resistance of an austenite (martensite) domain without strain. If we consider a linear mixture law, we can write

$$r(z) = r_{0a}(1 - z) + r_{0m}(z) \Rightarrow z = \frac{r(z)/r_{0a} - 1}{r_{0m}/r_{0a} - 1}. \tag{2.3}$$

2.1.3. Measurement of acoustic emission

a. Introduction

Acoustic emission (A.E) (more exactly stress waves emission) is a phenomenon of creation of transient elastic waves due to local microdisplacements inside the material.

The ultrasound A.E. results from a rough and very localized energy relieving, which is produced, inside the material, after a quick microstructural change.

When we obtain this A.E. by means of appropriate sensors, we can determine the mechanism which lead to this energy relieving.

The emitted ultrasound wave gives us workable information, and moreover, the signal contains a lot of dynamic information on the mechanism of the emission. Therefore, an analysis of the signal seems to be a very attractive tool to study dynamics of the physical phenomena which provide A.E. These phenomena are very varied: plastic deformation, cleavage and fracture inside the materials fracture produced by thermal shock, twinning, displacement of domain walls, martensite transformation.

In the case of thermoelastic martensite transformation of SMA, the observed A.E. is "discrete".

It is difficult to give an accurate analysis of this A.E., which is observed as an electric signal by a piezoelectric transducer, followed by amplificators and filters. It is usually analyzed by counting the number of times the electric signal furnished by the transducer crosses a pre-established threshold level (ring-down counting technique).

This technique is very sensitive but provides only qualitative information: hence, the physical origin of the A.E. source cannot be obtained from this kind of measurements.

b. Equipment and data processing

SOURCE — SENSOR

Ultrasonic waves, which carry the A.E. information, are changed into an electric voltage by means of a A.E. sensor which often uses the piezoelectric effect. This sensor is indexed at the end of the sample. It resonates in a mechanical way because the ultrasonic wave is jammed between two interfaces: the entrance face and the exit face of the piezoelectric element.

AMPLIFICATION — FILTERING

The signals coming from the sensor have usually a very small amplitude, so they have to be amplified.

RING DOWN COUNTING

The signals coming from the sensors, in response to the waves coming to the sensor, seem to be random not only in amplitude but also in duration. So, we have first to change them in measurable and registrable values, regarded with another parameter (time, temperature, strain, stress).

In order to try to measure the martensitic transformation, the chosen measurable value is the cumulated energy E_t.

2.2. Elementary analysis of the tensile curves

The tension-unloading curves for the Al composition will be examined first ($\dot{\varepsilon} = 10^{-4}\ s^{-1}$ with the hypothesis of small strains).

2.2.1. Strain in the martensitic phase. ($T \leq M_F$). In the temperature interval from $-196°C$ to $-97°C$, the strain ε of the purely martensite phase, with the platelets oriented in an

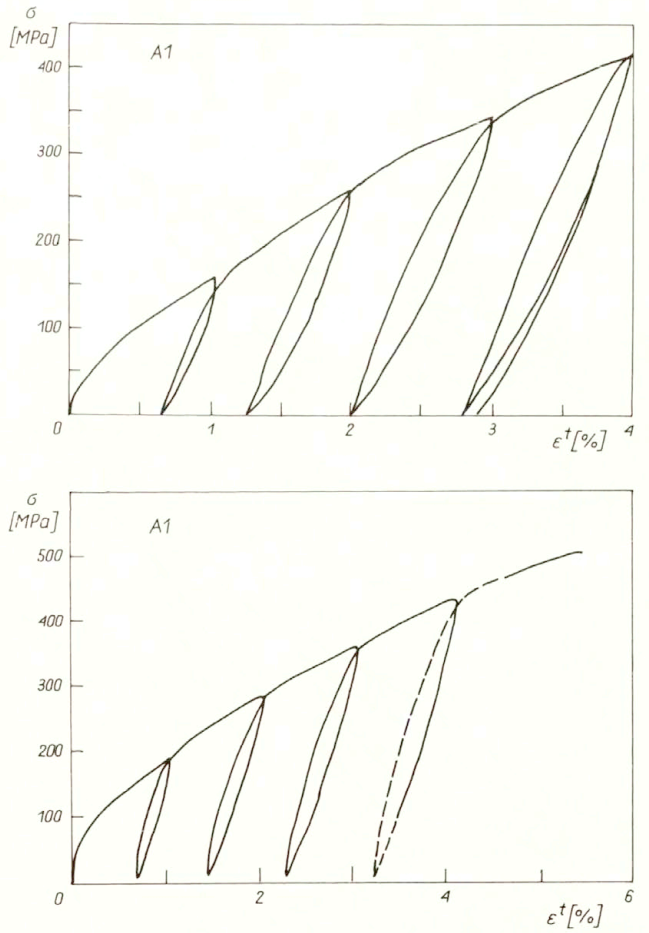

FIG. 1. Strain curve ($\sigma - \varepsilon$) in the pure martensitic state (A_1, $\dot{\varepsilon} = 10^{-4} s^{-1}$, $T = -115°C$, $-129°C$).

initially random fashion, can be divided into a reversible strain $\varepsilon_{\text{el}}^{TM}$

$$\varepsilon_{\text{el}}^{PM} = \frac{\sigma}{E_M}, \tag{2.4}$$

where E_M is Young's modulus of martensite of the order of 3.4 10^4 MPa and nearly independent of the temperature, and an irreversible strain $\varepsilon_{\text{pl}}^{TM}$ which is mainly produced by the movements of the interface between the variants which orient themselves under the effect of the external stress applied. In the case of extreme strain up to 17%, which is not the case here, a transformation of this martensite into a new martensitic structure can be obtained [8]. Figure 1 ($T = -115$, -129°C) shows a very slight hysteresis corresponding to a partial reorientation of the martensitic variants at unloading (caoutchouc effect).

$\varepsilon_{\text{pl}}^{TM}$ can be found at unloading as

$$\varepsilon_{\text{pl}}^{TM} = a_M \langle \sigma + b(T - A_s) \rangle, \tag{2.5}$$

with a_M of the order of $1 \cdot 10^{-4}\text{MPa}^{-1}$, and b around 2MPa°C^{-1}.

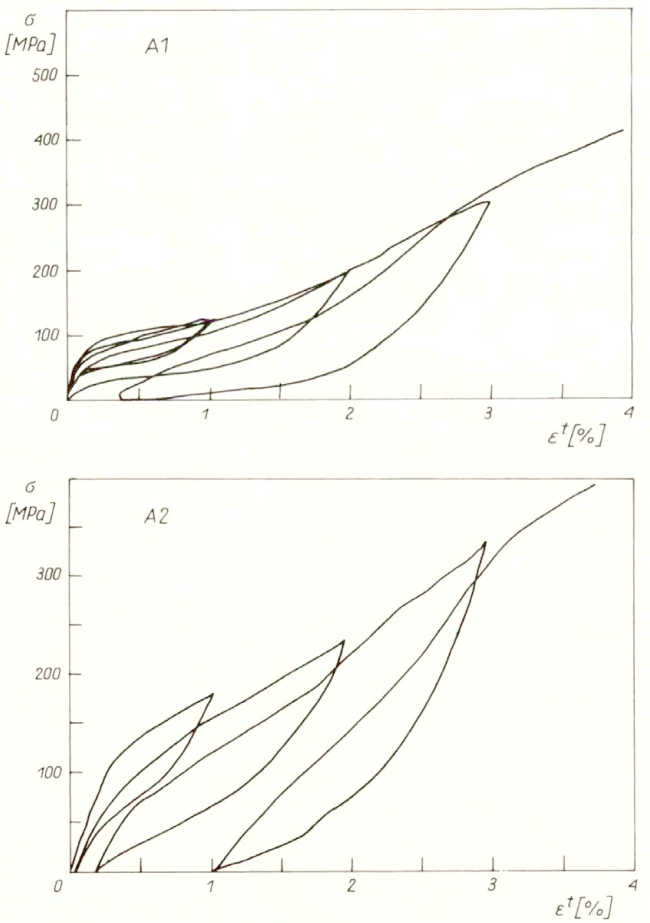

FIG. 2. Coupled transformation plasticity curve ($\dot{\varepsilon} = 10^{-4}\ \text{s}^{-1}$, A_1, $T = -73$°C, A_2, $T = -130$°C).

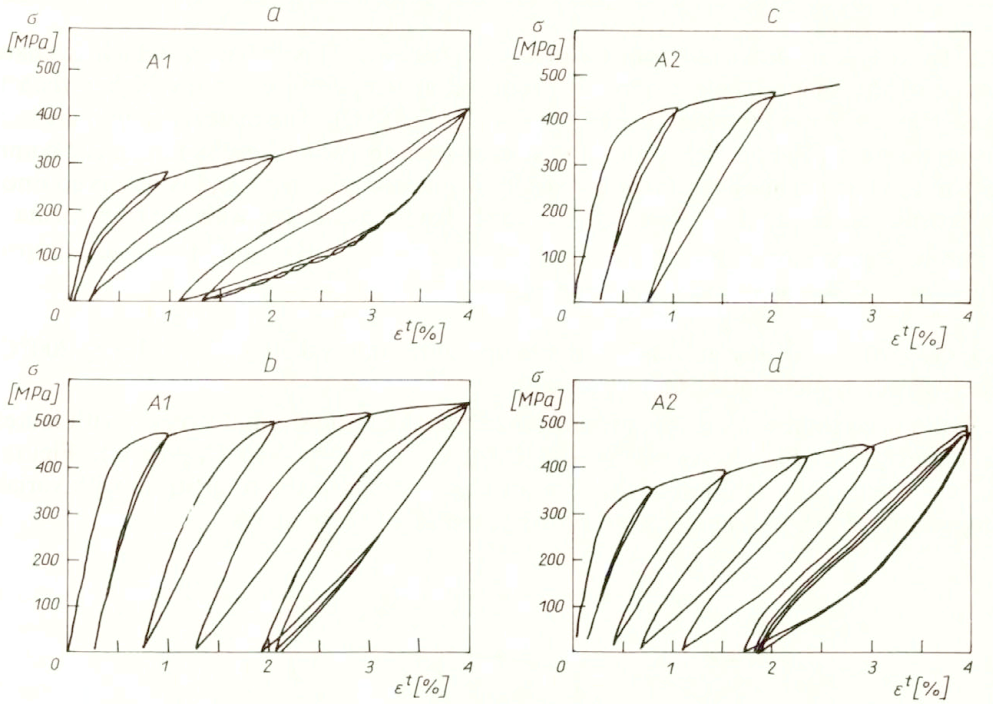

FIG. 3. Pure pseudoelasticity curve ($\dot{\varepsilon} = 10^{-4}\ \mathrm{s}^{-1}$, $A_1, T = -44^\circ\mathrm{C}, 20^\circ\mathrm{C}$, $A_2, T = -40^\circ\mathrm{C}, -70^\circ\mathrm{C}$).

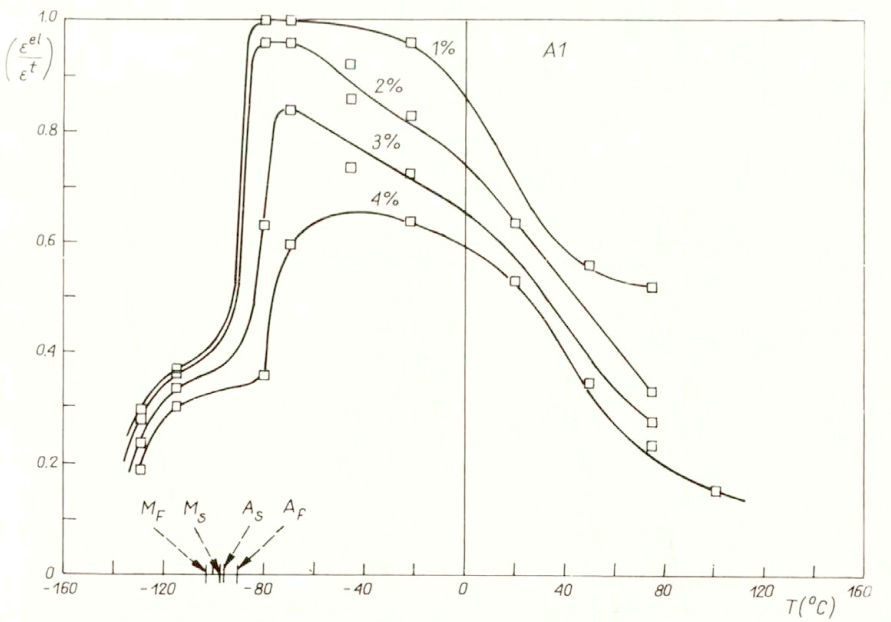

FIG. 4. Evolution of the ratio $\varepsilon^{\mathrm{el}}/\varepsilon^T$ as a function of the temperature (at fixed $\varepsilon^T = 1\%, 2\%, \ldots 4\%$).

2.2.2. Purely hyperelastic behavior (pure transformation plasticity). This behavior, which is characteristic of the shape memory alloy, is produced at temperature slightly higher than the phase transformation temperature ($0 \leq (T - A_s) < 20°C$). The material is initially in the austenitic state. The application of an external stress σ (which results in a shear component in the habit plane) can favor the strain by microscopic shear and is observed once a martensitic variant appears. For $\varepsilon \leq 2\%$, the behavior associated with the transformation is purely pseudoelastic (Fig. 2, $\dot{\varepsilon} = 10^{-4}s^{-1}$, $A_1 : T = -73°C$ and $A_2 : T = -130°C$), while for $\varepsilon = 3\%$, a plastic strain appears.

2.2.3. Coupled transformation plasticity. In the temperature interval $30 \leq (T - A_s) \leq 200°C$, a purely hyperelastic domain no longer exists.

For a fixed total strain ε, the proportion of pseudoelastic strain decreases with increasing temperature (Fig. 3, $A_1 : T = -44°C, 20°C$, $A_2 : T = -40°C, -70°C$). Figure 4, which presents the evolution of the ratio of elastic strain to the total strain with variable temperature T, shows the decrease of the potential of these alloys.

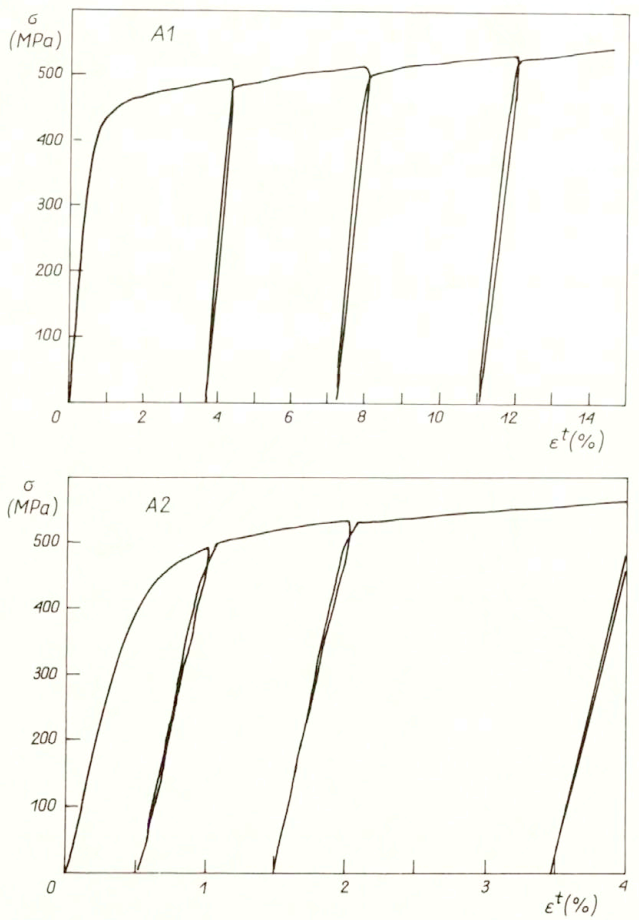

FIG. 5. Elastoplastic behaviour of pure austenite ($\dot{\varepsilon} = 10^{-4}s^{-1}$, $A_1, T = 100°C$, $A_2, T = 80°C$).

2.2.4 Elasto-viscoplastic behavior of pure austenite. For a temperature $(T - A_s)$ of the order of 200°C, the pseudoplastic strain disappears completely; there exists a temperature M_d (Martensite death) from which, regardless of the applied stress, martensite no longer forms (Fig. 5, $A_1 : T = 100°C$, $A_2 : T = 80°C$).

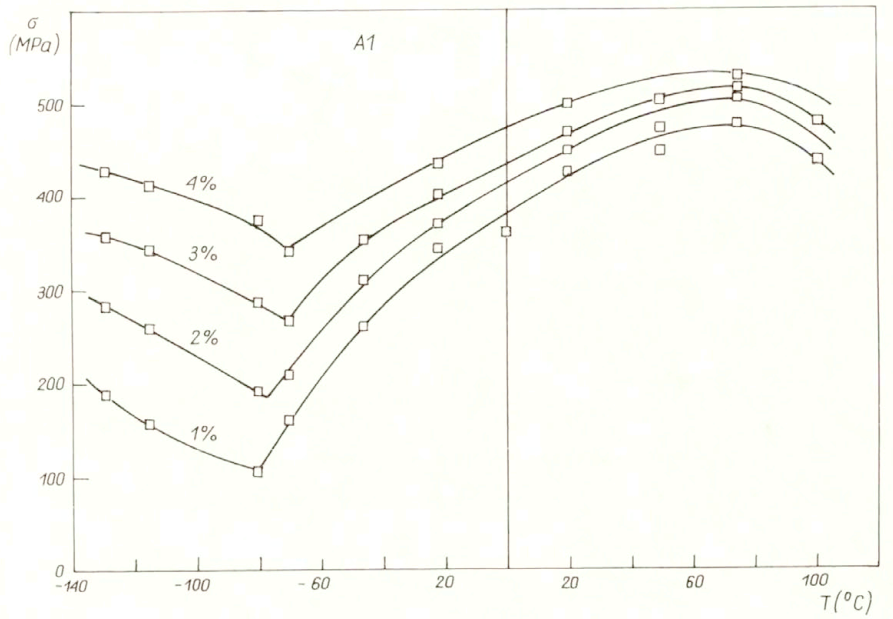

FIG. 6. Evolution of the applied stress with the temperature (at fixed $\varepsilon^T = 1\%, 2\%, \ldots 4\%$).

2.2.5. Evolution of the applied stress with the temperature (at a fixed total strain). Figure 6 shows that the stress σ:

- attains a minimum nearly coinciding with the phase transformation temperature (the energy necessary either to orient the platelets ($T \leq M_F$), or to form oriented platelets directly ($T > M_s$), increases with the distance from the phase transition temperatures),
- passes by a maximum near the temperature M_d; from $(T - A_s) > 30°C$, the viscoplasticity of the austenite plays a more and more important role with increasing temperature, and its evolution is the inverse of that of the energy necessary to the transformation.

2.2.6. Simplified approach to the hyperelastic and plastic behavior. For uniaxial tensile tests, the total strain ε can be partitioned in the classical fashion

$$\varepsilon = \varepsilon_c^{\mathrm{el}} + \varepsilon^{\mathrm{PE}} + \varepsilon^{\mathrm{pl}} \tag{2.6}$$

with the classical elastic strain defined by

$$\varepsilon_c^{\mathrm{el}} = \frac{\sigma}{E_A}. \tag{2.7}$$

The obtained pseudoelastic strain can be approximated by a linear law (even though this is not altogether the case at the beginning of the phase transformation)

$$\varepsilon^{\mathrm{PE}} = a\langle \sigma - \sigma_0 \rangle \tag{2.8}$$

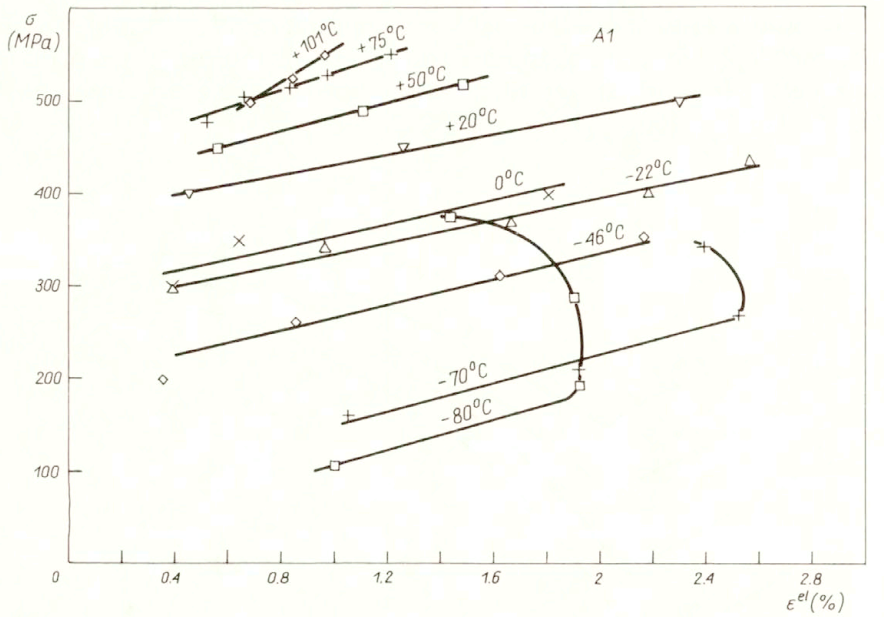

FIG. 7. Modelling of the pseudo-elastic strain ε^{PE}.

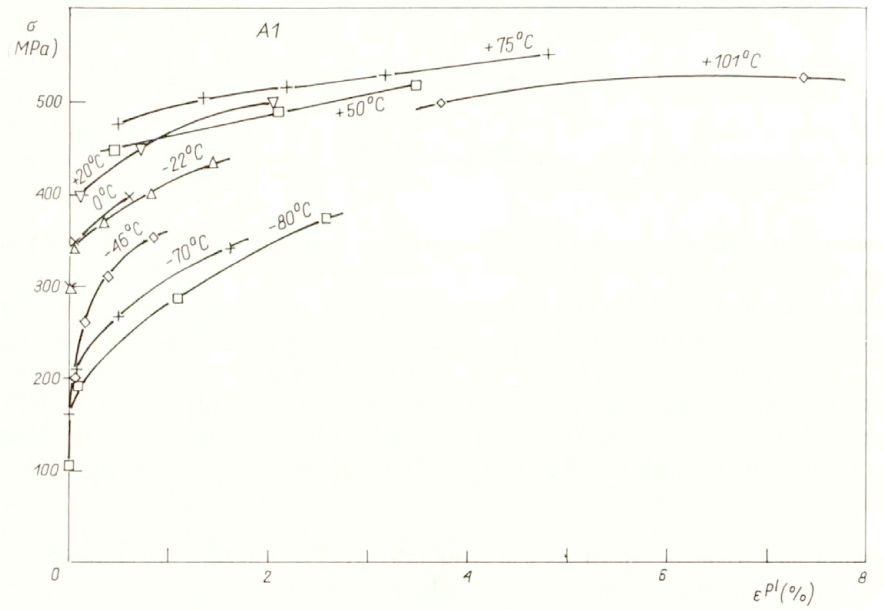

FIG. 8. Evolution of the plastic strain ε^{pl} with the applied stress.

with σ_0 yield stress for the phase transformation,

$$\sigma_0(T) = b(T - M_s) \quad \text{with} \quad \begin{cases} a = 1.1 \cdot 10^{-4}\ \text{MPa}^{-1}, \\ b = 3.45\ \text{MPa/°C} \quad \text{(Fig.7)}. \end{cases} \tag{2.9}$$

Note that the value of b obtained experimentally is higher than the value of 2 MPa/°C usually obtained on these Cu-Zn-Al alloys.

The plastic strain is represented in Fig. 8. As a first approximation, a viscous hardening law is chosen,

$$(\sigma - \sigma_0(T)) = K(T)(\dot{\varepsilon}_{\mathrm{pl}})^{1/N(T)}(\varepsilon_{\mathrm{pl}})^{1/M(T)}. \tag{2.10}$$

This partition of the strain allows for a simple modelling. But is does not take into account the particular character of the martensite transformation.

2.3. Determination of the volume fraction x of the martensite formed

As we explain in Sec. 2.1.2, the resistivity measurements are used in a classical way as an indication of the fraction of martensite that has formed during the mechanical test.

If the effect of the martensitic transformation induced under stress on the elasto-plastic behavior of the material is to be modelized, it is necessary to measure the fraction x of the martensite formed.

During the tension tests, at imposed $\dot{\sigma}$ (A_1 : $\dot{\sigma} = 0.55$ MPa/s the variation of the voltage at the sample boundaries has been measured by the four points method.

In the pure martensitic state (A_1, $-115°\mathrm{C} = T < M_F$), the strain due to the orientation of the martensite platelets under the influence of σ has the property of slightly increasing the resistivity of the sample (Fig. 9). The variation of this resistivity $r_M(\varepsilon_{11})$ with the axial strain ε_{11} has been taken into account. At those temperature values where no more martensite is induced under stress (A_1, $T = 101°\mathrm{C}$, Fig. 10), the measurements show that even significant plastic strains (up to around 10%) barely modify the resistivity of the austenite (variation less than 5%).

The volume fraction of the formed martensite is given by a slight modification of Eq. (2.3) by taking into account the low variation of r_M with ε_{11}:

$$x = \frac{\left(\dfrac{r(x)}{r_{0A}} - 1\right)}{\left(\dfrac{r_M(\varepsilon_{11})}{r_{0A}} - 1\right)}, \tag{2.11}$$

where the resistivity of pure austenite is $r_{0A} = r_A(\varepsilon_{11})$, and the resistivity of the martensite at strain ε_{11} is $r_M = r_M(\varepsilon_{11})$ and $r_{0M} = r_M(\varepsilon_{11} = 0)$.

2.3.1. Evolutionary law of the transformation austenite ⇒ martensite. The evolution of x_c with the applied stress σ is nonlinear (A_1, Fig. 11). The threshold value for the beginning of transformation obtained from resistivity measurements is nearly the same as that which governs the pseudoelastic strain equation (relation (2.8)). This observation is logical.

A classical formulation is chosen for the kinetics of the phase transformation. It was expressed by KOISTINEN and MARBURGER [9] and applied to shape memory alloys by TANAKA *et al.* [10],

$$x_c = 1 - \exp(-a_c < \sigma - \sigma_0 >), \tag{2.12}$$

with

$$\sigma_0 = b(T - M_S).$$

The plot of $\ln(1 - x_c)$ allows a_c of the order of $7 \cdot 10^{-3}$ MPa to be obtained (Fig. 12), which gives a rather slow kinetic effect as compared to that which could be obtained by the effect of only the temperature (austenite ⇒ martensite by cooling of the sample of M_s to M_F, $\sigma = 0$).

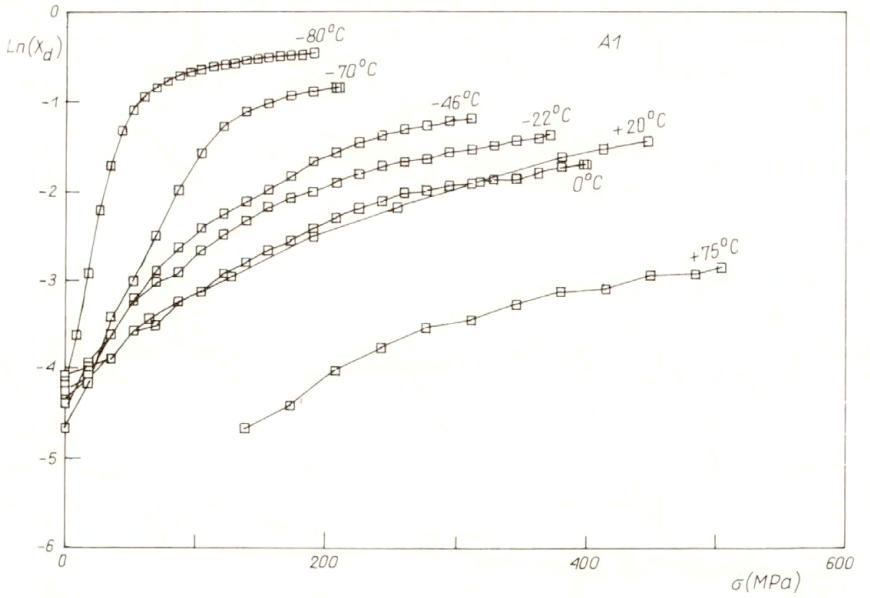

FIG. 13. Determination of the equation of evolution of the restituted martensite at unloading.

For simple thermal effects, the term $a_c b$ can be calculated using the metallurgical hypothesis that the transformation is complete when $x = 0.99$

$$a_c b = \frac{2 \operatorname{Ln} 10}{M_S - M_F} \Rightarrow a_c - 0.184 \text{ MPa}^{-1}.$$

In fact, when self-accomodating variants are formed by purely temperature effects and preferentially oriented variants by an external stress, it is logical that the rates of the processes are not the same.

2.3.2. The law governing evolution of the fraction of residual martensite x_d (at unloading). It might be supposed that just after the sign inversion of the stress ($d\sigma > 0 \Rightarrow d\sigma < 0$), the resistivity decreases slightly due to the partial reorientation of the martensitic variants previously polarized under the effect of the external stress during loading.

This means that $x_0 = x_0$ (1%, 2% ...) should not change. When σ decreases to attain the threshold value $\sigma_{0d} = b(T - A_S)$ then the inverse transformation martensite $\Rightarrow$ austenite can begin. This analysis is confirmed by examination of the Fig. 13.

Experimentally, the kinetics of the fraction of residual martensite is obtained,

$$x_d = x_0(n\%) \exp(-ad < \sigma_{0d} - \sigma >), \tag{2.13}$$

with a_d decreasing with the temperature, a_d can be modelled by

$$a_d = \frac{1.1}{T - A_s} \text{ MPa}^{-1}.$$

For pure temperature test, we obtain

$$a_d b = \frac{2 \operatorname{Ln} 10}{A_F - A_S} \Rightarrow a_d = 0.92.$$

As the temperature moves farther and farther away from the transformation temperature A_S, the restitution of the martensite becomes more and more difficult, apparently blocked by the plastic strain (which also increases with $\varepsilon = 1\% \ldots 4\%$) in tension-unloading. In any case, the reversed kinetics (martensite $\Rightarrow$ austenite) is always slower than that obtained under the effect of only the temperature (T varying from A_S to A_F, $\sigma = 0$).

2.4. Acoustic emission data [11]

As we have explained in Sec. 2.1.3, in order to try to quantify the martensitic transformation, the cumulated energy E_t has been calculated at the instant t.

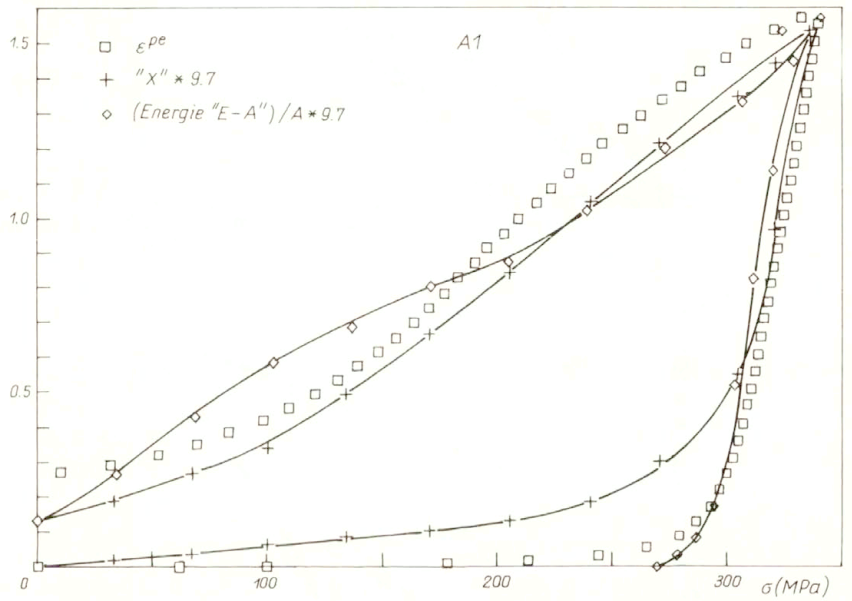

FIG. 14. Evolution of the fraction x of martensite and the cumulated energy (measured by acoustic emission).

In reference to a thermodynamic formulation of the energy associated with the transformation [1], the following hypothesis is made:

$$E_t = Ax, \tag{2.14}$$

and the parameter A chosen such that

$$A = \frac{(E_t)_{\max}}{(x_{0c})}, \tag{2.15}$$

where $(E_t)_{\max}$ — maximal cumulated energy obtained by acoustic emission at the end of loading, (x_{0c}) — volume fraction x_{0c} measured by resistivity at the end of loading.

The results show that the plot of the normalized cumulated energy E_t/A as a function of the stress σ, coincides with the evolution of x with σ (Fig. 14).

Even if the numerical value of the measured cumulated energy E_t is not assumed to be accurate, its evolution seems to coincide with that of the fraction of the martensite formed.

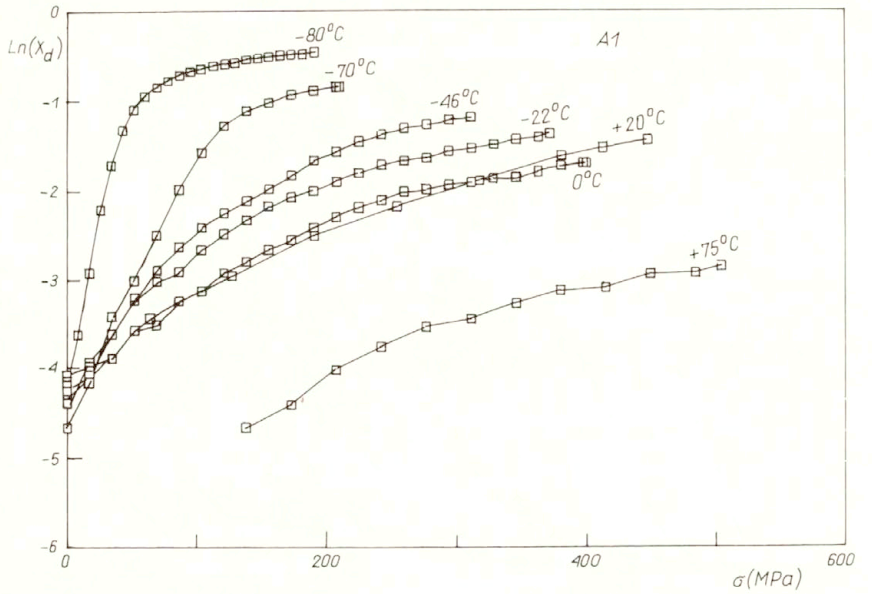

FIG. 13. Determination of the equation of evolution of the restituted martensite at unloading.

For simple thermal effects, the term $a_c b$ can be calculated using the metallurgical hypothesis that the transformation is complete when $x = 0.99$

$$a_c b = \frac{2 \operatorname{Ln} 10}{M_S - M_F} \Rightarrow a_c - 0.184 \text{ MPa}^{-1}.$$

In fact, when self-accomodating variants are formed by purely temperature effects and preferentially oriented variants by an external stress, it is logical that the rates of the processes are not the same.

2.3.2. The law governing evolution of the fraction of residual martensite x_d (at unloading). It might be supposed that just after the sign inversion of the stress ($d\sigma > 0 \Rightarrow d\sigma < 0$), the resistivity decreases slightly due to the partial reorientation of the martensitic variants previously polarized under the effect of the external stress during loading.

This means that $x_0 = x_0$ (1%, 2% ...) should not change. When σ decreases to attain the threshold value $\sigma_{0d} = b(T - A_S)$ then the inverse transformation martensite $\Rightarrow$ austenite can begin. This analysis is confirmed by examination of the Fig. 13.

Experimentally, the kinetics of the fraction of residual martensite is obtained,

$$x_d = x_0(n\%) \exp(-ad < \sigma_{0d} - \sigma >), \tag{2.13}$$

with a_d decreasing with the temperature, a_d can be modelled by

$$a_d = \frac{1.1}{T - A_s} \text{ MPa}^{-1}.$$

For pure temperature test, we obtain

$$a_d b = \frac{2 \operatorname{Ln} 10}{A_F - A_S} \Rightarrow a_d = 0.92.$$

As the temperature moves farther and farther away from the transformation temperature A_S, the restitution of the martensite becomes more and more difficult, apparently blocked by the plastic strain (which also increases with $\varepsilon = 1\% \ldots 4\%$) in tension-unloading. In any case, the reversed kinetics (martensite $\Rightarrow$ austenite) is always slower than that obtained under the effect of only the temperature (T varying from A_S to A_F, $\sigma = 0$).

2.4. Acoustic emission data [11]

As we have explained in Sec. 2.1.3, in order to try to quantify the martensitic transformation, the cumulated energy E_t has been calculated at the instant t.

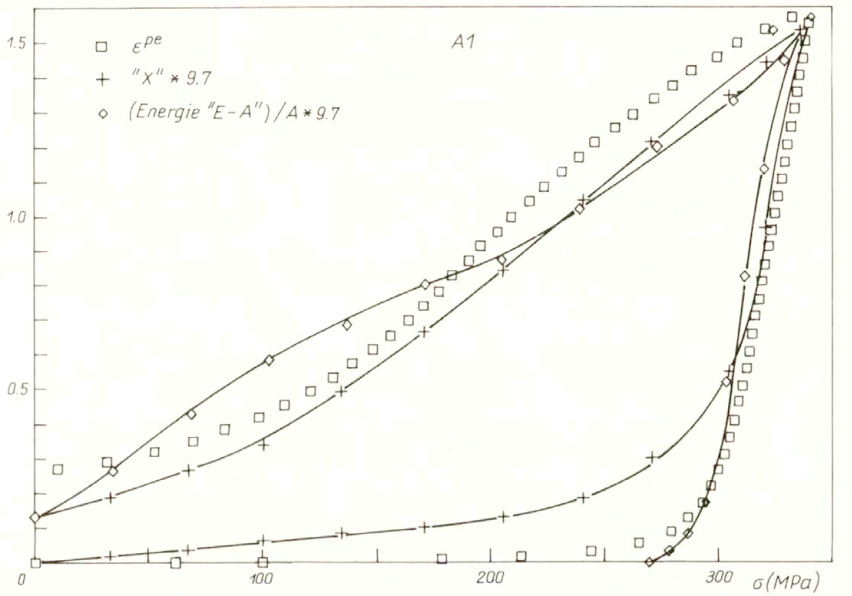

FIG. 14. Evolution of the fraction x of martensite and the cumulated energy (measured by acoustic emission).

In reference to a thermodynamic formulation of the energy associated with the transformation [1], the following hypothesis is made:

$$E_t = Ax, \tag{2.14}$$

and the parameter A chosen such that

$$A = \frac{(E_t)_{\max}}{(x_{0c})}, \tag{2.15}$$

where $(E_t)_{\max}$ — maximal cumulated energy obtained by acoustic emission at the end of loading, (x_{0c}) — volume fraction x_{0c} measured by resistivity at the end of loading.

The results show that the plot of the normalized cumulated energy E_t/A as a function of the stress σ, coincides with the evolution of x with σ (Fig. 14).

Even if the numerical value of the measured cumulated energy E_t is not assumed to be accurate, its evolution seems to coincide with that of the fraction of the martensite formed.

3. Brief thermodynamic analysis and comparison with other models

3.1. Associated thermodynamic model for pseudoelastic behaviour

In the conditions of pure hyperelastic behaviour ($A_1, T = -80, -70°C$, $\varepsilon^T \leq 2\%$, $\mathring{\sigma} = 0.55$ MPa/s), Fig. 15 shows that correlation between the pseudoelastic strain ε^{PE}

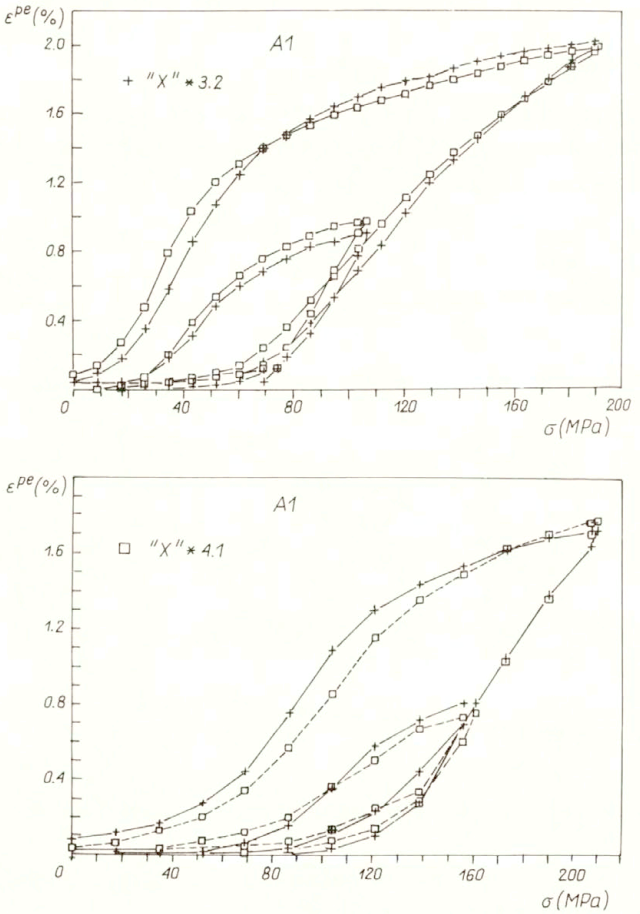

FIG. 15. Proportional evolution between ε^{PE} and x with the stress ($A_1 = T = -80°C$, $-70°C$, $\varepsilon^T \leq 2\%$, $\mathring{\sigma} = 0.55$ MPa/s).

and the martensite fraction x is possible (in loading as well as in unloading). This yields

$$\boxed{\varepsilon^{PE} = \gamma(T)x} \tag{3.1}$$

with $\mathring{T} = 0$, $\mathring{\sigma} = \text{const}$.

For a one-dimensional approach, we consider the extended specific free energy of two-phase system (see for instance MÜLLER [12])

$$\boxed{\Phi = (1-x)\Phi^{(1)} + x\Phi^{(2)} + \Phi_{\text{conf}}}, \tag{3.2}$$

where $\Phi^{(\alpha)}$ is the specific free energy of the parent phase ($\alpha = 1$, austenite) and product phase ($\alpha = 2$, martensite).

The term of configurational energy Φ_{conf} represents the hysteresis. According to MÜLLER and XU [13], the main term of Φ_{conf} is the interfacial energy, but hysteresis may also be due to lattice defects such as dislocations, elastic misfits of the phases and elastic interaction of the neighbouring domains.

RANIECKI, LEXCELLENT, TANAKA [14] write the expression of Φ_{conf} in the form

$$\Phi_{\text{conf}} = x(1-x)\Phi_{\text{it}}(T), \tag{3.3}$$

with

$$\Phi_{\text{it}}(T) = \overline{u}_0 - T\overline{s}_0. \tag{3.4}$$

MÜLLER [12] shows that we can approximate $\overline{s}_0$ at 0 for single crystals, but not for the case of polycrystals.

A common expression of the specific free energy $\Phi^{(\alpha)}$ in non-equilibrium state is written in the form

$$\Phi^{(\alpha)} = u_0^{*(\alpha)} - Ts_0^{*(\alpha)} + \frac{E_0}{2}(\varepsilon_{(\alpha)} - \varepsilon_{(\alpha)}^f)^2 - \alpha_0(T-T_0)E_0(\varepsilon_{(\alpha)} - \varepsilon_{(\alpha)}^f) + c_v[(T-T_0) - T\,\text{Ln}(T/T_0)] \tag{3.5}$$

with $-E_0 = E/\varrho$ (E — Young's modulus, ϱ — mass density).

In the first approximation, suppose that

$$\varrho^{(1)} = \varrho^{(2)} - \varrho,$$
$$E^{(1)} = E^{(2)} = E.$$

Here $u_0^{*(\alpha)}$, $s_0^{*(\alpha)}$ — specific internal energy (entropy) of each phase at stress-free state, and at a chosen reference temperature T_0, α_0 — thermal expansion coefficient, c_v — specific heat at constant volume.

The austenitic and martensitic strains purely associated with the phase transformation, are

$$\varepsilon_{(1)}^f = 0 \quad \text{and} \quad \varepsilon_{(2)}^f = \gamma. \tag{3.6}$$

Thus, we assume that the austenite strain is elastic and equal to the elastic strain of martensite

$$\varepsilon_{(1)} = \varepsilon_{(2)} - \gamma. \tag{3.7}$$

The intrinsic Cauchy stress $\sigma_{(\alpha)}$ corresponding to total strain $\varepsilon_{(\alpha)}$ is defined by

$$\sigma_{(\alpha)} = \varrho\frac{\partial\Phi^{(\alpha)}}{\partial\varepsilon_{(\alpha)}}. \tag{3.8}$$

With the expression for $\Phi^{(\alpha)}$ Eq. (3.5) and hypothesis (3.7), we obtain with Eq. (3.8)

$$\sigma_{(1)} = \sigma_{(2)} = \sigma. \tag{3.9}$$

Properties at constrained thermodynamic equilibrium

RANIECKI *et al.* [14] adopt at thermodynamic equilibrium the concept of KESTIN and RICE [15] of "constrained equilibrium".

Using the expression of the total strain ε

$$\varepsilon = (1-x)\varepsilon_{(1)} + x\varepsilon_{(2)} \tag{3.10}$$

with

$$\varepsilon_{(1)} = \varepsilon_{(2)} - \gamma, \tag{3.11}$$

we can determine $\varepsilon_{(1)}$ and $\varepsilon_{(2)}$

$$\varepsilon_{(1)} = \varepsilon - x\gamma, \qquad \varepsilon_{(1)} = \varepsilon + (1-x)\gamma, \tag{3.12}$$

which implies

$$\sigma = \varrho\frac{\partial \Phi}{\partial \varepsilon} = E(\varepsilon - x\gamma - \alpha_0(T - T_0)). \tag{3.13}$$

By substituting Eqs. (3.12), into Eq. (3.5) and the result obtained into Eq. (3.2), we obtain the following form of the free energy function at constrained equilibrium:

$$\begin{aligned} \Phi_c(\varepsilon, x, T) &= \frac{1}{2}E_0(\varepsilon - x\gamma)^2 - \alpha_0(T - T_0)E_0(\varepsilon - x\gamma) \\ &\quad + c_v[(T - T_0) - T\,\mathrm{Ln}(T/T_0)] + \Phi^*(x, T), \\ \Phi^* &= u_0^{*(1)} - Ts_0^{*(1)} - x\pi_0^f(T) + \Phi_{\mathrm{conf}}(x, T), \end{aligned} \tag{3.14}$$

with

$$\pi_0^f(T) = \Delta u^* - T\Delta s^* \begin{cases} \Delta u^* = u_0^{*(1)} - u_0^{*(2)}, \\ \Delta s^* = s_0^{*(1)} - s_0^{*(2)}. \end{cases} \tag{3.15}$$

$\pi_0^f(T)$ represents the "driving force" for temperature-induced martensitic transformation at the stress-free state.

It can be verified that the pseudoelastic part of the total strain is

$$\varepsilon^{\mathrm{PE}} = x\gamma. \tag{3.16}$$

The specific entropy s can be defined in a classical manner and thus the driving force of the phase transformation π^f is given by

$$s = -\frac{\partial \Phi_c}{\partial T}, \qquad \pi^f = -\frac{\partial \Phi_c}{\partial x}, \tag{3.17}$$

and the Clausius–Duhem inequality by

$$dD = \pi^f dx \geq 0. \tag{3.18}$$

The Clausius–Duhem inequality preludes the parent-martensite transformation at states where $\pi^f < 0$ and prevents the reverse transformation when $\pi^f > 0$. $\pi^f = 0$ corresponds to a line of unstable equilibrium separating two domains (the one where $A \rightarrow M(\pi^f > 0)$ and the other where $M \rightarrow A$ $(\pi^f < 0)$).

To specify the flow rules, we assume, as in "plasticity", that there exist two functions $\psi^{(\alpha)}(\pi^f, x)(\alpha = 1, 2)$ such that an active process of parent phase decomposition, $(dx > 0$, the forward transformation) can proceed only when $\psi^{(1)} = \mathrm{const}(d\psi^{(1)} = 0)$, and an active process of martensite decomposition, $(dx < 0$, the reverse transformation) can occur only if $\psi^{(2)} = \mathrm{const}$ $(d\psi^{(2)} = 0)$

$$\psi^{(1)} = \pi^f - k^{(1)}(x), \qquad \psi^{(2)} = -\pi^f + k^{(2)}(x). \tag{3.19}$$

In order to model the external loops (corresponding to complete phase transformations), the direct transformation is governed by $\pi^f = k^{(1)}(x)$ (i.e. $\psi^{(1)} = 0$) and the reverse transformation by $\pi^f = k^{(2)}(x)$ (i.e. $\psi^{(2)} = 0$).

For internal loops, if $\overline{x}$ is the extreme point attained before inversion of stress, there is a slight modification

$$
\begin{aligned}
A \to M \qquad & \psi^{(1)} = -k^{(1)}(\overline{x}) = cte < 0, \\
M \to A \qquad & \psi^{(2)} = +k^{(2)}(\overline{x}) = cte < 0.
\end{aligned} \tag{3.20}
$$

To be in accordance with the phase transformation kinetic laws suggested by expressions (2.12), (2.13) [10], we assume

$$
\begin{aligned}
k^{(1)}(x) &= -(A_1 + B_1 x)\,\mathrm{Ln}(1-x) + C_1 x\,, \\
k^{(2)}(x) &= (A_2 - B_2(1-x))\,\mathrm{Ln}\,x - C_2(1-x),
\end{aligned} \tag{3.21}
$$

with

$$
\begin{aligned}
C_1 &= 2\Phi_{\mathrm{it}}(M_2^0), \qquad & C_2 &= 2\Phi_{\mathrm{it}}(A_s^0), \\
a_1 A_1 &= \Delta s^* - \overline{s}_0, \qquad & a_2 A_2 &= \Delta s^* + \overline{s}_0, \\
a_1 B_1 &= a_2 B_2 = \overline{s}_0.
\end{aligned} \tag{3.22}
$$

Note that the pseudoelastic strain is bounded by the value $\gamma(T)$, which is logical from the physical point of view.

3.2. Introduction of a training variable X_e

The models developed in pure pseudoelasticity can be used to model a training processing by slight modification to introduce an internal auxiliary variable $\mathbf{X}_e$ [16]. A cyclic tension-unloading test (A_1, $\dot{\varepsilon} = 10^{-3}\ \mathrm{s}^{-1}$, $0 \leftrightarrow 2\%$, $T = -70°\mathrm{C}$) has been performed. These thermomechanical conditions correspond to a purely hyperelastic behavior.

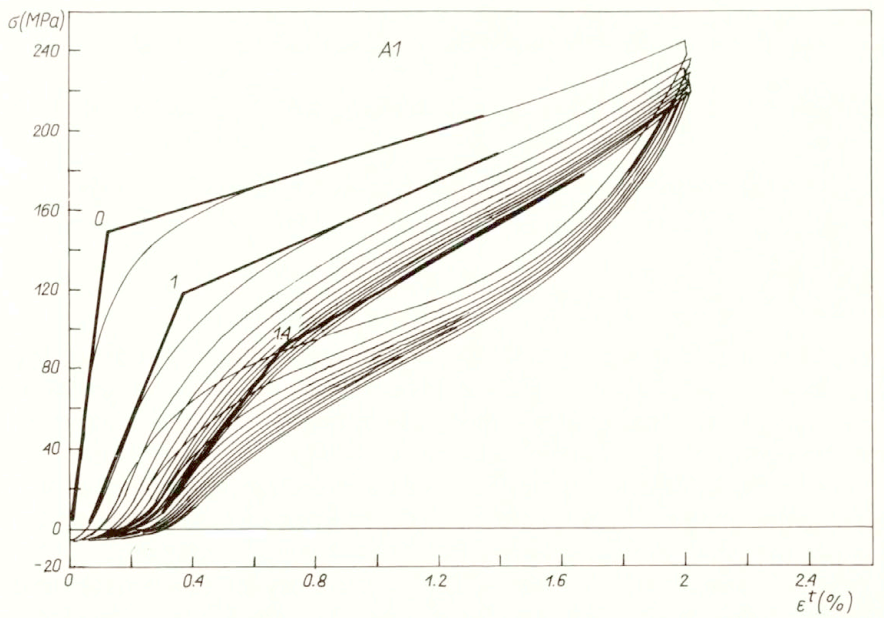

FIG. 16. Purely mechanical education curve A_1 (cycle $0 \leftrightarrow 2\%$) $T = -70°\mathrm{C}$, $\dot{\varepsilon} = 10^{-3}\ \mathrm{s}^{-1}$.

The stress threshold of the transformation diminishes with the number of increasing cycles (Fig. 16). At the first loading, the equation of the surface criteria is written,

$$\sigma - b(T - M_s) = \sigma - \sigma_0 = 0; \tag{3.23}$$

at the n-th loading

$$\sigma + X_e - b(T - M_S) = 0. \tag{3.24}$$

In uniaxial tests, X_e constitutes the measure of decrease of the transformation threshold with the number of cycles.

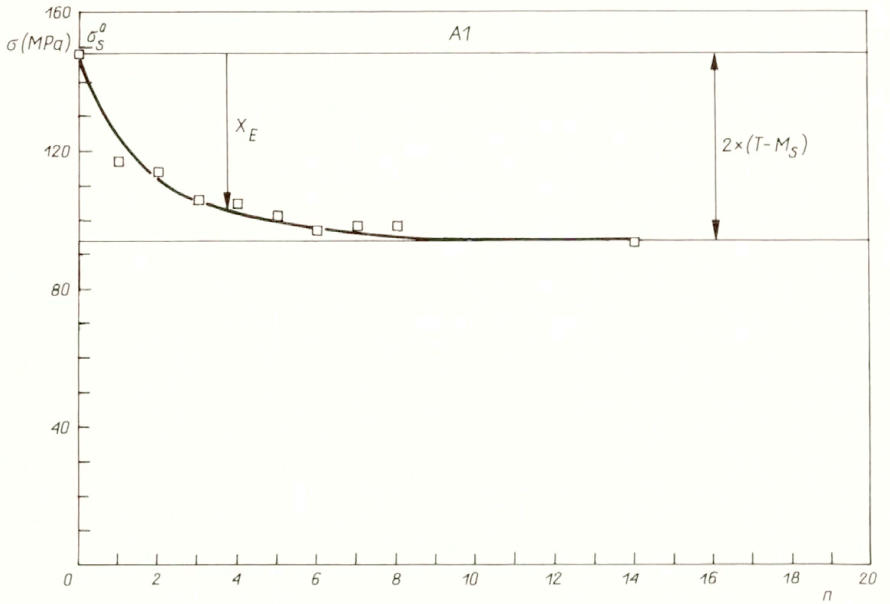

FIG. 17. Evolution of the internal variable X_e with the number of cycles.

As the cycle (σ, ε) tends to close in a stabilized form, X_e stabilizes after 15 cycles (Fig. 17).

$$x_c = 1 - \exp(-a_c < \sigma + X_e - b(T - M_S) >), \qquad \varepsilon^{\mathrm{PE}} = \gamma' x, \tag{3.25}$$

with $X_e = X_e(N)$, N — number of cycles.

4. Conclusion

The tension-unloading tests $(1\%, 2\%, \ldots 4\%)$ enable the separation of the hyperelastic and plastic strains. Resistivity measurements constitute an important indicator of the volume fraction x of the martensite formed. These observations are complemented by the information provided by acoustic emission recordings. However, a problem of discontinuity in the classical formulation [9, 10] of the evolutionary law for the martensite fraction (in loading and unloading) is observed, depending on whether the transformation is made under the effect of applied stress (at constant temperature) or at variable temperature (and zero stress). In other words, if x is a necessary internal variable to describe the hyperelastic behavior, it is not a sufficient one. An orientation parameter must be introduced to indicate the nature of the formed martensite, which is different under the

effect of a uniaxial loading on a polycristalline sample than by isotropic cooling. This is apparently the reason why certain models [17] are constructed using a local approach. Then, a homogenization method allows to obtain more realistic behavior laws.

Finally, the modelling of the general behavior, where pseudoelasticity is coupled with plasticity, constitutes a difficult subject of research.

Aknowledgement

We are very gratefull to Professor B. RANIECKI (Center of Mechanics, IFTR, Warszawa) for his help in the thermodynamic model formulation [14].

References

1. J. R. PATEL and M. COHEN, Acta Met., 1, 531, 1953.
2. R. ROMERO, F. C. LOVEY and M. AHLERS, Phil. Mag., **A. 58**, 881, 1988.
3. H. ONODERA, I. TAMURA, N.S.F. US/Japan, Seminar, 12, 1979.
4. R. ROMERO and M. AHLERS, Phil. Mag., **A. 59**, 5, 1103, 1989.
5. S. DENIS, S. SJOSTROM and A. SIMON, Met. Trans. A, **18 A.**, 1203, 1987.
6. J. B. LEBLOND, G. MOTTET and J. C. DEVAUX, J. Mech. Phys. Solid, **34**, 44, 395, 1986.
7. *Rapport de contrat de programme DGRST*, 81-P-0578, Trefimetaux-INSA Lyon, Partie INSA.
8. L. CONTARDO, These INSA, Lyon 1988.
9. D. P. KOISTINEN and R. E. MARBURGER, Acta Met., **7**, 59, 1959.
10. K. TANAKA, S. KOBAYASHI and Y. SATO, Int. J. Plasticity, **2**, 59, 1986.
11. C. LEXCELLENT and P. VACHER, Euromech 263, The Effect of Phase Transformations in Solides on Constitutive Laws, July 2–4, Vienna 1990.
12. I. MÜLLER, Continuum Mech. Thermodyn., **1**, 125, 1989.
13. I. MÜLLER and H. XU, Acta Met. Mater., **29**, 3, 263, 1991.
14. B. RANIECKI, C. LEXCELLENT and K. TANAKA, Arch. Mech., **44**, 3, 261, 1992.
15. J. KESTIN and J. R. RICE, *Paradoxes in the application of thermodynamics to strained solids*, B. B. STURAT, B. GALOR and A. I. BRAIMARD [Eds.], [in:] A Critical Review of Thermomechanics, Monobook. Corps Baltimore, 275, 1970.
16. M. BERVEILLER, *Propriétés thermomécaniques des alliages a mémoire de forme*, Conférence aux journées A.M.F. d'Aix-en-Provence, ENSAM Aix-en-Provence, 11 mai 1989.
17. E. PATOOR, A. EBERHARDT and M. BERVEILLER, Acta Met., **25**, 11, 2779, 1987.

LABORATOIRE DE MECANIQUE APPLIQUEE, ASSOCIE AU CNRS,
UFR SCIENCE ET TECHNIQUES, BESANCON, FRANCE.

Received March 3, 1992, *new version January* 18, 1993.

Arch. Mech., 45, 1, pp. 157–158, Warszawa 1993

BOOK REVIEWS

M. KLEIBER and T.D. HIEN, **The stochastic finite element method. Basic perturbation technique and computer implementation**, J. Wiley, Chichester–New York–Brisbane–Toronto–Singapore 1992, pp. 322.

THE BOOK containing 322 pages has been divided into two parts. Its principal contents is presented in Part II FEM in Stochastic Analysis; Part I. Preliminaries represents a general introduction enabling the reader to understand and utilize the information presented in Part II.

Part I consists of two chapters. Chapter 1 is devoted to the foundations of the probability theory and to the discrete data representation, first of all the discrete Fourier transform. Chapter 2 deals with a deterministic description of the Finite Element Method in the range of linear elasticity theory, with a brief presentation of nonlinear phenomena. Statical and dynamical problems are discussed.

Part II is divided into seven chapters 3–9, two appendices, bibliography, index and glossary of the symbols used in the book. Stochastic approach and the perturbation method are used to analyze the following particular problems:

- Variational principles of linear mechanics (Chapter 3);
- Stochastic finite element analysis (Chapter 4);
- Theory of sensitivity in static problems (Chapter 5);
- Computer program SFESTA for the analysis of deterministic and stochastic problems of spatial 3D trusses (Chapter 6);
- Problems of the sensitivity theory in structural dynamics (Chapter 7);
- Computer program SPEDYN for the analysis of deterministic and stochastic problems of dynamics and sensitivity theory of 3D frames (Chapter 8);
- Elements of the stochastic Finite Element Method FEM used in nonlinear mechanics (Chapter 9).

Two appendices A and B represent user's manuals for two SFESTA and SPEDYN computer programs. The corresponding IBM PC modules are available from the Publisher. The bibliography contains 126 references.

To the best knowledge of the reviewer, the book reviewed is the second monograph dealing with the problems of stochastic FEM. The first one was the book by E. Ghanem and P.D. Spanos, „Stochastic finite elements: a spectral approach, Springer Verlag, 1991. The stochastic Finite Element Method is concerned, first of all, with linear problems of structural mechanics characterized by random properties. The randomness of the material and geometric characteristics of structural elements leads to nonlinearity of the stochastic type, thus making it impossible to obtain accurate solutions. The most popular method of solving such problems is the perturbation method which, together with the FEM, constitutes a certain variant of the stochastic finite elements. The authors of the book apply consistently the second-order perturbation approach to the expected values, and the first-order approach to the covariance matrices.

It is generally known that the stochastic FEM may be used in the cases when the range of variability of the random parameters or functions is small enough.

According to reviewer's opinion, the principal advantages of the book are the following:

Part I of the book, which enables the unprepared reader to follow the considerations presented in Part II.

Formulation of the mathematical foundations of the stochastic FEM.

Analysis of a wide range of stochastic problems of mechanics of structures, such as the static and dynamic problems, sensitivity of structures, and inclusion of the computer programs enabling the readers to perform the numerical analysis of the problems discussed in the book.

The scope of the book is very close to the needs of modern design engineers, since the mechanical properties and dimensions of real structural elements usually exhibit a random character, and the sensitivity analysis is tightly connected with the optimization of structures.

To conclude the remarks concerning the valuable and interesting monograph, the question may be posed whether the theoretical considerations and the computer programs presented in the book will be actually used not

only by the research staff members of scientific institutes, but also by professional engineers active in structural design practice? In my opinion, the actual level of theoretical preparedness of civil and mechanical engineers is still insufficient to enable them to comprehend and implement in practice all the results derived in the book. However, modern development of technology proves that certain theoretical approaches and solutions may be well ahead of the actual level of design methods used in technology. The book may also have a considerable impact on the teams active in standardization of the engineering design.

E. Bielewicz

30th POLISH SOLID MECHANICS CONFERENCE

organized by

CENTER OF MECHANICS
of the INSTITUTE OF FUNDAMENTAL TECHNOLOGICAL RESEARCH
and
COMMITTEE OF MECHANICS
of the POLISH ACADEMY OF SCIENCES

Zakopane, September 5–9, 1994

The 30th Polish Solid Mechanics Conference will be held in Zakopane, a renowned resort at the foot of the Tatra Mountains.

Following a long tradition going back to the 1st Polish Solid Mechanics Conference in 1953, the objective of the 30th Conference is to bring together researchers engaged in all major areas of contemporary mechanics of solids and structures.

The program of the conference will include a number of general (invited) lectures and contributed papers. The contributed papers will be presented either in oral form or at poster sessions. The language of the conference will be English.

Social events and tours are planned.

Further details regarding the submission of abstracts will be announced in the first circular.

Scientific Committee

Prof. R. Bogacz
Prof. A. M. Brandt
Prof. H. Frąckiewicz
Prof. W. Gutkowski
Prof. M. Kleiber
Prof. Z. Mróz
Prof. W. K. Nowacki — chairman
Prof. Z. Peradzyński
Prof. P. Perzyna
Prof. B. Raniecki
Prof. D. Rogula
Prof. J. Sławianowski
Prof. K. Sobczyk
Prof. M. Sokołowski
Prof. W. Szczepiński
Prof. W. Szemplińska-Stupnicka
Prof. H. Zorski
Prof. M. Życzkowski

Organizing Committee

Prof. W. K. Nowacki — chairman
Dr. M. Basista
Dr. K. Doliński

Address for correspondence

30th Polish Solid Mechanics Conference
Center of Mechanics — IPPT PAN
Świętokrzyska 21
00-049 Warszawa, Poland
phone: 26-88-02, fax: 269815,
telex: 825638 ippt pl
e - mail: zakopane@lksu.ippt.gov.pl

First International Symposium
on
Thermal Stresses and Related Topics

THERMAL STRESSES '95

will be held at
Shizuoka University, Hamamatsu, Japan
June 5–7, 1995

The Symposium will be comprised of invited lectures and of the presentation and discussion of contributed papers. Ladies Program will be arranged. A post-symposium tour of Kyoto and Nara will be organized. Group flights from the United States to Japan will be planned.

Write for the First Announcement brochure to:

Richard B. Hetnarski, Chairman
International Organizing Committee
James E. Gleason Professor
of Mechanical Engineering
Rochester Institute of Technology
Rochester, NY 14623, U.S.A.

Naotake Noda, Chairman
International Organizing Committee
Dept. of Mechanical Engineering
Shizuoka University
5-1, Johoku 3 chome
Hamamatsu, 432, JAPAN

11th Aachen Colloquium on Fluid Power Technology
"call for papers"

The Aachen Colloquium on Fluid Power Technology (AFK) has been established as one of the eminent international conferences for current topics from the fields of hydraulics and pneumatics during the previous two decades. The colloquium has been met with an extraordinarily good response from producers and users of fluid power technology, as well as other interested parties. Besides reports and discussions, the three-day colloquium includes an exhibition and poster-session where exhibits from the fields of equipment, measuring systems and software are presented. At the same time, those guests who are interested in the Department of Fluid Power Transmission and Control of the University of Technology Aachen, can take the opportunity to view the laboratories and to inform themselves on current research projects and new developments.

The main topics of the 11th AFK, which lasts from **March 8th, 1994, until March 10th, 1994**, will deal with the field of hydraulics during the first two days and with pneumatics at the final day. The main topics of the 11th AFK are as follows:

1. Improvement of the Competitiveness of Fluid Power
2. Energy Saving Measures
3. New Concepts in Mobile Hydraulics
4. Hydraulics in the Plastics Industry and Metal Forming
5. Economical and Environmental Use of Pneumatics
6. New Developments of Pneumatic Components and Systems

On each of the main conference topics several lectures, which last for maximally 15 minutes, will be held. Anyone interested in contributing a **paper** to the conference is requested to forward an abstract (maximal two letter-size pages) of his article to the following address by **May 31, 1993,** at the latest.

nstitut für Hydraulische und Pneumatische Antriebe und Steuerungen der RWTH Aachen,
Steinbachstrasse 53, W-5100 Aachen, Germany

Archives of Mechanics

Archiwum Mechaniki Stosowanej

volume 45 **Authors' Index**

Polish Scientific Publishers PWN

Warszawa 1993

Book Reviews